HYBRID MODELLING AND OPTIMISATION OF OIL WELL DRILLSTRINGS

M. Y. A. ALKARAGOOLEE

PHD

2018

Hybrid Modelling and Optimisation of Oil Well Drillstrings

Mohammed Yaseen Abdullah ALKARAGOOLEE

Submitted for the Degree of

Doctor of Philosophy

Faculty of Engineering and Informatics

University of Bradford

2018

Abstract

Mohammed Yaseen Abdullah Alkaragoolee

Hybrid Modelling and Optimisation of Oil Well Drillstrings

Keywords: Drilling, Oil Rig, Drillstring, Stick-Slip, Modelling, Simulation, Distributed-Lumped, Optimisation, Genetic Algorithms.

The failure of oil well drillstrings due to torsional and longitudinal stresses caused by stick-slip phenomena during the drilling operation causes great expense to industry. Due to the complicated and harsh drilling environment, modelling of the drillstring becomes an essential requirement in studies.

Currently, this is achieved by modelling the drillstring as a torsional lumped model (which ignores the length of the drillstring) for real-time measurement and control. In this thesis, a distributed-lumped model including the effects of drillstring length was developed to represent the drillstring, and was used to simulate stick-slip vibration. The model was developed with increasing levels of detail and the resultant models were validated against typical measured signals from the published literature.

The stick-slip model describes the friction model that exists between the cutting tool and the rock. Based on theoretical analysis and mathematical formulation an efficient and adaptable model was created which was then used in the application of a method of species conserving genetic algorithm (SCGA) to optimise the drilling parameters.

In conclusion, it was shown that the distributed-lumped model showed improved detail in predicting the transient response and demonstrated the importance of including the drillstring length. Predicting the response of different parameters along the drillstring is now possible and this showed the significant effect of modelling the drillcollar. The model was shown to better represent real system and was therefore far more suited to use with real time measurements.

List of Publications

a- Published

- Alkaragoolee, MYA, Ebrahimi, KM and Whalley, R. A hybrid model for a drilling process for hydrocarbon well-boring operations, Proceedings of the Institution of Mechanical Engineers, Part K: Journal of Multi-body Dynamics, 2017.

- **b- In progress**

- M Y A Alkaragoolee, D Bryant, N Rahmanian, Jian-Ping Li, K Ebrahimi, Development of the Distributed-Lumped Parameter Model (Hybrid) of an Oilwell Drillstring.

- M Y A Alkaragoolee, D Bryant, N Rahmanian, Jian-Ping Li, Optimisation of Drilling Parameters to Prevent Stick-slip Vibrations of Oilwell Drillstrings Using Species Conserving Genetic Algorithm Technique.

- M Y A Alkaragoolee, D Bryant, N Rahmanian, Jian-Ping Li, The Effect of Decay Factor (the Stribeck effect) on Stick-Slip Behaviour of Oilwell Drillstring

Acknowledgements

I would like to thank my supervisors, Dr David Bryant, Dr JP Li and Dr N. Rahmanian for their supervision and invaluable guidance provided to accomplish the project. Special thanks to Professor K. M. Ebrahimi and Professor Martin Priest for help and support.

I would also like to express my deep thanks and appreciation to the Iraqi government represented by the Ministry of Higher Education and Scientific Research for their financial support and granting the opportunity to do my PhD at the University of Bradford. A special word of thanks is given to Mr Ali Hussian Ahmed the driller in the Iraq Driller Company (IDC) for helping me to understand the mechanism of drilling.

Finally, I would like to thank my wife, children, sisters and brothers for their never ending support, patience and prayers.

List of Contents

Abstract……i

List of publications……..ii

Acknowledgments……..iii

List of contents……...iv

Appendices……ix

List of figures……...x

List of tables……..xix

Nomenclature……xx

List of abbreviation……xxv

CHAPTER 1: INTRODUCTION……...1

1.1 Well drilling for hydrocarbons 2

1.2 Scope of this research.....4

1.3 Aim…… 5

1.4 Objectives of the work 5

1.5 Contributions 6

1.6 Structure of the thesis.....8

CHAPTER 2: LITERATURE REVIEW.....11

2.1 Principle of oil well drilling.....12

2.1.1 Hoisting system….....16

2.1.2 Rotating system… 18

2.1.3 Circulating system 22

2.1.4 Control and monitoring system 24
2.2 Drillstring Vibrations 26
2.2.1 Longitudinal or axial vibrations (bit bouncing phenomenon) 28
2.2.2 Lateral vibrations (whirl motion) 30
2.2.3 Stick-slip vibrations 31
2.3 Modelling methods for stick-slip vibrations 35
2.3.1 Torsional pendulum model 36
2.3.2 Distributed parameter model 39
2.4 Stick-slip prevention methods 43
2.4.1 Active stick-slip suppression approaches 44
2.4.2 Passive stick-slip suppression approaches 48
2.5 Summary 50
CHAPTER 3: THEORY & METHODOLOGY 52
3.1 Lumped model of drilling system 53
3.2 Equation of motion of the drive system 54
3.2.1 DC motor 55
3.2.2 Gearbox and bevel gear 56
3.2.3 The rotary table 56
3.3 Mathematical model of the drillstring 58
3.4 The model of friction torque ($\boldsymbol{T_{fb}}$) 60
3.5 Distributed-Lumped model 63
3.6 The general representation of a hybrid model 65

3.6.1 Torsional distributed shaft 66

3.7 Distributed-Lumped model of a rotary system with inertia and damping…….....69

3.8 Summary 71

CHAPTER 4: SIMULATION OF THE DRILLING SYSTEM.....72

4.1 Lumped model simulation.....74

4.2 Distributed-Lumped model simulation 76

4.2.1 Lumped-Distributed-Lumped Model (LDLM) 77

4.3 Lumped-Distributed-Distributed-Lumped Model (LDDLM).....82

4.4 Lumped-Distributed-Distributed-Distributed-Lumped Model (LDDDLM)……. 87

4.5 Model parameters.....93

4.5.1 Fixed parameters.....93

4.5.2 Variable parameters 94

4.6 Development of Lumped and Lumped-distributed-lumped models…….96

4.6.1 NO Stick-slip…….....97

4.6.2 Stick-Slip Phase….....100

4.7 Validation of models 105

4.8 Summary 113

CHAPTER 5: COMPARISON BETWEEN HYBRID MODELS AND LUMPED MODEL…….....114

5.1 Comparison between Distributed-Lumped (Hybrid) Models and the Lumped Model……..116

5.1.1 Case study one ($l_{dp} = 500m$) 116

5.1.2 Case study two ($l_{dp} = 2000m$) 125

5.1.3 Case study three ($l_{dp} = 5700m$) 136

5.2 Investigating the effect of key drilling parameters on critical speed……144

5.2.1 Simulation results of the key parameters.....146

5.3 Summary 150

CHAPTER 6: OPTIMISATION OF DRILLING PARAMETERS.....152

6.1 Drilling optimisation 154

6.2 Genetic algorithms (GAs) 156

6.2.1 Selection……. 159

6.2.2 Crossover…… 159

6.2.3 Mutation…….. 160

6.3 Species Conserving Genetic Algorithms 160

6.4 Optimisation Problems 163

6.4.1 Objective function ……...165

6.4.2 Constraints…….....167

6.5 Results and Discussion 167

6.5.1 Case study one (length of drillpipe 500 m) 168

6.5.2 Case study two (length of drillpipe 2000 m).....173

6.5.3 Case study three (length of drillpipe 5700m) 179

6.6 Summary 184

CHAPTER 7: CONCLUSION AND RECOMMENDATIONS FOR FURTHER WORK……..... 186

7.1 Summary 187

7.2 Recommendations for Further Work..... 189

References…… 191

Appendices

Appendix A……..……A

A .1 Electrical transmission line ……..……A

A .1.1 Lossy transmission line..……..……B

A .1.1 Lossles transmission line……..……I

Appendix B……..……K

B.1 General solution of second order linear differential equation……..K

Appendix C……..L

Table C-1-1 Simulation results of the key parameters……L

List of Figures

Figure 2-1 Classification of rotary drilling rigs (Bourgoyne Jr et al. 1986) 13

Figure 2-2 Conventional land rig 15

Figure 2-3 Hoisting system (Oil and Gas Portal 2014) 16

Figure 2-4 Kelly system 19

Figure 2-5 Stabiliser (Mitchell et al. 2011) 21

Figure 2-6 Types of bits, a) Fixed-Cutter, b) Roller-Cone c) Hybrid (Mitchell et al. 2011) 22

Figure 2-7 Drill-mud circulation system (Rich Mineral Corporation 2007) 24

Figure 2-8 Example of stick-slip oscillation of a drillstring (Kriesels et al. 1999.) 33

Figure 3-1 Representation of a drilling system as a torsional pendulum driven by a DC motor 55

Figure 3-2 Friction torque at the bit: (1) dry friction with exponential-decaying law in the sliding phase; (2) switch, friction model with a variation of Karnopp's friction model 62

Figure 3-3 Block diagram of the drilling system (lumped model) (blue: drive system; red: drillpipe; bright blue & green: BHA) 63

Figure 3-4 Distributed-lumped parameter system 65

Figure 3-5 A simple torsional shaft 66

Figure 3-6 Free body diagram of a rotary system 69

Figure 3-7 Block diagram representation of a simple rotary system (blue: prime mover; red: load; purple: sold shaft) 70

Figure 4-1 Simulink model of a lumped parameter drillstring in an oil drilling system (blue: drive system; red: drillpipe; light blue: BHA; green: friction torque on the bit) 75

Figure 4-2 Representation of a drilling system as a torsional transmission line driven by a DC motor 77
Figure 4-3 Block diagram of the drilling system (LDLM) (blue: drive system; red: drillpipe; light blue & green: BHA) 79
Figure 4-4 LDLM of drillstring in an oil drilling system (LDLM) (blue: drive system; red: drillpipe; light blue & green: BHA) 81
Figure 4-5 Representation of oil drilling system as a Lumped-Distributed-Distributed-Lumped Model (LDDLM) 82
Figure 4-6 Block diagram of the drilling system (LDDLM) (blue: drive system; red: drillpipe; yellow: HWDP; dark blue: drill collar; purple: common point between drillpipe and HWDP) 84
Figure 4-7 Simulation of LDDLM of oil drilling system in Matlab Simulink (blue: drive system; red: drillpipe; yellow: HWDP; dark blue: drill collar; purple: common point between drillpipe and HWDP).....86
Figure 4-8 Subsystem to calculate the output velocity of the drillpipe (blue: inlet velocity of drillpipe; dark blue: velocity of drill bit; purple: outlet velocity of drillpipe) 87
Figure 4-9 Representation of oil drilling system as LDDDL model 88
Figure 4-10 Block diagram of the drilling system (LDDDLM) (blue: drive system; red: drillpipe; dark blue: drillcollar; purple: common point between drillpipe and HWDP; bright blue: common point between HWDP and drillcollar; dark red: drill bit).....90
Figure 4-11 Simulation of LDDDLM of oil drilling system in Matlab Simulink (blue: drive system; red: drillpipe; dark blue: drillcollar; dark blue: drill bit) 91

Figure 4-12 Subsystem to calculate the output velocity of drillpipe and HWD (blue: inlet velocity of drillpipe; purple: outlet velocity of drillpipe; bright blue: outlet velocity of HWD; dark red: velocity of drill bit) 92
Figure 4-13 Applied torque on the bit of LDLM (no stick-slip) 98
Figure 4-14 Applied torque on the bit of LM (no stick-slip).....98
Figure 4-15 Friction torque on the bit of LDLM (no sticking) 99
Figure 4-16 Friction torque on the bit of LM (no sticking).....99
Figure 4-17 Angular velocity of LDLM (no stick-slip).....100
Figure 4-18 Angular velocity of LM (no stick-slip) 100
Figure 4-19 Applied torque on the bit LDLM with stick-slip motion.....102
Figure 4-20 Applied torque on the bit versus bit speed for the LDLM with stick-slip motion.....102
Figure 4-21 3D plot of applied torque on the bit and bit speed against time for the LDLM 102
Figure 4-22 Applied torque on the bit of LM with stick-slip motion 103
Figure 4-23 Applied torque on the bit versus bit speed for the LM with stick-slip motion 103
Figure 4-24 3D plot of applied torque on the bit and bit speed against time for the LM.....103
Figure 4-25 Friction torque on the bit of LDLM with stick-slip motion.....104
Figure 4-26 Friction torque on the bit of LM with stick-slip motion 104
Figure 4-27 Stick-slip oscillation: LDLM 105
Figure 4-28 Stick-slip oscillation: LM.....105
Figure 4-29 Real measurements of stick-slip vibration reproduced from(Veeningen 2011) 108
Figure 4-30 Stick-slip vibration of LDDDLM (W_{ob} =200KN,μ_{sb}=0.8, γ_b=0.9) ...108

Figure 4-31 Stick-slip vibration of LDDDLM (W_{ob} =250KN,μ_{sb}=0.8, γ_b=0.9) ...108
Figure 4-32 Stick-slip vibration of LDDDLM (W_{ob} =200KN,μ_{sb}=0.8, γ_b=0.2) ...109
Figure 4-33 Stick-slip vibration of LM (W_{ob} =200KN,μ_{sb}=0.8, γ_b=0.2).....109
Figure 4-34 Real measurements of stick-slip vibration (drillstring length = 550m)(Ledgerwood et al. 2013) 110
Figure 4-35 Stick-slip vibration of LDDDLM (drillstring length = 550m).....110
Figure 4-36 Real measurements of stick-slip vibration (drillstring length = 1500m) (Ledgerwood et al. 2013) 111
Figure 4-37 Stick-slip vibrations of LDDDLM (drillstring length=1500m) 111
Figure 4-38 Stick-slip vibration of LDDDLM (drillstring length =2840m) (Ledgerwood et al. 2013) 112
Figure 4-39 Stick-slip vibration of LDDDLM (drillstring length = 2840m; Wob = 100kN; sticking time = 4s).....112
Figure 5-1 Angular velocity of Lumped model (LM) and Distributed-Lumped models (LDLM, LDDLM and LDDDLM) at 125rev/min (case 1) 118
Figure 5-2 Applied torque on bit of Lumped model (LM) and Distributed-Lumped models (LDLM, LDDLM and LDDDLM) at 125rev/min (case 1) 119
Figure 5-3 Torque at the top of Lumped model (LM) and Distributed-Lumped models (LDLM, LDDLM and LDDDLM) at 125rev/min (case 1) 119
Figure 5-4 Comparison between critical speed of Lumped model (LM) and Distributed-Lumped models (LDLM, LDDLM and LDDDLM) (case 1).....121
Figure 5-5 Stick-slip below the critical speed of Lumped model (LM) and Distributed-Lumped models (LDLM, LDDLM and LDDDLM) (A: stick-slip torque of LDDLM; B: stick-slip torque of LDDLM and LDLM; C: stick-slip torque of LDDLM, LDLM and LM; D: stick-slip torque of LDDLM, LDLM, LM and LDDDLM) (case 1).....122

Figure 5-6 Stick-slip at low velocity for the Lumped model (LM) and Distributed-Lumped models (LDLM, LDDLM and LDDDLM) (case 1).....124
Figure 5-7 Applied torque on the bit in the stick-slip phase for the Lumped model (LM) and Distributed-Lumped models (LDLM, LDDLM and LDDDLM) (case 1).....124
Figure 5-8 Torque at the top of drillstring at the stick-slip phase for the Lumped model (LM) and Distributed-Lumped models (LDLM, LDDLM and LDDDLM) (case 1).....125
Figure 5-9 Angular velocity of the Lumped model (LM) and Distributed-Lumped models (LDLM, LDDLM and LDDDLM) at 125rev/min (case 2).....127
Figure 5-10 Applied torque on the bit of the Lumped model (LM) and Distributed-Lumped models (LDLM, LDDLM and LDDDLM) at 125rev/min (case 2).....128
Figure 5-11 Torque at the top of the drillstring for the Lumped model (LM) and Distributed-Lumped models (LDLM, LDDLM and LDDDLM) at 125rev/min (case 2).....128
Figure 5-12 Comparison between critical speed of Lumped model (LM) and Distributed-Lumped models (LDLM, LDDLM and LDDDLM) (case 2).....129
Figure 5-13 Stick-slip under critical speed of Lumped model (LM) and Distributed-Lumped models (LDLM, LDDLM and LDDDLM) (A: stick-slip torque of LDDDLM; B: stick-slip torque of LDDDLM and LDDLM; C: stick-slip torque of LDDDLM, LDDLM and LDLM; D: stick-slip torque of LDDDLM, LDDLM, LDLM and LM) (case 2).....130
Figure 5-14 Stick-slip at low velocity of Lumped model (LM) and Distributed-Lumped models (LDLM, LDDLM and LDDDLM) (case 2).....132

Figure 5-15 Applied torque on bit at stick-slip phase of Lumped model (LM) and Distributed-Lumped models (LDLM, LDDLM and LDDDLM) (case 2).....132
Figure 5-16 Torque at the top of drillstring at stick-slip phase of Lumped model (LM) and Distributed-Lumped models (LDLM, LDDLM and LDDDLM) (case 2) 133
Figure 5-17 Example of stick-slip oscillation of a drill string (Kriesels et al. 1999.) (Also shown in Figure 2-8) 134
Figure 5-18 Stick-slip of the LM at steady state 134
Figure 5-19 Stick-slip of LDLM at steady state 135
Figure 5-20 Stick-slip of LDDLM at steady state 135
Figure 5-21 Stick-slip of LDDDLM at steady state 136
Figure 5-22 Angular velocity of the Lumped model (LM) and Distributed-Lumped models (LDLM, LDDLM and LDDDLM) at 125rev/min (case 3) 138
Figure 5-23 Applied torque on the bit for the Lumped model (LM) and Distributed-Lumped models (LDLM, LDDLM and LDDDLM) at 125rev/min (case 2).....138
Figure 5-24 Torque at the top of the drillstring for the Lumped model (LM) and Distributed-Lumped models (LDLM, LDDLM and LDDDLM) at 125rev/min (case 3).....139
Figure 5-25 Comparison between the critical speed of the Lumped model (LM) and Distributed-Lumped models (LDLM, LDDLM and LDDDLM) (case 3).....140
Figure 5-26 Stick-slip below the critical speed of the Lumped model (LM) and Distributed-Lumped models (LDLM, LDDLM and LDDDLM) (A: stick-slip torque of LDDDLM; B: stick-slip torque of LDDDLM and LDDLM; C: stick-slip torque of LDDDLM, LDDLM and LDLM; D: stick-slip torque of LDDDLM, LDDLM, LDLM and LM) (case 3).....141

Figure 5-27 Stick-slip at low velocity for the Lumped model (LM) and Distributed-Lumped models (LDLM, LDDLM and LDDDLM) (case 3).....143
Figure 5-28 Applied torque on the bit in the stick-slip phase for the Lumped model (LM) and Distributed-Lumped models (LDLM, LDDLM and LDDDLM) (case 3).....143
Figure 5-29 Torque at the top of the drillstring in the stick-slip phase for the Lumped model (LM) and Distributed-Lumped models (LDLM, LDDLM and LDDDLM) (case 3).....144
Figure 5-30 Interaction plot of key drilling parameters (characteristic impedance of the drillpipe (ξ_{dp}), inertia of drillcollar (J_{dc}), weight on bit (W_{ob})) and damping along BHA(C_{bh})).....147
Figure 5-31 Surface plot of the key drilling parameters (characteristic impedance of the drillpipe (ξ_{dp}), inertia of drillcollar (J_{dc}), weight on bit (W_{ob})) vs critical speed (ω_{cr}).....147
Figure 6-1 A simple one point crossover.....160
Figure 6-2 Mutation in binary genetic algorithm 160
Figure 6-3 A sample distribution of species in a two-dimensional domain (Li et al. 2002).....162
Figure 6-4 The structure of the species conserving genetic algorithm(Li et al. 2002).....163
Figure 6-5 Block diagram of the drilling system with two inputs and two outputs 165
Figure 6-6 Block model representing the objective function.....165
Figure 6-7 The objective function as coded in Matlab.....167
Figure 6-8 Three dimensional plot of rate of penetration (R_{op}) when velocity of the bit was ≤125rev/min ($l_{dp} = 500m$).....170

Figure 6-9 Maximum rate of penetration (Rop) at a bit velocity of 124.9925 rev/min ($l_{dp} = 500m$).....170

Figure 6-10 Velocity of drilling at maximum rate of penetration (Rop) ($l_{dp} = 500m$).....171

Figure 6-11 Surface plot of rate of penetration (Rop) vs weight on bit (Wob) and torque of rotary table (T_{rt}) ($l_{dp} = 500m$).....171

Figure 6-12 Surface plot of velocity of bit (ω_b) vs weight on bit (Wob) and torque of rotary table (T_{rt}) ($l_{dp} = 500m$).....172

Figure 6-13 Surface plot of rate of penetration (Rop) vs velocity of bit (ω_b) and weight on bit (Wob) ($l_{dp} = 500m$).....173

Figure 6-14 Three dimensional plot of rate of penetration (Rop) when velocity of the bit was ≤125rev/min ($l_{dp} = 2000m$).....175

Figure 6-15 Maximum rate of penetration (Rop) at a bit velocity of 124.4267rev/min($l_{dp} = 2000m$).....176

Figure 6-16 Velocity of drilling at maximum rate of penetration (Rop) ($l_{dp} = 2000m$).....176

Figure 6-17 Surface plot of rate of penetration (Rop) vs weight on bit (Wob) and torque of rotary table (T_{rt}) ($l_{dp} = 2000m$).....177

Figure 6-18 Surface plot of velocity of bit (ω_b) vs weight on bit (Wob) and torque of rotary table (T_{rt}) ($l_{dp} = 2000m$).....178

Figure 6-19 Surface plot of rate of penetration (Rop) vs velocity of bit (ω_b) and weight on bit (Wob) ($l_{dp} = 2000m$).....178

Figure 6-20 Three dimensional plot of rate of penetration (Rop) at a velocity of ≤125rev/min ($l_{dp} = 5700m$).....181

Figure 6-21 Maximum rate of penetration (Rop) at a bit velocity of 124.4267rev/min ($l_{dp} = 5700m$).....181
Figure 6-22 Velocity of drilling at maximum rate of penetration (Rop) ($l_{dp} = 5700m$).....182
Figure 6-23 Surface plot of rate of penetration (Rop) vs weight on bit (Wob) and torque of rotary table (T_{rt}) ($l_{dp} = 5700m$).....182
Figure 6-24 Surface plot of velocity of bit (ω_b) vs weight on bit (Wob) and torque of rotary table (T_{rt}) ($l_{dp} = 5700m$).....183
Figure 6-25 Surface plot of rate of penetration (Rop) vs velocity of bit (ω_b) and weight on bit (W_{ob}) ($l_{dp} = 5700m$).....184
Figure A-1 Generic transmission-line section.....B

List of Tables

Table 4-1 Fixed parameters of the drilling system (Jansen et al. 1995; Christoforou and Yigit 2003; Navarro-López and Licéaga-Castro 2009)…… 94

Table 4-2 Parameters of drillstring (case study one)…… 95

Table 4-3 Parameters of drillstring (case study two)…… 95

Table 4-4 Parameters of drillstring (case study three)…….. 96

Table 4-5 Validation parameters of drillstring (Veeningen 2011 and Ledgerwood et al.2013)……106

Table 4-6 Parameters are taken from table 4.1…… 106

Table 5-1 Simulation result of case one ($l_{dp} = 500m$)…… 118

Table 5-2 Simulation result of case two (drillpipe=2000m)…… 127

Table 5-3 Simulation result of case three (drillpipe=5700m)…….. 137

Table 5-4 Parameter values for the study into critical velocity……146

Table 6-1 Number of solutions at ≤125rev/min (case one)…… 169

Table 6-2 Number of solutions at ≤125rev/min (case two)…… 174

Table 6-3 Number of solutions at ≤125rev/min (case study three)……180

Table C-1 Simulation results of the key parameters…… L

Nomenclature

A, B, C', D	Arbitrary constants
a	Constant represent characteristic impedance of drillpipe (ξ_{dp})
b	Constant represent characteristic impedance of HWDP(ξ_{hw})
b'	Damping coefficient
c	Constant represent characteristic impedance of drillcollar (ξ_{dc})
c_1^*, c_2^*	Constants representing the rock characteristics
C	Capacitance per unit length (F/m)
C_0	Coefficient damping of bearing on the motor side (Nms/rad)
C_1	Coefficient damping of bearing on the load side (Nms/rad)
C_{bh}	The equivalent damping of BHA of LDLM (Nms/rad)
C_{ds}	Equivalent viscous damping of drive system (Nms/rad)
C_{dp}	Equivalent viscous damping along the drillpipe (Nms/rad)
C_{eb}	Equivalent viscous damping of the BHA of LM (Nms/rad)
$d_{o,dp}$	Outer diameter of the drillpipe (mm)
$d_{i,dp}$	Inner diameter of the drillpipe (mm)
$d_{o,dc}$	Outer diameter of the drillcollar (mm)
$d_{i,dc}$	Inner diameter of the drillcollar (mm)
$d_{o,hdp}$	Outer diameter of the HWDP (mm)
$d_{i,hdp}$	Inner diameter of the HWDP (mm)
$D\omega$	Limit velocity interval (rev/min)
G	Conductance per unit length (N/m^2)
$G(t)$	Generation
G_*	Shear modulus of rigidity(N/m^2)
G_s	Shear modulus of steel (N/m^2)
G_0	Shear modulus of distributed shaft (N/m^2)

I_j, I_{j+1}	Input and output current of element of a transmission line(A)
$\mathrm{i}(\mathrm{x},\mathrm{t})$	Current at distance x and time t (A)
I_0	Inertia of distributed shaft (m^4)
J	Shaft polar moment of inertia (m^4)
J_m	Mass moment of inertia of the motor (kgm^2)
J'_m	Mass moment of inertia of drillstring (kgm^2)
J_{bh}	The equivalent mass moment inertia of BHA (kgm^2)
J_{rt}	Mass moment of inertia of the rotary table (kgm^2)
J_{ds}	Equivalent mass moment of inertia of the drive system (kgm^2)
J_{eb}	Equivalent mass moment of inertia of the BHA plus 1/3 of drillpipe (kgm^2)
J_b	Mass moment of inertia of bit plus shock absorber (kgm^2)
J_dc	Mass moment of inertia of drillcollar plus J_b (kgm^2)
J_{hdp}	Mass moment of inertia of the HWDP (kgm^2)
J_{dp}	Mass moment of inertia of the drillpipe (kgm^2)
J_{dc}	Mass moment of inertia of the drillcollar (kgm^2)
J_0	Mass moment of inertia of distributed shaft (kgm^2)
J_1	Mass moment of inertia of load (kgm^2)
K_{dp}	Equivalent torsional stiffness of the drillpipe $(Nm\ /\ rad)$
L	Inductance per unit length of electrical transmission line
l_{dp}	Length of drillpipe (m)
l_{dc}	Length of drillcollar (m)
l_{hdp}	Length of HWDP (m)
l_0	Length of torsional distributed shaft (m)
n	A combined gear ratio of gearbox and bevel gear
p	Constant

P_n	Population
r	Radius of shaft (mm)
R_b	Radius of the bit (m)
R	Resistance per unit length (Ω/m)
s	Laplace operator
S_i	Species set
t	Time
t_{dp}	The delay time of drillpipe (s)
t_{dc}	The delay time of heavyweight drillpipe (s)
t_{hw}	The delay time of heavyweight drillpipe (s)
T_j, T_{j+1}	Input and output torque of distributed shaft(Nm)
T_m	Torque of motor (Nm)
T_{rt}	Torque of the rotary table (Nm)
T_{vb}	Viscosity damping torque over the BHA (Nm)
T_{fb}	Friction torque on the bit (Nm)
T_{ab}	External torque applied by drillstring on the bit (Nm)
T_{sb}	Static friction torque on the bit (Nm)
T_{cb}	Colum friction torque (cutting torque) (Nm)
T_0	Input torque to distributed shaft (Nm)
T_1^*	Torque output from distributed shaft (Nm)
T_{dp}	The torque of drillpipe
T_1	Input torque to drillpipe (Nm)
T_2	Output torque from drillpipe (Nm)
T_3	Output torque from HWDP (Nm)
T_4	Output torque from drillcollar (Nm)
$\mathrm{u}_0, u_1, u_{n-1}$	Input variable to element

U_j	Input variable (j= ith element -1)
V_j, V_{j+1}	Input and output voltage of element of a transmission line
$\mathrm{v(x,t)}$	Voltage at distance x and time t (v)
W_{Ob}	Weight on bit (WOB) (N)
w_j	Transform variable
w_0	Transform variable associated with distributed shaft
w_1	Transform variable associated with drillpipe
w_2	Transform variable associated with heavyweight drillpipe
w_3	Transform variable associated with drillcollar
x^*	Species seed
X_s	Species set
y	Non-dominating individual
$\mathrm{y}_0, y_1, y_{n-1}$	Output variable from element
$Y_j(s)$	Output variable (j= ith element -1)
σ_s	Species distance
γ	Shear strain
γ_b	Positive constant defining the decaying velocity of T_{fb}
Γ	Propagation constant of the electrical transmission line (s/m)
Γ_j	Propagation constant (s/m)
Γ_0	Propagation constant of the distributed shaft (s/m)
Γ_{dp}	Propagation constant of the drillpipe (s/m)
Γ_{dc}	Propagation constant of the drillcollar (s/m)
Γ_{hp}	Propagation constant of the heavyweight drillpipe (s/m)
ξ_i	Characteristic impedance
ξ	Characteristic impedance of electrical transmission line (v/A)
ξ_0	Characteristic impedance of distributed shaft (Nms)

$\xi_1 = \xi_{dp}$	Characteristic impedance of the drillpipe (Nms)
$\xi_2 = \xi_{hw}$	Characteristic impedance of the heavyweight drillpipe (Nms)
$\xi_3 = \xi_{dc}$	Characteristic impedance of the drillcollar (Nms)
μ_b	Friction coefficient at the bit
μ_{cb}	Coulomb friction coefficient
μ_{sb}	Static friction coefficient
θ_m	Angular displacement of the motor (rad)
θ_{rt}	Angular displacement of the rotary table (rad)
θ_b	Angular displacement of the bit (rad)
θ	Angle of twist (rad)
ρ	Density of steel (kg/m^3)
ρ_0	Density of distributed shaft (kg/m^3)
ω	Angular velocity (rev/min)
ω_{cr}	Critical velocity (rev/min)
ω_m	Angular velocity of the motor shaft (rev/min)
ω_j, ω_{j+1}	Input and output angular velocity of distributed shaft (rev/min)
ω_{rt}	Angular velocity of the rotary table (rev/min)
ω_b	Angular velocity of the bit (rev/min)
ω_0	Angular velocity at the inlet of distributed shaft (rev/min)
ω_1^*	Angular velocity at the outlet of distributed shaft (rev/min)
ω_1	Angular velocity at the inlet of drillpipe (rev/min)
ω_2	Angular velocity at the outlet of drillpipe (rev/min)
ω_3	Angular velocity at the outlet of HWDP (rev/min)
ω_4	Angular velocity at the outlet of drillcollar (rev/min)

List of Abbreviations

Abbreviation	Meaning
BHA	Bottom Hole Assembly
DLM	Distributed-Lumped Model
DoF	Degree of Freedom
D-OSKIL	Drill Oscillation Killer
FEM	Finite Element Method
FE	Finite Element
GAs	Genetic Algorithms
HWDP	Heavyweight Drillpipe
LM	Lumped Model
LDLM	Lumped-Distributed-Lumped Model
LDDLM	Lumped-Distributed-Distributed-Lumped Model
LDDDLM	Lumped-Distributed-Distributed-Distributed-Lumped Model
MWD	Measurement While Drilling
NWS	Next Well Service
PDC	Polycrystalline-Diamond-Compact
PDE	Partial Differential Equation
PID	Proportional-Integral-Derivative
PI	Proportional-Integral
ROP	Rate of Penetration
RTS	Real-time Service
STRS	Soft Torque Rotary System
SCGA	Species Conserving Genetic Algorithm
WOB	Weight on Bit
XO sub	Crossover Sub

CHAPTER 1: INTRODUCTION

Chapter 1

Introduction

1.1 Well drilling for hydrocarbons

With the development of the petroleum industry for exploration or production of hydrocarbons deep beneath the earth, the problems of drilling are increased and also the cost has become very high (Leonov et al. 2014). The drilling at high depth leads to an increase in the probability of stick-slip vibrations due to the increasing strength of rocks, decreasing stiffness of the drillpipe and poor circulation of the drilling fluid (Brett 1992). Also with the progress of drilling and casing, the well becomes very narrow at a high depth which leads to increased friction between the borehole wall and the drillstring.

The elimination of stick-slip vibrations is a target for drillers and scientists in order to reduce the cost of drilling per metre by reducing the drilling time and improving the drilling performance. In addition, it will increase the quality of the borehole and increase the lifetime of the drilling system. Analysing and understanding the behaviour of the drillstring during stick-slip oscillation can be used effectively to reduce the harmful effect of these vibrations on the drilling system.

The vibrations of the drillstring are the main parameters considered in hydrocarbon drilling, which can maximise or minimise the drilling performance. The stick-slip motion is the main cause of drillstring vibrations (Mason and Sprawls 1998). Optimising and controlling of the surface drilling parameters (e.g. torque and speed) to reduce stick-slip oscillations have become necessary for hydrocarbon drilling.

The stick-slip oscillation of the drillstring is considered to be a self-excited vibration due to the friction between the bit and formation (Dawson et al. 1987; Dareing et al. 1990). A mathematical model of stick-slip including the effect of friction on the drill bit by Kyllingstad and Halsey (1988) was the first attempt to study the dynamics of the drillstring under stick-slip motion by considering the drillstring as a simple torsional pendulum. Based on the concept of Kyllingstad and Halsey many studies have modelled the drillstring as a torsional pendulum with differing degrees of freedom; this will be covered in the following chapters.

There are many solutions available to suppress stick-slip vibrations in drilling systems; one method is by manipulating the different drilling parameters such as: increasing the speed of operation, decreasing the weight on the bit (WOB) and modifying the drilling mud characteristics (Pavone and Desplans 1994).

The angular velocity of the drillstring is one of the surface parameters which can lead to a decrease or increase in the stick-slip vibrations. One of the important velocities during the drilling operation is the critical speed of the drilling system which is defined as the speed over and above which stick-slip does not occur and below which it appears (Dufeyte and Henneuse 1991). Therefore drilling above the critical speed will reduce stick-slip vibrations and the probability of downhole equipment damage. Hence, a predrilling analysis by using modelling and simulation in addition to real analysis of drillstring dynamics is very significant for drilling and the oil and gas industry.

The modelling and control of stick-slip vibrations of the drilling system are considered a challenge for the modeller due to the complexity of the drilling phenomena. Most of the parameters which affect the sensitivity of the model are unknown or insufficiently studied during the process of modelling, which means the model does not have universal acceptability. Laboratory experiments

or historical field data are often used to validate the result of the drillstring model.

1.2 Scope of this research

One of the most serious problems encountered in oil drilling is the occurrence of stick-slip vibrations, which limits both operational efficiency and drilling system lifetime. Hence, the cost of drilling will be increased.

Most of the previous studies for solving the stick-slip vibrations in the oil drilling system model the drillstring as a torsional pendulum with different degrees of freedom, from one degree to several degrees, as will be shown briefly in the next chapters. The main concept of a torsional pendulum is to consider the drillstring as a lumped mass connected by a torsional spring.

In a lumped model (LM), the length of drillstring is not considered during the modelling and the mass of drillpipe is lumped at certain points depending on the number of degrees of freedom. Also in a lumped model, the time for propagation is ignored, which is acceptable when the length is small, but when the drillstring length is very long, the length should be taken into consideration.

Zhu et al. (2015) and Patil et al. (2013) have shown in their literature review of the modelling and control of stick-slip vibration that no researchers have used the concept of the distributed-lumped model (DLM) (also known as a hybrid model) to model and control the drilling system to suppress the stick-slip vibrations. Therefore, this work will use this type of modelling (DLM) to model and simulate the drillstring. Also, as a comparison, the drillstring will be modelled as a torsional pendulum with two degrees of freedom as in the previous studies which means that the effect of the increased length will be ignored and can be compared.

A comparison between the distributed-lumped model and purely lumped model will be made by choosing three different lengths of drillpipe to show the importance of considering the length of drillstring in the modelling, especially in deep well drilling. Also, all the past studies used one parameter to control stick-slip vibration by using a single input, single output (SISO) approach either by controlling the speed of the rotary table and fixing the weight on bit or reversing the process by fixing the speed and changing the weight on bit. In this project, the stick-slip vibration will be suppressed by optimising the drilling parameters (the speed of the rotary table and weight on bit) together by using a species conserving genetic algorithm approach (SCGA).

1.3 Aim

The aim of this research is to develop a new model which hitherto has not been considered for the modelling of oil well drillstring stick-slip vibrations, and has the ability to take the length of drillstring in consideration and can be used for real-time measurement to study the response of different drilling parameters under different drillstring lengths.

1.4 Objectives of the work

The objectives of the thesis can be summarised as follows:

- To undertake a detailed literature review to identify the current state of the art in the field of modelling and suppression of stick-slip vibration of oilwell drillstrings and to identify the gaps in the knowledge pool.
- To develop a mathematical model of a general oil drilling system using a distributed-lumped (hybrid) modelling approach and to solve the resulting matrix of equations to get the system response.

- To study the effect of taking into consideration the length of the heavyweight drillpipe and drill collar when modelling the drillstring instead of neglecting the length as in the previous studies.
- To incorporate a lumped model with two degrees of freedom in order to study the main differences between the two types of modelling (DLM and LM) in reflecting the behaviour of the main drilling parameters such as the speed of rotary table, the speed of bit, the torque at the top of drillstring and the applied torque on the bit in the slip phase and stick-slip phase when drilling at small depths and at comparably deeper depths.
- To make comparisons between the lumped and hybrid models using Matlab software package with the Simulink toolbox in order to show which model is best for describing the dynamic behaviour of a drillstring in the ordinary phase and under the stick-slip motion when the depth of the well changes while the other parameters remain constant.
- To use the species conserving genetic algorithm (SCGA) approach to optimise the rotary torque and weight on bit to prevent the stick-slip vibration and maximise the rate of penetration (ROP) at the desired drilling speed.
- Draw sound conclusions based on the results and analysis which will enable engineers and future researchers to use the new hybrid model to study and analysis the drilling parameters more deeply.

1.5 Contributions

To avoid a drillstring shaft failure, the stick-slip phenomena inherent in the cutting of rock should be mitigated. The input command signals to the drive control systems determine the feed rate of the drilling depth and the cutting speed. To avoid stick-slip and reduce possibility of shaft failure the two input

command signals should be regulated in a coordinated manner. The main contributions of this thesis are summarised as follows:

1- Accurate models of the drillstring for online control and monitoring of the cutting process during the rock cutting operations. The drill string is represented as a distributed-lumped model (DLM) or hybrid model. All the previous studies either considered the drillstring to be a lumped shaft or used finite element modelling to represent the drillstring. The distributed-lumped modelling will result in an accurate representation of the drilling system.

2- All the past studies using distributed-lumped models to model rotary systems ignore any action in the final lumped element, such as cutting torque, and take only the action of mass moment of inertia and use the transfer function and inverse matrix to calculate the response of the system. The inverse matrix method is very complex and tedious especially when more than two distributed elements are used. In this study, the action of the cutting torque is included and the method of getting the output response is very effective and can be used for a large number of distributed elements.

3- Using species conserving genetic algorithms (SCGA) which have not previously been used for the sake of preventing the stick-slip, vibration via optimisation of two parameters. The first parameter is the torque of the rotary table and the second is the weight on bit (WOB). All the past studies have used either passive or active control to suppress the vibration after occurring, however, the results from this study will prevent the stick-slip from occurring by optimising the rotary torque and weight on bit to get the best rate of penetration.

1.6 Structure of the thesis

The structure of this thesis is presented below:

Chapter 1: Introduction

The general background of well drilling for hydrocarbon problems due to increasing the drilling depth is presented. The main causes of vibration are presented. The objectives and contributions of this thesis are outlined.

Chapter 2: Literature review

This chapter presents a literature review about three subjects. First, the main types of rigs and their components are presented by classifying the rig types into offshore and onshore rigs. Also, the main systems inside the conventional oil rig are described to show the role and main parts of every system inside the oil rig. Secondly, torsional, lateral and longitudinal vibrations of the drillstring are explained. The mechanisms of stick-slip are also introduced, and the causes and the effect of stick-slip on the drilling operation are presented. Finally, the previous methods for the modelling and prevention of stick-slip vibration are reviewed.

Chapter 3: Methodology

The Methodology used throughout this thesis is divided into two parts. First, the mathematical model of the drilling system (Lumped model) and the equations of the different parts of the drilling system are introduced in order to model and simulate stick-slip vibration. Secondly, the modelling of drillstrings using a distributed-lumped model (DLM) technique where the length of the drillstring plays a major role in the derivation of the model. For the sake of illustrating the distributed-lumped scheme, the general representation is then applied to a simple torsional system consisting of a shaft carrying a load with inertia and

viscous damping when the shaft is considered as a distributed element and the load as a lumped element.

Chapter 4: Simulation of the drilling system

The simulation methods for the Lumped and Distributed-Lumped (Hybrid) models are introduced. Three types of distributed-lumped model approach are presented, lumped-distributed-lumped model (LDLM), lumped-distributed-distributed-lumped (LDDLM) and lumped-distributed-distributed-distributed-lumped model (LDDDLM) depending on the number of lumped and distributed elements. The parameters of the drilling system are presented, and LDDDLM is validated against real measurement from past studies, also the behaviour of different drilling parameters is demonstrated when there is no stick-slip motion and when stick-slip happens.

Chapter 5: Comparison between Hybrid Models and Lumped Model

In this chapter, the comparison between distributed-lumped (hybrid) models and a purely lumped model are presented. In this comparison, three case studies are used in order to show the difference between the two models when the length of drilling is increased. Also, the interaction effect between the drilling parameters on the value of critical speed is investigated.

Chapter 6: Optimisation

This chapter is devoted to showing the significance in the optimisation of the drilling parameters of an oil drilling system. The principle of genetic algorithms (GAs) is demonstrated together with an explanation of species conserving genetic algorithms (SCGA). Optimisation of the weight on bit and torque of rotary table is carried out with three different lengths of drillpipe.

Chapter 7: Conclusion and recommendation for further work

In this chapter, the conclusions that can be gathered from the comparison between the hybrid models and lumped model and the implement of optimisation are presented. Finally, proposals for further work are suggested.

.

CHAPTER 2: LITERATURE REVIEW

Chapter 2

Literature Review

This chapter gives a literature review focussed upon three subjects. First, the principle of oil well drilling is clarified to give a better understanding of the drilling operation for hydrocarbons. Also, the main systems inside the conventional oil rig are described to show the role and main parts of every system inside the oil rig.

Secondly, the vibration of the drillstring during drilling operations is explained by giving the types of vibrations (torsional, lateral and longitudinal) and the main cause of each type of vibration in order to have clear insight about these types of vibration. Since the research focus in this thesis deals primarily with the modelling of stick-slip vibration, the mechanisms of stick-slip are explained and the causes and the effect of stick-slip on the drilling operation are introduced to show the importance of mitigating this type of vibration on drilling performance.

Finally, existing methods for the modelling and prevention of stick-slip vibration are a reviewed to give a broad picture about the different approaches that are used for the modelling and prevention of stick-slip vibration. The conventional techniques using a torsional pendulum to model the drillstring are given in detail to allow later comparisons with the proposed models and methods that have been developed as part of this research to allow the prevention stick-slip vibration by manipulating the drilling parameters.

2.1 Principle of oil well drilling

Currently, for oil and natural gas exploration and production, wells are drilled by using rotary drilling rigs. These are various in their characteristics such as size, the capability of drilling, the level of automation and environment in which they

can be operated. Despite the considerable variety of rig types, however, all the types have the same basic components with just a few exceptions (Mitchell et al. 2011).

Rigs, in general, can be divided into two main categories dependent on the location of drilling: Onshore (Land rigs) and Offshore (Marine rigs). Figure 2-1 shows the rig classification under these categories (Bourgoyne Jr et al. 1986).

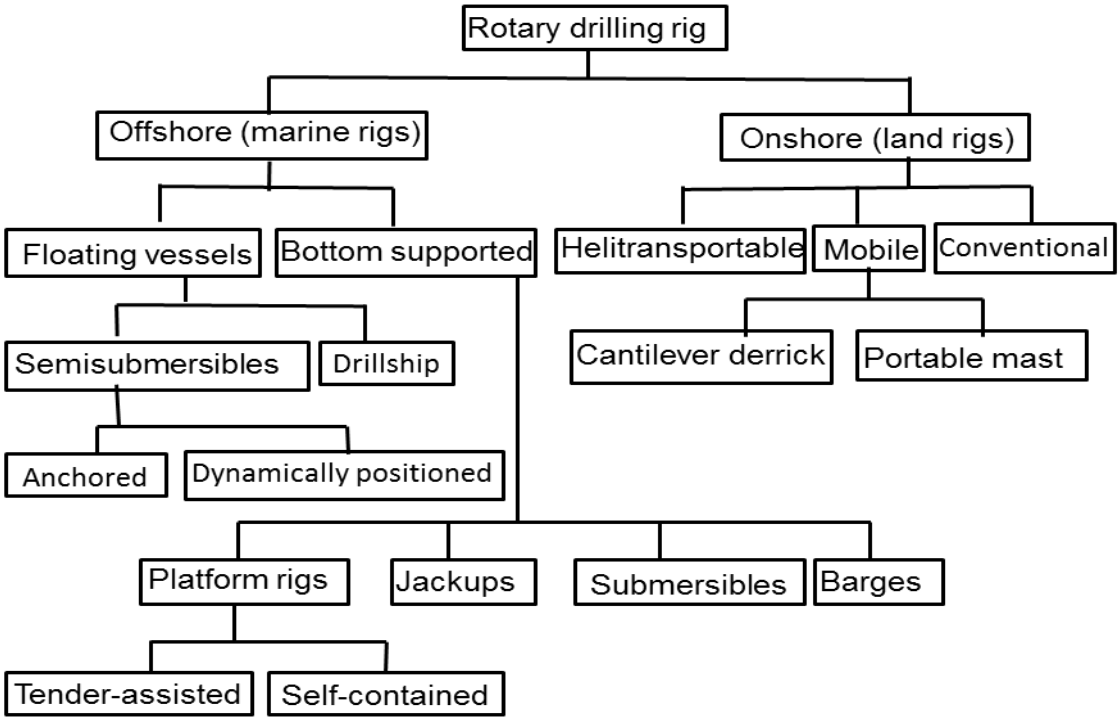

Figure 2-1 Classification of rotary drilling rigs (Bourgoyne Jr et al. 1986)

The production of oil and gas are accomplished by drilling a small borehole in the earth's surface using a cutting device, called the bit, by cutting rock either by chipping or by using a crushing action. The energy required for rock cutting arises from the motor torque which is transmitted to the cutting bit by a long shaft known as the drillstring. The cutting debris from drilling is removed from

the borehole via a fluid circulation system. Mud is pumped into the top of the drillstring and exits through an orifice in the bit. This fluid is returned using the annulus between the drillstring and the borehole wall.

The rig of any of the different types comprises of four main systems, a hoisting system, rotating system, circulating system and monitoring system as shown in Figure 2-2 which depicts a conventional land rig. These systems work together to accomplish the drilling operation. Also, there are other supplementary systems not associated with drilling processes, such as power system, motion compensation system and prevention system (Baker Houghes INTEQ 1996).

In this thesis, the focus will be on the main four systems that have a significant influence on the drilling process.

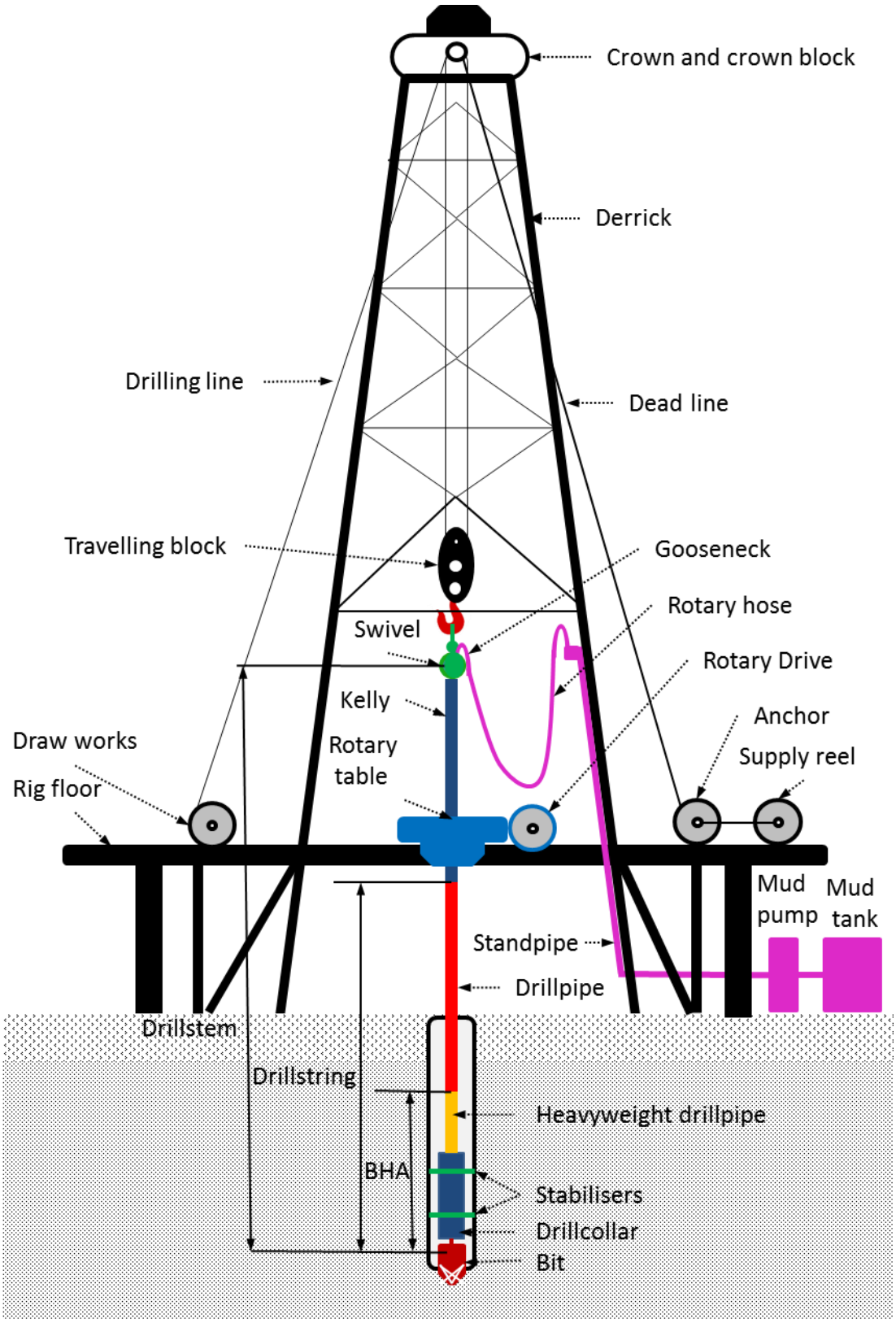

Figure 2-2 Conventional land rig

2.1.1 Hoisting system

The hoisting system is responsible for raising, lowering and suspending the drillstring in and out the well during the drilling operation (Baker Houghes INTEQ 1996). It consists of many parts that are assembled to construct the system as shown in Figure 2-3. For the sake of simplicity and better understanding for the reader, the hoisting system as shown in Figure 2-3 and Figure 2-2 will be divided into parts, and a description of each part and the main function of each one inside the system will be given.

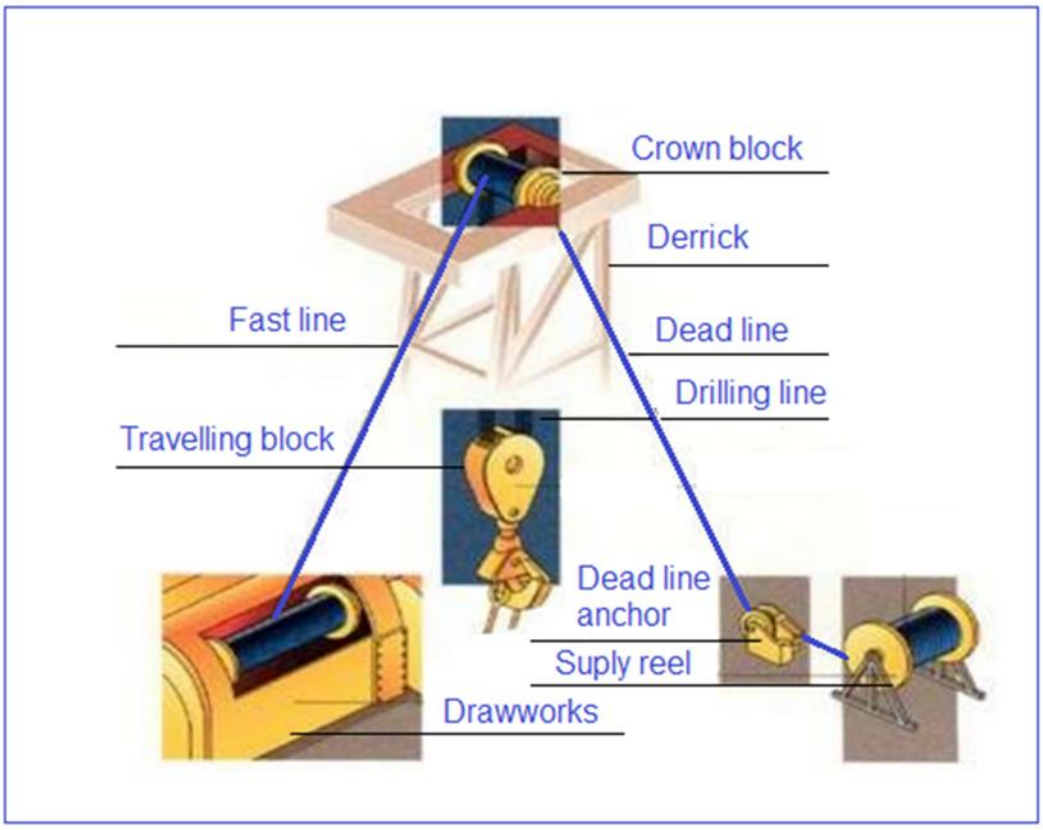

Figure 2-3 Hoisting system (Oil and Gas Portal 2014)

a) The derrick or mast: a steel tower fixed above the well with a length of around 24.4-57m (Mitchell et al. 2011). The main function of the derrick or mast

is to support the travelling and crown blocks as well as storage to keep the drill pipes in a vertical position when they are pulled from the well. A derrick is used in a land rig while a mast is used on an offshore rig. They are classified with respect to the loads they can withstand and the wind load, around 160 to 208km/h (Mitchell et al. 2011). The cross-section of the derrick or mast is square with four legs made of structural steel. They have a steel base called a rig floor located at 3-10m above the ground where most of the drilling activities occur. The space between the rig floor and the ground are very important for the wellhead equipment such as the blowout preventer (Baker Houghes INTEQ 1996).

b) The drilling or hoisting line is a braided steel wire with a diameter around 0.3m and is used for lifting the drillstring (Mitchell et al. 2011). The line made by winding a steel braid wire around a core made from fibre or steel. The types of core, the number of strands around the core and individual wires per strand are used for describing the characteristic of the hoisting line. The drilling line is wound around the reel of the drawworks and goes through the crown block to the travelling block and ends on the supply reel. A dead line anchor is used to keep the dead line fixed. The supply reel is used to replace the drilling line when it wears or is damaged due to any other cause. The hook load sensor is fixed inside dead line anchor in order to calculate the tension in drilling line and then to calculate the weight on bit (WOB) (Baker Houghes INTEQ 1996).

c) The drawworks is a steel frame with a horizontal shaft supporting the reel which is used for winding the drilling line around it. A depth sensor is fixed on the horizontal shaft of the drawworks for calculating the total depth of the well and also the location of the bit while pulling the drillstring. The drilling line is wound and unwound by a motor which drives the drawworks. A brake and hand

lever is used by the driller to control the speed of the drawworks. The reel can rotate in both forward and backwards directions to lower and raise the travelling block and hook (Baker Houghes INTEQ 1996).

d) The crown and travelling block is a fixed block located at the top of the derrick and is used to support the drilling line while the travelling block with hook is moving up and down to raise and lower the drillstring inside the well. The travelling block has a sheave where the drilling line from the fixed crown block comes and returns 4-12 times to carry the travelling block and hook (Mitchell et al. 2011).

2.1.2 Rotating system

The rotating system is used to create a borehole by a rock-crushing tool called a bit. The system consists of all the equipment and devices which are used to rotate the bit. It can be divided into two main parts, the drillstem which is responsible for transmitting the rotational motion to the bit and the prime mover (lower rotating system or top drive rotary system) which generates rotational motion (Mitchell et al. 2011).

The drillstem is the part responsible for transmitting the rotation of the bit. In addition to this function, the drillstem is used to lower and raise the bit in the well, put weight on the bit and as a conduit to transmit the mud under pressure from the surface to the bottom of the well. It consists of three main parts that are arranged in descending order from the top of the rig to the bottom of the well as shown in Figure 2-2.

a) Swivel or power swivel: a large handle suspended from the hook that does not rotate. It supports the kelly and carries the weight of the drillstem and gives the ability to rotate on a bearing inside it. A power swivel is used instead of

swivel in the top drive system when a standpipe replaces the kelly to rotate the drillstring (Mitchell et al. 2011).

b) Kelly: a high-grade molybdenum steel pipe, square or hexagonal on the outside and hollow throughout to allow the drilling mud to pass through it, with length of 40-54 ft (12.2-16.5m) (Mitchell et al. 2011). The kelly is attached to the swivel at the top end and the drillpipe at the bottom. It receives rotating power from the rotary table, a large disc centrally located on the rig floor and transmits this power to the drillstring. The kelly passes through the kelly bushing which contains rollers that allow the kelly to slide up and down as shown in Figure 2-4 when the drilling operations are progressing.

The rotational motion transfers from the rotary table to the master bushing and then to the kelly, through the kelly bushing which fits onto the master bushing in the rotary table in the lower rotary system. A kelly cock safety valve is present at the top of the kelly to prevent mud back pressure damaging the swivel, rotary hose, and other surface devices.

Figure 2-4 Kelly system

c) Drillstring: this term includes all the components used to drill below the kelly or top drive, such as drillpipe and bottom hole assembly (BHA) (drillcollar, heavyweight drillpipe, specialised subs and a rotary bit).

The drillpipe is a heat-treated alloy steel of circular cross-section with an individual length that ranges from 5.5 to 13.7m, but the popular length that is used in most drilling operations is 9m. The outer diameter ranges from 73 to 140mm (Mitchell et al. 2011). Each pipe is screwed with the other to construct the drillpipe.

The bottom hole assembly (BHA) consists of, heavyweight drillpipe (HWDP), drillcollar, specialised subs, and a bit. The HWDP is a pipe with intermediate strength and weight, having the same outer diameter as the drillpipe, but a smaller inner diameter, therefore, its weight is greater than the drillpipe (Mitchell et al. 2011). It is used as a transition section between the drillpipe and drillcollar to reduce the stress between the two and to prevent failure in the area of connection between the two pipes.

The drillcollar is a heat-treated alloy steel similar to the drillpipe with length of 9m but with an outer diameter reaching up to 320mm and small inner diameter. The weight of the drill and collars may reach 1814kg or more (Mitchell et al. 2011). The drillcollar has several functions, such as, put weight on bit (WOB); keep the drillpipe in tension and introduce the pendulum effect in order to help the bit to drill a nearly vertical hole (Baker Houghes INTEQ 1996).

Specialised subs are any short segment of pipe, collars, casing, etc., used for special functions:

- Crossover Sub (XO sub): for connecting between two different pipes in size or type (drillpipe, drillcollar) with different end threads.

- The stabiliser is a short sub with fins that contacts with the well walls as shown in Figure 2-5. In general two stabilisers are located between the drillcollar to keep the drillcollar in the centre of the well.
- Shock Sub: The impact of the bit bouncing on hard formation is reduced by using a shock sub as a steel or rubber packing behind the bit.
- Bit Sub: The connection between the bit and drillcollar is made using a bit sub which has a box with internal threads at both ends in order to connect with the pin of bit and drillcollar.

Figure 2-5 Stabiliser (Mitchell et al. 2011)

The bit is the final part of the drillstring and is used for crushing the rock. It is designed in different shapes and made from a different material appropriate to the rock formation to be drilled. There are three main types of the bit; roller-cone, fixed-cutter and hybrid bits as shown in Figure 2-6. Each type can be classified into other categories, but the most common bit is the rotary cone bit with three rotating cones (Mitchell et al. 2011).

The lower rotating system is located on the rig floor; it uses the rotary table, master bushing, and kelly bushing to transmit the rotation to the drillstring. While the top drive rotary system is a hydraulic or electrical motor used to rotate the drillstring. It is located at the head of the rig, suspended in the derrick, and

moves up and down with the drillstring. In this system, the kelly and kelly bushing are not required (Mitchell et al. 2011).

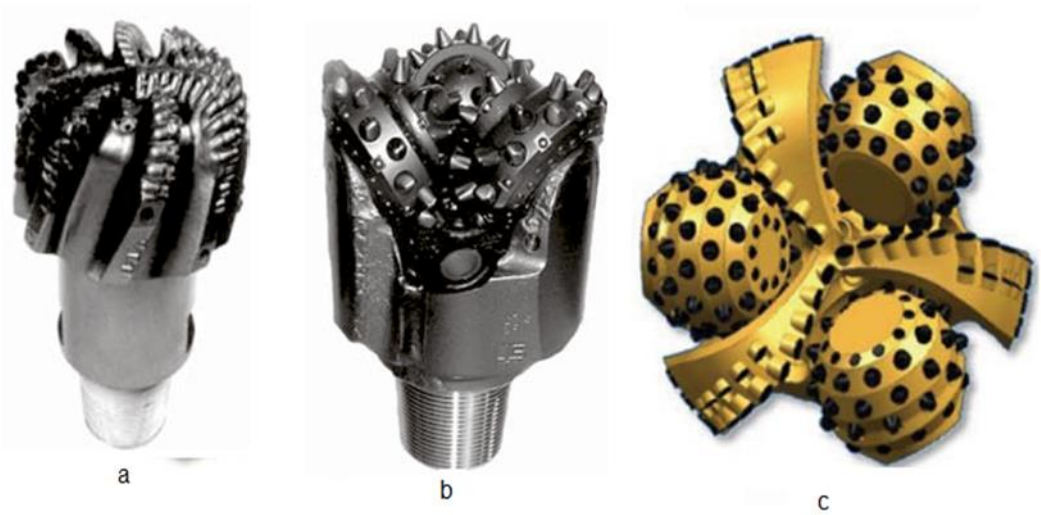

Figure 2-6 Types of bits, a) Fixed-Cutter, b) Roller-Cone c) Hybrid (Mitchell et al. 2011)

2.1.3 Circulating system

The circulating system is used to circulate the drilling mud (mixture of water, clay, weighting material and chemicals, used to lift cutting formation from the drill bit to the surface) from a mud tank at the surface through the rotating drillstem to the bit and return it to the surface in the space (annulus) between the drillstring and well walls as shown in Figure 2-7. Duplex and triplex pumps usually are used on drilling rigs to circulate the drilling mud under pressure from the mud tank to the bit (Mitchell et al. 2011). The mud goes from the pump through a long rubber tube to the standpipe which is firmly fixed to the derrick and connected to a rotary hose and then to a gooseneck on the swivel. The return mud from the well passes through shale shaker in order to separate the coarse rock cuttings and is then collected in the mud pits while the rock cuttings go to the reserve pit. The mud in the mud pits is mixed with new mud coming from the mud mixing hopper to reuse again (Mitchell et al. 2011).

Two types of fluid pressure are present at the bottom of the well, the hydrostatic pressure of the mud due to its weight and the formation pressure of the fluid in the rocks. When the hydrostatic pressure is greater than formation pressure in the rocks, it will prevent the fluid in the rock rushing inside the well. If the formation pressure is higher than the hydrostatic pressure, this will lead to fluid flow inside the well and cause the side of the well to be damaged. Therefore, it is important to ensure that the hydrostatic pressure is higher than the formation pressure. The hydrostatic pressure should be maintained within a specific tolerance since if it is very high this will lead to a rush of drilling mud into the rock and cause wastage of drilling fluid (Baker Houghes INTEQ 1996).

The circulating drilling mud is used for many purposes in the drilling operation (Cherutich 2009):

- Remove cuttings from the bit face at the bottom of the hole to allow drilling process to progress.
- Clean the well of cuttings and return to the surface for reuse again (circulating condition).
- Suspend the cuttings suspension in the drilling fluid when the drilling operation stops.
- Remove cuttings from the drilling fluid at the surface.
- Cool, and lubricate the bit.
- Lubricate the drillstring.
- Cool the well and keep the temperature of the liquid in the well below boiling point.

- Prevent the well from a blowout by controlling the pressure downhole. Control the downhole pressure, preventing the well from flowing.
- Increase the drilling fluid density by carrying a weighted material to increase the hydrostatic pressure to prevent flow and the possibility of a blowout.
- Provide a transmit medium for measurement while drilling (MWD) by using pressure pulses through the drilling fluid mud.

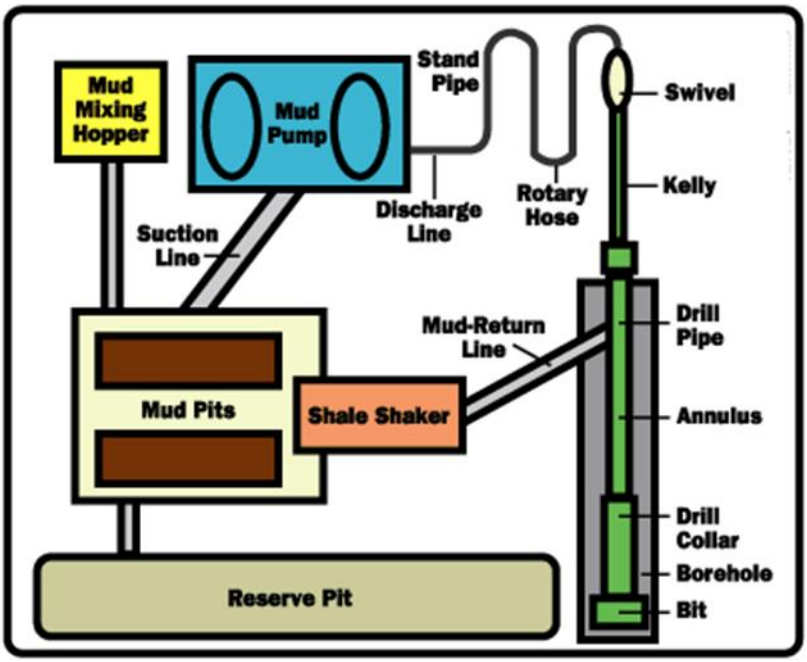

Figure 2-7 Drill-mud circulation system (Rich Mineral Corporation 2007)

2.1.4 Control and monitoring system

To accomplish successful drilling without delay or waste of time and money, requires close control of a number of drilling parameters. The rig personnel (e.g. driller, drilling supervisor, drilling and mud engineer) must continuously monitor the development in the drilling operation so as to make necessary adjustments and to identify quickly and correct drilling problems (Baker Houghes INTEQ

1996). The parameters related to the drilling operation which can be measured automatically in the modern rig are continuously recorded and displayed on devices at the control unit. While the parameters such as mud properties which cannot be measured continuously or automatically will be measured and recorded at specific intervals.

The parameters which play an imperative role in drilling operation which require monitoring and control can be summarised as follows (Mitchell et al. 2011).

- Well depth
- Weight on bit (WOB)
- Rotary speed
- Rotary torque
- Pump pressure
- Pump rate
- Fluid- flow rate
- Flow return
- Rate of penetration
- Hook load
- Fluid properties (e.g., density, temperature, viscosity, gas and sand content, salinity, solids content)
- Bit level

The driller can predict and identify possible drilling problems when these parameters are monitored continuously along with a reliable historical record of previous similar operations.

2.2 Drillstring Vibrations

For oil and gas exploration, drillstring vibrations are considered to be the leading cause of loss performance in the drilling process, premature wear of drill bit, tear of drilling equipment due to fatigue and induce failures such as pipe wash-out and twist-off (Mason and Sprawls 1998). A significant wasting of drilling energy (Macpherson et al. 1993) and induce borehole instabilities reducing the directional control (Dunayevsky et al. 1993) considered another cause of these vibrations.

In the hydrocarbon industry, the process of drilling an oil well can reach tens of millions of dollars (Macdonald and Bjune 2007). This figure can be increased by 2% to 10% due to unwanted vibrations (Jardine et al. 1994) therefore, the improvement of drilling performance has an economic interest.

Many studies have been conducted to identify drillstring vibrations during the drilling operation. These have led to the identification and classification of vibrations, dependent upon their direction, into three primary modes: torsional (stick-slip); longitudinal (bit bouncing); and lateral (whirling) modes (Christoforou and Yigit 2003; Kovalyshen 2013). These vibrations occur due to the cutting of rock by the bit and the contact between the drillstring (drillpipe, drillcollar, and stabilisers) and the wall of the wellbore. Also, bent or misaligned drillstrings are considered as other causes of drillstring vibrations (Khulief et al. 2007).

The change of axial force from tension to compression along the drillstring, the coupling nature of bit–rock interaction, high static driving torque and the curvature of the drillstring are major causes of the coupling of vibration modes of the drillstring. These vibrations represent an extreme example of coupling and are very complex in nature and can occur simultaneously due to the aforementioned causes (Ghasemloonia et al. 2015).

The high amount of energy stored in the drillstring during the stick-slip phenomena can lead to longitudinal and lateral vibrations when the energy is finally released, resulting in a decrease in the efficiency of drilling (Christoforou and Yigit 2003). Also, when the velocity of the rotary table increases above a threshold value, this leads to eliminating the stick-slip vibration, however, this high-velocity can cause lateral problems such as backwards and forward whirling (Yigit and Christoforou 1998). Therefore, the desired velocity of drilling should be chosen carefully to overcome this issue.

These vibrations (lateral, longitudinal and torsional) frequently manifest themselves in multiple modes and are considered an important cause of deteriorated drillstring performance and can lead to premature failure of bits, motors and other drillstring components (Sassan and Halimberdi 2013).

At lower speed, the stick-slip vibration is considered to be the main reason for torsional vibrations and most damage compared with the other two types of vibrations (Mensa-Wilmot et al. 2000; Abdulgalil and Siguerdidjane 2005; Khulief et al. 2005). Stick-slip vibration is a familiar phenomenon in many engineering systems, not solely limited to oil drilling operations. For example, brake systems (Crowther and Singh 2007), manufacturing systems (Tarng and Cheng 1995), vehicle systems (Sun and Simson 2008) and earthquake triggers (Johnson et al. 2008) can all experience stick-slip vibrations. This type of oscillation, known as limit-cycling, can occur due to hysteresis, backlash between contacting parts, dry friction between sliding parts, nonlinear damping, and geometrical imperfections (Dubinsky and Baecker 1998).

Since the work in this thesis is related to torsional vibrations, or more precisely to the stick-slip phenomenon, the focus of the following literature review will be

only on this area. Before going further in the discussion of this phenomenon, stick-slip needs to be defined, categorised and clearly explained.

2.2.1 Longitudinal or axial vibrations (bit bouncing phenomenon)

Longitudinal vibration is the bouncing of the drilling bit on the rock during the cutting operation due to the interactions between the bits and the hole bottom. This vibration can cause many problems during the drilling operation such as fluctuations of the weight on bit (WOB), irregular rate of penetration(ROP), damage to the surface equipment at shallow depths due to shake, damage to the tool face, increases in total drilling time and poor directional control (Mongkolcheep 2009; Saldivar et al. 2014a).

This pattern of vibration is associated with a roller-cone bit, also called tricone or rock bit, which leads to bit bounce and a loss of contact between the bit and formation, detected by the driller at the surface as bouncing motion or axial vibration.

Coupling between axial and vibrations in other directions have been studied by many researchers; for example, Saldivart et al. (2013) presented a comprehensive analysis of the modelling and control of coupling between axial and torsional vibrations which occur in a vertical oilwell drilling system. A distributed parameter model was used to reproduce the mutual coupling between the two modes of vibrations. The results of the simulation showed that increasing the rotational speed of the rotary table led to a reduction of the stick-slip vibration but at the same time high rotational speeds caused lateral instabilities resulting in whirl motion. Also, the results showed that suppressing the stick-slip vibration led to an elimination of the bit bouncing due to the coupling between torsional and axial vibrations.

Saldivart et al. (2014b) used two wave equations with nonlinear coupled boundary conditions, one for torsional vibration and the other for axial vibration, to model the coupling between the two types of vibrations. The rotary torque and weight on bit were used as a controller variable to control torsional and axial vibrations using a flatness-based control approach.

Zamanian et al.(2007) studied the coupling between axial and torsional vibrations by using a discrete model with three degrees of freedom; two for torsional vibration and one for axial vibration. This study showed that bit-rock interaction leads to a coupling between axial and torsional vibration and the results from the simulation showed that an increase in the damping of the drilling mud would decrease the stick-slip vibration.

Richard et al. (2007) presented a discrete model with two degrees of freedom; one for torsion and the other for an axial motion to study the self-excited stick-slip vibration of the drillstring by considering the coupling between axial and torsional vibrations. The coupling between the two modes of vibration takes place due to the bit-rock interaction. The study showed that a delay caused by the tooth-rock interaction and rotational speed of the bit was responsible for the existence of self-excited vibrations which were transformed into torsional or axial vibrations under certain conditions.

Kamel and Yigit (2014) presented a study of coupled axial and torsional vibrations by using a lumped model with two degrees of freedom for torsion and two degrees of freedom for axial vibration. This study confirmed that the coupling between axial and torsional vibration was attributed to the bit-rock interaction, and also confirmed that the stick-slip vibration can be eliminated by increasing the rotary speed above a threshold value. The drilling efficiency was

found to increase with an increase in the rotary speed and then decrease when the velocity reached a threshold value.

2.2.2 Lateral vibrations (whirl motion)

Lateral vibrations occur when the drillstring moves laterally from its axis of rotation due to interactions between the bits and the rock formation, the pipe eccentricity, bit whirl, and from fluid forces around the drillstring (Brett 1992; Mongkolcheep 2009; Fubin et al. 2010). These vibrations are classified into two types: forward and backwards whirls. Forwards whirl occurs when the axis of the bit rotates in the same direction as the rotation of bit, whilst backwards whirl takes place when the axis of the bit rotates in the opposite direction to the rotation of the bit.

Whirl vibration is common with polycrystalline-diamond-compact (PDC) bits especially when drilling with high velocity and low WOB, and it is considered responsible for the premature damage of the bit (Brett 1992). Imbalance of the bottom hole assembly(BHA) is considered to be the leading cause of whirl instability, and most of the published models are based on this assumption (Kovalyshen 2013). This imbalance is attributed either to mass imbalance (Dykstra et al. 2001) or cutting structure imbalance (Abbassian and Dunayevsky 1998). Also, there are other factors that can lead to an increase in whirl vibration such as the bit-rock interaction (Johnson 2008), bit vibration (Brett 1992) and bit geometry (Kovalyshen 2013).

Lateral vibrations have been studied by many modellers, whilst in some of the earliest work from Yigit and Christoforou (1998) the authors studied the coupling between torsional and bending vibrations of the drillstring using a lumped parameter model. The simulation results, combined with laboratory and field

observations, showed that control of the rotary torque could be used to eliminate stick-slip vibrations and reduce the lateral vibration. In other work, (Yigit and Christoforou 2000) the authors added the interactions between the drillstring and the wellbore to the coupling between the torsional and bending vibrations and this interaction was found to cause more significant interaction between lateral and torsional motions.

Al-Hiddabi et al. (2003) used a nonlinear dynamic inversion control design approach to suppress the coupled torsional and lateral vibrations of a non-linear drillstring. The study showed that suppressing the torsional vibration led to a significant reduction of the lateral vibration.

Leine and Van Campen (2005) used a simple model with three degrees of freedom; 1DOF for torsional vibration and 2DOF for lateral vibration to study the coupling between the two modes of vibration. The study showed that there was an interaction between the stick-slip and whirl vibrations in an oilwell drilling system and this interaction was attributed to the hydrodynamic fluid forces.

A discrete model with eight degrees of freedom was developed by Liu et al. (2013b) to study the coupled axial, torsion, and lateral dynamics of a drillstring by taking into consideration both the stick-slip oscillation and time delay associated with both the axial and lateral cutting process. The results showed that the stick-slip oscillation and delay time due to cutting action led to the emergence of self-excited motion.

2.2.3 Stick-slip vibrations

Duff (2013) defined the stick-slip in oil drilling operation as ‘The cyclic reduction and corresponding increase of instantaneous rotation speed.’ This vibration occurs due to the nonlinear interaction between bit/formation and

drillstring/borehole (Leine and Van Campen 2005), which leads to the BHA sticking for a finite time interval and then slipping. It should be noted that this definition differs from the classical definition of stick-slip of tribological systems where the stick-slip is related to the generation (stick) and breaking (slip) of adhesive bonds. During the 'slip' phase, the angular velocity of the BHA can exceed the imposed velocity by two to three times as shown in Figure 2-8 (Kriesels et al. 1999.). This vibration can continue for several minutes (Sassan and Halimberdi 2013).

The period of stick-slip oscillation depends on many factors such as the length of the drillpipe, rotary speed, nature and location of the friction. It is possible for the stick-slip to appear in up to 50% of the drilling time (Brett 1992; Jardine et al. 1994; Christoforou and Yigit 2001).

The main parameters of drilling such as weight on bit(WOB), rotary torque and rotary speed range from 0 to 3000kN, 0.5 to 70kN and 50 to 200 rev/min respectively (Macdonald and Bjune 2007). However, during the drilling operation the desired speed of drilling is typically in the range of 120 to 125rev/min in the ordinary mode when there is no stick-slip (slip phase) and 50 rev/min when stick-slip occurs (Kriesels et al. 1999.). It has been observed by several authors that the stick-slip vibration occurs mostly with low angular velocity and a significant weight (when compared to the type of rock formation) on the bit (Brett 1992; Yigit and Christoforou 2000; Abdulgalil and Siguerdidjane 2005). Another cause can be attributed to the high difference between the static and dynamic friction which leads to a transfer of the stored energy in the drillpipe to inertial energy in the BHA, subsequently increasing the rotational speed of the BHA (Brett 1992). Some researchers have attributed the stick-slip vibration to the mechanical structure of the bit and type of bit as stick-slip is

more common with polycrystalline diamond compact (PDC) bits (Brett 1992). However, other authors refer to the size of the bit since an increase the size this leads to an increase in the reactive torque on the bit (Jain et al. 2011).

Besides the associations with the drill bit, other factors such as the condition and tortuosity of the wellbore, the type of formation and the lubricity of the drilling fluid have a significant impact on the occurrence of stick-slip (Sassan and Halimberdi 2013).

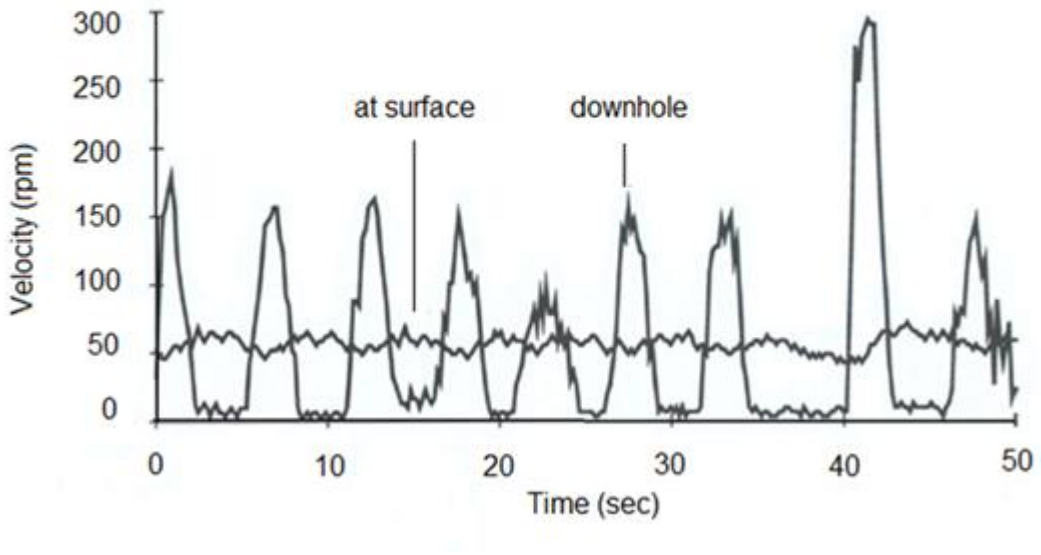

Figure 2-8 Example of stick-slip oscillation of a drillstring (Kriesels et al. 1999.)

The stick-slip mechanism can be explained as follows: the bit may become trapped due to many factors such as formation characteristics, significant drag torque or tight bit/hole clearance which leads to the BHA becoming stationary whilst the rotary table continues to rotate. This leads to wind-up of the shaft (similar to a wound-up torsional spring) and an increase in the torsional energy trapped in the drillstring causing an increase in the applied torque. When this torque overcomes the frictional force at the bit/rock interface (static friction), suddenly the bit will start to rotate at a high speed, this high speed leads to the

generation of a torsional wave which travels up to the rotary table before being reflected back to the bottom hole assembly (Macdonald and Bjune 2007; Saldivar et al. 2011). The process may repeat many times until the stick-slip decays. Hence, this oscillatory motion is similar to classical stick-slip motion in tribological systems where the build-up and release of energy generates the stick-slip motion.

Stick-slip vibration is undesirable in the oil drilling process due to many reasons which can be summarised as follows:

1- Reduction in the rate of penetration (ROP) of the drilling operation due to the lateral and longitudinal vibrations in the slip phase (Halsey et al. 1988; Sassan and Halimberdi 2013; Liu 2015).
2- Increase in the cost of drilling due to a decrease in the ROP and increase in the drilling duration (Jardine et al. 1994; Dubinsky and Baecker 1998; Kriesels et al. 1999.; Guerrero and Kuli 2007; Sassan and Halimberdi 2013; Zhu et al. 2015).
3- Affecting the borehole quality resulting in lateral vibration (backwards and forward whirling) (Zhu et al. 2015).
4- Fatigue problems in the drillpipe due to the large cyclic stresses which lead to an increase in tool failures (Kriesels et al. 1999.; Christoforou and Yigit 2001).
5- Failures of the components of the BHA (measurement while drilling (MWD) sensors, and motors) due to severe lateral vibration in the slip phase (Kriesels et al. 1999.).
6- Instability of the wellbore structure which may lead to collapse (Placido et al. 2002; Paic et al. 2007)

7- Severe axial and lateral vibrations in the bottom hole assembly due to the high speed in the sliding phase. These vibrations lead to excessive bit wear (Henneuse 1992; Warren and Oster 1998; Macpherson et al. 2001; Besselink et al. 2011).
8- Decrease in the accuracy of measurement while drilling (MWD) as a result of noise due to the vibrations; this could lead to inaccurate measurement of sensitive parameters (velocity and torque on bit signals) (Bailey et al. 2008).
9- Decrease the drilling efficiency (Besselink et al. 2011).

Therefore, due to these problems, the understanding of the stick-slip mechanism, the causes, and the methods that are used to suppress it is a very significant field of research in the oil drilling industry to improve overall performance.

2.3 Modelling methods for stick-slip vibrations

The modelling of the drillstring is significant for many reasons, such as:

- To be able to analyse the drillstring vibration pattern either in the frequency domain or time domain.
- To predict the effect of adjusting surface parameters (rotary speed, rotary torque, and weight on the bit) on the generated vibrations.
- To visualise the complete drilling operation, cutting process under different types of formation.
- To study the system stability, to develop and test different methods of damping to damp the vibration.
- To control the vibration by using different control strategies, etc.

The stick-slip oscillations of the drillstring are attributed to the nonlinear interaction between the bit and the rock formation, and these oscillations are regarded as self-excited vibrations (Richard et al. 2004; Gulyaev et al. 2009). The drillstring vibrations have been studied by using experimental and numerical approaches, however, there are two basic methods for modelling the dynamic phenomena of the drillstring: lumped modelling of a torsional pendulum, and distributed parameter models.

2.3.1 Torsional pendulum model

A torsional pendulum approach is the most widely used method to model the drillstring. This method considers the drillstring to consist of a lumped mass, torsional spring, and damper to keep the model simple for quick analysis when compared with other methods (Rudat and Dashevskiy 2011). However, this approach has two limitations. First the effect of the increasing length of the drillstring with the progress of drilling is not modelled; secondly, the vibrations along the drillstring are not modelled (Kapitaniak et al. 2015).

All of the previously mentioned authors have used the same concept of a torsional pendulum with the primary difference being in the number of degrees of freedom (DoF), whilst the damping along the drillstring is sometimes neglected because it is small when compared with damping in the BHA and drive system.

The first model of this type was by Halsey et al.(1988) who introduced the torsional pendulum by treating the drillstring as a torsional pendulum with one degree of freedom (1DoF). Despite this model being simple, it was possible to study the stick-slip vibration and has been used to suppress stick-slip

oscillations (Mensa-Wilmot et al. 2000). After that, many modellers used the same model (1DoF) to study the stick-slip.

Kyllingstad and Halsey (1988) studied the torsional oscillations caused by the stick-slip motion of the drillcollar section by using a torsional pendulum with one degree of freedom (1DoF). The authors assumed in their analysis that the stick-slip motion would occur with the given parameters. They proposed that the stick-slip vibration could be reduced or even eliminated by accurate control of the rotary-table speed or by reducing the downhole friction.

Lin and Wang(1991) used a torsional pendulum with one degree of freedom to study the effect of viscous damping, rotary speed and natural frequency on the stick-slip vibration. The study showed that stick-slip would not occur when the length of the drillstring was shorter than the critical length, which was defined as a function of rotary speed, dry friction and viscous damping.

Rudat and Dashevskiy (2011) used a drillstring model with one degree of freedom to monitor stick-slip oscillations in order to apply a model based stick-slip control system. This approach was based on running a model in parallel with an actual drilling system with a view to identifying the appropriate surface drilling parameters (rotary speed and WOB) which would prevent stick-slip vibration.

After Halsey et al. (1988), many modellers used a lumped model with two degrees of freedom to model the stick-slip vibrations. For example: (Javanmardi and Gaspard 1992a; Javanmardi and Gaspard 1992b; Sananikone et al. 1992; Jansen et al. 1994; Jansen et al. 1995; Yigit et al. 1996; Serrarens et al. 1998; Navarro-Lopez and Suarez 2004) all used similar 2-DoF models to apply different control strategies to the stick-slip problem. The various authors

considered the system to consist of a drive part (motor, gearbox, and turntable) connected to the BHA by a torsional spring and viscous damper. However, as previously mentioned, the damper was sometimes neglected because it was considered to be very small when compared to the damping in the BHA (Jansen and van den Steen 1995; Jansen et al. 1995; Serrarens et al. 1998). The authors demonstrated that this model was accurate to some extent in describing the stick-slip vibrations and could be used for a control analysis (Serrarens et al. 1998). However, the disadvantage of this model was that an increase in the length of the drillpipe led to a decrease in the accuracy of modelling due to the inability to represent the delay time. This is considered one of the primary factors of stick-slip vibration and in some cases delay time will be significant with an increase in the drillpipe length.

Navarro-Lopez (2009) proposed a model of three degrees of freedom by considering the drillstring to consist of three elements: top rotary system, drillpipe and BHA connected by a linear torsional spring. This method was to some extent, better than the 2DoF models due to increasing the number of degrees of freedom, but it did not solve the problem of modelling the delay time, which can be considered to be another important cause of self-excited vibrations in drill bits (Liu et al. 2013a).

Navarro-Lopez and Cortes (2007b) carried out work aimed at the mitigation of stick-slip vibrations by using dynamical sliding-mode control combined with a 4DoF lumped parameter torsional drillstring model. The study showed the ability of the controller to eliminate the stick-slip vibrations, and the desired dynamics were achieved, however, their effect on the bit-bouncing and whirl phenomenon were not analysed.

In the 4DoF models, the drillstring consists of four elements: top rotary system, drillpipe, drillcollar and bit connected by a linear torsional spring. This approach is very similar to three degrees of freedom models with the only difference being that the bit is separated from the drillcollar and is not a single lumped mass. By comparing the mass of the drill bit to that of the drillcollar, there is not a significant difference between the three and four degrees of freedom models.

After four degrees of freedom, the division of drillpipe and drillcollar can be increased to get a multi-dimensional lumped parameter model. Navarro-Lopez and Cortes (2007a) introduced a generic lumped-parameter model with n degrees of freedom. They used a model with six and eight degrees of freedom to study the self-excited bit stick-slip oscillations and bit sticking phenomena at the BHA. Increasing the number of degrees of freedom may be more realistic to describe the stick-slip vibration, but becomes computationally expensive and does not necessarily provide clear insight into the effect of parameters on system behaviour.

2.3.2 Distributed parameter model

The oscillation of a physical system can be reproduced by using the wave equation. Bailey and Finnie (1960) and Finnie and Bailey (1960) were one of the earliest researchers to develop dynamic models using the classical wave equation to describe the stick-slip oscillation behaviour of a drillstring supported by experimental validation.

The general wave equation which is used to describe a drillstring of length L_{ds}, subjected to a purely torsional excitations can be written as (Challamel 2000; Boussaada et al. 2012):

$$G_* J \frac{\partial^2 \theta}{\partial^2 x}(x,t) - b' \frac{\partial \theta}{\partial t}(x,t) - J'_m \frac{\partial^2 \theta}{\partial^2 t}(x,t) = 0 \qquad 2.1$$

Where θ is the drillstring twist angle which depends on the drillstring length and time(x,t). The parameters G_*, J, b' and J'_m are the shear modulus, the geometrical moment of inertia, damping and inertia mass moment respectively.

The boundary condition, which is used to solve the general wave equation of a drillstring (equation 2.1), depends on the dynamics of the drillstring at the upper and lower parts. Challamel (2000) used the following boundary condition to solve equation 2.1.

$$\theta(0,t) = \omega t \qquad 2.2$$

$$G_* J \frac{\partial \theta}{\partial x}(l,t) + J_{bh} \frac{\partial^2 \theta}{\partial^2 t}(l,t) = -T\left(\frac{\partial \theta}{\partial t}(l,t)\right) \qquad 2.3$$

The boundary equations in equation 2.2 and 2.3 assume that the speed at the top of the drillstring is restricted to a constant value ω which represents the speed of the motor, while the bottom of the drillstring is represented by a lumped inertia, J_{bh}, of the BHA and the bit subjected to torque T which is a function of speed at $x = l$ (total drillstring length). These boundary conditions constrain the dynamic behaviour at the BHA, however the velocity of the motor the does not match the rotational speed at the top of drillstring $\frac{\partial \theta}{\partial t}(l,t)$ and this slight difference results in the local torsion at the top of the drillstring. In order to overcome this limitation Saldivar et al. (2011) and Saldivar and Mondié (2013) presented the following boundary condition:

$$G_* J \frac{\partial \theta}{\partial x}(0,t) = -b'\left(\frac{\partial \theta}{\partial t}(0,t) - \omega\right) \qquad 2.4$$

The analysis and simulations of a distributed parameter model are very complex tasks especially when it subjected to nonlinearities and uncertainties. To solve this problem, the distributed model was simplified by ignoring the minor parameters and involving only the main parameters that have a large impact on

the dynamic behaviour. A neutral-type time delay equation was used to simplify the distributed model by transforming the partial differential equation of the model to that of a delay system of a neutral type.

This is a suitable method to simplify the model of the drillstring, by ignoring the damping along the drillstring, because most of the energy dissipation in drilling systems takes place at the bit-rock interaction (Saldivar et al. 2011; Boussaada et al. 2012; Boussaada et al. 2013). The distributed parameter model of the drillstring (equation 2.1) can be reduced to the unidimensional wave equation (Saldivar et al. 2011).

$$\frac{\partial^2\theta}{\partial^2 x}(x,t) = p^2 \frac{\partial^2\theta}{\partial^2 t}(x,t) \qquad 2.5$$

Where p is a constant and $= \sqrt{\frac{J'_m}{G_* J}}$.

The modelling of stick-slip oscillation using a lumped approach based on the assumption that the mass, damping and stiffness of the system can be represented at a certain discrete points, results in a model that is fast and efficient for analysis and can be used for control when compared with finite element method (FEM). However, in real systems, these parameters are distributed, and therefore most accurate way to determine the nature and the magnitude of influence of these parameters on the system behaviour is by representing them as a distributed.

Therefore, Finite Element Methods (FEM) focussed on the distributed approach, have been used to study the drillstring vibration by considering the main parameters of system (mass, inertia, and damping) to be distributed along the drillstring. Millheim et al.(1978) is one of the earliest published articles in which FEM is applied to model the dynamics of the bottom hole assembly.

Apostal et al.(1990) used FEM to investigate the harmonic response of the bottom hole assembly (BHA). Included in this study were the effects of damping due to mud viscosity and structural damping along the BHA. However, the damping along the drillpipe was neglected which is considered a significant factor when the length of drillsring is increased.

Khulief and Al-Naser (2005) used a Lagrangian approach to formulating the FE model to describe a rotating vertical drillstring that included drillpipe and drillcollar. The coupling between torsional and bending vibrations, gyroscopic effect and axial stiffness were considered in this study. This model was able to predict the more simplistic response of the drilling operation, but cannot predict correctly the dynamical response of a real system due to the fact that the model is too simple compared to a real system and uncertainties are not taken into account.

Khulief and Al-Sulaiman(2007) calculated the time-response of the drillstring system in the presence of stick-slip excitations by developing a dynamic model of the drillstring which included the drillpipe and drillcollar and used the Lagrangian approach in conjunction with the finite element method to derive the governing equations of motion. Whilst the model accounted for the stick-slip interaction forces the hydrodynamic damping due to the presence of drilling mud are were not modelled or investigated which was a limitation of the study.

Models built using the finite element method are computationally expensive and inefficient when compared to lumped parameter models. Whilst they do provide additional detail or fidelity, it is with both great computational and time expense and it can be seen that the models are not compatible with real-time measurement and control.

2.4 Stick-slip prevention methods

The problems of torsional vibration increase with increasing drilling depths due to the increasing in the hardness of the rocks and decrease in the stiffness of the drillpipe (Kyllingstad and Halsey 1988; Brett 1992). These vibrations lead to a reduction in the rate of penetration and subsequent increase in the price of oil production. Therefore, the solution for suppression and control becomes a very significant topic for both academics and industrialists.

The act of drilling for oil is considered to be a costly and risky activity (Richard 2001). Therefore, drilling techniques have been rapidly developed to decrease the cost and increase the efficiency of drilling. During drilling vibration is considered to the leading cause of failure and increase the cost of drilling, especially stick-slip vibration (Patil and Teodoriu 2013b). Therefore, active researchers in the area have performed numerous studies in the laboratory and in the field to solve the problem of stick-slip oscillation by developing the equipment used in the drilling operation or by controlling the parameters of drilling (Halsey et al. 1988; Jansen and van den Steen 1995).

The common strategies that have been used for suppressing the stick-slip oscillation are passive and active vibration control methods. The passive control schemes focus on the study of drillstring dynamic behaviour under different conditions and the analysis of the dynamics to optimise the BHA with regards to the type of bit that is appropriate to the rock formation, redesign of the bit and criteria for use of the downhole equipment; whilst active control deals with the optimisation of the drilling parameters based on real-time measurement.

2.4.1 Active stick-slip suppression approaches

The active control approach can be used effectively to suppress the drillstring vibrations when real-time details are provided. The active control approach can be classified into two types: use of active control systems and drilling parameter optimisation based on real-time measurements.

Many researchers have used active control, for example, torque feedback by Hasley (1988) by modifying the drive's characteristics. The results showed that the system is able to mitigate the stick slip vibration and even prevent it from beginning. However, it does have drawbacks because the measurement of torque at the rotary table is inconvenient during actual drilling operations and the expensive sensors can be prone to failure due to vibration and shock loads.

Soft torque rotary system (STRS) by Javanmard and Gasapard (1992a; 1992b) modified the torque feedback system of Hasley by eliminating the sensor for torque measurement at the rig floor by using the current and voltage of the rotary drive motor to directly measure the torque and speed of the drillstring by reducing the accumulated energy by reflecting the torsional waves. These systems still cannot provide immediate reaction due to the delay time between stick slip beginning at the bit and the response being detrected at the drive system.

Jansen and Van den Steen (1995) used an active damping system to reduce the critical angular velocity threshold value of the drillstring. The active damping approach is one of the effective solutions that is currently in use to mitigate the stick-slip oscillations. The principle of active damping is based on making the rotary table behave as a soft rotary table rather than stiff; its speed is permitted to vary inversely with the change of torque on the drillstring: decrease with increasing torque and increase with decreasing torque with the use of a

feedback circuit. The active damping system acts as a tuned vibration damper to mitigate stick-slip vibration. The drawback of this system is that the rig needs to be modified to run the feedback control system by completely changing the drive system.

In other work by Jansen and van den Steen (1995), the authors used the principle operation of an active damping system that had been developed for electrical rotary drives for a hydraulic top drive in order to suppress the stick-slip oscillation of the drillstring of a semi-submersible drilling rig. The stick-slip oscillations in this system were eliminated by controlling the energy flow through the hydraulic top drive. In this system, the measurement of pressure fluctuations was used to adapt the flow rate of the pumps that powered the top drive. While in Jansen and Van den Steen (1994) the measurement of current fluctuations was used to adapt the voltage of the electrical motor.

Serrarens et al. (1998) modified the classical concept of H_∞ control design technique to suppress the stick-slip oscillation in the drillstring system. The result shows that H_∞controller can be used to mitigate stick-slip oscillation and fast transient response in the bit speed after the elimination of stick-slip oscillation. However, this approach considers the controller to be linear and time-invariant in spite of the fact that the friction at the bit is nonlinear due the unknown and time varying forces where the stability of the system is critical.

A classical PID controller at the surface was used by (Pavone and Desplans 1994; Abbassian and Dunayevsky 1998; Navarro-Lopez and Suarez 2004) and Navarro-López (2009) developed a proportional-integral controller (PI) in order to eliminate stick-slip oscillation. All of these techniques use single input single output control to supress stick-slip vibration by increasing the velocity of the

rotary table or by decreasing the WOB. However, increasing the rotary speed may cause undesired effects such as lateral vibration (e.g. backward and forward whirling) resulting in impacts with the borehole wall, increased wear of the drill bit; or the desired speed may be beyond the capacity of motor. Whilst decreasing the WOB below the threshold value will lead to zero cutting force.

Canudas-De-Wit et al. (2005) presented D-OSKIL (drill oscillation killer) technics to mitigate stick-slip vibration by using the weight on the bit (WOB) forces as an additional control variable. The stick slip oscillation can be indeed eliminated by D-OSKIL, however, the drawback of this approach is that the whole analysis is based on the approximated bias describing function that uses the angular rotary speed of the rotary table to estimate the angular speed of the bit, and is not based on direct measurement of the angular velocity of the bit.

A nonlinear dynamic inversion control design method was used by Al-Hiddabi, Samanta and Seibi (2003) to reduce the lateral and torsional vibration of the drillstring. The dynamic inversion was used to design two controllers, one to control the speed of the table and the second to control the bit speed. The result of the simulation showed that the design of a non-linear controller of the bit eliminates the torsional vibrations and suppresses the lateral vibrations significantly. However, the robustness of such a technique has not yet been demonstrated.

Kyllingstad and Nessjen (2009; 2010) presented a new smart tuning system called Soft Speed for suppressing and preventing harmful stick-slip vibration. This system was a standard proportional integral type speed controller (PI) which used the stick-slip frequency to suppress stick-slip oscillations effectively instead of using torque feedback or motor torque, therefore, it is considered as passive in a sense. The results showed the ability of this system to suppress

the fundamental stick-slip vibration but not the higher stick-slip modes because they are far outside the absorption band of the system.

Jijón et al. (2010) used the D-OSKIL mechanism proposed by Canudas-de Wit et al. (2005) to the design of an observer for oilwell drilling. In this approach, the measurement of the angular velocity of the rotary table is added to the measured angular velocity of the bit, however, based on the technological constraint of the drillstring length, the signal from the bit arrives with significant delay affecting the accuracy of the system.

Pavković, Deur and Lisac (2011) proposed an automatically tuned active damping control to attenuate the torsional vibration (stick-slip) of the drillstring. This strategy was based on estimated drillstring torque used as an additional term in the feedback loop for the proportional-integral controller (PI), therefore, due to this modification, the PI controller is referred to as PIm controller. In addition, to mitigate the stick-slip vibration an appropriate back-spinning prevention algorithm was used to prevent back spinning of the drillstring which is attributed to the stick-slip tool friction, and restricted braking power of the power converter.

Manipulation of the drilling parameters is one of the solutions to suppressing the stick-slip oscillation, such as: increasing the driving speed (rotary speed), reducing the weight on bit (WOB), enhance the viscosity of the drilling mud or increase the friction at the bit (Canudas-de-Wit et al. 2005). The manipulation of these parameters has been shown to be very efficient in mitigating the stick-slip vibration in the field (Sananikone et al. 1992).

Dufeyte and Hennneuse (1991) studied the stick-slip vibration by analysing the drilling parameters and downhole measurement simultaneously, and the results

showed that manipulating the surface parameters (WOB, rotary speed, and mud characteristics) can lead to a reduction of the stick-slip vibration and thus minimises the problem of drillpipe fatigue and bit wear.

Omojuwa, Osisanya, and Ahmed (2011; 2012) showed that by increasing the rotary speed and decreasing the weight on the bit (WOB) led to reduced stick-slip vibration. However, increasing the rotary speed can cause increases in lateral and longitudinal vibration, whilst decreasing the WOB will typically reduce the rate of penetration (ROP). Therefore a balance must exist between stick-slip oscillations and ROP.

2.4.2 Passive stick-slip suppression approaches

Control and mitigation of the vibrations of a mechanical system are considered the first target of the designer to mitigate the unwanted effects of vibration which may eventually lead to the fatigue and failure of the equipment. Passive control approaches are considered to be one of the most effective ways to control and suppress the unwanted vibrations; this method has been used by many researchers to control the dynamic behaviour of the drillstring for the suppression of stick-slip vibration. The methods which use passive stick-slip suppression can be classified as: optimisation of bottom hole assembly (BHA) configurations; optimisation of drilling input parameters; bit selection and bit design; and use of downhole tools.

Due to the fact that the BHA is an important part of the drillstring and plays a significant role in stick-slip vibrations, many researchers have attempted to overcome this problem by optimising the BHA configurations to improve the drillstring dynamics and drilling performance. Fear et al. (1997) studied the BHA configuration by focusing on the effect of the drill bit on the drillstring dynamics

by changing the location of the stabilisers. This study revealed that stick-slip increased when the bit had more freedom to move laterally.

Janwadkar et al.(2006) demonstrated that the redesign of the BHA taking into consideration weight buckling and critical speed could lead to an improvement of the ROP by 42-121% with minimal bit damage. Also, Baily and Remmert (2009) showed that redesign of the BHA could be effective in stick-slip suppression and provide an improvement in the rate of penetration. Increasing the stiffness of the BHA to improve the transmission of the energy to the bit can reduce the occurrence of stick-slip vibration as shown by (Pastusek et al. 2005).

Mahyari et al. (2010) investigated the best location of one, two or three sets of stabilisers to give stable lateral motion of the drillstring and maximum WOB while Jansen (1990) studied the effect of stabiliser clearance and stabiliser friction on whirl and stick-slip vibrations of the drillstring. Control of stabiliser clearance reduces the rotary speed at which the whirl amplitude is maximum, while stabiliser friction decreases the maximum amplitude and can produce self-excited backward whirl of the drillcollar.

Chen et al. (2002) studied the vibrations of the drillstring when the bit was of roller cone type. The study showed that this type of bit, which includes bearings, could reduce the torsional vibration and increase the rate of penetration (ROP). The bit was found to drill more smoothly and had better durability than conventional bits.

Patil and Teodoriu (2013c) studied the effect of surface drilling parameters (rotary speed and WOB) on the stick-slip oscillations. They revealed that an increase in the rotary speed would convert the stick-slip vibration to torsional

vibration, but the ROP would increase; whilst decreasing the WOB would eliminate the stick-slip oscillation but also reduced the ROP.

Tang et al. (2015) analysed the torsional vibrations of a drilling system with different rotary table speed by modelling the drillstring as a torsional pendulum. The result of the simulations showed that by increasing the velocity above a threshold value (critical speed), the stick-slip disappeared and below this value would start again. Also, this study showed that many parameters play a significant role in stick-slip vibration such as WOB, drillstring length, drill bit type, damping, and rock formation and the stick-slip can be controlled by carefully considering and matching these parameters.

2.5 Summary

The literature review has introduced the main types of oil drilling rigs with an overview of the main systems to show the role of each system inside the rig, to understand the overall procedure of oil drilling and the problems faced. Drillstring vibrations (torsional, longitudinal and lateral) have been shown to be considered as the main cause of drillstring failure and subsequent increase in the cost of drilling.

The prevention and suppression of the stick-slip vibrations are considered to be the main target to researchers and oil companies to reduce the cost of drilling. The methods that have been used to suppress stick-slip oscillation have been classified as either passive or active approaches.

Since the stick-slip vibration is very significant when compared with other types of vibrations (longitudinal and lateral) (Abdulgalil and Siguerdidjane 2005) the focus of this thesis will be on the efficient modelling of this vibration and on strategies for mitigation.

As can be seen from the literature review, a significant effort has been devoted to studying the stick-slip vibrations of drillstring by using lumped or distributed model. However, robust and reliable models that adequately capture all phenomena related to stick-slip vibrations still need to be developed. Work by Apostal et al. (1990) showed that vibration could be modelled using distributed approach (FE), but this is very time consuming. Work by Halsey et al. (1988) showed that the vibrations could be modelled using the lumped approach but lacked appropriate fidelity. This leaves a gap between the highly detailed but computationally taxing distributed approach and the more simplistic but faster lumped approach. Therefore, the hybrid model is considered to be an ideal compromise as it has the accuracy of FE with less computational expense and can be used for real-time measurements and control analysis just like a lumped model.

A model that takes into consideration the fact that the real drilling system consists of lumped and distributed elements has not yet been developed. In this thesis, such a model will be developed which can be used to prevent the stick-slip vibration by manipulating the weight on bit (WOB) and rotary torque by using the genetic algorithm approach.

In the next chapter, the concept of the torsional lumped model and distributed-lumped (hybrid) model will be used for modelling the drillstring to provide an accurate but efficient model to describe the stick-slip vibration.

CHAPTER 3: THEORY & METHODOLOGY

Chapter 3

Theory & Methodology

This chapter introduces the mathematical models used in the research for the modelling and simulation of the stick-slip vibration of an oil well drilling system. Two types of modelling are used in this thesis: a conventional lumped model approach and a new approach for the modelling of oil drilling systems, based on the work by Whalley (1988), which is called lumped-distributed modelling (hybrid).

First, the basic theory of lumped modelling is covered by describing the drillstring as a torsional pendulum with two degrees of freedom, where the driving system has been considered as a lumped mass mechanically coupled to the bottom hole assembly (BHA) by a torsional spring and torsional damper. The basic equations of the different parts of the drilling system that will be used in the modelling of the stick-slip vibration are derived.

Secondly, the bit-rock interaction and the concept of dry friction is presented by deriving the general equation of torsional friction torque on the bit.

Finally, the idea of the distributed-lumped approach and the analogy between the transmission line and other physical systems is presented. The mathematical equations for the distributed-lumped model (DLM) of a general torsional distributed shaft are presented to use in the next chapter for modelling the drillstring.

3.1 Lumped model of drilling system

Drilling operations in the oil industry exposed to dynamic damage lead to a decrease in the drilling efficiency and failure of the drillstring, drill bit and

measurement-while-drilling tools (MWD) (Jansen et al. 1995). The control and reduction of these effects are effectively restricted by two obstacles. First, the harsh medium of cutting leads to damage of the sensors and difficulty in measuring the down hole conditions, resulting in poor observation of the drillstring. Secondly, the delay in transmission of the signal from the bit to the surface (about 20 bits/Sec) (Beck et al. 1996) makes the real-time control difficult. The solution to progressing research in these areas is the replacement of the original drilling system either by modelling and simulation or by experimental test stand.

The modelling and simulation of drilling system have been examined by a significant number of researchers and companies and are documented in many published articles, for example, (Worrall et al. 1992; Patil and Teodoriu 2013a; Ghasemloonia et al. 2015; Zhu et al. 2015). Also, the experimental test stand is treated in a literature review by Patil (2013a).

Two main problems face modellers when studying the drillstring behaviour; the first issue is the accurate modelling of the drilling system and the second issue is modelling the bit-rock interaction. Bit-rock interaction is usually modelled by a dry friction model, whilst the drilling system for the purposes of modelling can be divided into three main parts as follows: drive system, drillstring, and cutting process.

3.2 Equation of motion of the drive system

The drive system consists of three main components as shown in Figure 3-1 (Jansen et al. 1995; Beck et al. 1996).

- Electrical motor (DC or sometimes AC) with mass moment of inertia J_m, angular velocity ω_m and angular displacement θ_m is used to deliver the energy for cutting operations .
- A bevel gear and a gearbox with a combined gear ratio of $1:n$.
- Rotary table with a mass moment of inertia J_{rt}, angular velocity ω_{rt} and angular displacement θ_{rt} .

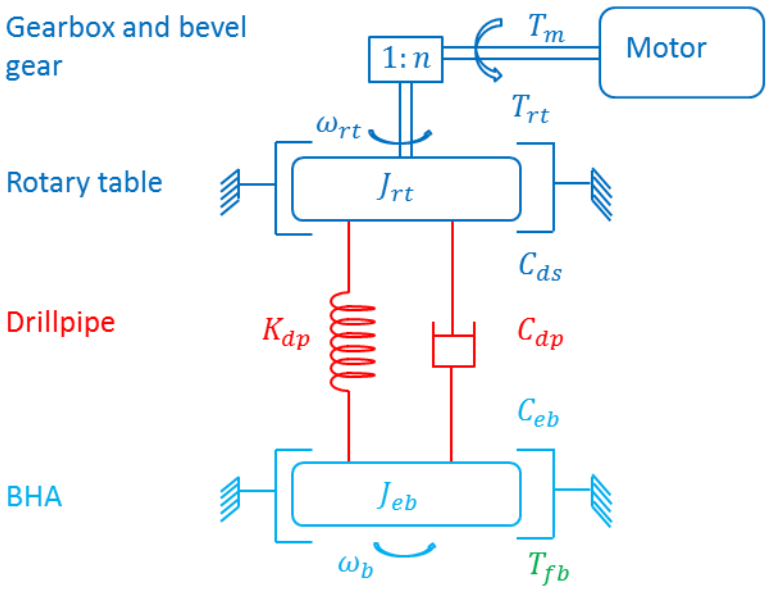

Figure 3-1 Representation of a drilling system as a torsional pendulum driven by a DC motor

3.2.1 DC motor

The equations that describe the electrical behaviour of the motor depend upon the type of motor. In this study, the motor dynamics will be neglected and it will be assumed that a torque T_m can be applied, disregarding the actuator dynamics that are required to generate this torque.

3.2.2 Gearbox and bevel gear

The gearbox is used as a reduction transformer and is considered as a pure frictionless, inertia-less and inelastic device having a gear ratio denoted by n. Since the gearbox is a reduction transformer, the speed of the motor shaft is greater than the speed of the rotary table and drill string as follows:

$$\dot{\theta}_m = n\,\dot{\theta}_{rt} \tag{3.1}$$

$\dot{\theta}_m$ The angular velocity of motor.

$\dot{\theta}_{rt}$ The angular velocity of rotary table.

For the purpose of this study, the efficiency of the gearbox is assumed to equal to 100%. Therefore, the torque transmitted to the rotary table from the motor can be calculated as follows:

$$T_{rt} = \eta n T_m \tag{3.2}$$

Where

T_{rt} - The torque delivered by the motor to rotate the drillstring via the gearbox, rotary table and kelly.

η - The efficiency of the gearbox.

3.2.3 The rotary table

The rotary table as shown in the last chapter in Figure 2-4 is a large disc centrally located on the rig floor used to transmit the rotating power from the DC motor to the drillstring through the Kelly. The speed of rotary table is assumed constant regardless of the applied load during cutting. The rotary table has a moment of inertia J_{rt} which is lumped with the inertia of motor to calculate the overall inertia of drive system J_{ds} as follows:

$$J_{ds}\ddot{\theta}_{rt} = J_{rt}\ddot{\theta}_{rt} + n\,J_m\ddot{\theta}_m = J_{rt}\ddot{\theta}_{rt} + n\,J_m n\,\ddot{\theta}_{rt} = (J_{rt} + n^2\,J_m)\ddot{\theta}_{rt} \tag{3.3}$$

In addition to the lumped inertia, the viscous damping in the various components of the drive system can be lumped into an equivalent viscous damping C_{ds} at the motor side which will be applied as a damping torque $C_{ds}\dot{\theta}_{rt}$.

The differential equation which represents the mechanical components of the drive system plus the drill pipe can be written as:

$$J_{ds}\,\ddot{\theta_{rt}} + C_{ds}\dot{\theta_{rt}} + K_{dp}(\theta_{rt} - \theta_b) + C_{dp}(\dot{\theta_{rt}} - \dot{\theta_b}) = T_{rt} \qquad 3.4$$

$$K_{dp} = \frac{G_s}{l_{dp}}\frac{\pi}{32}(d_{o,dp}^4 - d_{i,dp}^4) \qquad 3.5$$

Where K_{dp} represents the equivalent torsional stiffness of the drillpipe; C_{dp} is the equivalent viscous damping coefficient along the drillpipe due to the drilling mud and must be calculated experimentally; l_{dp} is the length of the drillpipe; G_s is the shear modulus (steel) of the drillstring; whilst $d_{o,dp}$ and $d_{i,dp}$ are the outer and inner diameters of the drillpipe respectively.

Substituting $\dot{\theta}_{rt}$ and $\dot{\theta}_b$ with ω_{rt} and ω_b in equation 3.4 and taking the Laplace transformation with zero initial conditions, the transfer functions can be obtained which are a convenient and commonly used representation of the system for use with control algorithms.

The initial conditions are taken as zero and the system is linear in order to obtain the transfer function. Without this assumption then the differential equations become nonlinear and the transfer function method cannot be used.

$$J_{ds}\,s\omega_{rt}(\mathrm{s}) + C_{ds}\omega_{rt} + \frac{K_{dp}}{s}\big(\omega_{rt}(\mathrm{s}) - \omega_b(s)\big) + C_{dp}(\omega_{rt}(\mathrm{s}) - \omega_b(\mathrm{s})) = T_{rt} \qquad 3.6$$

Let $\omega_{rt}(\mathrm{s}) - \omega_b(\mathrm{s}) = \Delta\,\omega$ and substitute into equation 3.6 then

$$(J_{ds}\,s + C_{ds})\omega_{rt}(\mathrm{s}) + (\frac{sC_{dp}+K_{dp}}{s})\Delta\,\omega = T_{rt}$$

$$\frac{T_{rt}-T_{dp}}{\omega_{rt}(s)} = \frac{1}{J_{ds}\,s+\,C_{ds}} \quad 3.7$$

Where

$$T_{dp} = (\frac{sC_{dp}+K_{dp}}{s})\Delta\,\omega \quad 3.8$$

T_{dp} represents the drillpipe torque.

3.3 Mathematical model of the drillstring

In many cases, the drillstring is considered as a simple torsional pendulum with different degrees of freedom as demonstrated in the literature review. The assumptions are as follows. First, the BHA (Bottom Hole Assembly) is considered as a rigid body with negligible twist compared with the twisting of the drillpipe. Therefore, it will be neglected. Secondly, the round-trip time of the torsional wave is small when compared to the natural oscillation period. Finally, the speed of the rotary table is constant regardless of the applied load (Pavković et al. 2011; Tikhonov and Safronov 2011).

In this thesis, the drillstring will be considered as a torsional pendulum, initially with two degrees of freedom driven by an electric motor where the drillpipe is represented as a torsional spring with a stiffness of K_{dp} and torsional dampingC_{dp}, due to the drilling mud, structural damping of the drillpipe and friction between drillpipe and wellbore as shown in Figure 3-1.

The rotary table rotates at constant speed regardless of the applied load while the BHA behaves as a rigid body with an equivalent moment of inertia J_{eb} which includes the drillcollar inertia J_{dc} , the HWDP (Heavyweight drillpipe) inertia J_{hdp}, and the third regular drillpipe inertia J_{dp} (Jansen 1993):

$$J_{eb} = J_{dc} + J_{hdp} + \frac{1}{3}J_{dp} \quad 3.9$$

$$J_{eb} = G\,\rho\frac{\pi}{32}[l_{dc}\left(d_{o,dc}^4 - d_{i,dc}^4\right) + l_{hdp}\left(d_{o,hdp}^4 - d_{i,hdp}^4\right) + \frac{l_{dp}}{3}\left(d_{o,dp}^4 - d_{i,dp}^4\right) \quad 3.10$$

As the drilling progresses, the drillpipe length will increase while the bottom hole assembly (BHA) length remains constant. The above assumptions will permit the study of the dynamics of the drillpipe and BHA separately. Some further assumptions are made to obtain the equations of motion:

- There is no inclination in the borehole and the drillstring and borehole both remain vertical.
- The friction between drillpipe and borehole are neglected.
- There is no lateral motion of the bit.
- The viscosity of mud is considered constant along the drillstring.
- Drive torque is constant and positive.
- The motion of drilling mud is assumed to be laminar, i.e., without turbulence.

The equation of motion for the BHA connected to a drive system by a torsional spring and damper can be written as follows by applying Newton's second law:

$$J_{\text{eb}}\,\ddot{\theta_b} + C_{eb}\dot{\theta_b} - K_{dp}(\theta_{rt} - \theta_b) - C_{dp}(\dot{\theta_{rt}} - \dot{\theta_b}\,) = -T_{fb} \quad 3.11$$

Where

C_{eb} is the equivalent viscous damping coefficient associated with the BHA.

$T_{fb}(\dot{\theta_b})$ is a non-linear friction torque due to bit-rock interaction and represents the classical Coulomb plus static friction (dry friction) torque along the BHA.

Taking the Laplace transformation of equation 3.11 with zero initial conditions:

$$J_{\text{eb}}\,s\omega_b(\text{s}) + C_{eb}\omega_b - \frac{K_{dp}}{s}\left(\omega_{rt}(\text{s}) - \omega_b(s)\right) + C_{dp}(\omega_{rt}(\text{s}) - \omega_b(\text{s})\,) = -T_{fb}$$

$$(J_{\text{eb}}\,s + C_{eb})\omega_{rt}(\text{s}) - (\frac{sC_{dp} + K_{dp}}{s})\Delta\,\omega = -T_{fb}$$

$$\frac{T_{dp}-T_{fb}}{\omega_b(s)} = \frac{1}{J_{eb}\,s+\,C_{eb}} \qquad 3.12$$

3.4 The model of friction torque (T_{fb})

The stick-slip vibrations in the oilwell drilling shaft are driven by a nonlinear reactive torque, which is combined with the viscous damping torque (T_{vb}), due to drilling fluid, and friction torque $(T_{fb}(\dot{\theta}_b))$ due to the bit contact with rocks by cutting process and friction along the BHA. The friction torque depends on a wide range of factors, for example the types or rock, the bit type and the vertical force applied on the bit (WOB) (Pavković et al. 2011); therefore the function representing the friction torque is highly uncertain.

Since friction torque on the bit is directly proportional to the weight on the bit, the coefficient of friction and the radius of the bit, the equation of $(T_{fb}(\dot{\theta}_b))$ can be written as:

$$T_{fb} = W_{Ob} R_b \mu_b(\dot{\theta}_b) \qquad 3.13$$

Where

W_{Ob}, is the weight on bit (WOB), which is related with the hook-on-load applied at the surface, R_b is the radius of the bit and $\mu_b(\dot{\theta}_b)$, friction coefficient at the bit which is bit speed dependent. Since the coefficient of friction depends on speed there will be a transition between static and dynamic friction. These two frictions coefficients lead to discontinuous differential equations making the stick-slip vibration challenging to model (Tikhonov and Safronov 2011).

Many methods are used for modelling the friction torque on the bit; most of these models use a decreasing and continuously differentiable velocity when the velocity of the BHA is not equal to zero and discontinuous otherwise because of the presence of the Coulomb friction. The work in this thesis will use

a model proposed by Navarro-Lopez and Suarez (2004) which used a dry friction model together with Stribeck effect to model the friction torque on the bit (Armstrong-Helouvry et al. 1994). Also, the dry friction model when the friction torque on the bit (T_{fb}) is multi-valued at $\dot{\theta}_b$=0 will be approximated by a combination of the model proposed by Leine (1998; 2000) and the Karnopp's models (1985) with a zero velocity band as shown in equation 3.14.

$$T_{fb}(\dot{\theta}_b) = \begin{cases} T_{ab} & if\ |\dot{\theta}_b| < \mathrm{D}\omega\ \ T_{ab} \le T_{sb} \text{ stick} \\ T_{sb} sign(T_{ab}) & if\ |\dot{\theta}_b| < \mathrm{D}\omega\ \ T_{ab} > T_{sb} \text{ stick to slip transition} \\ T_{cb}\, sign(\dot{\theta}_b) & if\ |\dot{\theta}_b| > \mathrm{D}\omega \quad \text{slip} \end{cases} \qquad 3.14$$

Where

- T_{ab} represent the external torque applied by drillstring on the bit which must overcome the static friction torque T_{sb}, to move the bit.

$$T_{ab} = T_{dp} - T_{vb} = K_{dp}(\theta_{rt} - \theta_b) + C_{dp}(\dot{\theta}_{rt} - \dot{\theta}_b) - C_{\mathrm{eb}}\dot{\theta}_b \qquad 3.15$$

- T_{sb} is the static friction torque associated with J_{eb} .

$$T_{sb} = R_b W_{Ob} \mu_{sb} \qquad 3.16$$

- T_{cb} is the sliding friction torque (cutting torque).

$$T_{cb} = R_b W_{Ob} \mu_b(\dot{\theta}_b) \qquad 3.17$$

- μ_b, is the bit speed dependent bit friction coefficient.

$$\mu_b(\dot{\theta}_b) = [\mu_{cb} + (\mu_{sb} - \mu_{cb}) e^{-\gamma_b|\dot{\theta}_b|} \qquad 3.18$$

- μ_{cb} ,μ_{sb}, are the Coulomb and static friction coefficients associated with J_{eb}.

- R_b is the radius of the bit.
- W_{ob} is the weight on the bit WOB which is related to the hook on load applied at the surface.
- $D\omega$>0 a limit velocity interval specifies a small enough neighbourhood of $\dot{\theta}_b$=0.
- γ_b is a positive constant defining the decaying velocity of T_{fb}.

The resulting friction model is represented in Figure 3-2 and can be compared with a classical dry friction model with an exponential-decaying law in the sliding phase.

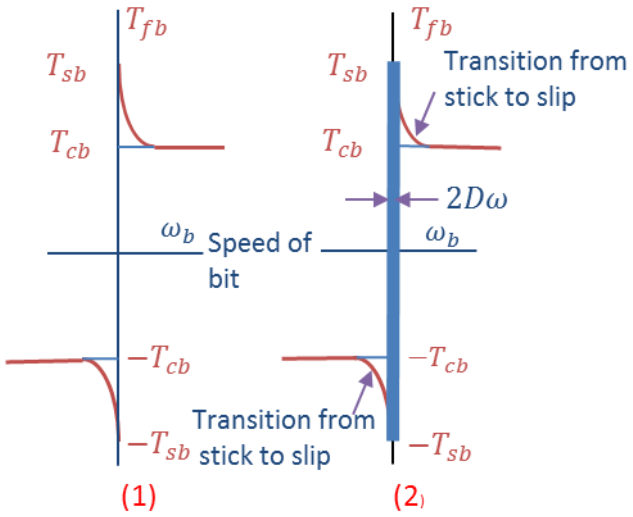

Figure 3-2 Friction torque at the bit: (1) dry friction with exponential-decaying law in the sliding phase; (2) switch, friction model with a variation of Karnopp's friction model

Leine et al. and Gradl et al. (1998; 2012) explains the equation of friction torque on the bit as follows: the first line of equation 3.14 is the case when the bit is in the stick phase for a limited interval, that means the bit speed is less than a limit velocity interval $D\omega$ and the applied torque less than or equal to the static friction torque (T_{sb}). During this phase the applied torque by the drillstring will

build up until it exceeds the static friction torque which initiates the transition from stick to slip with constant velocity$D\omega$. When the velocity of the bit exceeds the $D\omega$ velocity, the slip phase will start and the bit will finally go to constant speed with constant torque.

From equations (3.1- 3.12) the overall lumped model of a drilling system for the purposes of simulation is shown in Figure 3-3.

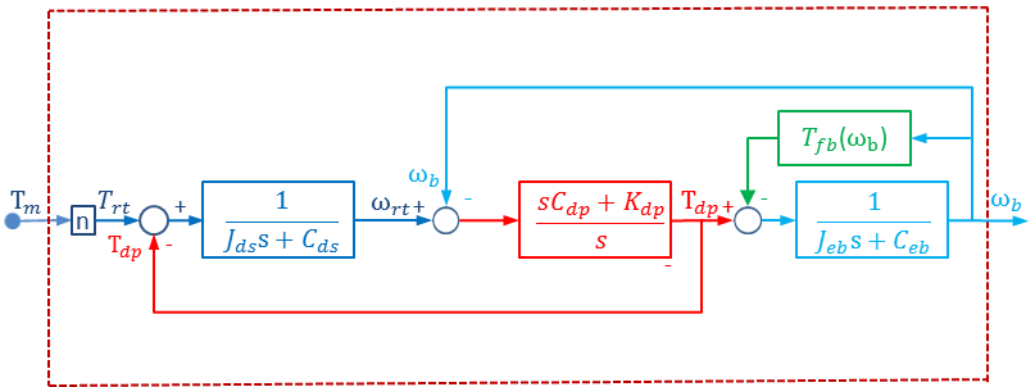

Figure 3-3 Block diagram of the drilling system (lumped model) (blue: drive system; red: drillpipe; bright blue & green: BHA)

3.5 Distributed-Lumped model

The main methods of system modelling for analysis, design and regulation purposes are lumped (or discrete) and continuous (or distributed) systems. The lumped system assumes that the mass, damping and elasticity of the system to be presented at a certain discrete point in the system, while the continuous system considers the mass, damping and elasticity to be distributed with space (Rao 1995). The governing equations of the discrete system are ordinary differential equations (O.D.E) which are to some extent easy to solve. On the other hand, partial differential equations (P.D.E) are the governing equations of the continuous modelling system which are sometimes harder to handle

compared with the ordinary differential equations. However, the result obtained from a P.D.E system can in some cases be more accurate than the result of O.D.E based system. The modeller should be careful when choosing between the two types of models and take into consideration many factors such as the purpose of the analysis, the influence of the analysis on design, and the computational time available before the choice (Rao 1995).

Brown (2001) states that all physical systems are distributed in space, so for the sake of modelling, the model also should be distributed in the space to represent the real system. The distributed system model has at least two or more independent variables and if the system is dynamic one of them should be the time. A lumped model system has only one independent variable (time). Therefore the O.D.E can be used to model the system. The lumped model system does not necessarily give less accurate results than the distributed system, also is not necessarily easier to solve than a distributed system. There are no simple rules for choice between distributed or lumped model, and the modelling becomes partly an art which depends on experience, knowledge and intuition.

The main feature of lumped systems is that the signal is assumed to be transmitted from the input of an element to the output without delay or distortion to the next element in the system without taking into consideration the distance between components. However, there are many systems in which the spatial configuration plays a major role in their dynamic behaviour. The most common example of the effect of dispersion on the dynamic behaviour is the electrical transmission line when the spatial configuration has a significant influence on the transfer of electricity over long distances. Similarly, in the mechanical system, for example, the deflection of beams and vibrating strings, the

dispersion should be taken into consideration for an accurate result. Also, chemical processes when the reaction takes place at a certain point and transmits through a pipe to another place. A system is called distributed-parameter system or simply distributed system if the spatial configuration is vital. On the other hand, if the spatial configuration is not important and ignored the system is called a lumped parameter system or simple lumped parameter (Schwarz and Friedland 1965).

3.6 The general representation of a hybrid model

A natural and more accurate procedure for the determination of the performance of the dynamic system can be achieved by representing the actual system as both a distributed and lumped model. This type of modelling, also known as hybrid modelling, is where distributed and lumped elements are used together to represent the system (Brown 2001).

Whalley (1988; 1990) introduced a Hybrid Model comprising a cascade of distributed parameter dynamical elements separated by lumped parameter dynamical elements as shown in Figure 3-4. Each of the distributed parameters is assumed to have an input such as force, voltage, pressure, etc. and output such as deflection, current, flow rate, etc. The output of each section represents the input of the following section. The series of alternating distributed and lumped sections should end with a lumped element.

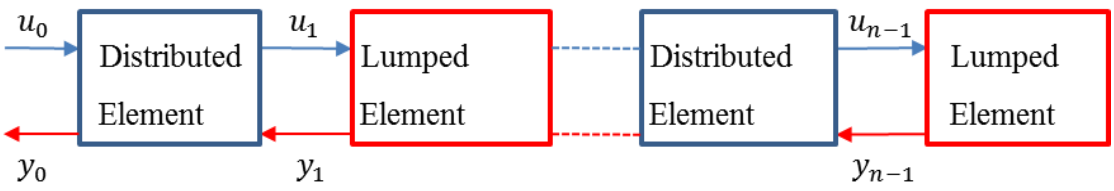

Figure 3-4 Distributed-lumped parameter system

According to Whalley (1988), the energy dissipation throughout the system occurs in the lumped element due to entry, exit and reaction losses. The analogy between the transmission line and other physical systems that have the same differential equation are used to derive the general equation for the distributed elements. The basic equation of the transmission line will be discussed in more detail in the next section.

3.6.1 Torsional distributed shaft

One of the examples of the transmission system is the torsional distributed shaft when the torque transmitted from the source to the place of application. The general equation of distributed shaft can be derived as follows.

From Figure 3-5 take a segment of length Δx at a distance x from the beginning of the shaft.

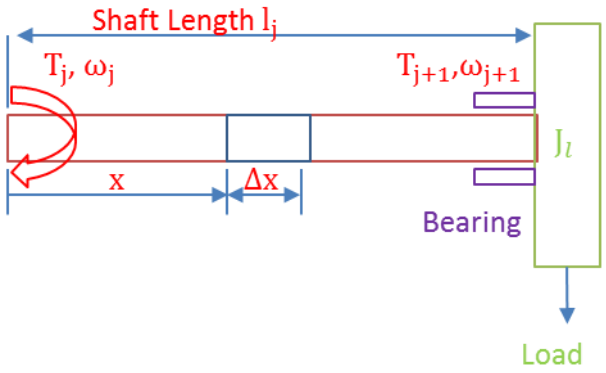

Figure 3-5 A simple torsional shaft

The relationship between the shear strain (γ) and angle of twist of an element of length Δx is:

$$\gamma = \frac{r\partial\theta(x,t)}{\partial x} \qquad 3.19$$

Where

θ is the angle of twist.

γ is the shear strain.

From Hooke's law:

$$G_* = \frac{\tau}{\gamma} = \frac{Tr/J}{r\partial\theta(x,t)/\partial x} \quad 3.20$$

$$T = G_* J \frac{\partial\theta(x,t)}{\partial x} \quad 3.21$$

Where

G_* is the shear modulus of rigidity.

J is the shaft polar moment of inertia $\frac{\pi}{32} d^4$.

The inertia torque acting on an element of length Δx is

$$J\rho \frac{\partial 2\theta}{\partial t^2} \Delta x \quad 3.22$$

Where ρ Is the density of the shaft (kg/m^3)

Jρ Is the mass polar moment of inertia of the shaft per unit length (kg.m)

From Newton's second law

$$\sum T = (J\ \ddot{\Theta}) \quad 3.23$$

The equation of motion can be expressed as:

$$\big(T(x,t)\ + \Delta T(x+\Delta x,t)\big) - T(x,t) = -J\rho \frac{\partial 2\theta}{\partial t^2} \Delta x \quad 3.24$$

Dividing by Δx and taking $(\text{limit}\ \Delta x \to 0)$

$$\frac{\partial T(x,t)}{\partial x} = -J\rho \frac{\partial^2\theta(x,t)}{\partial t^2} \quad 3.25$$

Derive equation 3.21 with respect to t:

$$\frac{\partial T(x,t)}{\partial t} = -G_* J \frac{\partial^2\theta(x,t)}{\partial x \partial t} \quad 3.26$$

Expressing:

$$\omega(x,t) = \frac{\partial\theta(x,t)}{\partial t} \quad 3.27$$

Equation 3.25 and 3.26 can be written as:

$$\frac{\partial T(x,t)}{\partial x} = -J\rho\frac{\partial\omega(x,t)}{\partial t} \quad 3.28$$

$$\frac{\partial\omega(x,t)}{\partial x} = -\frac{1}{G_* J}\frac{\partial T(x,t)}{\partial t} \quad 3.29$$

By comparison of equations 3.28 and 3.29 with equations A.36 and A.37 in Appendix A (Lossless Transmission Line), it can be realised that:

$$L = J\rho \text{ and } C = \frac{1}{G_* J}$$

$\frac{1}{G_* J}$ is the Compliance per unit length,

$J\rho$ is the shaft inertia per unit length

Also the characteristic impedance and propagation constant of the shaft are:

$$\xi = \sqrt{\frac{L}{C}} = J\sqrt{G_*\rho} \quad 3.30$$

$$\Gamma = s\sqrt{CL} = s\sqrt{\rho/G_*} \quad 3.31$$

Using the solution given in section A.1.2 (Appendix A), it follows that the equation of the torsional system of Figure 3-5 can be expressed as:

$$\begin{bmatrix} T_j(s) \\ T_{j+1}(s) \end{bmatrix} = \begin{bmatrix} \xi_j w_{j\,(s)} & -\xi_j\sqrt{\left(w_j{}^2(s) - 1\right)} \\ \xi_j\sqrt{\left(w_j{}^2(s) - 1\right)} & -\xi_j w_{j\,(s)} \end{bmatrix} \begin{bmatrix} \omega_j(s) \\ \omega_{j+1}(s) \end{bmatrix} \quad 3.32$$

Where

$$w_{j\,(s)} = \frac{e^{2\Gamma_j l_j} + 1}{e^{2\Gamma_j l_j} - 1} \quad 3.33$$

3.7 Distributed-Lumped model of a rotary system with inertia and damping

In order to demonstrate the procedure that is used for modelling a rotary system using a distributed-lumped model, the general arrangement shown in Figure **3-6**6 will be utilised to derive the distributed-lumped model (DLM) of this arrangement. Where T_m represents the drive torque from a prime mover such as electrical motor, J_0 the inertia of the gear box, motor, turntable etc, C_0 the damping in the bearing, l_0 the shaft that is used to transmit the torque to a load such as a flywheel, propeller, etc., which consists of inertia and bearing damping (J_1 , C_1)

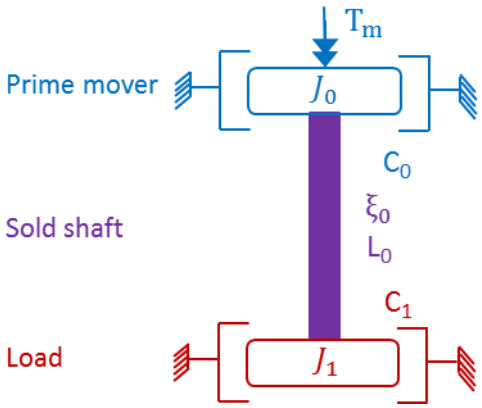

Figure 3-6 Free body diagram of a rotary system

Based on the general representation of a distributed element of torsional shaft equation 3.32 gives the following for a distributed element of a drillpipe

$$\begin{bmatrix} T_0(s) \\ T_1^*(s) \end{bmatrix} = \begin{bmatrix} \xi_0 w_{0\,(s)} & -\xi_0\sqrt{(w_0{}^2(s) - 1)} \\ \xi_0\sqrt{(w_0{}^2(s) - 1)} & -\xi_0 w_{0\ (s)} \end{bmatrix} \begin{bmatrix} \omega_0(s) \\ \omega_1^*(s) \end{bmatrix} \quad 3.34$$

Where

$T_0(s)$ is the input torque to distributed shaft.

$T_1^*(s)$ is the output torque from distributed shaft.

$\omega_0(s)$ is the angular velocity at the inlet of distributed shaft.

$\omega_1^*(s)$ is the angular velocity at the outlet of distributed shaft.

Since

$$\mathrm{T_0(s) = T_m - J_0 s\omega_0(s) - C_0\omega_0(s)} \quad 3.35$$

$$T_1^*(s) = J_1 s\omega_1^*(s) + C_1\omega_1^*(s) \quad 3.36$$

$$w_0(s) = \frac{e^{2l_0\Gamma_0(s)}+1}{e^{2l_0\Gamma_0(s)}-1} \quad 3.37$$

Equation 3.37 can be written in delay form

$$w_0(s) = \frac{1+e^{-2l_0\Gamma_0(s)}}{1-e^{-2l_0\Gamma_0(s)}} \quad 3.38$$

Moreover, upon evaluation

$$\sqrt{(w_0{}^2(s) - 1)} = \frac{2e^{-l_0\Gamma_0(s)}}{1-e^{-2l_0\Gamma_0(s)}} \quad 3.39$$

$$\Gamma_0(s) = s\sqrt{L_0C_0} = s\sqrt{\rho_0/G_0} \quad 3.40$$

$$\xi_0 = \sqrt{\frac{L_0}{C_0}} = I_0\sqrt{\rho_0 G_0} \quad 3.41$$

The block diagram which represents equation 3.34 is shown in Figure 3-77.

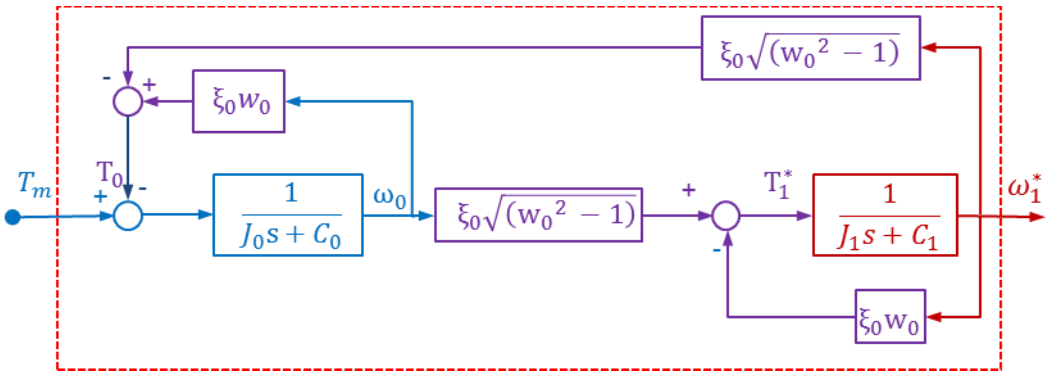

Figure 3-7 Block diagram representation of a simple rotary system (blue: prime mover; red: load; purple: sold shaft)

3.8 Summary

This chapter presented the mathematical models of the drilling system using the lumped model and distributed-lumped modelling approaches. First, the lumped model was derived by considering the drillstring as a torsional pendulum with two degrees of freedom. In general, the equation of motion of the drilling system is divided into three equations, the equation of drive system, the drillstring and the dry friction. All the necessary equations for the lumped modelling and simulation were introduced in this chapter. The block diagram shown in Figure 3-3 represents lumped model of the drilling system which is shown in Figure 3-1.

Secondly, the main difference between the lumped and distributed model was highlighted in this chapter. The distributed-lumped modelling scheme of Walley (1988; 1990) has been demonstrated by using the concept of the analogue between the electrical transmission line and other physical systems that have similar properties.

For illustration purposes, a simple torsional system was used to apply the distributed-lumped modelling technique to derive the general equation that can be used to simulate and analyse the system. Then the general equation of a torsional distributed system was used to model a general rotary system as in Figure 3-66 and the block diagram of the scheme shown in Figure 3-77.

In the next chapter, the parameters of the drilling system will be introduced, and the lumped model and distributed-lumped model approach will be used to model the rotary system of an oil drilling rig. The general and specific equations and relations that were developed in this chapter will be utilised for the purpose of modelling and simulation of the drillstring.

CHAPTER 4: SIMULATION OF THE DRILLING SYSTEM

Chapter 4

Simulation of the Drilling System

In this chapter, the simulation of Lumped and Distributed-Lumped (Hybrid) models are presented. First, the lumped model simulation of a drilling system as shown in Figure 3-1 and governing equations 3.1-3.14 is introduced. Secondly, the distributed-lumped approach as explained in the previous chapter, and shown graphically in Figure 3-75, is used to model and simulate the drilling system.

Three types of distributed-lumped modelling approaches are presented depending on the number of lumped and distributed elements:

- First is a lumped-distributed-lumped model (LDLM) which considers the drive system as a lumped element connected to the BHA (lumped element) by a distributed element (drillpipe).
- Secondly, a lumped-distributed-distributed-lumped model (LDDLM), where the HWDP is also considered as a distributed element.
- Finally, a lumped-distributed-distributed-distributed-lumped model (LDDDLM) where the three types of pipe (drillpipe, HWDP and drillcollar) are represented as distributed elements.

Validation of the model types will be carried out by comparing the velocity of the bit as a function of time in the stick-slip phase with real measurements from Veeningen (2011) and Ledgerwood (2013). Also the behaviour of different drilling parameters (Applied torque on the bit T_{ab}, Friction torque on the bit T_{fb}, speed of the rotary table ω_{rt} and speed of the bit ω_b) are demonstrated in two cases: when there is no stick-slip motion (slip phase); and when the stick-slip occurs (sticking phase), in order to prove that the models work properly.

4.1 Lumped model simulation

The entire lumped model of a drilling system was introduced in chapter three using the concept of the simple torsional pendulum with two degrees of freedom. In chapter three the drilling system, for the sake of modelling, was divided into three parts (rotary drive system, drillstring and friction torque on the bit) as shown in Figure 3-1, whilst equations 3.1 - 3.14 represent the mathematical model of the drilling system and Figure 3-3 represent the block diagram of the whole system.

The corresponding simulation model of the drilling system (Figure 3-1) as a lumped model for equations 3.7, 3.8 and 3.12 with friction torque on the bit (T_{fb}) as demonstrated in equation 3.14 is presented in Figure 4-1.For clarification, the Simulink model has different colours. These colours correspond to colour used in Figure 3-3 where the blue colour represents the drive system; red represents the drillpipe, light blue represents the BHA and green represents the friction torque on bit (T_{fb}). .

For the purpose of simulation, the lumped model (Figure 4-1) and the distributed-lumped models (hybrid) in the next section used a fixed-step solver type ode5 (Dormand-Prince) with fundamental sample time equal 0.001 sec. The input to the model is the torque of rotary table (T_{rt}) and the main output is the velocity of the bit (ω_b) together with other parameters such as the applied torque on the bit (T_{ab}), friction torque on the bit (T_{fb}) and speed of the rotary table (ω_{rt}) which can be calculated at different points in the models.

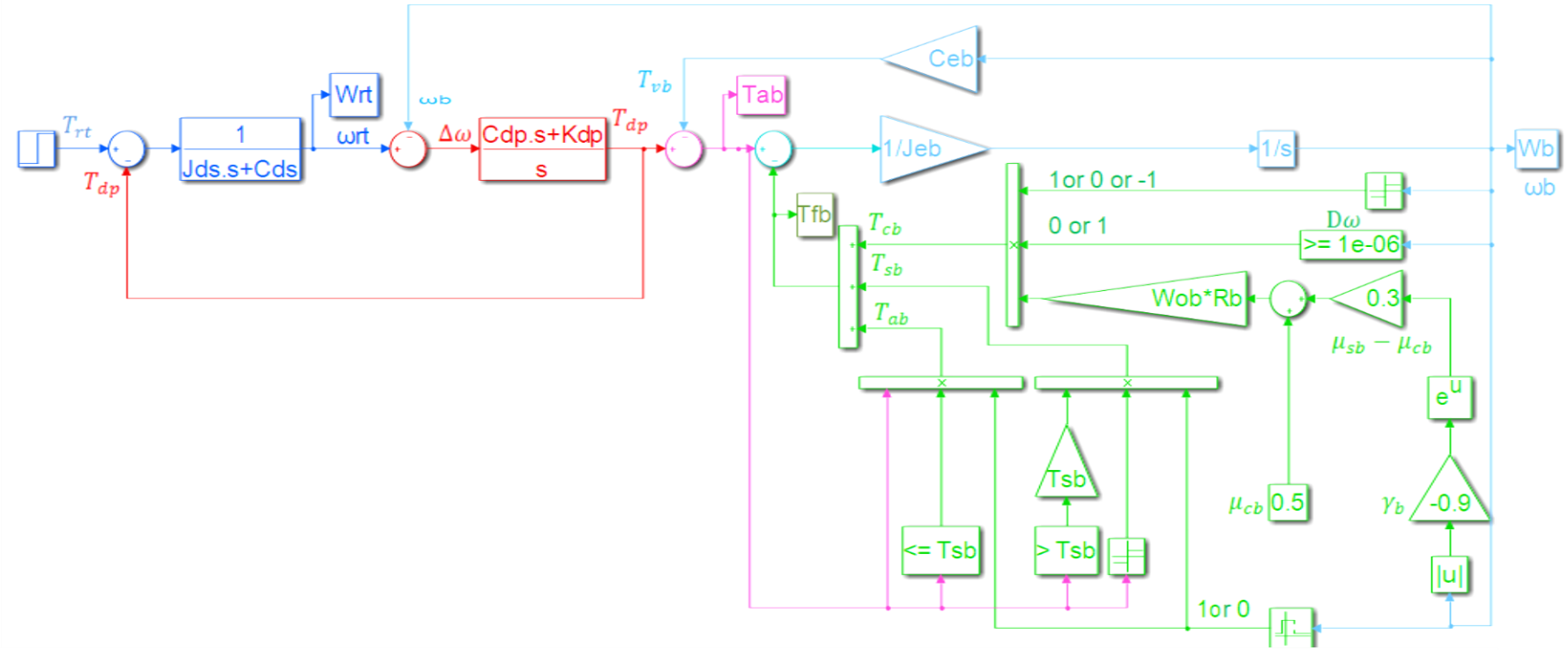

Figure 4-1 Simulink model of a lumped parameter drillstring in an oil drilling system (blue: drive system; red: drillpipe; light blue: BHA; green: friction torque on the bit)

4.2 Distributed-Lumped model simulation

In Chapter 3, the theoretical analysis of the DLM (Hybrid) for a general transmission line was presented. For the lossless transmission line, the general equation was introduced in equation A.40 (Appendix A), and this equation was used to derive the general equation of a torsional shaft (3.32) which was then used to derive the equation of a rotary system with inertia and damping load as shown in equation 3.34 and block diagram presented in Figure 3-77.

In this chapter, the concept of the lossless transmission line will be used to derive the DLM (hybrid) of the drilling system by depending on the general equation of a distributed torsional shaft (eq. 3.32). The drilling system can be represented in three different ways. First as a Lumped-distributed-lumped model (LDLM) by considering the drive system (motor, gearbox, and the turntable) as a lumped element connected to a distributed element which is the drillpipe has a characteristic impedance (ξ_{dp}) and the distributed element connected to bottom hole assemblies (BHA)(heavyweight drillpipe, drillcollar and bit) has an equivalent inertia (J_{bh}).

Secondly, as a lumped-distributed-distributed-lumped model (LDDLM) by considering the drive system as a lumped element, the drillpipe and heavyweight drillpipe as a distributed element and the drillcollar plus the bit as a lumped element.

Thirdly as a lumped-distributed-distributed-distributed-lumped model (LDDDLM) in this case, the model consists of a lumped element (drive system) connected to three distributed elements (drillpipe, heavyweight drillpipe and drillcollar) and end with the lumped element (the drill bit). In the next section, the derivation of each model will be presented.

4.2.1 Lumped-Distributed-Lumped Model (LDLM)

The drilling system, in this case, consists of the drive system as lumped model connected to the bottom hole assembly (BHA) by the drillpipe as shown in Figure 4-2.

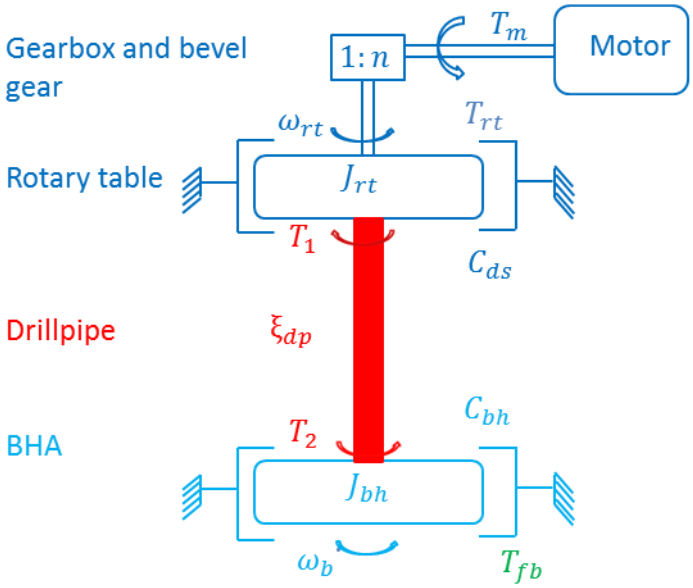

Figure 4-2 Representation of a drilling system as a torsional transmission line driven by a DC motor

From the equation of distributed torsional element (equation 3.32), the equation of a drillpipe can be represented in matrix form as follows by considering j=1 (where j relates to the element number).

$$\begin{bmatrix} T_1(s) \\ T_2(s) \end{bmatrix} = \begin{bmatrix} \xi_1 w_1(s) & -\xi_1\sqrt{(w_1{}^2(s) - 1)} \\ \xi_1\sqrt{(w_1{}^2(s) - 1)} & -\xi_1 w_1(s) \end{bmatrix} \begin{bmatrix} \omega_1(s) \\ \omega_2(s) \end{bmatrix} \quad 4.1$$

Where

$T_1(s)$ and $T_{2,}(s)$ are the torque at top and bottom of the drillpipe, $\omega_1(s)$ and $\omega_2(s)$ are the angular velocity at the top and bottom of the drillpipe and $\xi_1 = \xi_{dp}$ is the characteristic impedance of the drillpipe ($\xi_{dp} = J_{dp}\sqrt{G_s\rho}$).

Also

$$w_{1\,(s)} = \frac{e^{2\Gamma_1 l_1} + 1}{e^{2\Gamma_1 l_1} - 1} = \frac{1+e^{-2t_1 s}}{1-e^{-2t_1 s}} \qquad 4.2$$

$$\sqrt{(w_1{}^2(s) - 1)} = \frac{2e^{-\Gamma_1 l_1}}{1-e^{-2\Gamma_1 l_1}} = \frac{2e^{-t_1 s}}{1-e^{-2t_1 s}} \qquad 4.3$$

Where $\Gamma_1 = \Gamma_{dp} = s\sqrt{\rho/G_s}$ is the propagation constant of the drillpipe, $l_1 = l_{dp}$ is the length of the drillpipe and $\Gamma_1 l_1 = s l_1\sqrt{\rho/G_s} = s t_1$. Where $t_1 = t_{dp}$represents the delay time of the drillpipe relating to the time taken for a response to travel the full length of the drillpipe.

The governing equation of two lumped elements (drive system and BHA) can be calculated as follows by applying Newton's second law followed by Laplace transformation with zero initial conditions.

For the drive system:

$$T_1(s) = T_{rt}(s) - J_{ds}s\omega_{rt}(s) - C_{ds}\omega_{rt}(s)$$

$$\frac{\omega_{rt}(s)}{T_{rt}(s) - T_1(s)} = \frac{1}{J_{ds}s + C_{ds}} \qquad 4.4$$

Where J_{ds} and C_{ds} represent the equivalent inertia and viscous damping of the drive system respectively, $\omega_{rt}(s)$ is the angular velocity of the rotary table, equal to $\omega_1(s)$, whilst $T_{rt}(s)$ is the applied torque on the rotary table.

For the BHA:

$$T_2(s) = T_{fb} + J_{bh}s\omega_b(s) + C_{bh}\omega_b(s)$$

$$\frac{\omega_b(s)}{T_{fb}(s)-T_2(s)} = \frac{1}{J_{bh}s+ C_{bh}} \quad 4.5$$

Where T_{fb} is the friction torque on the bit as demonstrated in Eq. 3.14, but in the LDM the applied torque on the bit is

$$\mathrm{T}_{ab,d} = T_2 - T_{vb} \quad 4.6$$

C_{bh}, is the equivalent damping of the BHA, ω_b is the angular velocity of the bit, equal to ω_2, and J_{bh} is the equivalent mass moment of inertia of the BHA (drillcollar and HWDP)

$$J_{bh} = G_s\,\rho\,\frac{\pi}{32}[l_c(d_{o,\mathrm{dc}}^4 - d_{i,\mathrm{dc}}^4) + l_h(d_{o,hw}^4 - d_{i,hw}^4)] \quad 4.7$$

From equations 4.1 - 4.6 the block diagram representing the drilling system as a LDL model is presented in Figure 4-3.

For clarity, the blue colour represents the drive system as shown in equation 4.4; the red colour represents the drillpipe as shown in equation 4.1 and the light blue and green colours represent the BHA as demonstrated in equation 4.5.

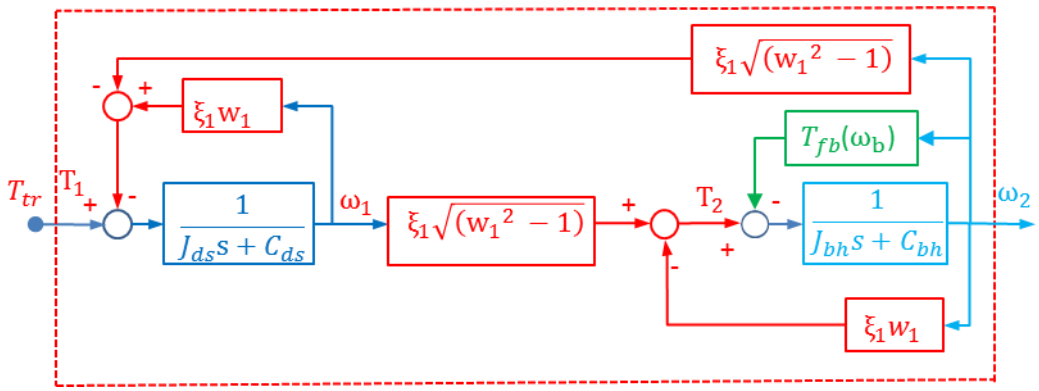

Figure 4-3 Block diagram of the drilling system (LDLM) (blue: drive system; red: drillpipe; light blue & green: BHA)

For the purpose of simulation, the input torque to the drillpipe can be calculated from equation 4.1 as follows

$$T_1 = \xi_1 w_1\, \omega_1 - \xi_1 \sqrt{({w_1}^2 - 1)}\omega_2 \qquad 4.8$$

Substituting equations 4.2 and 4.3 into equation 4.8 and simplifying gives:

$$T_1 = \frac{a + ae^{-2t_1 s}}{1 - e^{-2t_1 s}}\ \omega_1 - \frac{2ae^{-t_1 s}}{1 - e^{-2t_1 s}}\ \omega_2$$

$$T_1 - T_1 e^{-2t_1 s} = a\omega_1 + ae^{-2t_1 s}\omega_1 - 2ae^{-t_1 s}\ \omega_2$$

$$T_1 = T_1 e^{-2t_1 s} + 2ae^{-t_1 s}\ \omega_1 + a\omega_1 - ae^{-2t_1 s}\omega_2 \qquad 4.9$$

Where $a = \xi_1$ represent the characteristic impedance of the drillpipe.

Also, from equation 4.8

$$T_2 = \xi_1 \sqrt{({w_1}^2 - 1)}\omega_1 - \xi_1 w_1\, \omega_2 \qquad 4.10$$

Substituting equations 4.2 and 4.3 into 4.10 and simplifying:

$$T_2 = \frac{2ae^{-t_1 s}}{1 - e^{-2t_1 s}}\ \omega_1 - \frac{a - ae^{-2t_1 s}}{1 - e^{-2t_1 s}}\ \omega_2$$

$$T_2 - T_2 e^{-2t_1 s} = 2ae^{-t_1 s}\ \omega_1 - \ a\omega_2 - ae^{-2t_1 s}\omega_2$$

$$T_2 = T_2 e^{-2t_1 s} + a2e^{-t_1 s}\ \omega_1 - \ a\omega_2 - ae^{-2t_1 s}\omega_2 \qquad 4.11$$

From equations 4.4, 4.5, 4.6, 4.9, 4.11 and the equation of dry friction 3.14, the corresponding simulation model is shown in Figure 4-4. The colour used in this figure is the same as demonstrated in the block diagram of Figure 4-3.

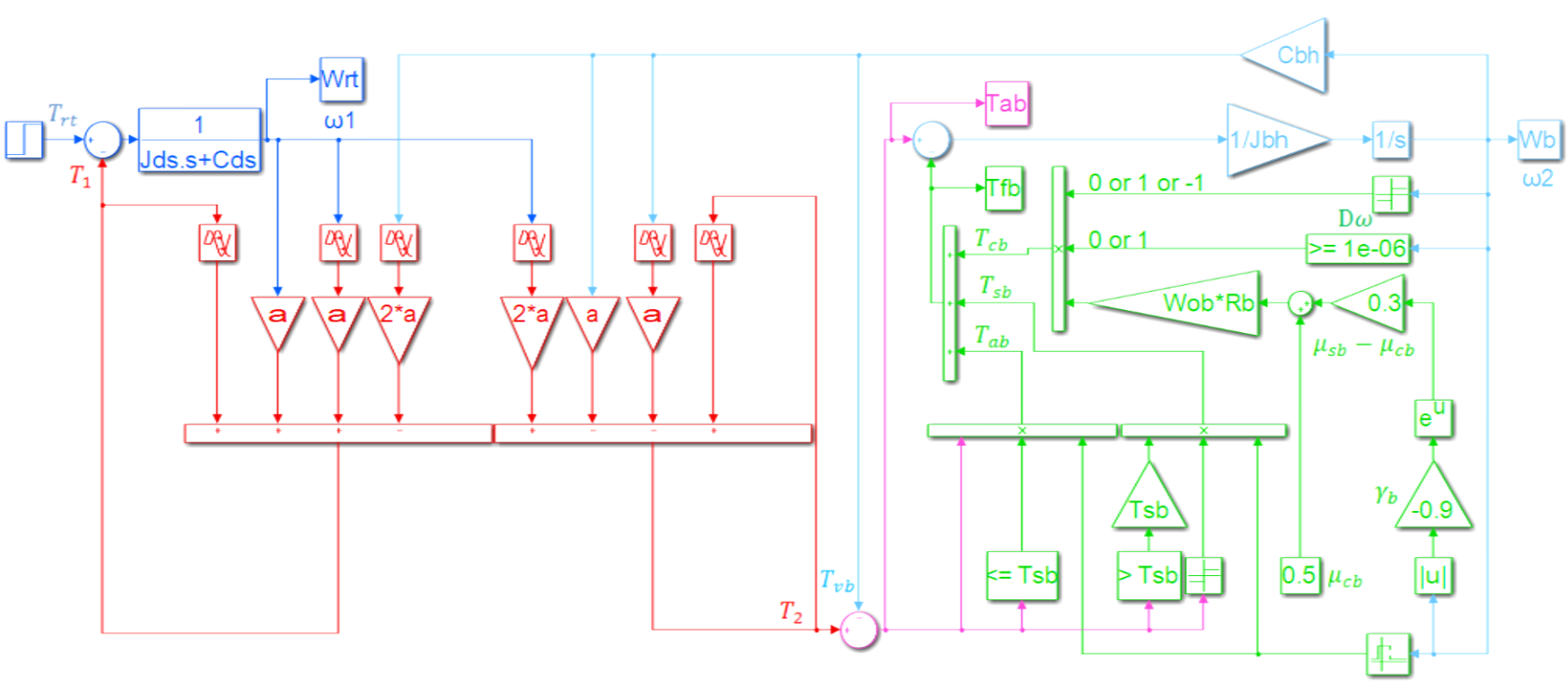

Figure 4-4 LDLM of drillstring in an oil drilling system (LDLM) (blue: drive system; red: drillpipe; light blue & green: BHA)

4.3 Lumped-Distributed-Distributed-Lumped Model (LDDLM)

The drillstring consists of three different types of pipes; drillpipe, heavyweight drillpipe and drillcollar. The drillpipe and HWDP will be considered as distributed elements in series. Therefore the drilling system can be modelled as a lumped element (drive system) connected to two distributed elements and ending with lumped element (drillcollar + bit). The whole drilling system is shown in Figure 4-5.

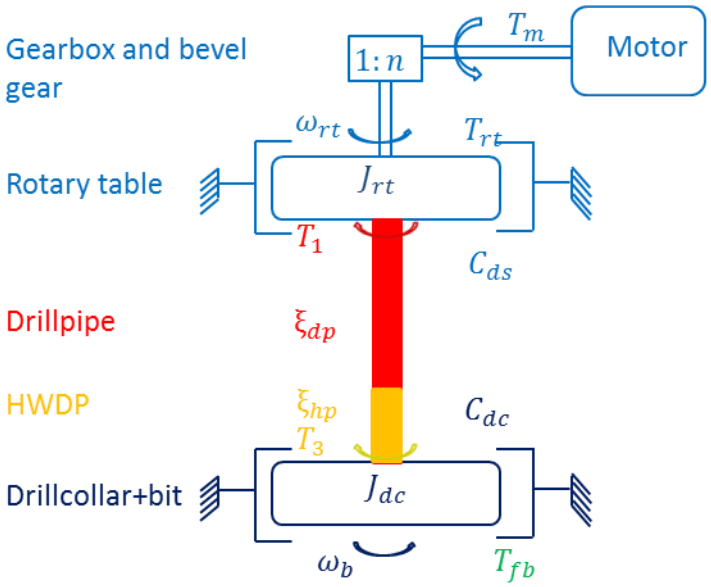

Figure 4-5 Representation of oil drilling system as a Lumped-Distributed-Distributed-Lumped Model (LDDLM)

From the general equation of distributed elements for a torsional shaft (equation 3.32), the Laplace transformed model of the distributed elements (drillpipe) is the same as equation 4.1 while for the HWDP it is:

$$\begin{bmatrix} T_2(s) \\ T_3(s) \end{bmatrix} = \begin{bmatrix} \xi_2 w_{2\,(s)} & -\xi_2\sqrt{(w_2{}^2(s) - 1)} \\ \xi_2\sqrt{(w_2{}^2(s) - 1)} & -\xi_2 w_{2\,(s)} \end{bmatrix} \begin{bmatrix} \omega_2(s) \\ \omega_3(s) \end{bmatrix} \quad 4.12$$

$T_2(s)$ is the input torque to the HWDP; $T_3(s)$ is the output torque from the HWDP; $\omega_2(s)$ is the angular velocity at the inlet of the HWDP; $\omega_3(s)$ is the angular velocity at the outlet of the HWDP and $\xi_2 = \xi_{hw}$ is the characteristic impedance of the HWDP ($\xi_{hw} = I_{hw}\sqrt{G_s\rho}$)

$$w_{2\,(s)} = \frac{e^{2\Gamma_2 l_2} + 1}{e^{2\Gamma_2 l_2} - 1} = \frac{1+e^{-2t_2 s}}{1-e^{-2t_2 s}} \qquad 4.13$$

$$\sqrt{(w_2{}^2(s) - 1)} = \frac{2e^{-2\Gamma_2 l_2}}{1-e^{-2\Gamma_2 l_2}} = \frac{2e^{-t_2 s}}{1-e^{-2t_2 s}} \qquad 4.14$$

Where $\Gamma_2 = \Gamma_{hw} = s\sqrt{\rho/G_s}$ is the propagation constant of the HWDP, $l_2 = l_{hw}$ is the length of the HWDP and $\Gamma_2 l_2 = s l_2\sqrt{\rho/G_s} = s t_2$. Where $t_2 = t_{hw}$ represents the delay time of the HWDP.

The system matrix for the complete model shown in Figure 4-5, can be obtained from equations 4.1 and 4.12 by eliminating the intermediate inputs as demonstrated by Whalley(1988) to give equation 4.15.

$$\begin{bmatrix} T_{1,dp}(s) \\ 0 \\ T_{3,hw}(s) \end{bmatrix} = \begin{bmatrix} \xi_1 w_{1\,(s)} & -\xi_1\sqrt{(w_1{}^2(s) - 1)} & 0 \\ \xi_1\sqrt{(w_1{}^2(s) - 1)} & -\xi_1 w_{1\,(s)} - \xi_2 w_{2\,(s)} & \xi_2\sqrt{(w_2{}^2(s) - 1)} \\ 0 & \xi_2\sqrt{(w_2{}^2(s) - 1)} & -\xi_2 w_{2\,(s)} \end{bmatrix} \begin{bmatrix} \omega_1(s) \\ \omega_2(s) \\ \omega_3(s) \end{bmatrix}$$

4.15

By the configuration shown in Figure 4-5, the governing equations for the system drive mechanism are the same as equation 4.4, and the equations for the drillcollar and bit following Laplace transformation with zero initial conditions are:

$$T_3(s) - T_{fb} = (J_{dc}s + C_{dc})\omega_3(s)$$

$$\frac{\omega_3(s)}{T_{fb}(s) - T_3(s)} = \frac{1}{J_{dc}s + C_{dc}} \qquad 4.16$$

From equation 4.4, 4.15 and 4.16 the block diagram representing the drilling system as LDDLM of Figure 4-5 is shown in Figure 4-6. The colours used in this block diagram are the same for the drive system, drillpipe and friction torque that are used in Figure 4-3 and the yellow is added for HWDP, dark blue for drillcollar and purple represents the common point between the drillpipe and HWDP which is used to calculateω_2.

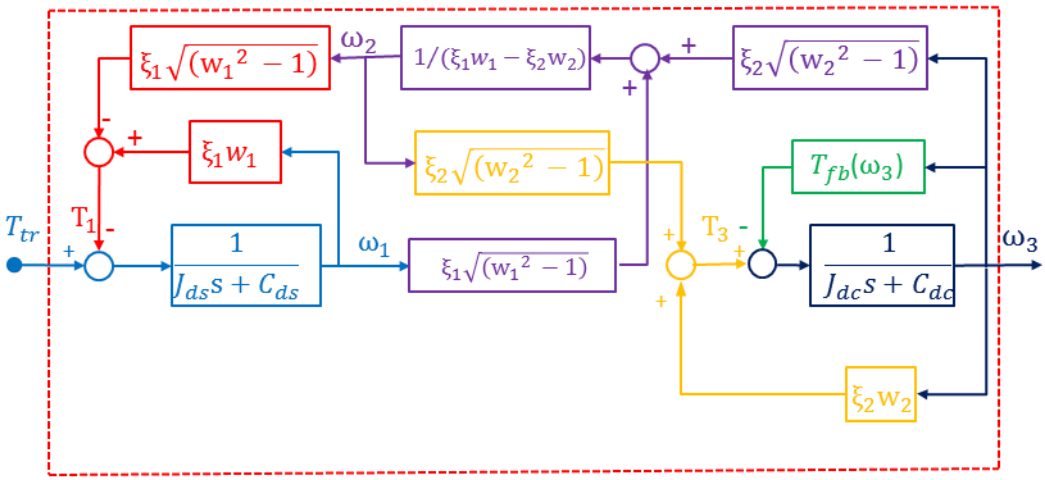

Figure 4-6 Block diagram of the drilling system (LDDLM) (blue: drive system; red: drillpipe; yellow: HWDP; dark blue: drill collar; purple: common point between drillpipe and HWDP)

For the purposes of simulation and from equation 4.15 inlet torque to the drillpipe is the same as equation 4.9, while

$$0=\xi_1\sqrt{(w_1{}^2-1)}\omega_1-\xi_1 w_1\ \omega_2-\xi_2 w_2\,\omega_2+\xi_2\sqrt{(w_2{}^2(s)-1)}\omega_3 \qquad 4.17$$

Substituting equations 4.2, 4.3, 4.12 and 4.13 into equation 4.17 and let $b=\xi$ gives:

$$0 = \frac{a2e^{-t_1 s}}{1 - e^{-2t_1 s}}\omega_1 - \frac{(a + ae^{-2t_1 s})}{1 - e^{-2t_1 s}}\omega_2 - \frac{(b + be^{-2t_2 s})}{1 - e^{-2t_2 s}}\omega_2 + \frac{2be^{-t_2 s}}{1 - e^{-2t_2 s}}\omega_3$$

$$0 = \frac{(1 - e^{-2t_2 s})(2ae^{-t_1 s}\ \omega_1) - (1 - e^{-2t_2 s})(a\omega_2 + ae^{-2t_1 s}\omega_2) -}{(1 - e^{-2t_1 s})(1 - e^{-2t_2 s})}$$

$$\frac{(1 - e^{-2t_1 s})(b\omega_2 + be^{-2t_2 s}\omega_2) + (1 - e^{-2t_1 s})(2be^{-t_2 s})\omega_3}{(1 - e^{-2t_1 s})(1 - e^{-2t_2 s})}$$

$$\omega_2 = 2e^{-t_1 s}\ \omega_1 - 2e^{-(t_1+2t_2)s}\omega_1 - \ e^{-2t_1 s}\omega_2 + e^{-2t_2 s}\omega_2 + e^{-2(t_1+t_2)s}\omega_2 - \frac{b}{a}\omega_2 -$$

$$\frac{b}{a}e^{-2t_2 s}\omega_2 + \frac{b}{a}e^{-2t_1 s}\omega_2 + \frac{b}{a}e^{-2(t_1+t_2)s}\omega_2 + 2\frac{b}{a}e^{-2t_2 s}\omega_3 - 2\frac{b}{a}e^{-(2t_{1+}t_2 s} \quad 4.18$$

From equations 4.4, 4.9, 4.16, 4.18 and the equation of dry friction 3.14, the corresponding simulation model of LDDLM is shown in Figure 4-7. The colour of the model is the same as demonstrated in Figure 4-6.

Figure 4-7 has two subsystem models: one for friction torque as evidenced in Figure 4-4, and the second model as shown in Figure 4-8 which is used to calculate the output velocity of the drillpipe, ω_2, as shown in equation 4.18.

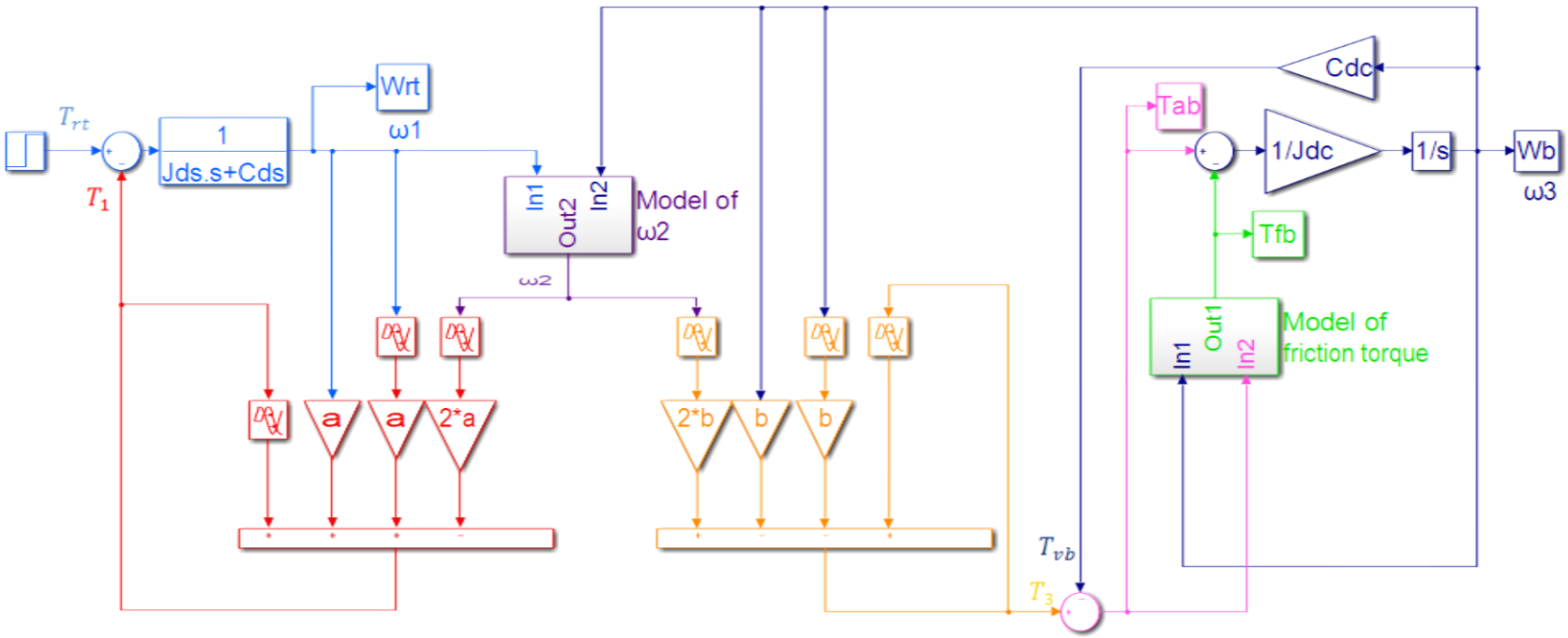

Figure 4-7 Simulation of LDDLM of oil drilling system in Matlab Simulink (blue: drive system; red: drillpipe; yellow: HWDP; dark blue: drill collar; purple: common point between drillpipe and HWDP)

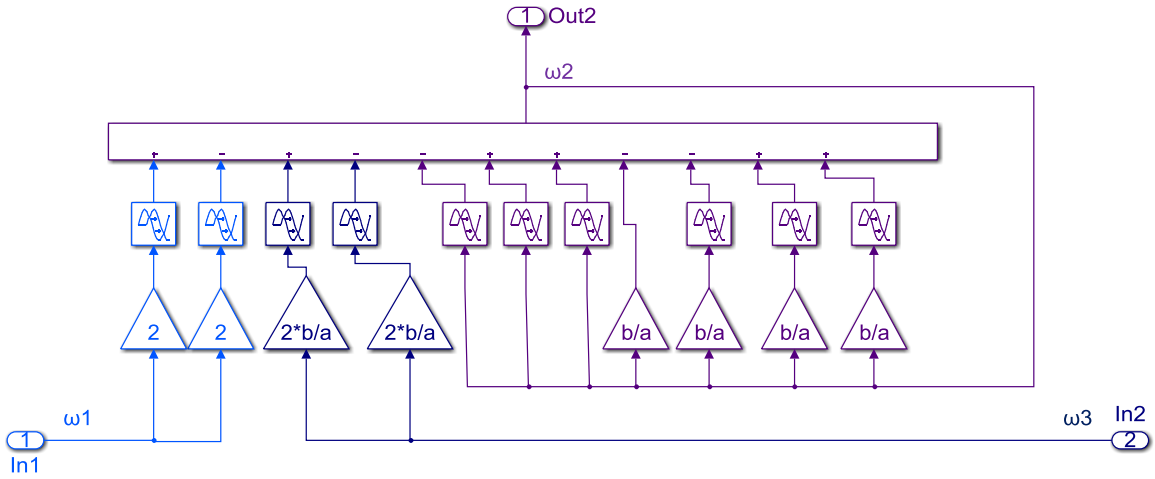

Figure 4-8 Subsystem to calculate the output velocity of the drillpipe (blue: inlet velocity of drillpipe; dark blue: velocity of drill bit; purple: outlet velocity of drillpipe)

4.4 Lumped-Distributed-Distributed-Distributed-Lumped Model (LDDDLM)

A lumped-distributed-distributed-distributed-lumped model (LDDDLM), for the oil drilling system, can be shown in Figure 4-9, where the motor, gearbox, the rotary table and the bit are modelled as rigid, lumped parameters, and pointwise. The drillstring (drillpipe, heavyweight drillpipe (HWDP) and drillcollar) are described as a distributed parameter elements, where the inertia and stiffness of these pipes are continuous functions of the pipe length.

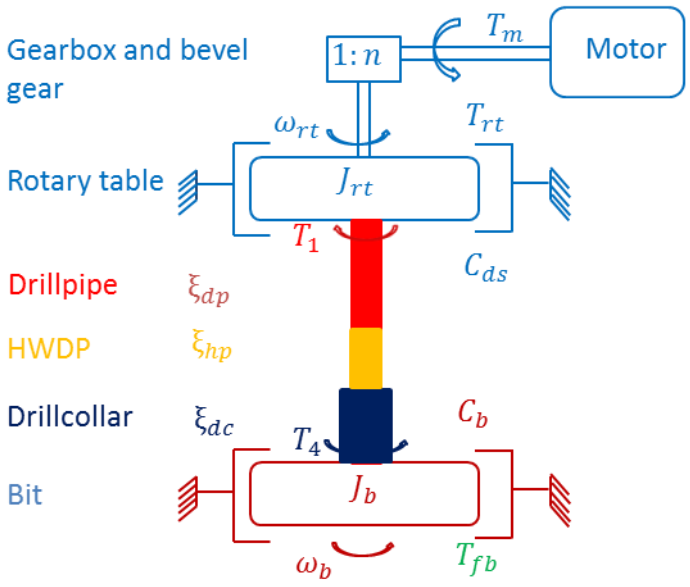

Figure 4-9 Representation of oil drilling system as LDDDL model

In accordance with Figure 4-9 and the general equation of distributed elements for a torsional shaft (equation 3.32), the Laplace transformed model of the distributed elements drillpipe and HWDP are equations 4.1 and 4.12, while for drillcollar is:

$$\begin{bmatrix} T_3(s) \\ T_4(s) \end{bmatrix} = \begin{bmatrix} \xi_3 w_{3\,(s)} & -\xi_3\sqrt{(w_3{}^2(s)\ -1)} \\ \xi_3\sqrt{(w_3{}^2(s)\ -1)} & -\xi_3 w_{3\ (s)} \end{bmatrix} \begin{bmatrix} \omega_3(s) \\ \omega_4(s) \end{bmatrix} \qquad 4.19$$

Where $\mathrm{T}_3(\mathrm{s})$ is the input torque to the drillcollar; $\mathrm{T}_4(\mathrm{s})$ is the output torque from the drillcollar; $\omega_3(\mathrm{s})$ is the angular velocity at the inlet of the drillcollar, $\omega_4(\mathrm{s})$ is the angular velocity at the outlet of the drillcollar $\xi_3 = \xi_{dc}$ Is the characteristic impedance of the drillcollar ($\xi_{dc} = I_{dc}\sqrt{G_s\rho}$).

$$\mathrm{w}_{3\,(\mathrm{s})} = \frac{\mathrm{e}^{2\Gamma_3 l_3}+1}{e^{2\Gamma_3 l_3}-1} = \frac{1+e^{-2t_3 s}}{1-e^{-2t_3 s}} \qquad 4.20$$

$$\sqrt{(w_3{}^2(s)\ -1)} = \frac{2e^{-2\Gamma_3 l_3}}{1-e^{-2\Gamma_3 l_3}} = \frac{2e^{-t_3 s}}{1-e^{-2t_3 s}} \qquad 4.21$$

The system matrix for the complete model shown in Figure 4-9 can be obtained from equations 4.1, 4.12 and 4.19 by eliminating the intermediate elements to give equation 4.22.

$$\begin{bmatrix} T_1(s) \\ 0 \\ 0 \\ T_4(s) \end{bmatrix} =$$

$$\begin{bmatrix} \xi_1 w_{1\,(s)} & -\xi_1\sqrt{({w_1}^2(s)\,-1)} & 0 \quad 0 \\ \xi_1\sqrt{({w_1}^2(s)\,-1)} & -\xi_1 w_1\,(s) - \xi_2 w_{2\,(s)} & \xi_2\sqrt{({w_2}^2(s)\,-1)} \quad 0 \\ 0 & \xi_2\sqrt{({w_2}^2(s)\,-1)} & -\xi_2 w_2\,(s) - \xi_3 w_{3\,(s)} \quad \xi_3\sqrt{({w_3}^2(s)\,-1)} \\ 0 & 0 & \xi_3\sqrt{({w_3}^2(s)\,-1)} \quad -\xi_3 w_3\,(s) \end{bmatrix}$$

$$\begin{bmatrix} \omega_1(s) \\ \omega_2(s) \\ \omega_3(s) \\ \omega_4(s) \end{bmatrix} \qquad 4.22$$

In accordance with the configuration shown in Figure 4-9, the governing equations for the system drive mechanism are equation 4.4, whilst for the drill bit following Laplace transformation with zero initial conditions are

$$T_4(s) - T_{fb} = (J_b s + C_b)\omega_4(s)$$

$$\frac{\omega_3(s)}{T_{fb}(s) - T_4(s)} = \frac{1}{J_b s + C_b} \qquad 4.23$$

From equation 4.4, 4.22 and 4.23 the block diagram representing the drilling system as LDDDLM from Figure 4-9 is shown in Figure 4-10. The dark red represents the bit, and the bright blue represents the common point between HWDP and drillcollar while the other colours the same as Figure 4-6.

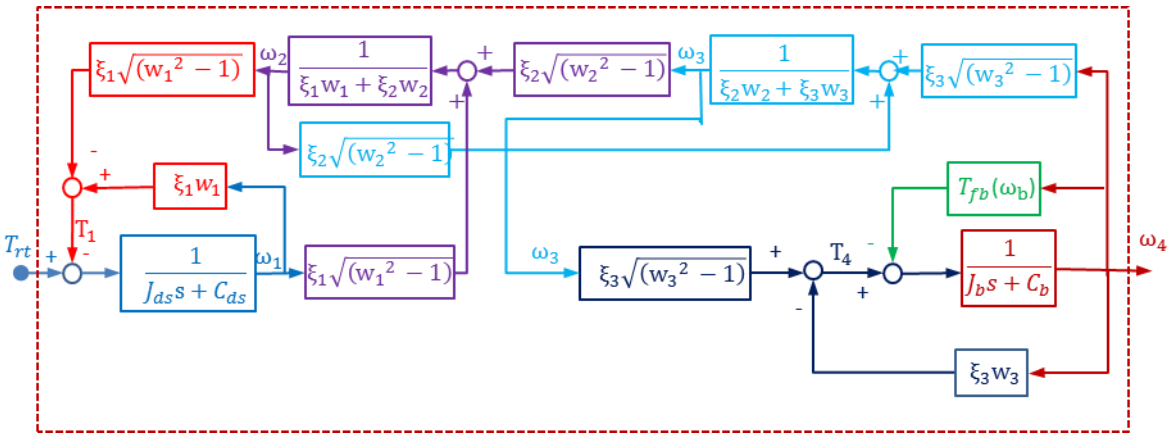

Figure 4-10 Block diagram of the drilling system (LDDDLM) (blue: drive system; red: drillpipe; dark blue: drillcollar; purple: common point between drillpipe and HWDP; bright blue: common point between HWDP and drillcollar; dark red: drill bit)

For the purposes of simulation and from equation 4.22, the inlet torque to the drillpipe is the same as equation 4.9, and the equation to calculate ω_2 is the same as equation 4.18 while ω_3 (common velocity between the drillcollar and HWDP) can be calculated from 4.22 as follows

$$0 = \xi_2\sqrt{(w_2^2-1)}\omega_2 - \xi_2 w_2\ \omega_3 - \xi_3 w_3\,\omega_3 + \xi_3\sqrt{(w_3^2(s)-1)}\omega_4 \qquad 4.24$$

Substituting equations 4.12, 4.13, 4.20 and 4.21 into equation 4.24 and let $c = \xi_3$.

$$\omega_3 = 2e^{-t_2 s}\,\omega_2 - 2e^{-(t_2+2t_3)s}\omega_2 - e^{-2t_2 s}\omega_3 + e^{-2t_3 s}\omega_3 + e^{-2(t_2+t_3)s}\omega_3 - \frac{c}{b}\omega_3 - \frac{c}{b}e^{-2t_3 s}\omega_3 + \frac{c}{b}e^{-2t_2 s}\omega_3 + \frac{c}{b}e^{-2(t_2+t_3)s}\omega_3 + 2\frac{c}{b}e^{-2t_3 s}\omega_4 - 2\frac{c}{b}e^{-(2t_2+t_3 s)}\omega_4 \qquad 4.25$$

Then From equations 4.4, 4.18, 4.23, 4.25 and the equation of dry friction 3.14, the corresponding simulation model is shown in Figure 4-11. The Simulink model has two subsystems; one for friction torque as demonstrated in Figure 4-4, and the other as shown in Figure 4-12 for calculating ω_2 and ω_3 as shown in equations 4.18 and 4.25 respectively.

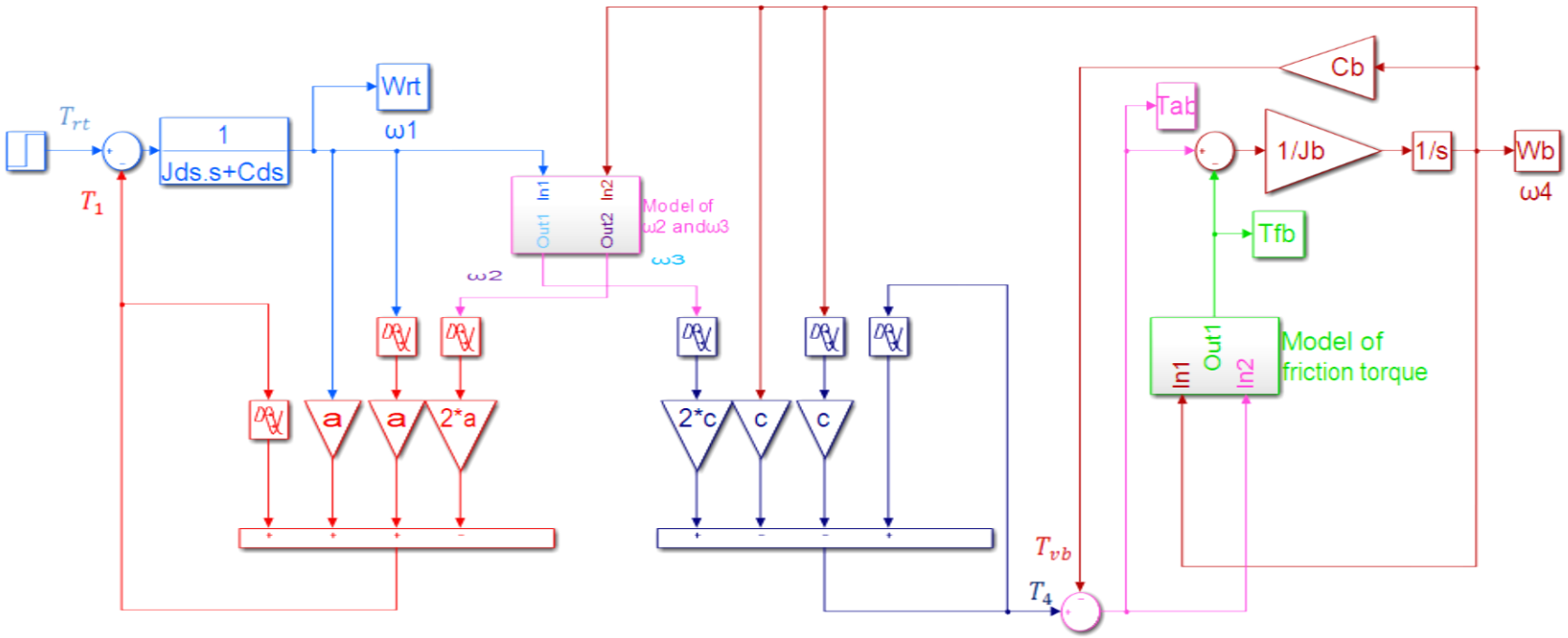

Figure 4-11 Simulation of LDDDLM of oil drilling system in Matlab Simulink (blue: drive system; red: drillpipe; dark blue: drillcollar; dark blue: drill bit)

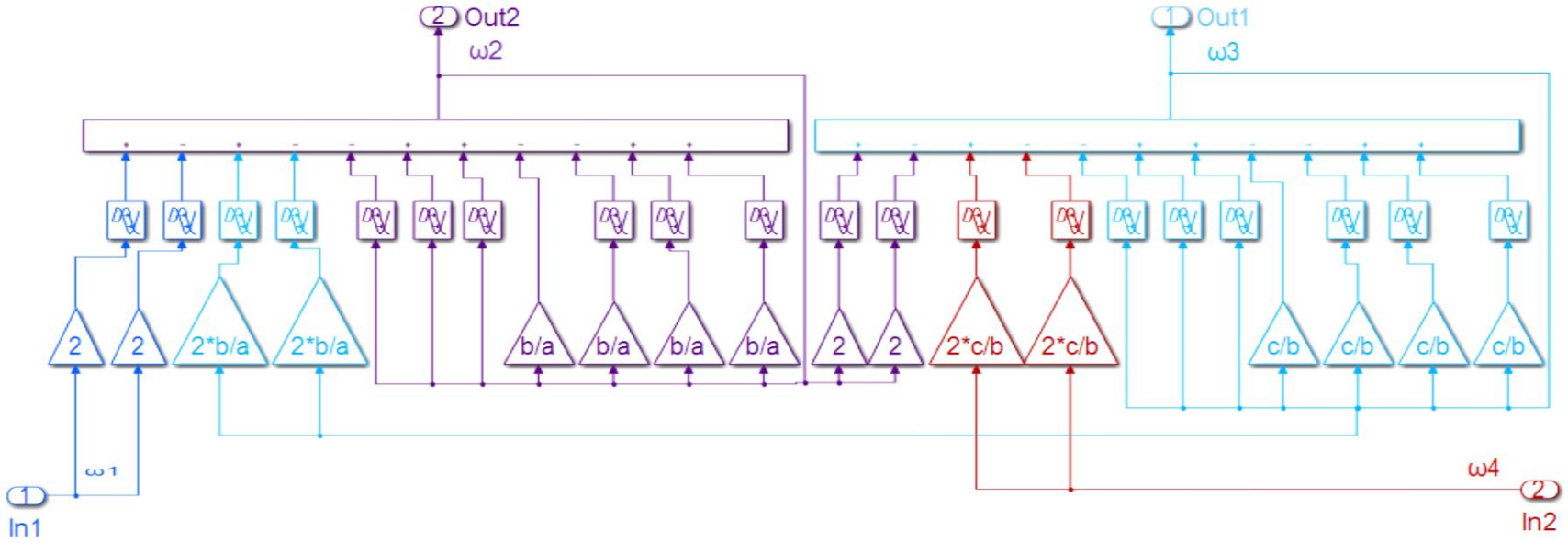

Figure 4-12 Subsystem to calculate the output velocity of drillpipe and HWD (blue: inlet velocity of drillpipe; purple: outlet velocity of drillpipe; bright blue: outlet velocity of HWD; dark red: velocity of drill bit)

4.5 Model parameters

The parameters used in this thesis for simulation correspond to a real drillstring design and are similar to the parameters used by (Jansen et al. 1995; Christoforou and Yigit 2003; Navarro-López and Licéaga-Castro 2009).

These parameters can be divided into two groups. The first group is referred to as fixed parameters which remain constant with the progress of drilling; while the second are variable parameters which change during the drilling operation and depend on the depth of the borehole. Regarding the fixed parameters, either they are fixed in a real drilling operations such as the inertia of rotary table, inertia of motor, shear modulus, etc. or fixed due to the assumption for the purposes of modelling and simulation such as viscosity damping along the drillstring, static and column friction etc.

4.5.1 Fixed parameters

Fixed parameters for both Lumped and Distributed- Lumped models are shown in Table 4-1

Table 4-1 Fixed parameters of the drilling system (Jansen et al. 1995; Christoforou and Yigit 2003; Navarro-López and Licéaga-Castro 2009)

Name	Symbol	Value	Unit
Shear modulus of steel	G_s	79.6×10^9	N / m^2
Density of steel	ρ	7850	kg / m^3
Weight on bit	W_{ob}	50000	N
Length of drillcollar	l_{dc}	210	m
Length of HWDP	l_{hw}	120	m
Outer diameter of drillpipe (5inch)	$d_{o,dp}$	127	mm
Inner diameter of drillpipe (4.408inch)	$d_{i,dp}$	108.6	mm
Outer diameter of HWDP	$d_{o,hw}$	127	mm
Inner diameter of HWDP	$d_{i,hw}$	76.2	mm
Gear ratio	n	7.2	
Inertia mass moment of motor	J_m	23	kgm^2
Inertia mass moment of rotary table	J_{rt}	930	kgm^2
Inertia mass moment of drive system	J_{ds}	2122.3	kgm^2
Equivalent inertia mass moment of BHA	J_{eb}	457.5795	kgm^2
Equivalent damping coefficient of the drive system	C_{ds}	425	Nms / rad
Propagation constant	Γ	0.0003140	s/m
Static friction coefficients	μ_{sb}	0.8	
Coulomb friction coefficients	μ_{cb}	0.5	
The constant of decaying	γ_b	0.9	
A limit velocity interval	$D\omega$	10^{-6}	rev/min
Characteristic impedance of the drillpipe	ξ_{dp}	297	Nms
Characteristic impedance of the HWDP	ξ_{hw}	555.68	Nms
Propagation time of HWDP	t_{hw}	0.0377	s
Propagation time of drillcollar	t_{dc}	0.0659	s

4.5.2 Variable parameters

Three case studies will be presented in this thesis by changing the length of drillpipe and the diameter of the drill bit. The length of the drillpipe ($\boldsymbol{l_{dp}}$) will equal 500m, 2000m and 5700m and the diameter of the drill bit will equal 17.5", 12.25" and 8.5" respectively for all the case study the parameters shown in Table 4-2, Table 4-3 and Table 4-4. The parameters for the three case studies were based upon published work by Jansen et al. 1995; Christoforou and Yigit 2003; Navarro-López and Licéaga-Castro 2009, whilst the remaining parameters were calculated.

Table 4-2 Parameters of drillstring (case study one)

Name	Symbol	Value	Unit
Length of drillpipe	l_{dp}	500	m
Radius of drill bit(8.75 in)	R_b	0.22225	m
Static friction torque on the bit	T_{sb}	8890	Nm
Coulomb friction torque on the bit	T_{cb}	5556.3	Nm
Outer diameter of drillcollar (9inch)	$d_{o,dc}$	228.6	mm
Inner diameter of drillcollar (3inch)	$d_{i,dc}$	76.2	mm
Viscous damping along drillpipe	C_{dp}	10	$Nms\ /\ rad$
Viscous damping along BHA	C_{eb}	30	$Nms\ /\ rad$
Viscous damping along drillcollar and bit	C_{dc}	30	$Nms\ /\ rad$
Viscous damping along bit	C_b	30	$Nms\ /\ rad$
Equivalent inertia mass moment of BHA plus 1/3 of drillpipe	J_{eb}	482.3	kgm^2
Equivalent inertia mass moment of BHA	J_{bh}	466.8	kgm^2
Equivalent inertia mass moment drillcollar plus bit	J_{dc}	445.85	kgm^2
Equivalent inertia mass moment of bit plus shock absorber	J_b	9.34	kgm^2
Drillpipe stiffness	K_{dp}	1892	$Nms\ /\ rad$
Propagation time of drillpipe	t_{dp}	0.1570	s
Characteristic impedance of the drillcollar	ξ_{dc}	6619	Nms

Table 4-3 Parameters of drillstring (case study two)

Name	Symbol	Value	Unit
Length of drillpipe	l_{dp}	2000	m
Radius of drill bit(6.125 in)	R_b	0.155575	m
Static friction torque on the bit	T_{sb}	6223	Nm
Coulomb friction torque on the bit	T_{cb}	3889	Nm
Outer diameter of drillcollar(9inch)	$d_{o,dc}$	228.6	mm
Inner diameter of drillcollar(3inch)	$d_{i,dc}$	76.2	mm
Viscous damping along drillpipe	C_{dp}	42	$Nms\ /\ rad$
Viscous damping along BHA	C_{eb}	40	$Nms\ /\ rad$
Viscous damping along drillcollar and bit	C_{dc}	35	$Nms\ /\ rad$
Viscous damping along bit	C_b	20	$Nms\ /\ rad$
Equivalent inertia mass moment of BHA plus 1/3 of drillpipe	J_{eb}	529	kgm^2
Equivalent inertia mass moment of BHA	J_{bh}	466.8	kgm^2
Inertia mass moment of drillcollar and bit	J_{dc}	445.85	kgm^2
Equivalent inertia mass moment of bit plus shock absorber	J_b	9.34	kgm^2
Drillpipe stiffness	K_{dp}	473	$Nm\ /\ rad$
Propagation time of drillpipe	t_{dp}	0.628	s
Characteristic impedance of drillcollar	ξ_{dc}	6619	Nms

Table 4-4 Parameters of drillstring (case study three)

Name	Symbol	Value	Unit
Length of drillpipe	l_{dp}	5700	m
Radius of drill bit(4.25 in)	R_b	0.10795	m
Static friction torque on the bit	T_{sb}	4318	Nm
Coulomb friction torque on the bit	T_{cb}	2698.75	Nm
Outer diameter of drillcollar(6.75inch)	$d_{o,dc}$	171.45	mm
Inner diameter of drillcollar(3inch)	$d_{i,dc}$	76.2	mm
Viscous damping along drillpipe	C_{dp}	85	$Nms\ /\ rad$
Viscous damping along BHA	C_{eb}	100	$Nms\ /\ rad$
Viscous damping along drillcollar and bit	C_{dc}	80	$Nms\ /\ rad$
Viscous damping along bit	C_b	50	$Nms\ /\ rad$
Equivalent inertia mass moment of BHA plus 1/3 of drillpipe	J_{eb}	335.57	kgm^2
Equivalent inertia mass moment of BHA	J_{bh}	158.32	kgm^2
Equivalent inertia mass moment drillcollar plus bit	J_{dc}	137.38	kgm^2
Equivalent inertia mass moment of bit plus shock absorber	J_b	3	kgm^2
Drillpipe stiffness	K_{dp}	166	$Nm\ /\ rad$
Propagation time of drillpipe	t_{dp}	1.79	s
Characteristic impedance of drillcollar	ξ_{dc}	2037.77	Nms

4.6 Development of Lumped and Lumped-distributed-lumped models

For the purposes of ensuring that the two models were working properly the parameters of the drilling operation such as applied torque on the bit, friction torque on the bit, speed of the rotary table and speed of the bit (T_{ab}, T_{fb}, ω_{rt}, ω_b) were analysed and are discussed below. Case study two (Table 4-3) was used for the LDL model because most of the published studies focussed on drillpipe lengths near to 2000m, where the length of the drillpipe is much larger than the drillcollar and HWDP, and the available measurements for validation were also performed at this length.

In the drilling operation, there are two cases, first when the operation of drilling progresses without any problem of vibration, which means that no stick-slip phenomenon occurs; secondly, when the stick-slip oscillation occurs.

4.6.1 NO Stick-slip

In this case, the stick-slip motion does not occur, and this should be the standard mode of cutting operation. The speed of drilling is typically between 50-250 rev/min depending on the type of formation, but the average speed preferred is 120-125 rev/min, which generally avoids both stick-slip oscillation at lower speeds and lateral whirling at higher speeds (Kriesels et al. 1999.).

As discussed in the derivation of lumped model and distributed-lumped models (section 4.1 and 4.2.1), to start the operation of drilling the applied torque from the drillstring on the bit (T_{ab}), should overcome the static friction torque required to rotate the drill bit and start cutting, as demonstrated in equation 3.15. When cutting continues, the value of the applied torque will be equal to the value of Coulomb friction torque (T_{cb}).

For the given model, the static and Coulomb friction torque were 12446Nm and 7778.8Nm respectively when the weight on the bit was 100KN. As shown in Figure 4-13 and Figure 4-14, the applied torque for LDLM and LM initially increased to overcome the static friction torque and then subsequently decreased in the steady-state period and continued cutting with that value of Coulomb friction torque. The damped natural frequency (ω_d) for both models (LDLM and LM) equals 1.047 rad/sec which is calculated from Figure 4.13 and Figure 4-14 by applying $\omega_d = 2\pi / \tau_d$ where τ_d is the time between two consecutive peaks.

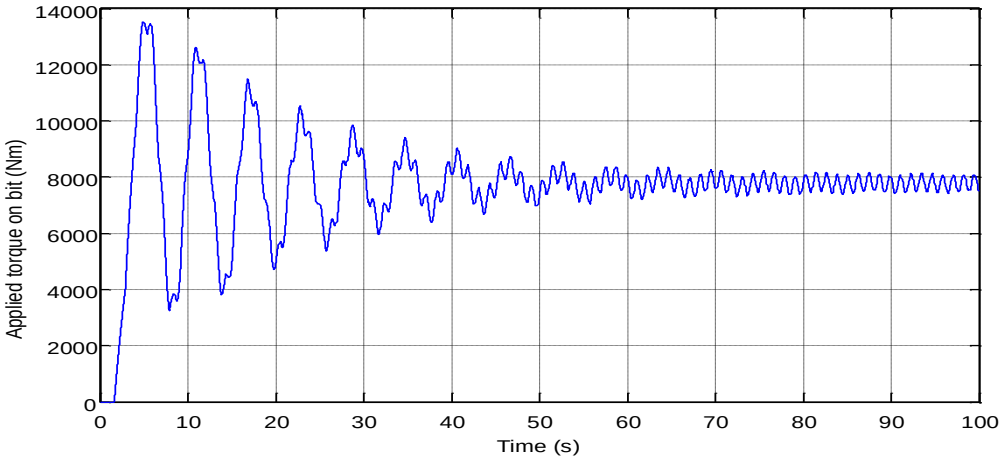

Figure 4-13 Applied torque on the bit of LDLM (no stick-slip)

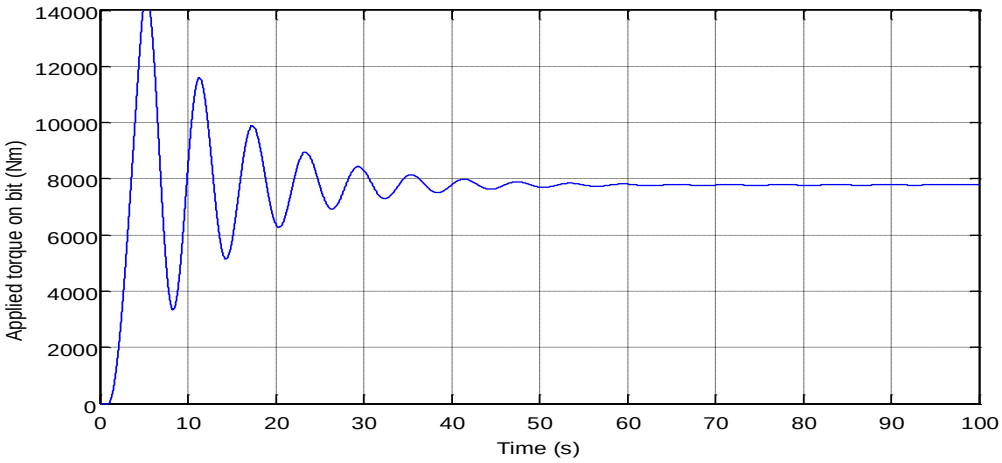

Figure 4-14 Applied torque on the bit of LM (no stick-slip)

In the slipping phase, the friction torque on the bit switches between three values (T_{ab}, T_{sb}, T_{cb}), as demonstrated in equation 3.14 and shown in Figure 3-2. The value of friction torque initially equals the applied load (T_{ab}), until it is equal to static friction torque ($T_{sb} = 12446$) and remains at the same value over a small interval of velocity ($\mathrm{D}\omega$) (in order to solve the problem of discontinuous friction torque) and then falls to the value of Coulomb friction torque ($T_{cb} = 7778.8$) as shown in Figure 4-15 and Figure 4-16.

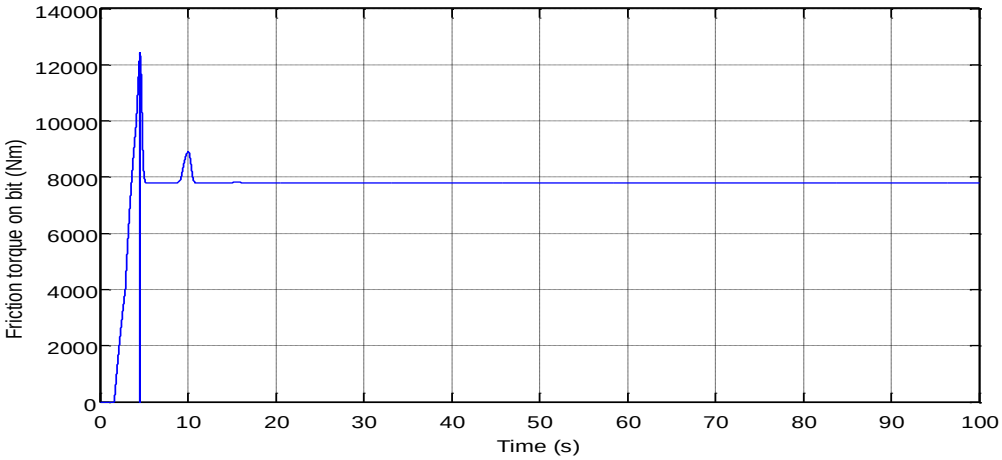

Figure 4-15 Friction torque on the bit of LDLM (no sticking)

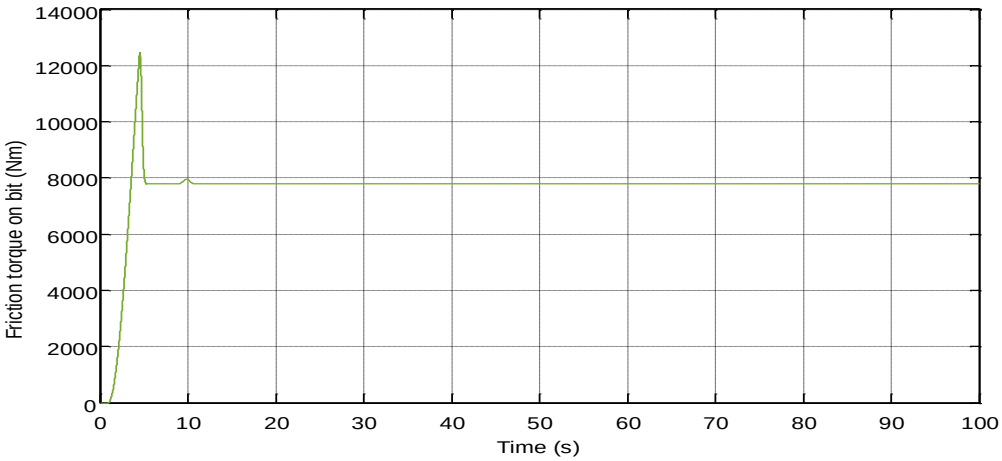

Figure 4-16 Friction torque on the bit of LM (no sticking)

The angular velocity of both the LDLM and LM was increased with the increase of the motor torque and when the transient phase had passed the velocity of the rotary table and BHA was equal for both models as shown in Figure 4-17 and Figure 4-18.

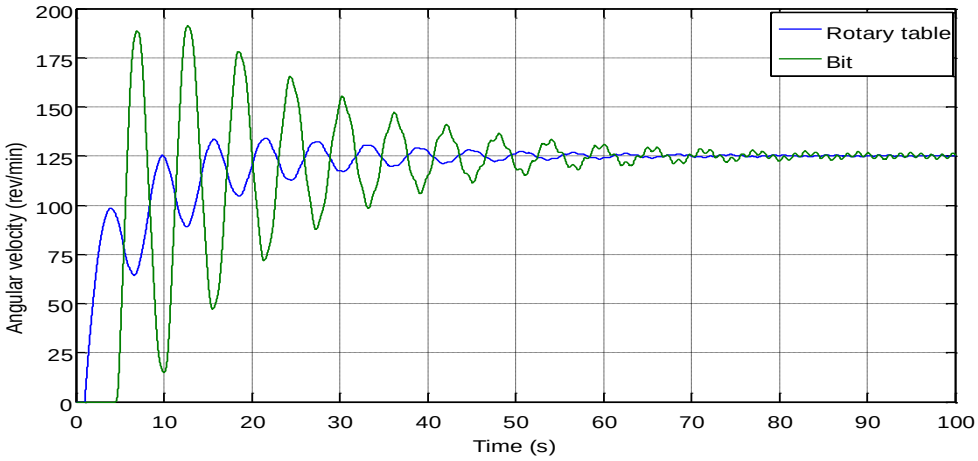

Figure 4-17 Angular velocity of LDLM (no stick-slip)

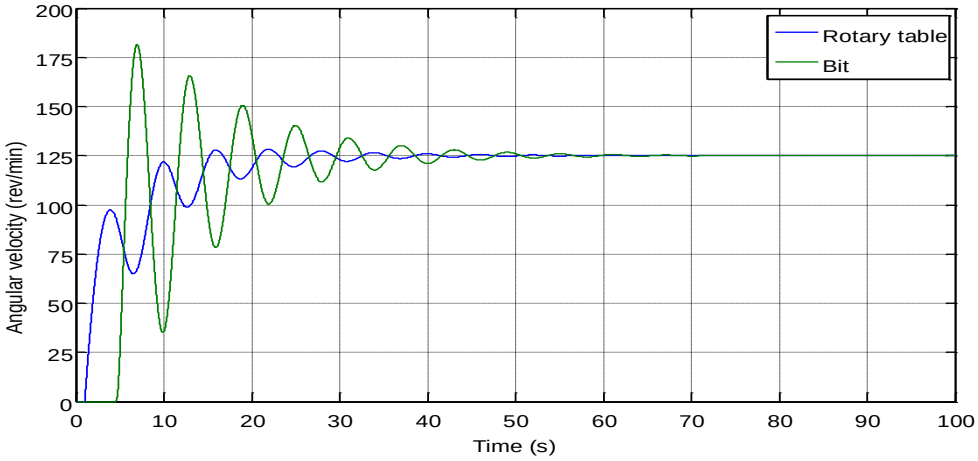

Figure 4-18 Angular velocity of LM (no stick-slip)

4.6.2 Stick-Slip Phase

The stick-slip phenomena occur when the velocity of the rotary table is below the critical rotational speed. Over and above this velocity, stick-slip does not take place whilst below it will occur (Dufeyte and Henneuse, 1991). When cutting hard rock formations where the velocity needs to be lower for a better rate of penetration, stick-slip typically occurs. The velocity recommended to the operators when stick-slip occurs is approximately 50 rev/min (Kriesels et al. 1999).

During stick-slip motion, the applied torque on the bit fluctuates between the static friction torque (T_{sb}) and Coulomb friction torque (T_{cb}) as shown in Figure 4-19. The behaviour of applied torque on the bit can be explained as follows; when the bit completely stops (stick) the velocity of the bit equals zero as shown in Figure 4-20, the applied torque starts to build up in the drillpipe because the rotary table continues to rotate which leads to twist of the drillpipe. When the value of applied torque increases from zero to a value above that of the static friction torque, the bit starts to rotate and reaches maximum value. When the velocity of the bit starts to decrease, the torque will also decrease until the velocity of the bit returns to zero and the torque increases again above static friction torque and the process repeats as shown in Figure 4-21 for LDLM.

The applied torque on the bit for the LM shows the same behaviour as the LDLM and the differences between the two types of models is that the LM shows very smooth response as shown in Figure 4-22, Figure 4-23 and Figure 4-24.

During the stick-slip motion the friction torque on the bit switches between the static friction torque (T_{sb}) and Coulomb friction torque (T_{cb}) as shown in Figure 4-25 and Figure 4-26 for the LDLM and LM respectively.

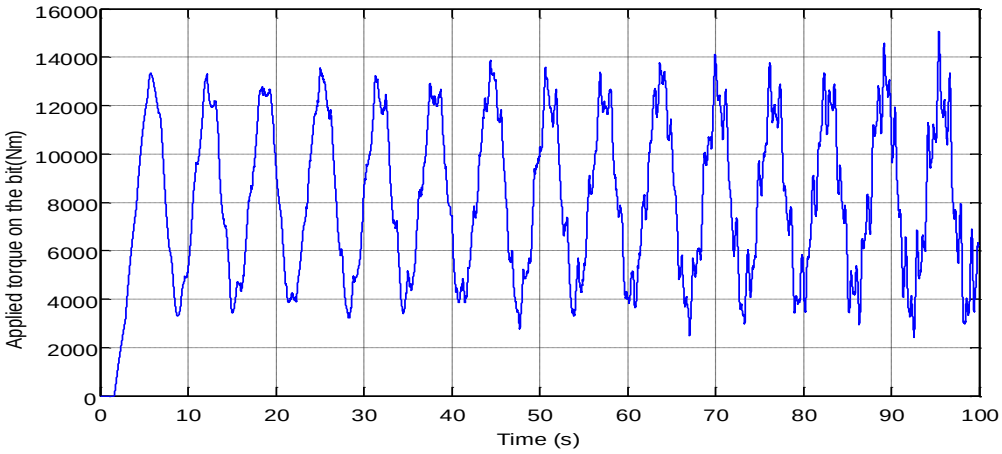

Figure 4-19 Applied torque on the bit LDLM with stick-slip motion

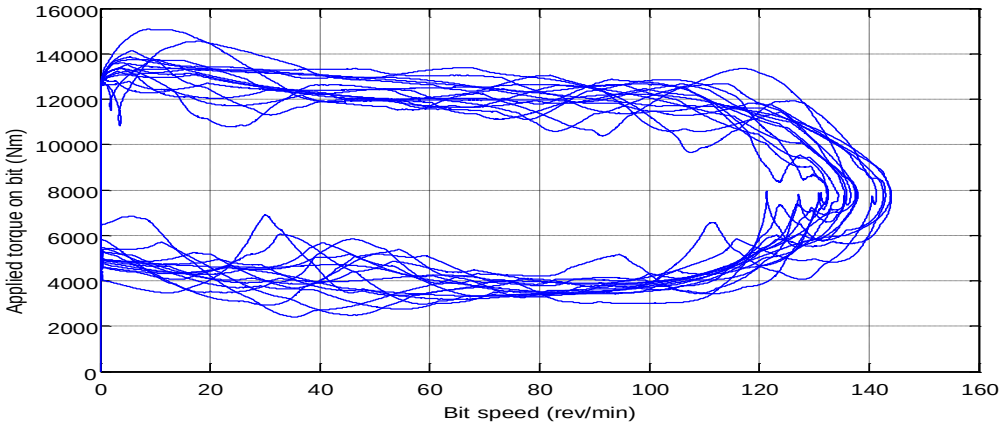

Figure 4-20 Applied torque on the bit versus bit speed for the LDLM with stick-slip motion

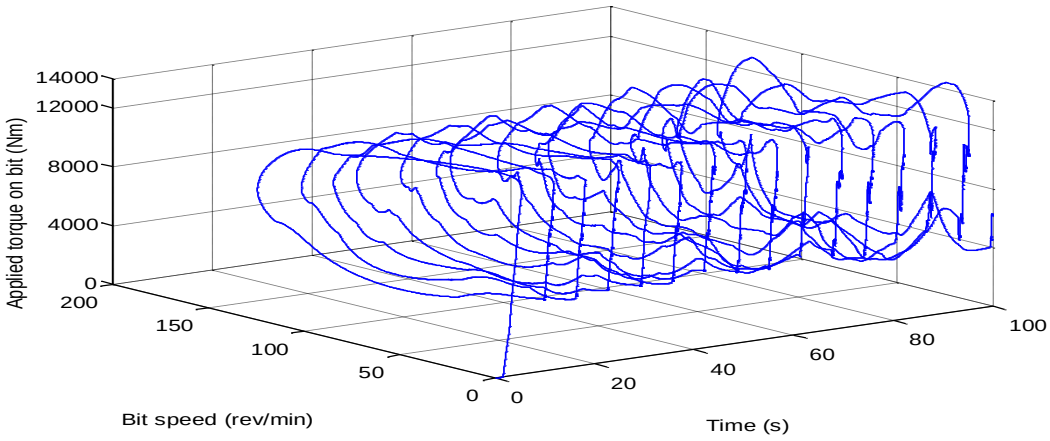

Figure 4-21 3D plot of applied torque on the bit and bit speed against time for the LDLM

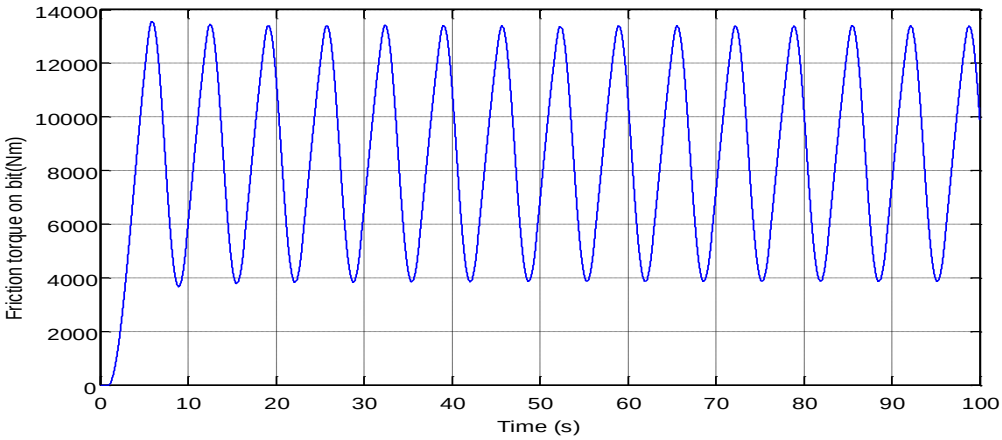

Figure 4-22 Applied torque on the bit of LM with stick-slip motion

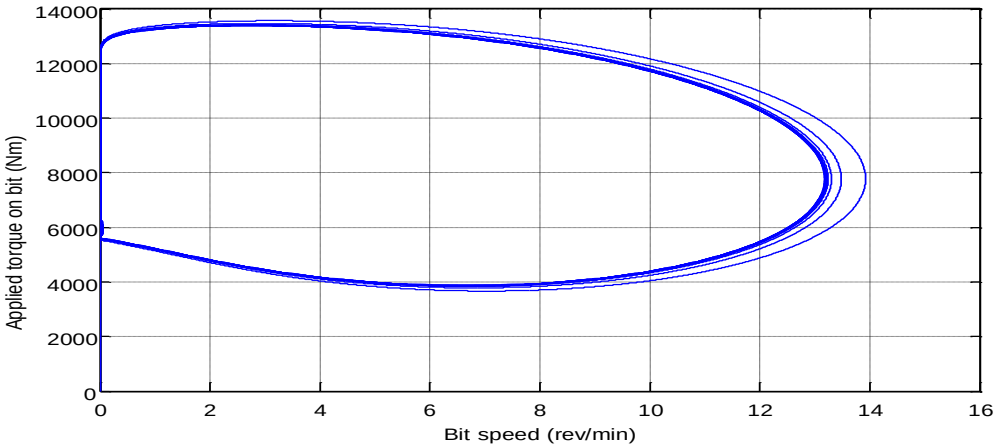

Figure 4-23 Applied torque on the bit versus bit speed for the LM with stick-slip motion

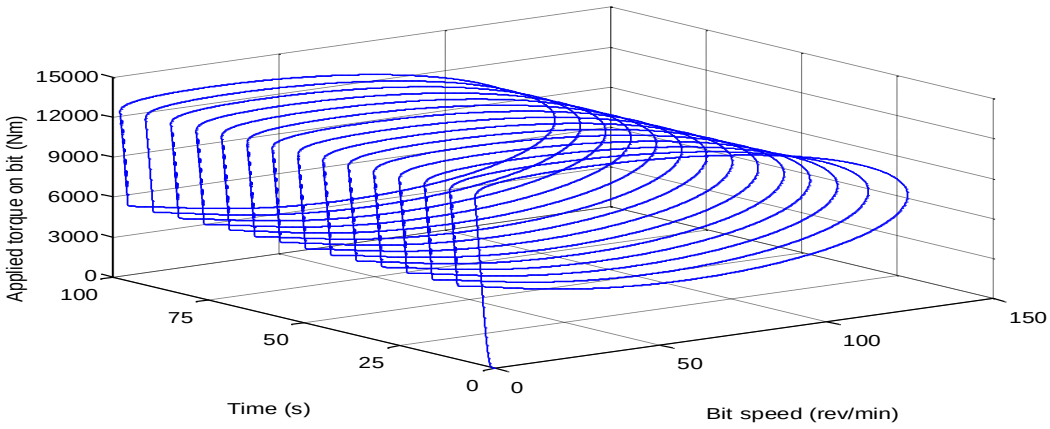

Figure 4-24 3D plot of applied torque on the bit and bit speed against time for the LM

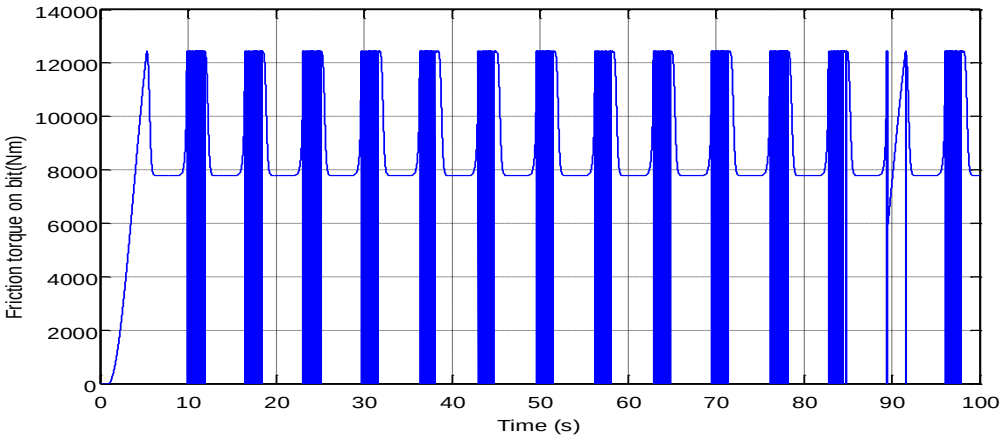

Figure 4-25 Friction torque on the bit of LDLM with stick-slip motion

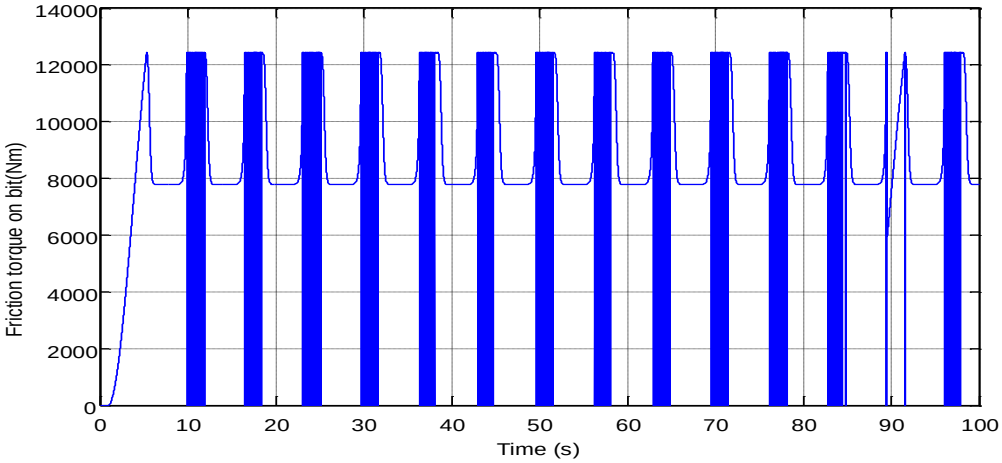

Figure 4-26 Friction torque on the bit of LM with stick-slip motion

In the real drilling process, the velocity of the rotary table fluctuates between two speeds during stick-slip motion, but the fluctuation is small due to the distance from the BHA and therefore the operator is not able to notice this fluctuation. However, the velocity of the BHA will be fluctuating between zero and two-to-three times the rotary table speed and the operator will recognise this by a vibration in the drillstring. The general trend of stick-slip oscillation is very clear in both models, as shown in Figure 4-27 and Figure 4-28 for the LDLM and LM respectively when the velocity of BHA fluctuated between zero

and two times the velocity of the rotary table. There is some difference in the shape of both models, and this will be discussed in the next chapter.

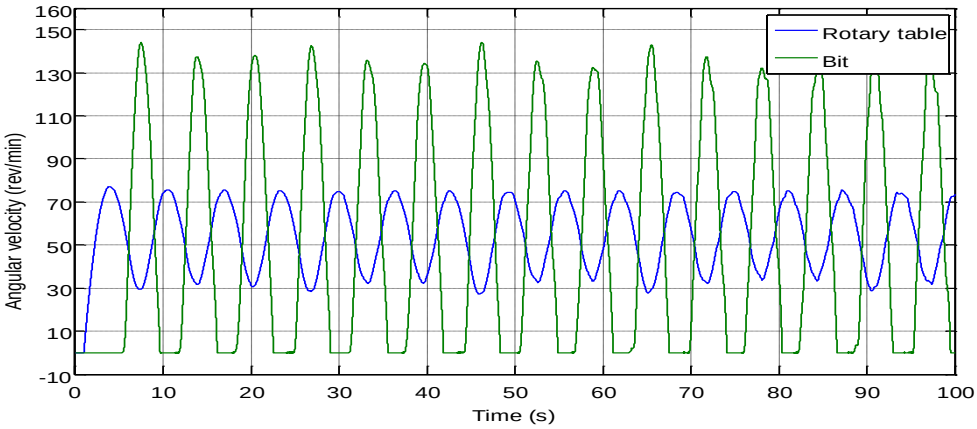

Figure 4-27 Stick-slip oscillation: LDLM

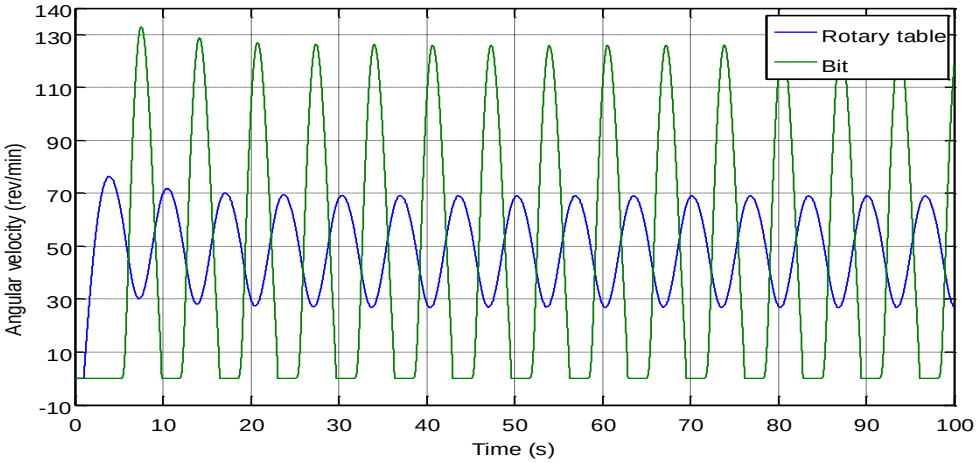

Figure 4-28 Stick-slip oscillation: LM

4.7 Validation of models

The LDDDLM and LM have been validated against a real measurement of bit velocity as a function of time for an approximate 25 second period of stick-slip vibration from (Veeningen 2011) and for 5 second from(Ledgerwood et al. 2013) . The real world data was obtained from (Veeningen 2011) and is reproduced in Figure 4-29. The data is for a 2000m long drillstring and shows that the drill bit exhibited stick-slip vibration with the velocity fluctuating between 0 and 300

rev/min. The parameters which are used in this validation for the simulations are similar to the parameters used by Veeningen (2011) and Ledgerwood et al. (2013) and are shown in Table 4.5 whilst other parameters are taken from Table 4-1 as shown in Table 4-6, with the remaining parameters being calculated from the drill string geometry. Using the same parameters for the LDDDLM and LM the simulated results can be seen in Figure 4-30, Figure 4-31 and Figure 4-32 for LDDDLM and Figure 4-33 for LM respectively.

Table 4-5 Validation parameters of drillstring (Veeningen 2011 and Ledgerwood et al.2013)

Name	Symbol	Value	Unit
Shear modulus of steel	G_s	79.6×10^9	N / m^2
Density of steel	ρ	7850	kg / m^3
Outer and inner diameter of drillpipe	$d_{o,dp}, d_{i,dp}$	127,108.6	mm
Outer and inner diameter of HWDP	$d_{o,hw,} d_{i,hw}$	127,76.2	mm
Outer and inner diameter of drillcollar	$d_{o,dc}, d_{i,dc}$	228.6,76.2	mm
Characteristic impedance of drillpipe	ξ_{dp}	297	Nms
Characteristic impedance of HWDP	ξ_{hw}	555.68	Nms
Characteristic impedance of drillcollar	ξ_{dc}	6619	Nms
Radius of drill bit(for,550,1500, 2000m)	R_b	0.155575	m
Radius of drill bit(for 2840m)	R_b	0.10795	m
Equivalent inertia mass moment of BHA	J_{eb}	457.5795	kgm^2
Equivalent inertia mass moment of bit	J_b	9.3	kgm^2
Weight on bit (for 550,1500,2840m)	W_{ob}	300,250,150	KN

Table 4-6 Parameters are taken from table 4.1

Name	Symbol	Value	Unit
Length of drillcollar and HWDP	l_{dc}, l_{hw}	210,120	m
Inertia mass moment of drive system	J_{ds}	2122.3	kgm^2
Equivalent damping coefficient of the drive system	C_{ds}	425	Nms / rad
Propagation constant	Γ	0,0003140	s/m
Viscous damping of drillpipe(for 2000m)	C_{dp}	42	Nms / rad
Viscous damping along BHA	C_{eb}	40	Nms / rad
Viscous damping along bit	C_b	20	Nms / rad
Static and Coulomb friction coefficients	μ_{sb}, μ_{cb}	0.8,0.5	
The constant of decaying	γ_b	0.9	
A limit velocity interval	$D\omega$	10^{-6}	rev/min

The LDDDL model shows a general trend similar to that of the system illustrated in Figure 4-29 where the velocity shows similar stick-slip behaviour between comparable speeds combined with higher frequency oscillations as shown in Figure 4-30. The difference between the LDDDLM and the real measurement is that the ‘stick’ period is shorter in the simulation compared to the actual system. This is because the friction between the stabilisers and the borehole wall was not modelled in the simulation; this would require more torque to overcome the static friction to start the rotation of the bit.

In Figure 4-31 the static friction was increased by increasing the weight on the bit from 200KN in Figure 4.14 to 250KN, but the amplitude was kept the same by increasing the torque on the bit from 22.5KNm to 25.6KNm. The time of sticking increased due to the increase in the static friction; this required more time to twist the drillpipe to get the applied torque to overcome the static friction. However, it can be seen that the sticking time in the real measurement was still longer than in the LDDDLM.

To compensate for this, the decay constant (γ_b) was changed from 0.9 in Figure 4-30 and Figure 4-31 to 0.2 in order to see if this parameter would have significant effect on the sticking time. Figure 4-32 shows that as a result of reducing the decay constant, the sticking time increased and the theoretical result were now very similar to the real measurement, both in terms of the higher frequency oscillations and period of sticking for LDDDLM.

To show the differences between the LM and LDDDLM the conventional two degrees of freedom lumped model was used to obtain Figure 4-33 by applying the same parameters as in Figure 4-32. It is clear from comparison of Figure 4-32 and Figure 4-33 that the LM did not show the high-frequency

oscillation and generated a far smoother shape compared with the LDDDLM and the real measurement.

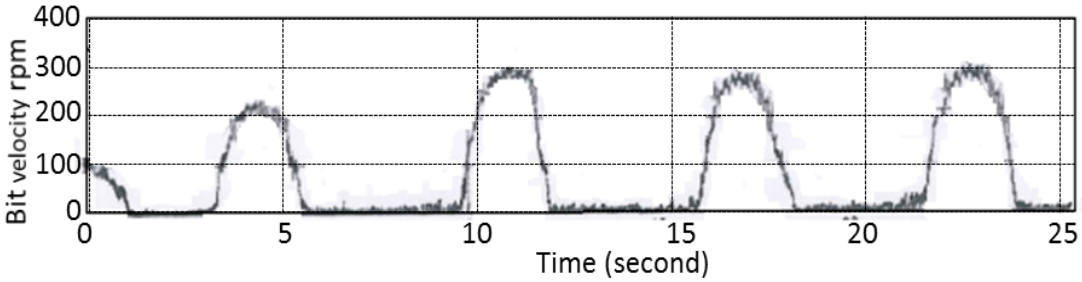

Figure 4-29 Real measurements of stick-slip vibration reproduced from(Veeningen 2011)

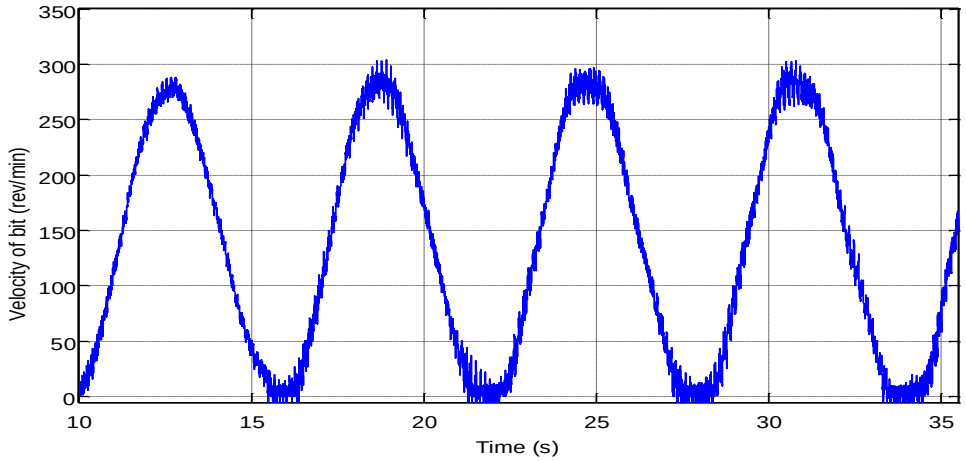

Figure 4-30 Stick-slip vibration of LDDDLM (Wob=200KN,μ_{sb}=0.8, γ_b=0.9)

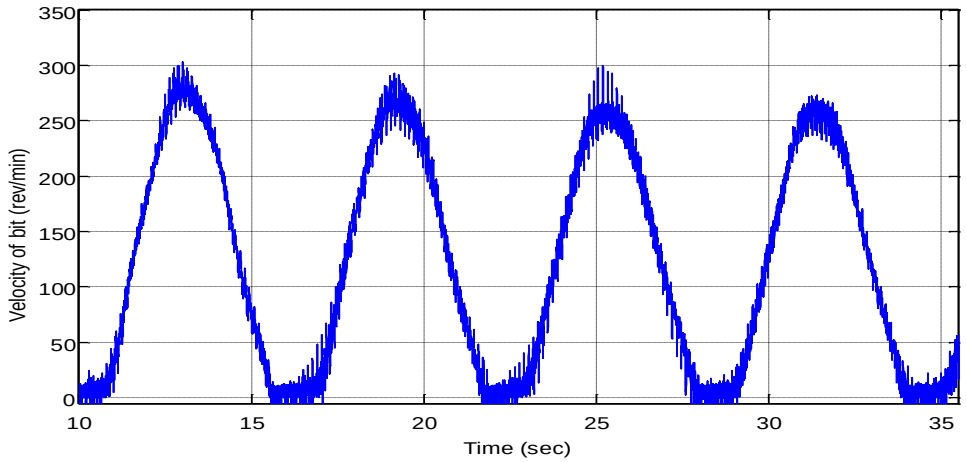

Figure 4-31 Stick-slip vibration of LDDDLM (Wob=250KN,μ_{sb}=0.8, γ_b=0.9)

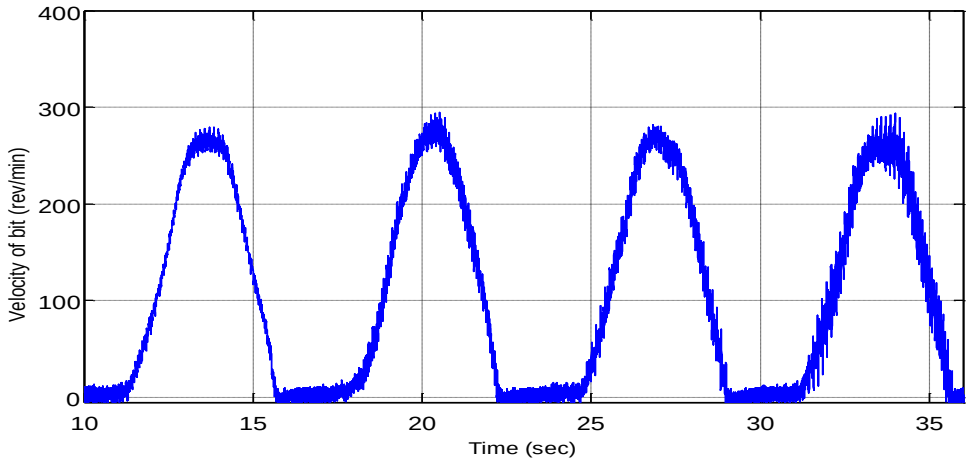

Figure 4-32 Stick-slip vibration of LDDDLM (Wob=200KN,μ_{sb}=0.8, γ_b=0.2)

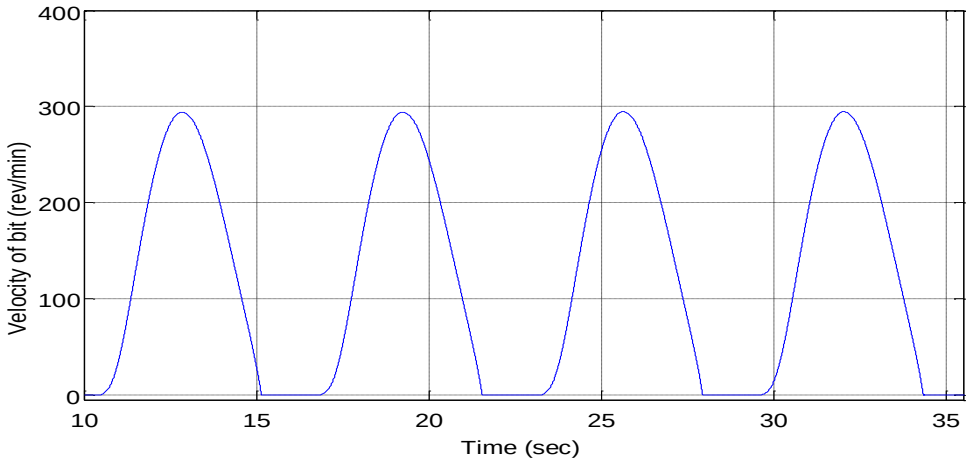

Figure 4-33 Stick-slip vibration of LM (Wob=200KN,μ_{sb}=0.8, γ_b=0.2)

The LDDDL model was also validated against a real measurement of bit velocity for an approximate 5 seconds period of stick-slip vibration in three different depths of oilwell (Ledgerwood et al. 2013). Figure 4-34 shows an example of the angular velocity of the bit measured using a MWD (measurement while drilling) vibration monitor during the stick-slip vibration in the field for a 550m well depth. The simulation result (Figure 4-35) shows excellent agreement with this measurement. It can be seen that the LDDDLM shows a high-frequency pattern of stick-slip vibration similar to real measurement; the differences in the time of sticking can be attributed to

different types of friction between the drillstring and oilwell wall that lead to an increase in the time of sticking.

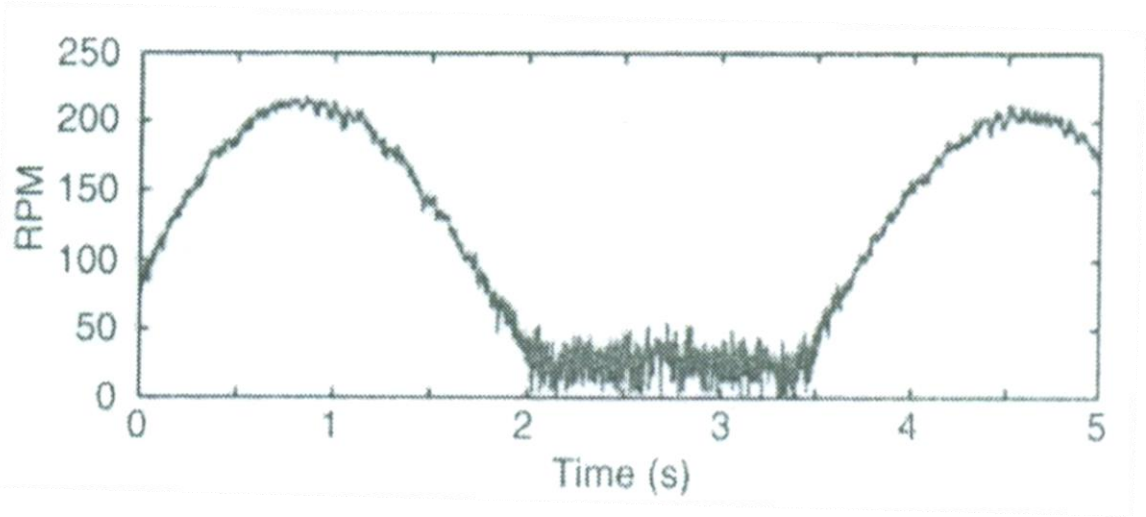

Figure 4-34 **Real measurements of stick-slip vibration (drillstring length = 550m)(Ledgerwood et al. 2013)**

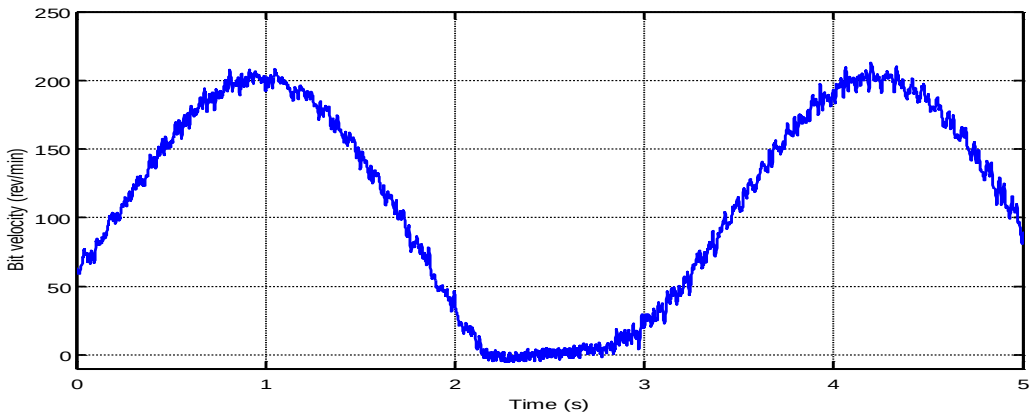

Figure 4-35 Stick-slip vibration of LDDDLM (drillstring length = 550m)

One of the issues that lead to an increase in the probability of stick-slip and increase in the time of sticking is increased drilling depths. These usually result in having to cut through harder rock formations and the longer drillstrings have a lower stiffness. Figure 4-36 shows an example from the real measurement where the time of sticking increased from the 1.5 sec of Figure 4-34, at a depth of 550m, to more than 2 sec at a depth of 1500m. The LDDDLM also correlates

well with this observation as shown in Figure 4-37 where the time of sticking increases near to 2 seconds. However, this was still less than the actual measurement due to the un-modelled well-bore friction as mentioned previously. In addition, the time taken for the bit velocity to fall from 200 rev/min to zero was approximately 1.2 seconds for the real measurement while in the simulation it was marginally longer at 1.5 seconds; again this can be attributed to the un-modelled bore-stabiliser friction which decreases the velocity more rapidly.

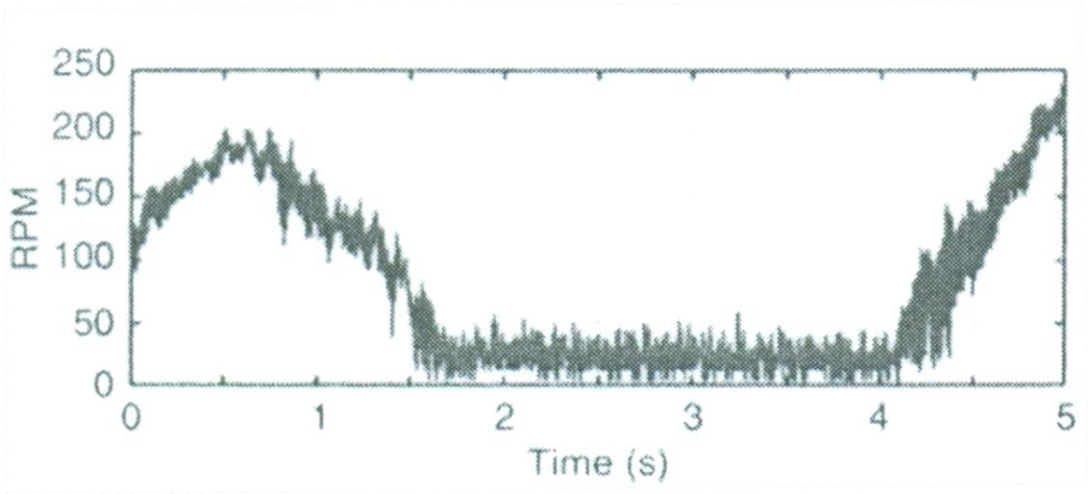

Figure 4-36 Real measurements of stick-slip vibration (drillstring length = 1500m) (Ledgerwood et al. 2013)

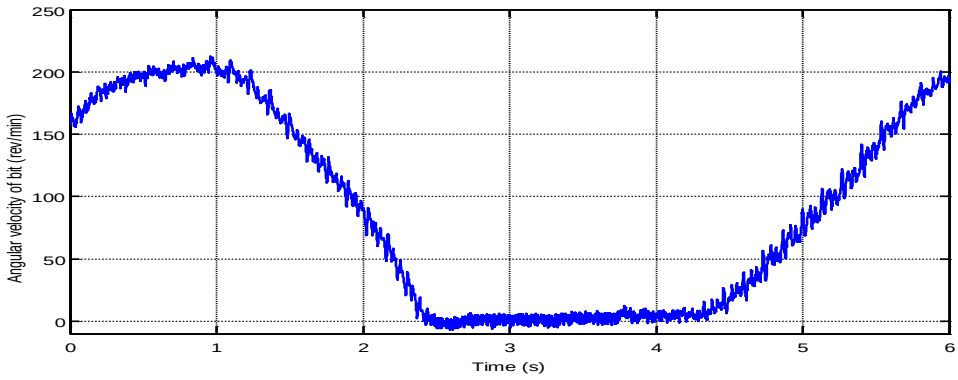

Figure 4-37 Stick-slip vibrations of LDDDLM (drillstring length=1500m)

The final comparison is conducted for a well of depth 2840m as shown in Figure 4-38. It can be seen from the figure that the period of stick-slip is so long

that it could not be completely captured in 5 seconds; the increase in the sticking time is due to the decrease in the stiffness of the drillstring and increase in the hardness of the rock at such depths. The simulation results at this depth, shown in Figure 4-39, showed apparent agreement with the actual measurement in both showing the high frequency and long sticking time.

From the three comparisons, it can be concluded that LDDDLM showed a very high similarity to the behaviour of real drillstrings under the stick-slip motion and therefore was deemed to be acceptably validated in order to progress with the parametric studies.

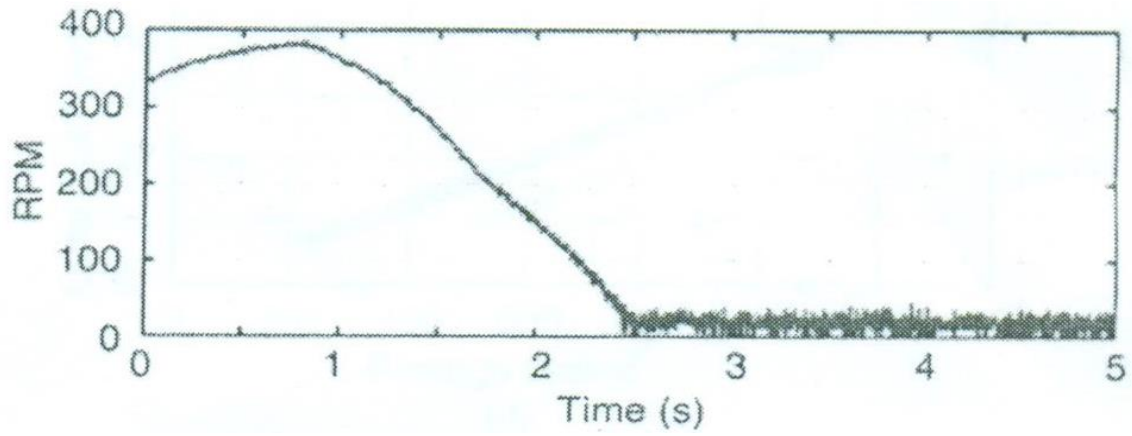

Figure 4-38 Stick-slip vibration of LDDDLM (drillstring length =2840m) (Ledgerwood et al. 2013)

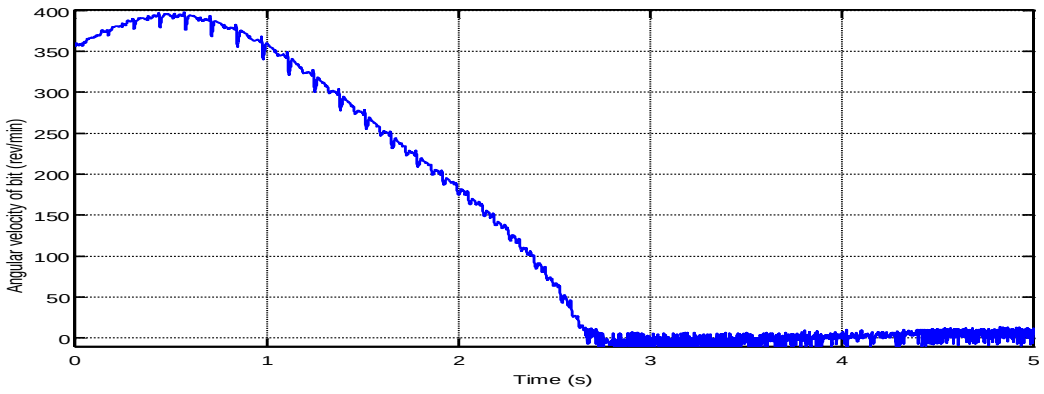

Figure 4-39 Stick-slip vibration of LDDDLM (drillstring length = 2840m; Wob = 100kN; sticking time = 4s)

4.8 Summary

This chapter has presented the simulation of LM and DLM. The simulation of the lumped model has presented as shown in Figure 4-1 by considering the drilling system as a torsional pendulum of two degrees of freedom. The DLM approach has been used to model the drilling system by depending on the general equation of distributed torsional shaft (3.73). Three types of DLM have been used to model the drilling system.

First LDL model by considering the drillpipe as a distributed element while the drive system and the BHA as a lumped elements. The whole derivative has presented, and the simulation model is shown in Figure 4-4. Secondly, the LDDLM was introduced by adding the HWDP as another distributed element in the drilling system as shown in Figure 4-5 and the simulation is demonstrated in Figure 4-7 and Figure 4-8. Finally, a LDDDLM was presented by considering the drillcollar also as a distributed element as shown in Figure 4-9 and the simulation model was shown in Figure 4-11 and Figure 4-12.

The parameters of the two models were divided into two groups as fixed parameters and variable parameters as shown in Tables 4.1-4.5.

The DLM type, LDDDLM, was validated against a real measurement Veeningen (2011) and Ledgerwood (2013). The two models, LDLM and LM, were analysed to demonstrate the behaviour of drilling parameters ($T_{ab}, T_{fb}, \omega_{rt}, \omega_b$), during a cutting operation in the two modes: no stick-slip motion and when the stick-slip oscillation occurs. In the next chapter the parameters will be used to provide comparisons between the DLM and LM.

CHAPTER 5: COMPARISON BETWEEN HYBRID MODELS AND LUMPED MODEL

Chapter 5

Comparison between Hybrid Models and Lumped Model

In Chapter 4, the lumped approach and hybrid approach with three types of models, LDLM, LDDLM and LDDDLM of an oil well drilling system were presented as shown in Figure 4-1, Figure 4-4, Figure 4-7 and Figure 4-11 respectively. Also the general behaviour of the main parameters ($T_{ab}, T_{fb}, \omega_{rt}, \omega_b$) of both models in the ordinary mode of drilling, where there is no stick-slip motion and when the stick-slip oscillation occurs, were demonstrated.

In this chapter the main differences between the hybrid and lumped modelling approaches in their ability to accurately describe the behaviour of the main parameters ($T_{ab},\ ,T_{rt}, \omega_{rt}\ and\ \omega_b$) of an oil drilling system will be discussed in order to show which is the best model that can be used to reflect the behaviour of these parameters in slip phase and stick-slip phase in a real oil drilling system.

Three cases will be used for comparison between the models by choosing differing lengths of drillpipe: 500m, 2000m and 5700m. The parameters of these cases were presented in Chapter 4 in Tables 4.1-4.4.

First, the comparison between the four types of models will be in the slip phase when the oil drilling system behaves in an ordinary manner, and the velocity of drilling is 125 rev/min. Secondly, the comparison between the models at the critical speed (ω_{cr}), to show which model is more sensitive in showing the

critical speed. Finally, at stick-slip when the velocity of the drilling is low between 20 rev/min to 50 rev/min.

5.1 Comparison between Distributed-Lumped (Hybrid) Models and the Lumped Model.

The modelling of an oil drilling system is considered one of the most effective ways to study the stick-slip vibration to use an optimum solution to suppress the stick-slip oscillation either by an active or passive approach, intending to reducing the damage to a drilling system, decrease the cost and other issues as demonstrated in the literature chapter.

The average speed that is used in oil drilling system is between 30 rev/min and 150 rev/min (Omojuwa et al. 2012). The typical speed that is used in the slip phase is around 120-125 rev/min where there is no stick-slip vibration and when the stick-slip occurs the desired speed of drilling is 50 rev/min. Therefore, the comparison between the four models will cover this range of velocity in order to show the ability of each model to give the whole picture of drilling in both low and high speed drilling.

5.1.1 Case study one ($l_{dp} = 500m$)

During the drilling operation, the desired speed of drilling in an ordinary mode where there is no stick-slip oscillation is around 125 rev/min. Therefore, the first comparison between the two types of modelling (lumped and hybrid) is at the desired speed where there is no stick-slip.

Table 5-1 shows the result of simulations of the four models when the length of the drillpipe is 500m. It can be seen from the results of the simulation that different values of rotary torque were applied to get the same speed of drilling for all models. Instead of that the rotary torque of LM and LDLM is the same

(11515 Nm) to get the desired speed of drilling but the transient responses for the velocity of bit (ω_b), as shown in Figure 5-1 for LM and LDLM, differs where the fluctuating and decay time in LDLM is 75sec whereas for the LM it is 50sec. This highlights one limitation of the lumped model in that it cannot predict the transient response.

The pattern of the velocity of the LDDLM as shown in Figure 5-1 is similar to LDLM in both fluctuation and decay time while the torque of the rotary table is 11445 Nm. The rotary torque of the LDDDLM is 11380 Nm, and the model shows more fluctuation and a larger decay time (>75 seconds) than all the other three models as shown in Figure 5-1. Despite this difference between the four models, in general the pattern of velocities is similar for all models.

Figure 5-2 shows the response of applied torque on the bit (T_{ab}) for the four models. It can be seen from this figure that the applied torque on bit for the LM, LDLM and LDDLM were similar but the fluctuation and decay time for the LDLM and LDDLM was bigger than that of the LM. This is due to the flexibility of both the drillpipe and HWDP and also due to the fact that hybrid modelling takes the length of drillpipe and HWDP into consideration when modelling the drillstring.

The applied torque on the bit for the LDDDLM as shown in Figure 5-2 demonstrated more stability than the other three models, and there was no fluctuation because the stiffness of the drillcollar is very high when compared with that of the drillpipe and HWDP. It can be seen from Figure 5-3 that the torque at the top of the drillstring (T_1) is similar for the four models and the fluctuation has increased for the hybrid models as a result of taking the length into consideration for all types of drillstring pipe (drillpipe, HWDP and drillcollar).

Table 5-1 Simulation result of case one ($l_{dp} = 500m$)

Model type	Torque at 125 rev/min	Torque at critical velocity	Stick-slip torque	Critical velocity (ω_{cr})	Torque at low velocity
LM	11515 Nm	10260 Nm	10250 Nm	98.7 rev/min	7000 Nm
LDLM	11515 Nm	10470 Nm	10460 Nm	103 rev/min	7000 Nm
LDDLM	11445 Nm	10520 Nm	10510 Nm	105.5rev/min	7000 Nm
LDDDLM	11380 Nm	10540 Nm	9970 Nm	107 rev/min	7000 Nm

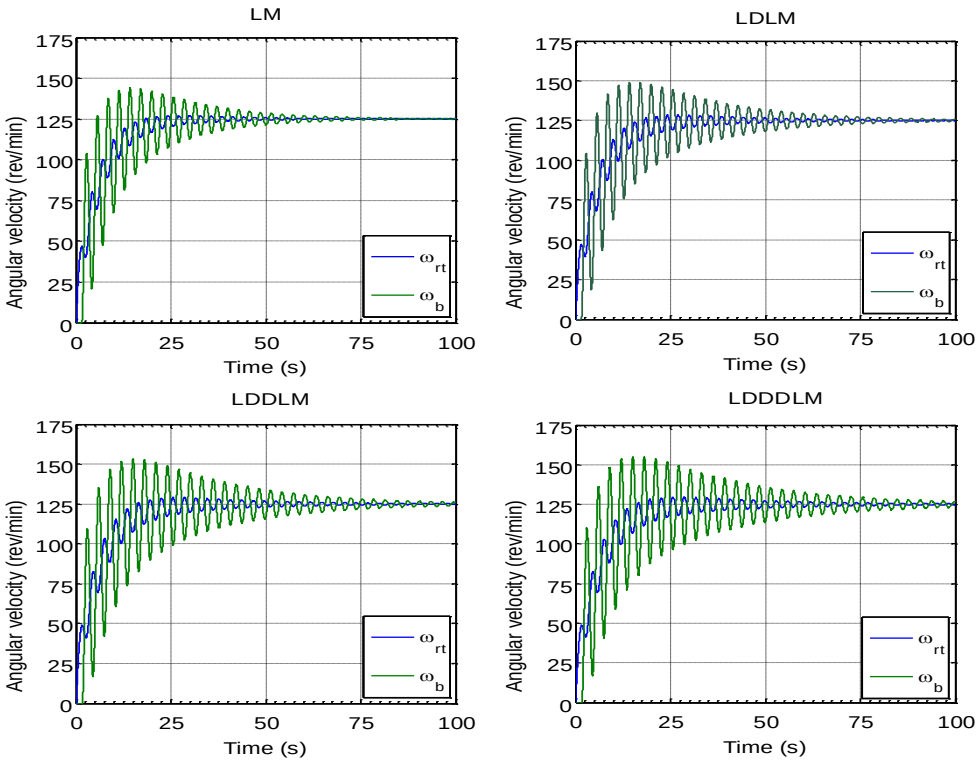

Figure 5-1 Angular velocity of Lumped model (LM) and Distributed-Lumped models (LDLM, LDDLM and LDDDLM) at 125rev/min (case 1)

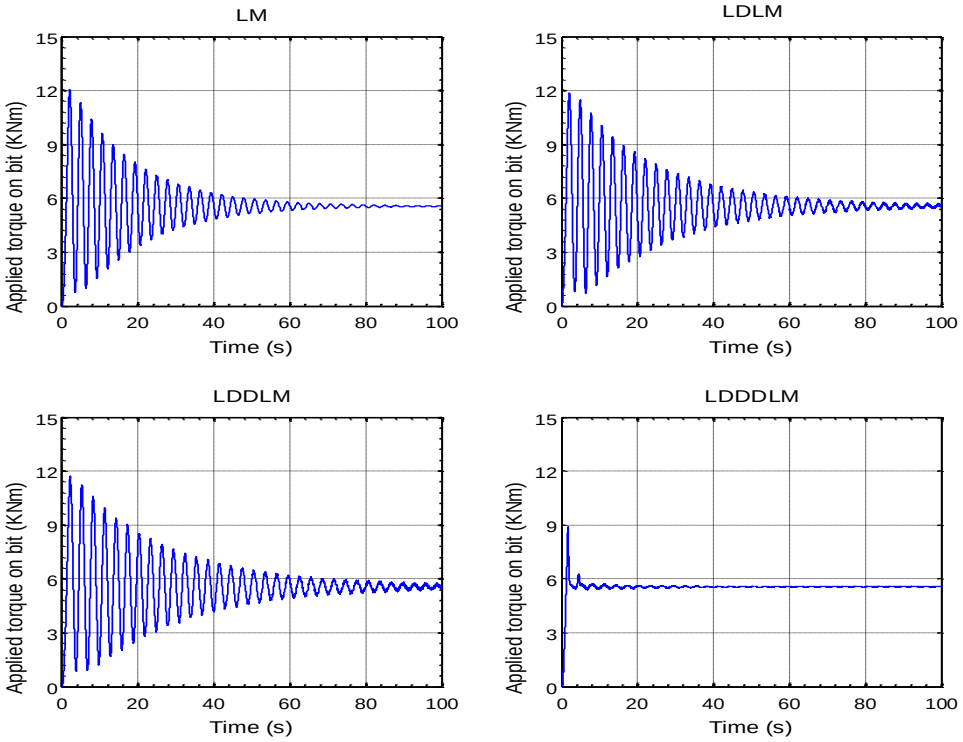

Figure 5-2 Applied torque on bit of Lumped model (LM) and Distributed-Lumped models (LDLM, LDDLM and LDDDLM) at 125rev/min (case 1)

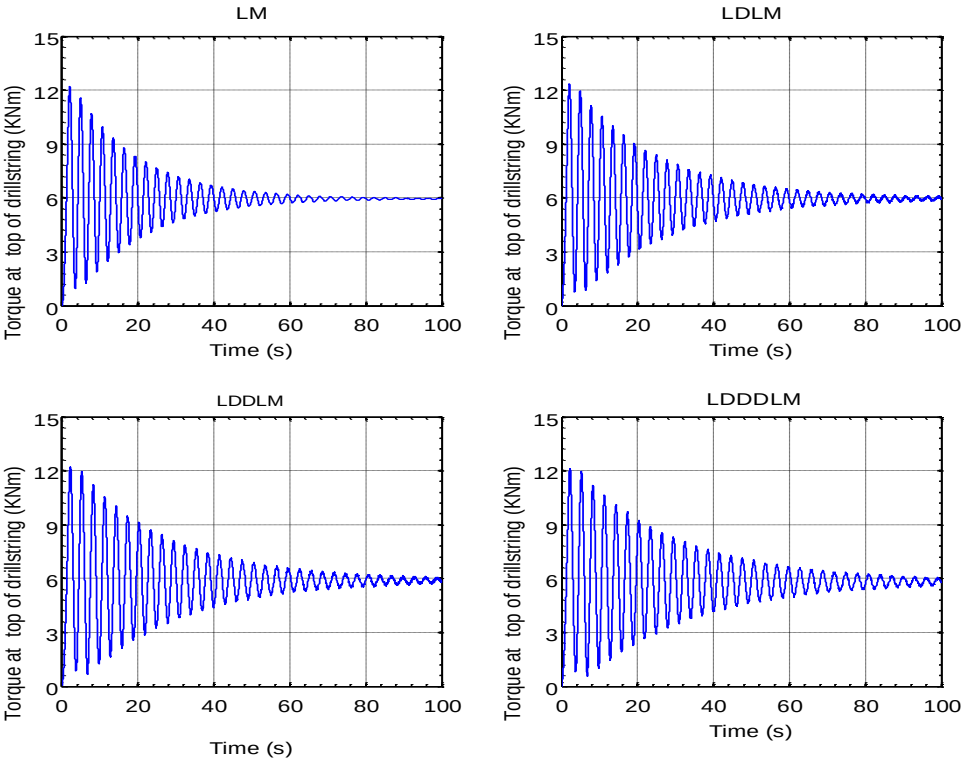

Figure 5-3 Torque at the top of Lumped model (LM) and Distributed-Lumped models (LDLM, LDDLM and LDDDLM) at 125rev/min (case 1)

One of the significant parameters which plays a fatal role in oil drilling system is the critical speed; above this velocity there is no stick-slip whilst under this velocity stick-slip oscillation occurs. The driller can recognise the critical speed from their experience when the sound of the motor starts to increase and decrease and also from the fluctuation of the motor current or torque. Therefore, the operator tries to keep the velocity above this value by choosing the appropriate weight on the bit.

Figure 5-4 shows the speed of the rotary table which represents the critical speed of each model. The value of this velocity is 98.7rev/min, 103rev/min, 105rev/min and 107rev/min for LM, LDLM, LDDLM and LDDDLM respectively. It can be seen from Figure 5-4 and the values of critical speed (Table 5-1) that the hybrid models predict a higher critical speed compared to the lumped model but in general, for this length of drillstring, there is no significant difference between each model.

In the case of decreasing the velocity of the rotary table below the critical speed, stick-slip will be initiated. Thus the effect of running each model at the four critical velocities predicted in Table 5-1 can be shown. Decreasing the torque of the rotary table to 10510Nm showed that stick-slip occurred for only 15 seconds for the LDDDLM and then converted to torsional vibrations with no bit stoppage, whilst the LDDLM predicted continuing stick-slip vibration as shown in Figure 5-5(A). By decreasing the torque of rotary table below 10460Nm, stick-slip also occurred in the LDLM as shown in Figure 5-5 (B).

When the torque of rotary table was decreased to 10250Nm stick-slip began in the LM while for LDDDLM, it still occurred for only 28 sec as shown in Figure 5.5 (C). When the torque was reduced to 9970Nm stick-slip continued for LDDDLM as shown in Figure 5-5(D). It can be seen that by decreasing the

torque of the LM, LDLM and LDDLM just below the critical velocity torque of by approximately 10Nm the stick-slip motion began, whilst for the LDDDLM stick-slip could not be sustained and it was required to decrease the torque by approximately 570 Nm to maintain the stick-slip behaviour.

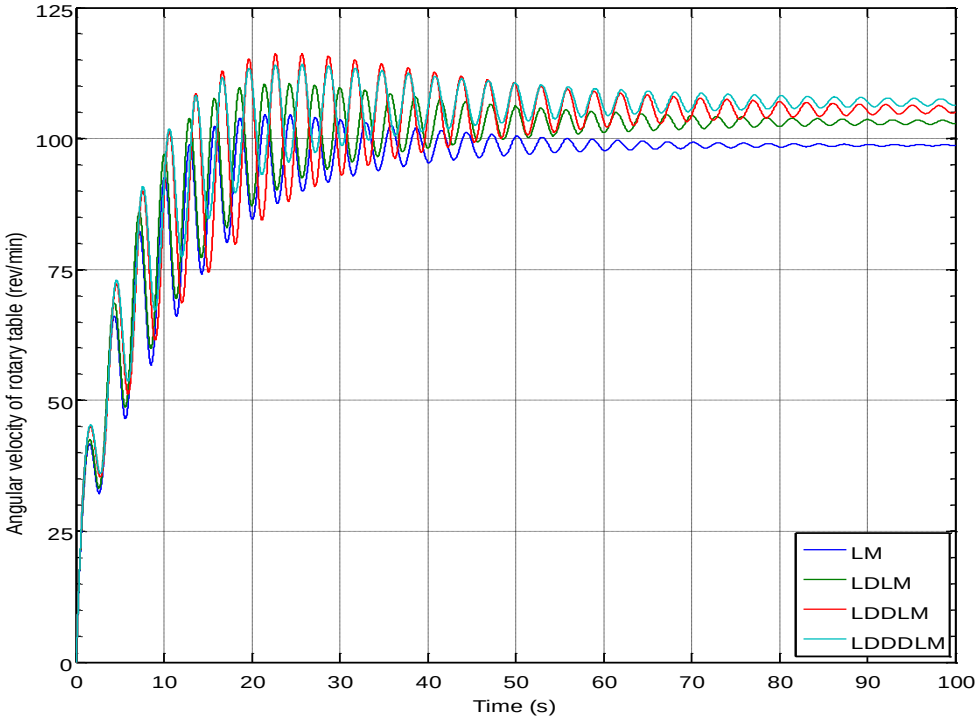

Figure 5-4 Comparison between critical speed of Lumped model (LM) and Distributed-Lumped models (LDLM, LDDLM and LDDDLM) (case 1)

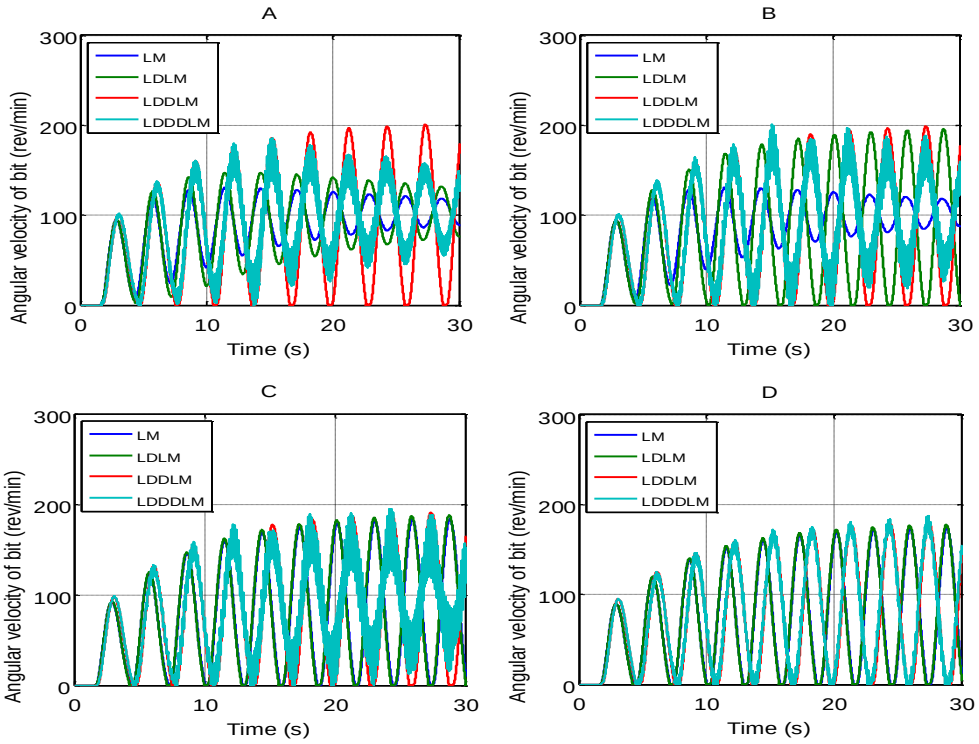

Figure 5-5 Stick-slip below the critical speed of Lumped model (LM) and Distributed-Lumped models (LDLM, LDDLM and LDDDLM) (A: stick-slip torque of LDDLM; B: stick-slip torque of LDDLM and LDLM; C: stick-slip torque of LDDLM, LDLM and LM; D: stick-slip torque of LDDLM, LDLM, LM and LDDDLM) (case 1)

Stick-slip is considered the leading cause of reducing ROP, increasing cost, premature bit wear, etc., therefore a study of the behaviour of the key drilling parameters under stick-slip is significant in increasing the understanding of the stick-slip phenomena.

For the following study, the torque of rotary table was reduced to 7000Nm for all four types of model, and it can be is seen from Figure 5-6 that all models showed the stick-slip oscillation where the velocity of the rotary table fluctuated between 0 and 60 rev/min. It can be seen from the LM, LDLM and LDDLM that the general trend of stick-slip vibration was similar where the velocity of the bit fluctuated between zero and a fixed upper value. This similarity is a result of the

relatively short length of drillpipe, which leads to an increase in the rigidity of the drillstring for all models; also, the delay time is small.

The LDDDLM showed a difference when compared to the other three models by demonstrating additional high-frequency vibration with the velocity of the bit fluctuating around zero in the stick phase and fluctuating around 60 rev/min in the slip phase.

Calculated values showed that the applied torque on the bit in the stick-slip phase would fluctuate between the static friction torque (8890 Nm) and dynamic friction torque (5556.3 Nm). It can be seen from Figure 5-7 that the LM, LDLM and LDDLM showed a similar pattern of applied torque on the bit, while the LDDDLM showed clear difference with higher frequencies present. This is because the LDDDLM includes the torsional stiffness of the drillcollar (100370 Nm/rad) which is very high when compared with both the drillpipe (1892 Nm/ rad/) and HWDP (14746 Nm/rad).

On the other hand, the torque at the top of drillstring exhibited a similar pattern for all models as shown in Figure 5-8 with a slight difference for the LDDDLM. This is because the high-frequency oscillations have mostly been damped out before reaching the top of the drillpipe.

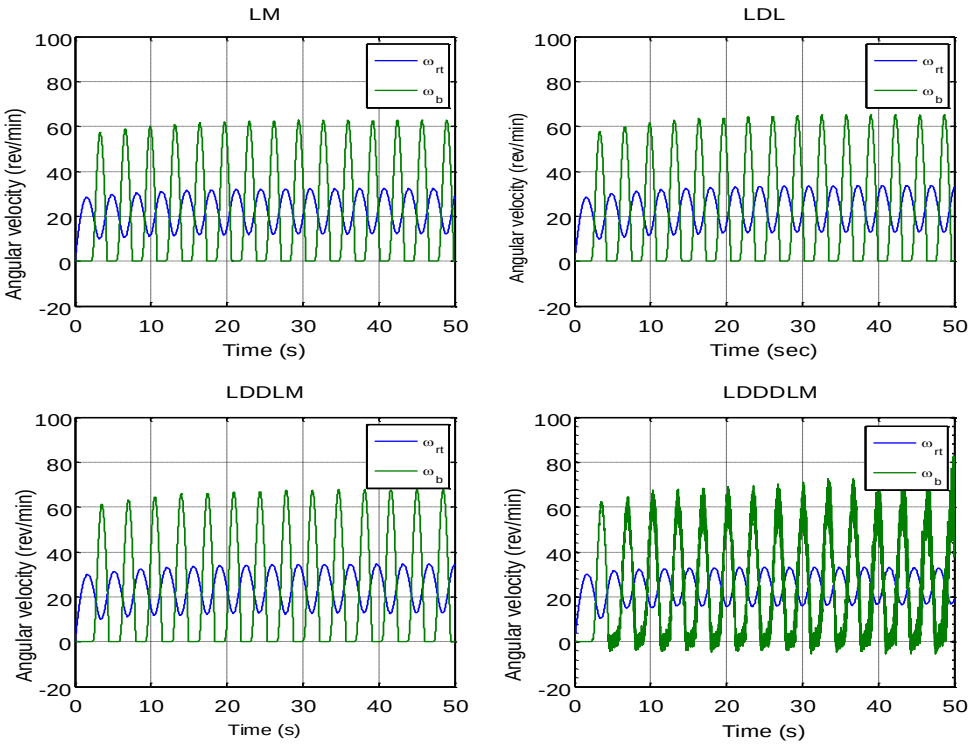

Figure 5-6 Stick-slip at low velocity for the Lumped model (LM) and Distributed-Lumped models (LDLM, LDDLM and LDDDLM) (case 1)

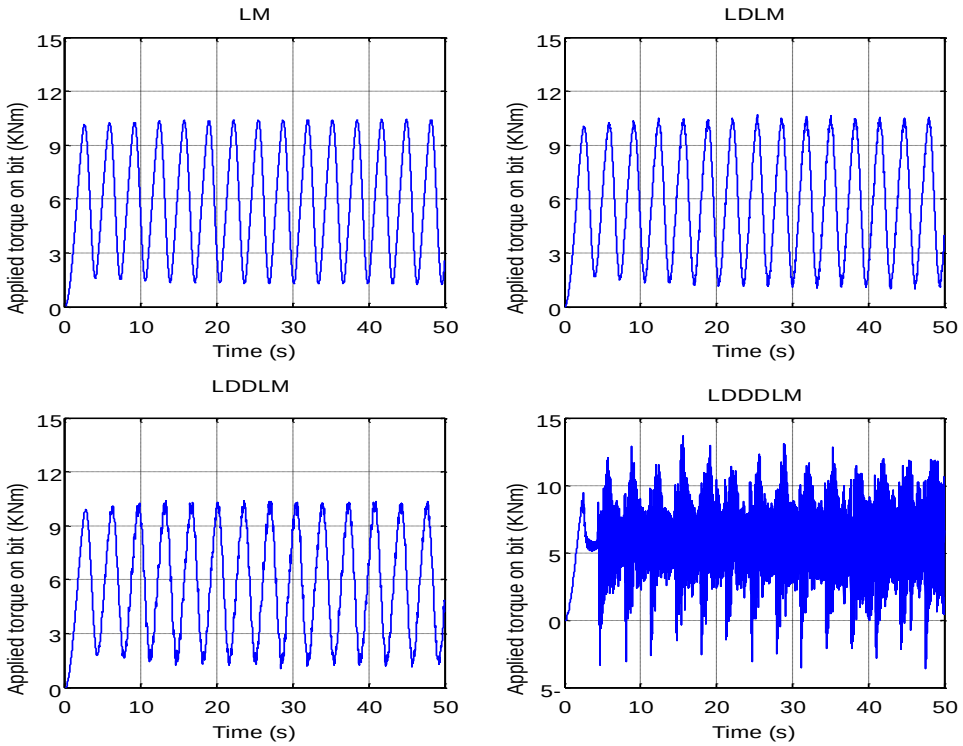

Figure 5-7 Applied torque on the bit in the stick-slip phase for the Lumped model (LM) and Distributed-Lumped models (LDLM, LDDLM and LDDDLM) (case 1)

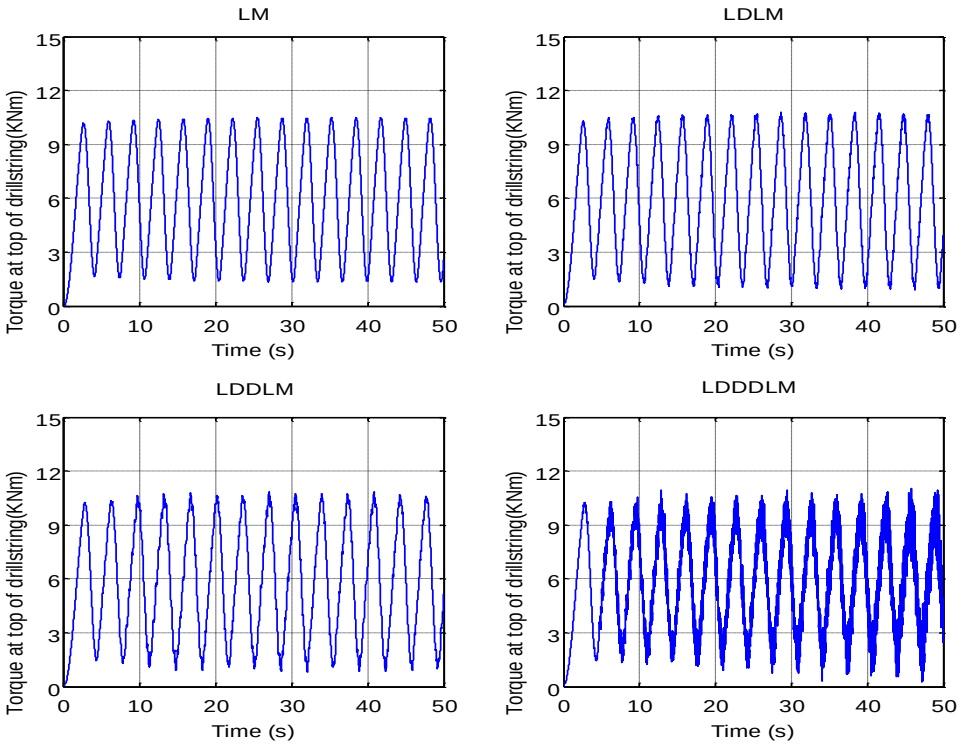

Figure 5-8 Torque at the top of drillstring at the stick-slip phase for the Lumped model (LM) and Distributed-Lumped models (LDLM, LDDLM and LDDDLM) (case 1)

5.1.2 Case study two ($l_{dp} = 2000m$)

With the increased depths of drilling, the hardness of rock will increase and also the length of drillpipe increases which leads to a decrease in its rigidity and therefore an increase in the possibility stick-slip.

Due to the casing operation to reinforce the borehole wall at increased depths, the diameter of both the borehole and the drill bit is reduced. In case study two, when the length of the drillpipe is 2000m and the diameter of the drill bit is 12.5 inches, the static friction torque reduces from 8890Nm (case study one) to 6223Nm; the dynamic friction torque reduces from 5556.3Nm to 3889Nm; and the stiffness of the drillpipe reduces from 1892N/m to 297N/m.

Table 5.2 represents the results of the simulations when the length of drillpipe is 2000m. Figure 5-9 shows a comparison between the four models at the desired drilling velocity (125rev/min). First, by comparing Figure 5-9 with Figure 5-1, it can be seen that the overshoot in the transient response for the LM model has decreased whilst for the LDLM, LDDLM and LDDDLM it increases. This increased overshoot is realistic due to decrease in the stiffness of the drillstring with increased length.

The second observation is that the decay time decreased in the LM, LDLM, and LDDLM and these models quickly transitioned to steady-state behaviour, whilst the decay time increased for LDDDLM due to the weight of the drillcollar.

The results demonstrate that at this depth of drilling the differences between the models are now clearer when compared with case study one; especially in the transient response. In addition, the differences between the torque values that are required to get the desired velocity have increased. The differences between LDLM and LDDLM are still slight but the additional detail of the LDDDLM is now clear.

Figure 5-10 shows the applied torque on the bit for all four models. When this figure is compared with Figure 5-2 (case study one), it can be observed that the frequency of torque oscillation is reduced due to the increase in the length of the drillstring. The lumped model is also faster than other models to go to steady state, and the behaviour of the LDLM and LDDLM is still similar with no a big differences between the two models. However, the applied load of the LDDDLM is entirely different from the other two hybrid models in both transient and steady conditions; the steady state response being due to the high stiffness of the drillcollar.

Figure 5-11 shows the torque at the top of the drillstring. It can be seen that the decay time of the LM is small when compared with the other models. The LDLM and LDDLM still show similar behaviour while the LDDDLM differs from the other models in both transient and steady response.

Table 5-2 Simulation result of case two (drillpipe=2000m)

Model type	Torque at 125 (rev/min)	Torque at critical velocity	Stick-slip torque	Critical velocity ω_{cr}	Torque at low velocity
LM	9985Nm	6890Nm	6880Nm	61.5rev/min	6600Nm
LDL	9975Nm	7680Nm	7670Nm	78rev/min	6450Nm
LDDLM	9910Nm	7770Nm	7760Nm	80.5rev/min	6400Nm
LDDDLM	9715Nm	7950Nm	7900Nm	87rev/min	6350Nm

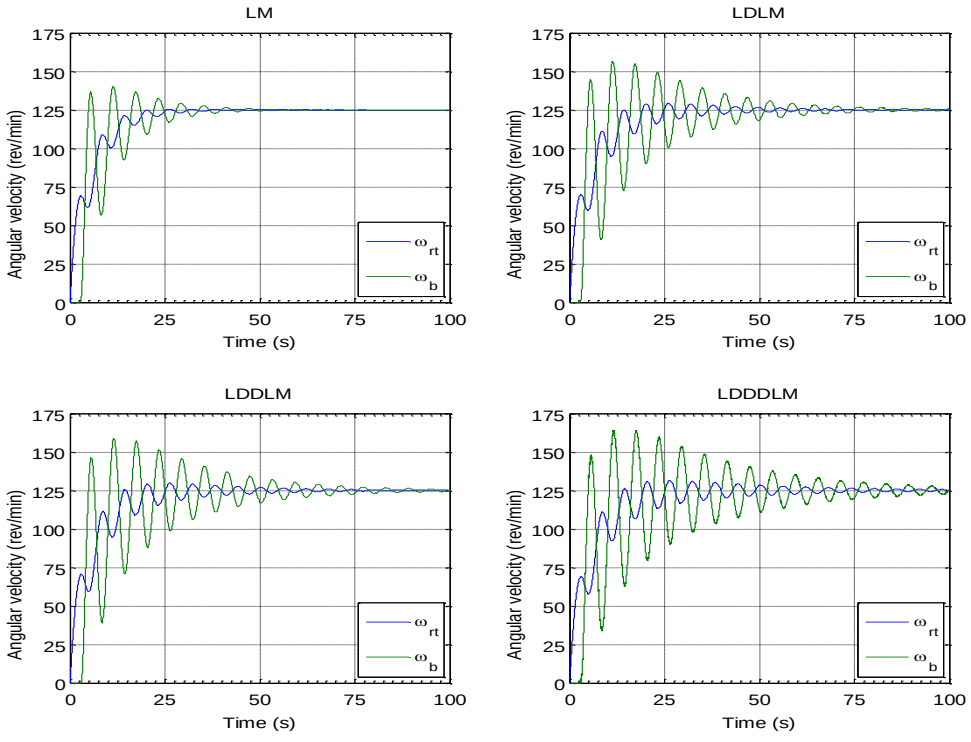

Figure 5-9 Angular velocity of the Lumped model (LM) and Distributed-Lumped models (LDLM, LDDLM and LDDDLM) at 125rev/min (case 2)

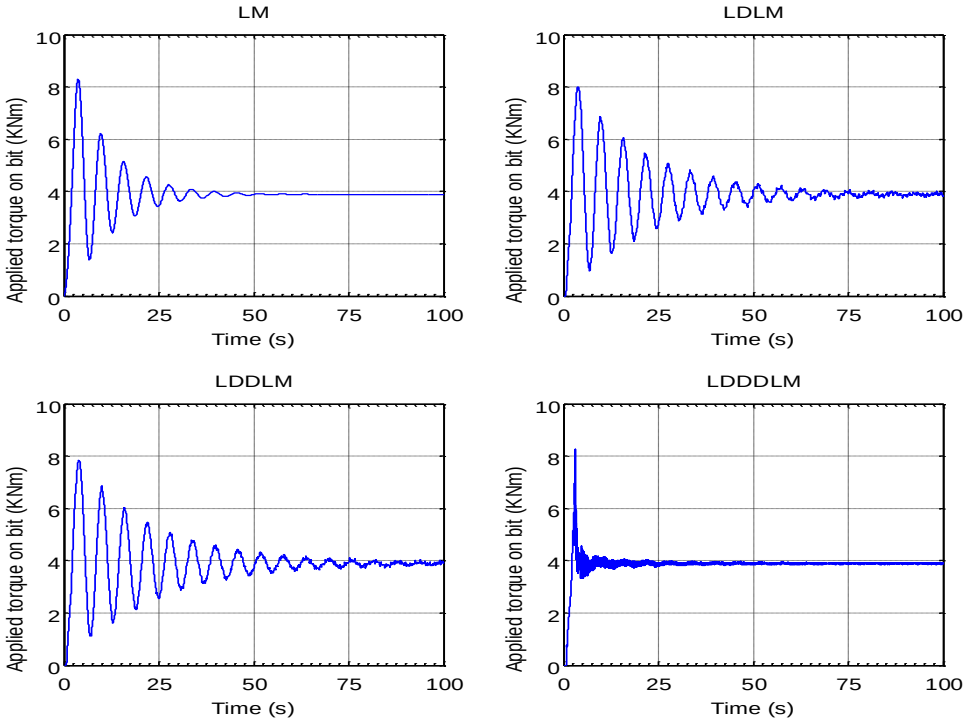

Figure 5-10 Applied torque on the bit of the Lumped model (LM) and Distributed-Lumped models (LDLM, LDDLM and LDDDLM) at 125rev/min (case 2)

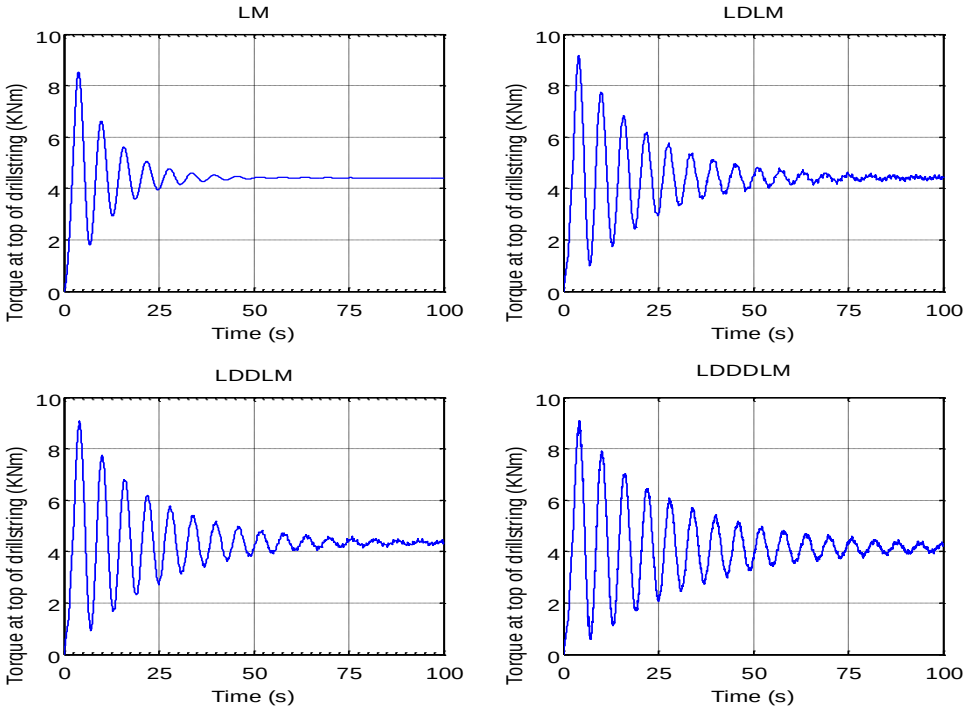

Figure 5-11 Torque at the top of the drillstring for the Lumped model (LM) and Distributed-Lumped models (LDLM, LDDLM and LDDDLM) at 125rev/min (case 2)

The biggest problem during the drilling operation is the stick-slip vibration. Therefore, the operator of the drill always tries to keep the drilling velocity above the critical speed. Comparison of Figure 5-12 and Figure 5-4 shows that the differences in critical speed of the four models had increased when the length of the drillpipe increased from 500m to 2000m.

Figure 5-13 shows that that stick-slip began in the four models when the torque of the rotary table decreased below the critical speed torque. In this case, the LDDDLM was the first to exhibit stick-slip behaviour as shown in Figure 5-13(A) when the torque decreased by 50Nm and then LDDLM, LDLM and LM respectively when the torque decreased only by 10 Nm as shown in Figure 5-13(B),(C)and (D) respectively.

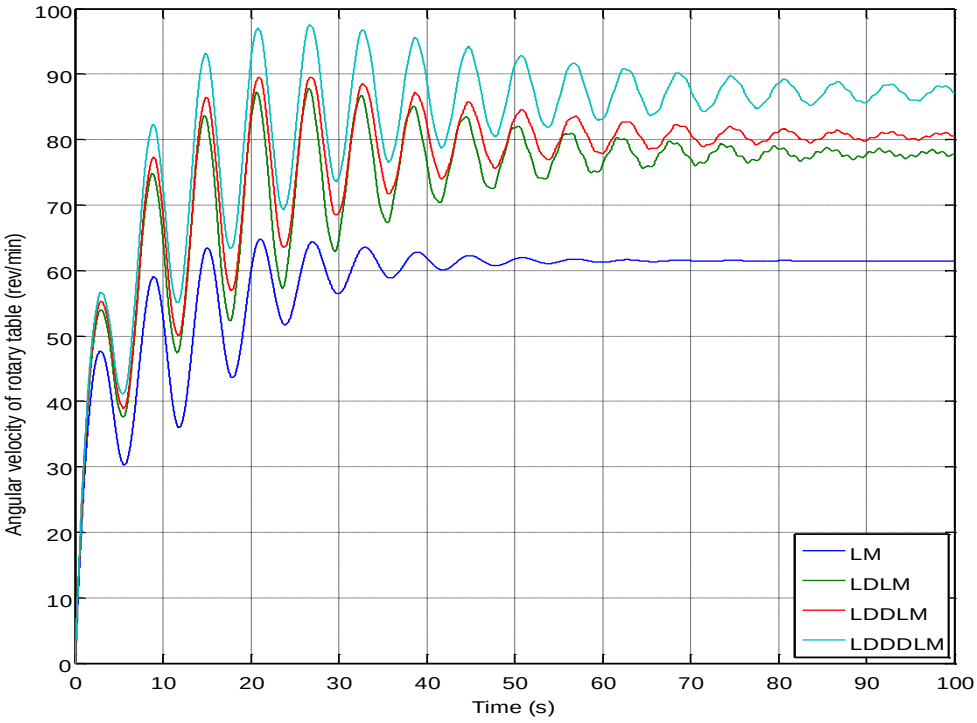

Figure 5-12 Comparison between critical speed of Lumped model (LM) and Distributed-Lumped models (LDLM, LDDLM and LDDDLM) (case 2)

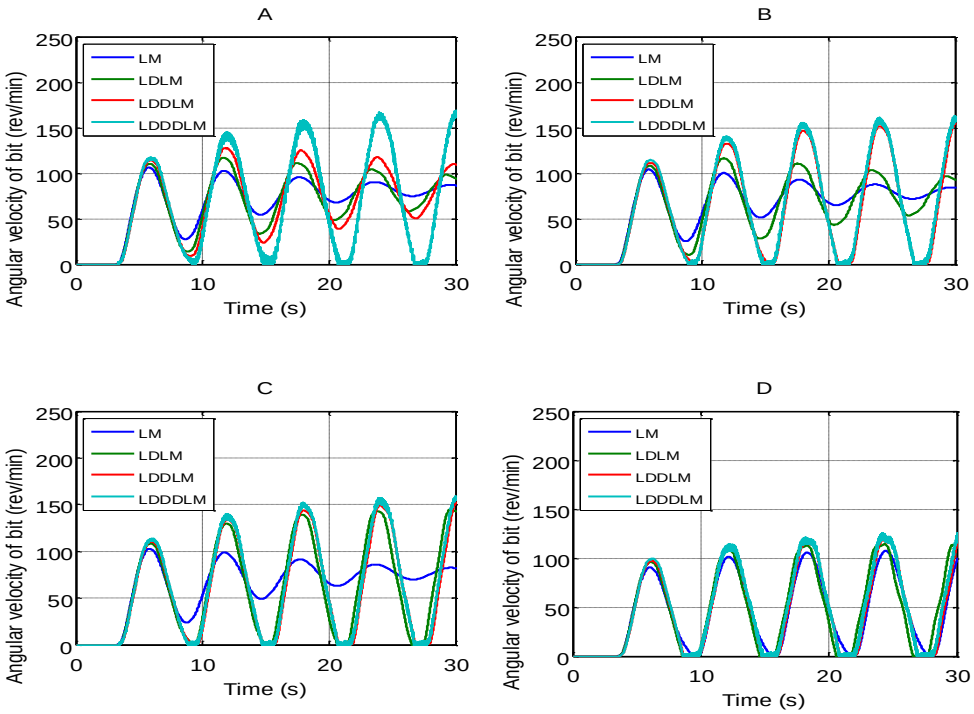

Figure 5-13 Stick-slip under critical speed of Lumped model (LM) and Distributed-Lumped models (LDLM, LDDLM and LDDDLM) (A: stick-slip torque of LDDDLM; B: stick-slip torque of LDDDLM and LDDLM; C: stick-slip torque of LDDDLM, LDDLM and LDLM; D: stick-slip torque of LDDDLM, LDDLM, LDLM and LM) (case 2)

Figure 5-14 shows the stick-slip vibration for each of the models over a 50-second period when the speed of the rotary table was approximately 50rev/min. The difference between the hybrid models and lumped model appears clearly when compared with case study one (Figure 5-6). This difference increases with an increase in the simulation time until quiescence in both model types. The main difference in both types of modelling can be summarised as follows:

- Whilst not apparent at the level of zoom shown in Figure 5-14, the angular velocity of the rotary table (ω_{rt}) for the hybrid models (LDLM, LDDLM and LDDDLM) showed more higher frequency fluctuations in comparison with the lumped model which had a smooth curve.

- The angular velocity of the drill bit for the LM, LDLM and LDDLM models varies between zero and fixed upper values. While in the LDDDLM model there is more fluctuation in the upper-value.
- The difference in the steady-state values increases between the hybrid models and lumped model.
- The average speed of the rotary table (50 rev/min) required a different value of rotary torque for each model as shown in Table 5.2.
- The applied torque on the bit as shown in Figure 5-15 showed that the LM fluctuates between static and dynamic friction torque on a smooth curve, while the LDLM and LDDLM fluctuated between these values on an irregular curve. The applied torque on the bit for the LDDDLM showed a very different pattern with higher frequency oscillations due to the higher stiffness of the drillcollar when compared to both the drillpipe and HWDP.
- The torque at the top of the drillstring as shown in Figure 5-16 showed that the torque predicted by the hybrid models fluctuated between static and dynamic on an irregular curve while the lumped model displayed a smooth curve.

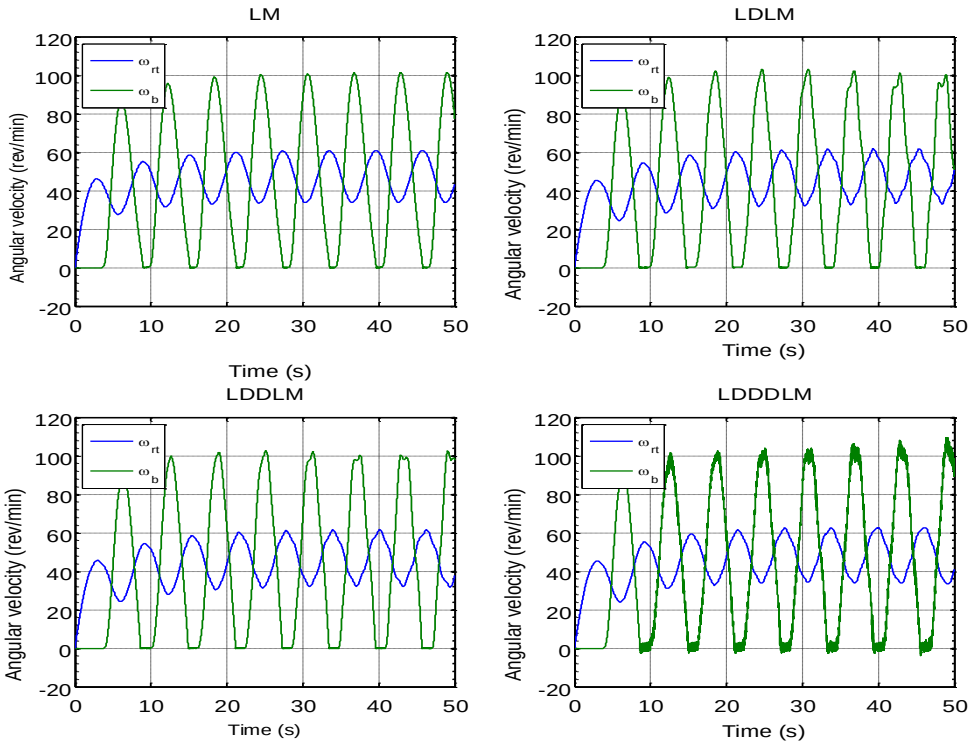

Figure 5-14 Stick-slip at low velocity of Lumped model (LM) and Distributed-Lumped models (LDLM, LDDLM and LDDDLM) (case 2)

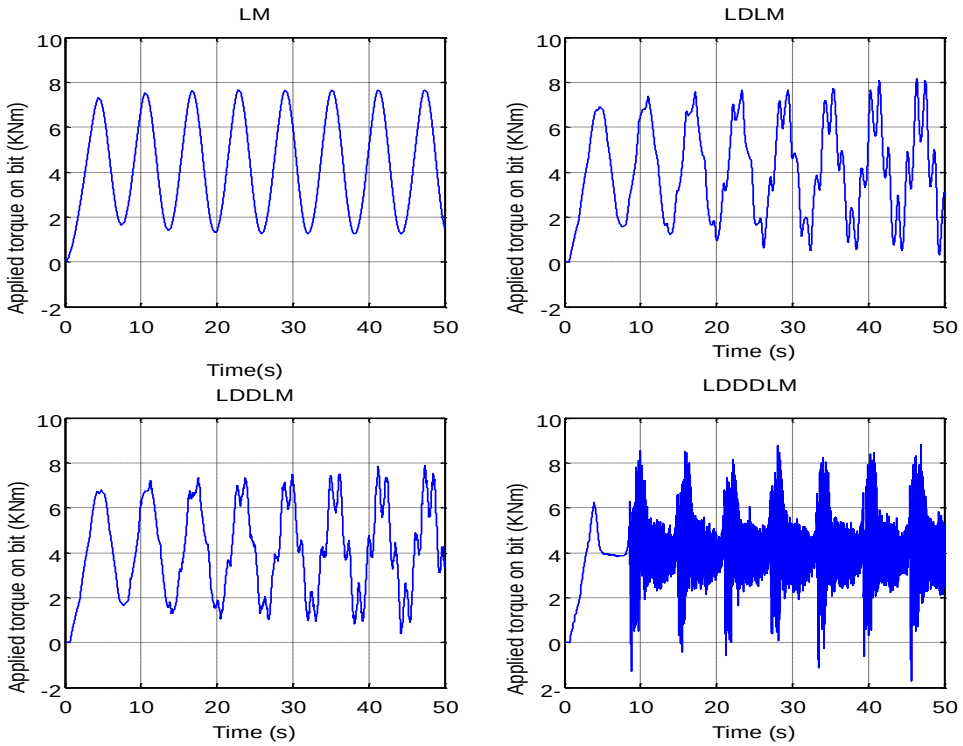

Figure 5-15 Applied torque on bit at stick-slip phase of Lumped model (LM) and Distributed-Lumped models (LDLM, LDDLM and LDDDLM) (case 2)

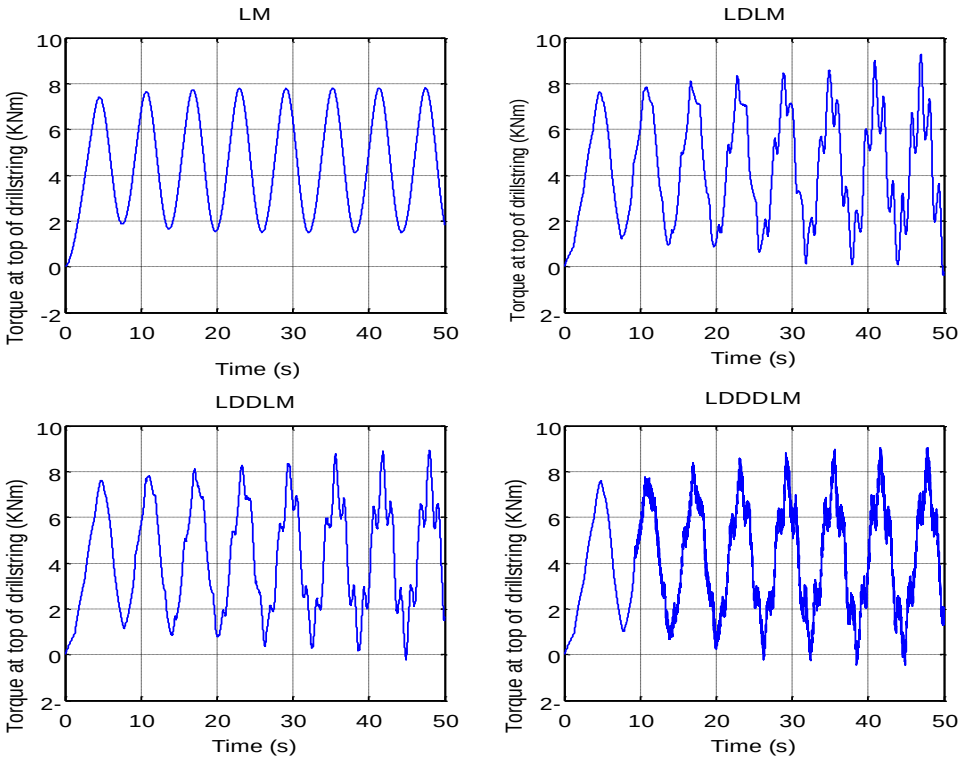

Figure 5-16 Torque at the top of drillstring at stick-slip phase of Lumped model (LM) and Distributed-Lumped models (LDLM, LDDLM and LDDDLM) (case 2)

The length of the drillstring in case study two is identical to that used for a real measurement available in published literature and is therefore suitable for further comparisons of the hybrid and lumped models. The real measurement can be seen reproduced in Figure 5.17. When comparing the lumped model and hybrid models in the steady state phase with this measurement, in addition to the conclusions drawn in section 4.7, it can be further concluded that:

- The general trend of the angular velocity of the drill bit (ω_b), as shown in Figure 5-18 to Figure 5-21, for the hybrid models was similar to the angular velocity measurement as shown in Figure 5-17. The angular velocity was shown to vary between zero and different upper values. The lumped model did not show this behaviour as it kept the same shape following the stick-slip vibration.

- The rotary table speed response of the actual measurement (Figure 5-17) is similar to hybrid models where the velocity fluctuated on an irregular curve.

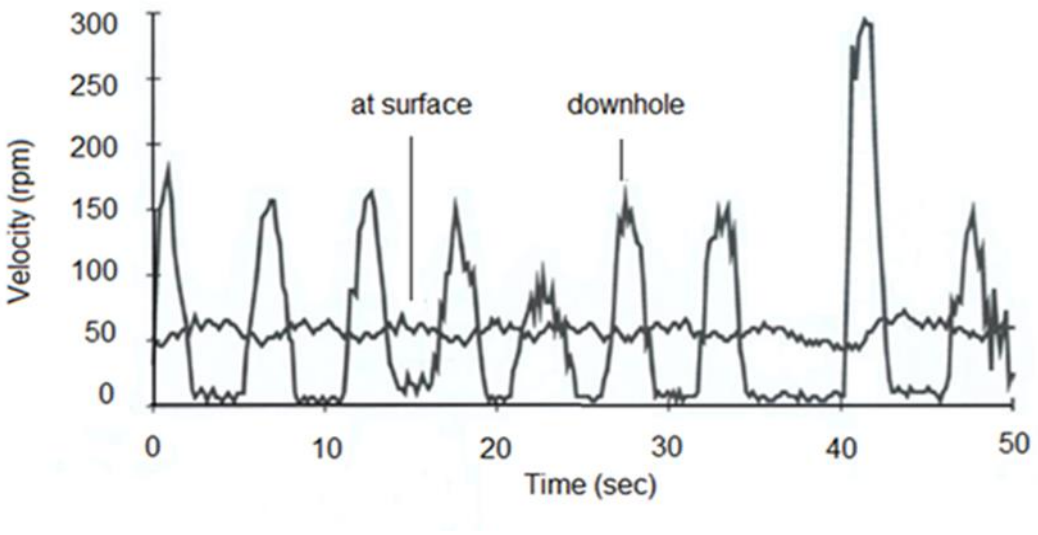

Figure 5-17 Example of stick-slip oscillation of a drill string (Kriesels et al. 1999.) (Also shown in Figure 2-8)

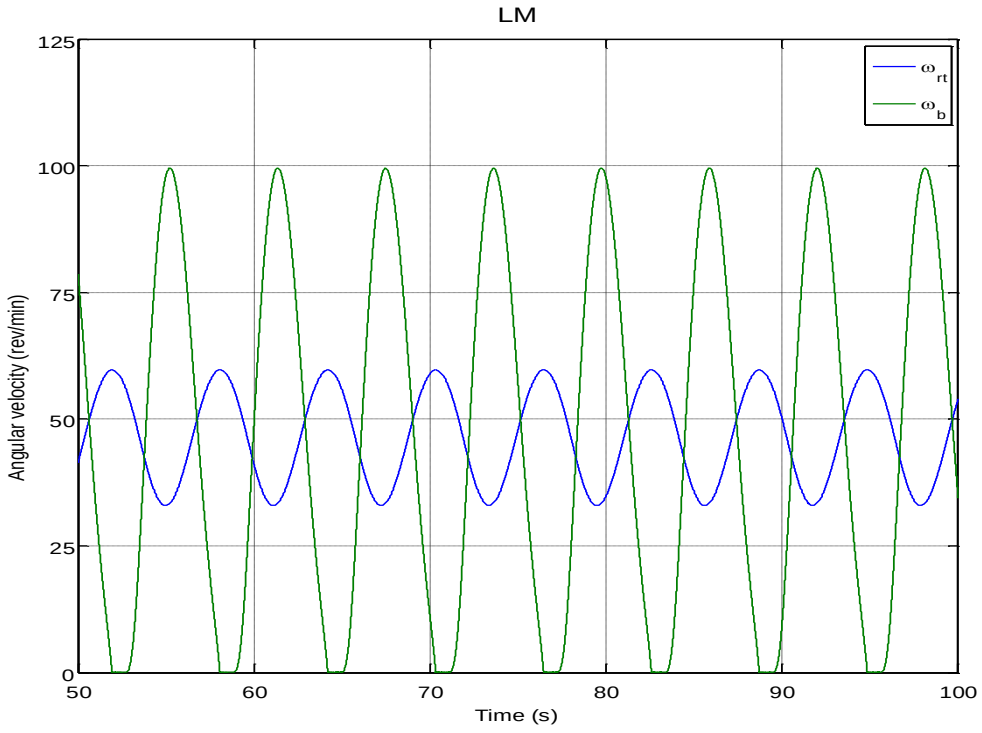

Figure 5-18 Stick-slip of the LM at steady state

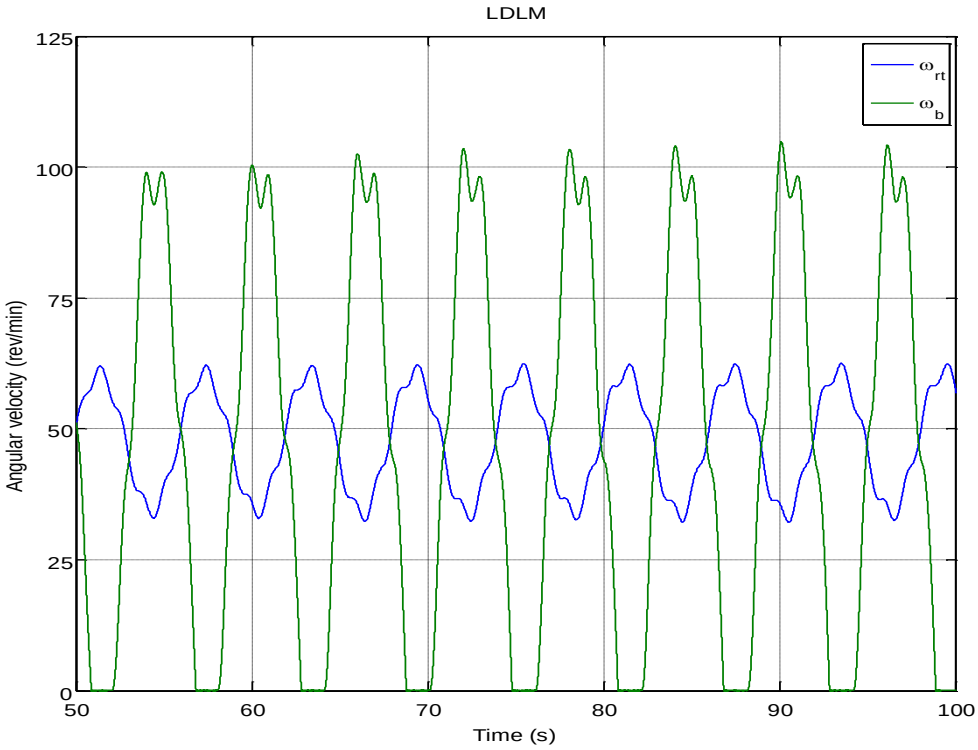

Figure 5-19 Stick-slip of LDLM at steady state

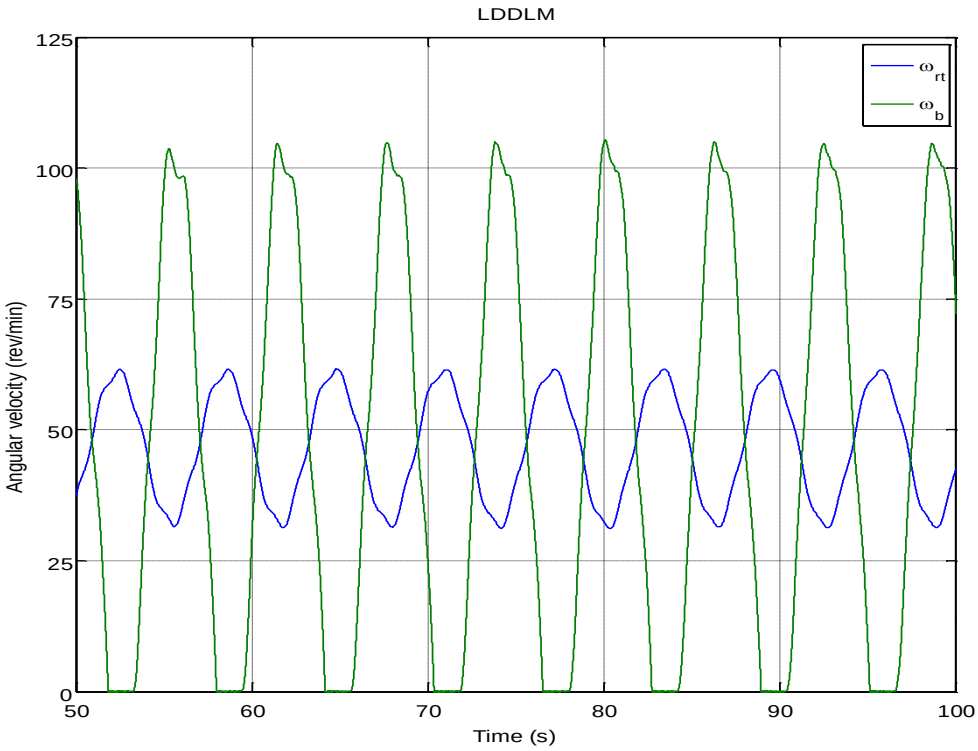

Figure 5-20 Stick-slip of LDDLM at steady state

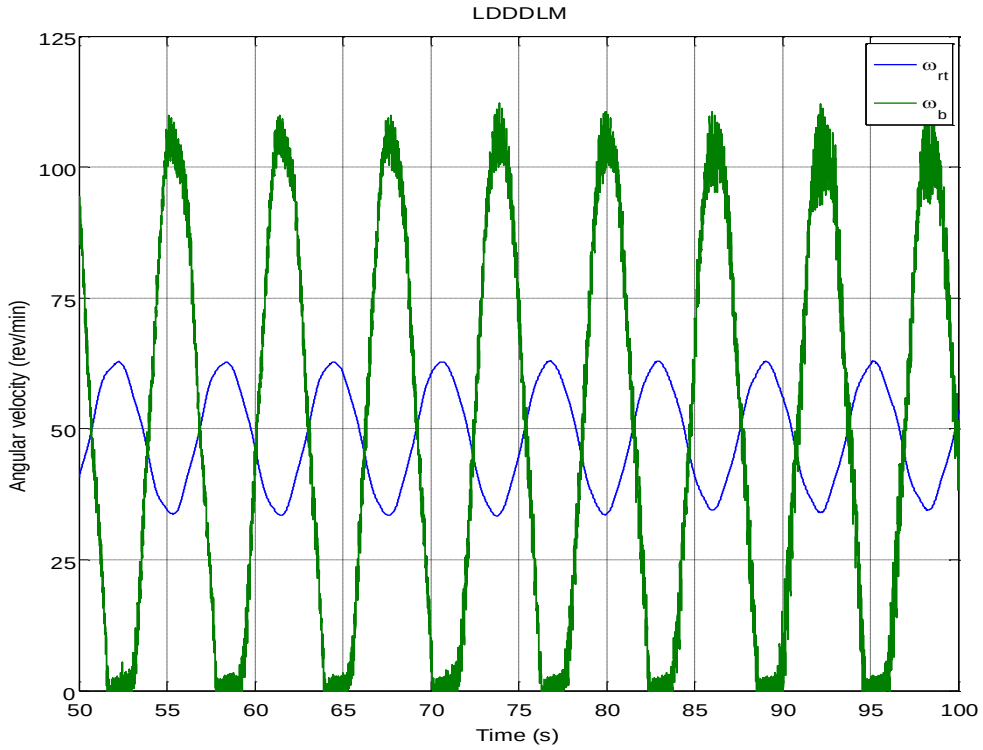

Figure 5-21 Stick-slip of LDDDLM at steady state

5.1.3 Case study three ($l_{dp} = 5700m$)

In case study three, the diameter of the drillcollar, shock-sub and the drill bit were further reduced due to the casing operation as shown in Table 4.4. The increased drillstring length and reduction in the diameter changes the similarity between the hybrid models and lumped model. Table 5.3 shows the results from the simulations. As in the previous two case studies, the first comparison between the hybrid models and lumped models is at the desired speed of drilling (125 rev/min) when there is no stick-slip motion.

Figure 5-22 shows the comparison between the two types of modelling. It can be seen that in general the decay time has decreased in each of the four models due to the increased viscous damping in the BHA for the hybrid models and along the drillpipe and BHA for the lumped model. The decay time for the

lumped model is still smaller than hybrid models, whilst the LDDDLM has the longest decay time.

The overshoot in the lumped model is smaller than the hybrid models and also lower than that found with shorter drillstring lengths. However, the overshoot in the hybrid models has increased when compared with the previous case studies; this is due to the increased length of the drillstring and the decreased stiffness of the drillpipe.

The frequencies of applied torque on the bit and the torque at the top of the drillstring have decreased for the lumped model and hybrid models as shown in Figure 5-23 and Figure 5-24 respectively due to the decrease in stiffness of the drillpipe and increase in the damping along the drillstring.

Table 5-3 Simulation result of case three (drillpipe=5700m)

Model type	Torque at 125(rev/min)	Torque at critical velocity	Stick-slip torque	Critical velocity ω_{cr}	Torque at low velocity
LM	9570Nm	4450Nm	4440Nm	30rev/min	4400NM
LDL	9570Nm	5260Nm	5250Nm	46rev/min	4400Nm
LDDLM	9310Nm	5430Nm	5370Nm	51rev/min	4400Nm
LDDDLM	8915Nm	5900Nm	5350Nm	64rev/min	4400Nm

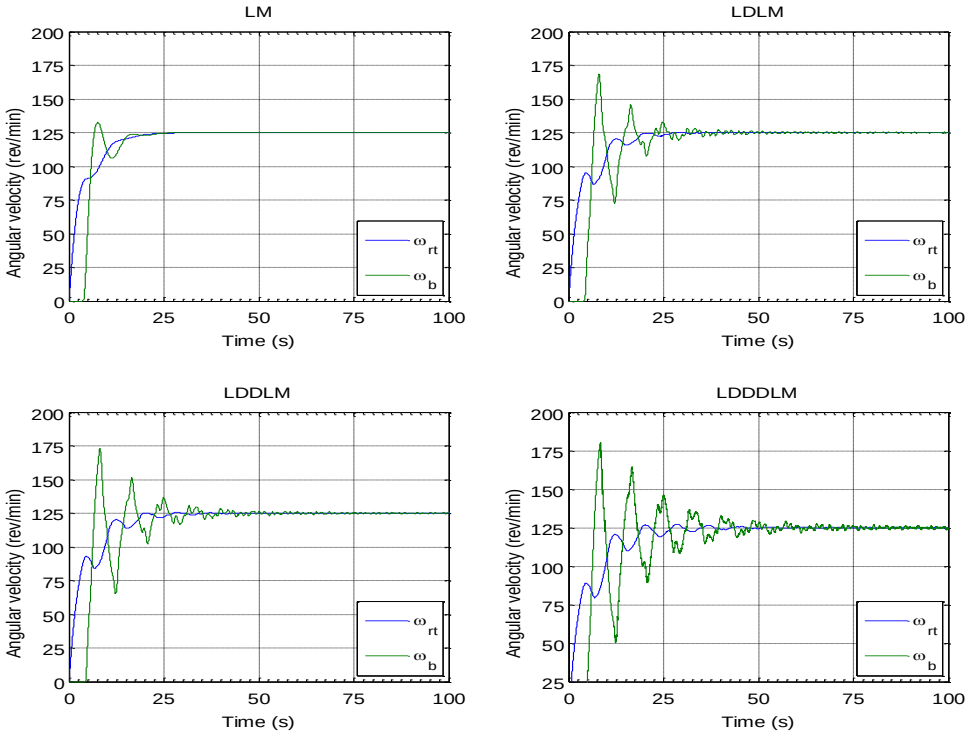

Figure 5-22 Angular velocity of the Lumped model (LM) and Distributed-Lumped models (LDLM, LDDLM and LDDDLM) at 125rev/min (case 3)

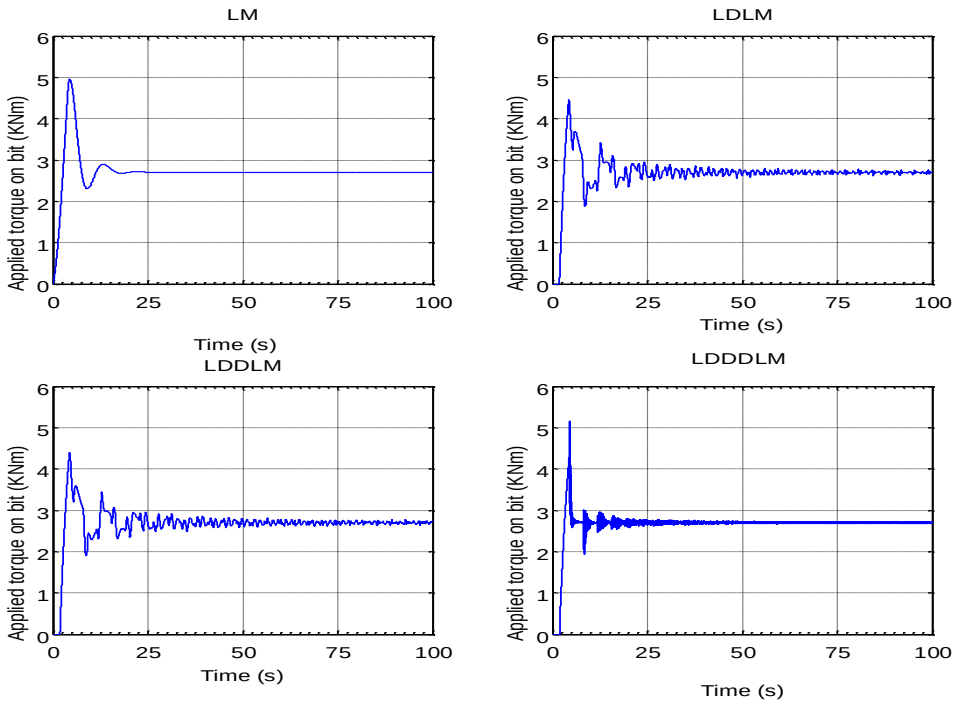

Figure 5-23 Applied torque on the bit for the Lumped model (LM) and Distributed-Lumped models (LDLM, LDDLM and LDDDLM) at 125rev/min (case 2)

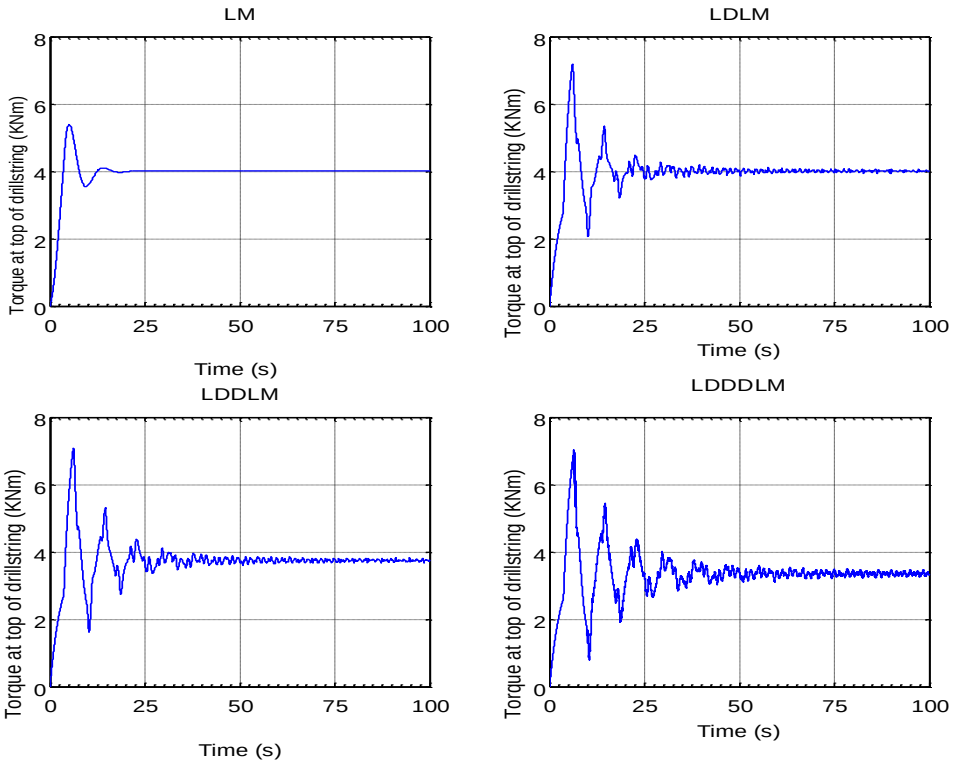

Figure 5-24 Torque at the top of the drillstring for the Lumped model (LM) and Distributed-Lumped models (LDLM, LDDLM and LDDDLM) at 125rev/min (case 3)

With the increase in the length of the drillstring, the critical speed of drilling decreases due to decrease the stiffness of drillpipe. Figure 5-25 shows the critical speed of hybrid models and lumped model; the first observation is that the critical speed has decreased when compared with the previous two case studies and this behaviour is similar to that which occurs in a real drilling system. The second observation is that the differences between the four models have increased, especially between the LM and LDDDLM where the critical speed of the LM is 30rev/min while for the LDDDLM is approximately 64rev/min. The differences between the LDLM and LDDLM are still small but have increased when compared with case study one and two.

When the torque of the rotary table decreases below the critical speed torque, the stick-slip in the LDDDLM was found to begin for a small period before converting to pure torsional vibration without complete stoppage while for the

LDDLM the stick-slip behaviour continues as shown in Figure 5-26(A). By decreasing the torque from 5900 Nm to 5350 Nm, the stick-slip of the LDDDLM continue as shown in Figure 5-26(B).

The behaviour of LM and LDLM below the critical speed was found to be similar to the previous case studies; decreasing the torque of the rotary table by approximately 10Nm induced the stick-slip oscillation in both models as shown in Figure 5-26(C) and Figure 5-26(D) respectively. The behaviour of the LDDDLM was found to be more realistic the other models when to compared with real drilling because the stick-slip generally occurs gradually when decreasing the torque below the torque of critical speed and not sharply.

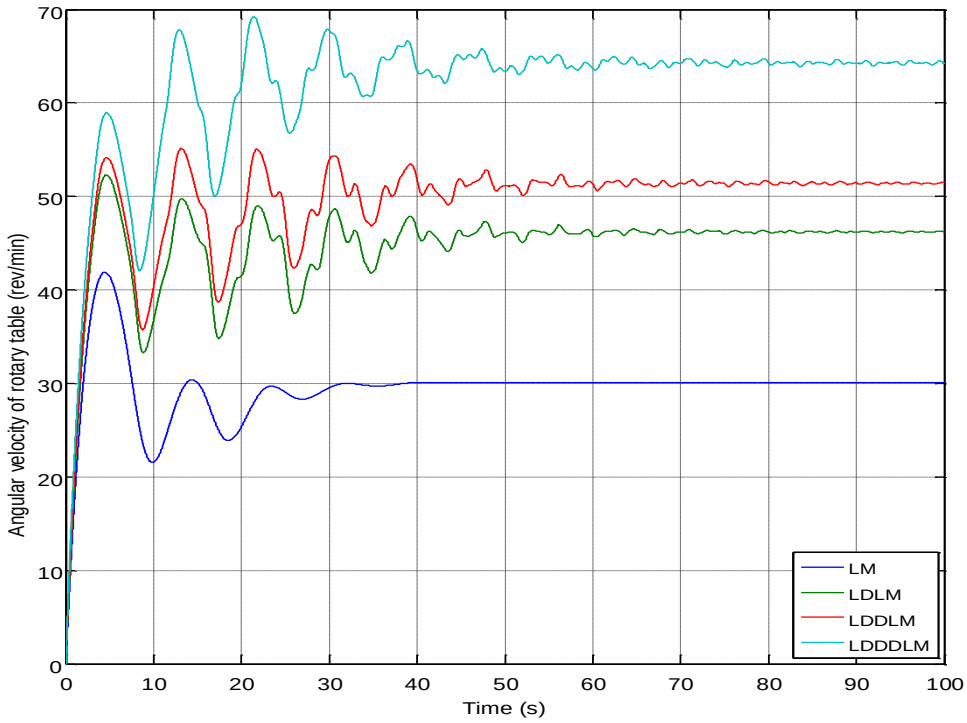

Figure 5-25 Comparison between the critical speed of the Lumped model (LM) and Distributed-Lumped models (LDLM, LDDLM and LDDDLM) (case 3)

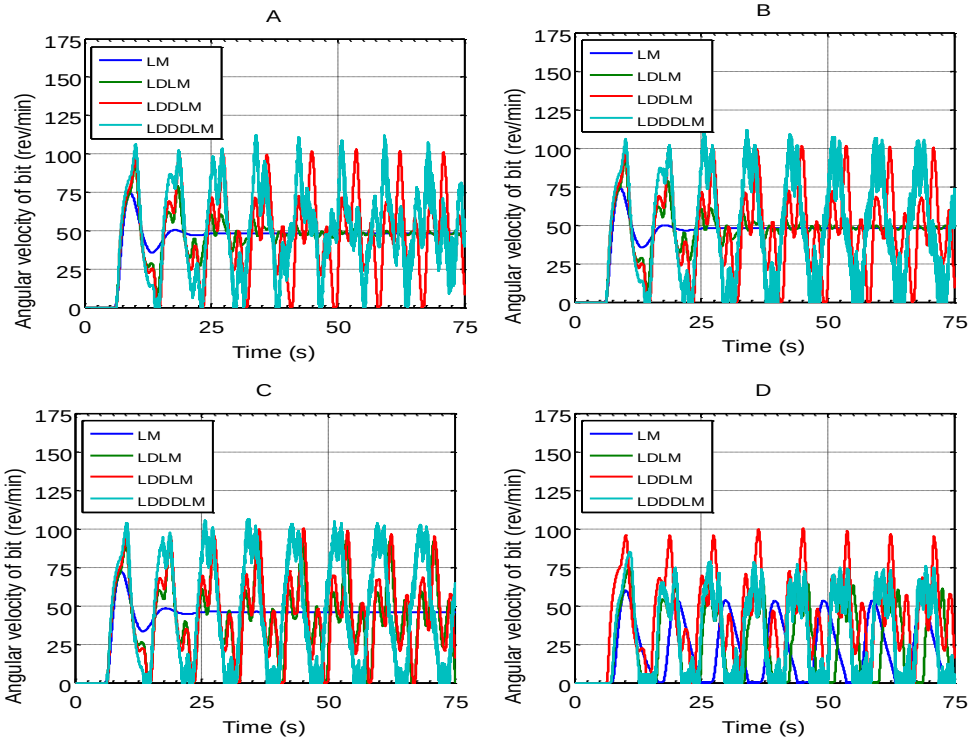

Figure 5-26 Stick-slip below the critical speed of the Lumped model (LM) and Distributed-Lumped models (LDLM, LDDLM and LDDDLM) (A: stick-slip torque of LDDDLM; B: stick-slip torque of LDDDLM and LDDLM; C: stick-slip torque of LDDDLM, LDDLM and LDLM; D: stick-slip torque of LDDDLM, LDDLM, LDLM and LM) (case 3)

When the depth of drilling is increased this leads to a decrease in the torsional stiffness (K_{dp}) of the drillpipe and it can bee seen that the stiffness decreased from $1892\ \mathrm{Nm/rad}$ when length of drillpipe was 500m to $166\ \mathrm{Nm/rad}$ when the length increased to 5700 m. It can be seen from Figure 5-27 that due to this decrease in the stiffness of drillpipe the number of stick-slip cycles in the shown time period decreased and the time of sticking increased for both the hybrid models and the lumped model.

The velocity of the rotary table for the LM was found to fluctuate as a smooth curve with the velocity of the bit fluctuating between zero and an upper fixed value. However, the velocity of the rotary table for the hybrid models fluctuated

on an irregular shape with the velocity of the bit transitioning between zero and fluctuating upper values for both the LDLM and LDDLM, with only a slight difference between the two models. The LDDDLM showed a different response of velocity of the drill bit with higher frequency fluctuations both around zero speed and at the upper value.

The decrease in the diameter of the bit leads to a reduction in both static and dynamic friction torque. It can be seen from Figure 5-28 that the LM fluctuated on a smooth curve between static and dynamic friction torque while for the LDLM and LDDLM the fluctuation was irregular. The difference between the responses of the applied torque on the bit for both models was small.

The applied torque on the bit for the LDDDLM showed a high-frequency fluctuation when compared with other three models as shown in Figure 5-28 and this was, as previously mentioned, due to the high stiffness of the drillcollar when compared with the drillpipe and HWDP; the stiffness of drillpipe was $166\ \mathrm{Nm/rad}$ while for drillcollar it was 30900 $\mathrm{Nm/rad}$.

The responses for the torque at the top of the drillstring (T_1) for the hybrid models and the lumped model are shown in Figure 5-29. It can be seen from this figure that the torque of LM, as in case study one and two, fluctuated on smooth curve and had a regular shape. However, for the LDLM and LDDLM the irregularity in the fluctuation increased when compared with case study one and two but the two models still showed similar response.

The LDDDLM again showed more irregularity in the fluctuation curve when compared with case study one and two, and also when compared with the LM, LDLM and LDDLM as shown in Figure 5-29.

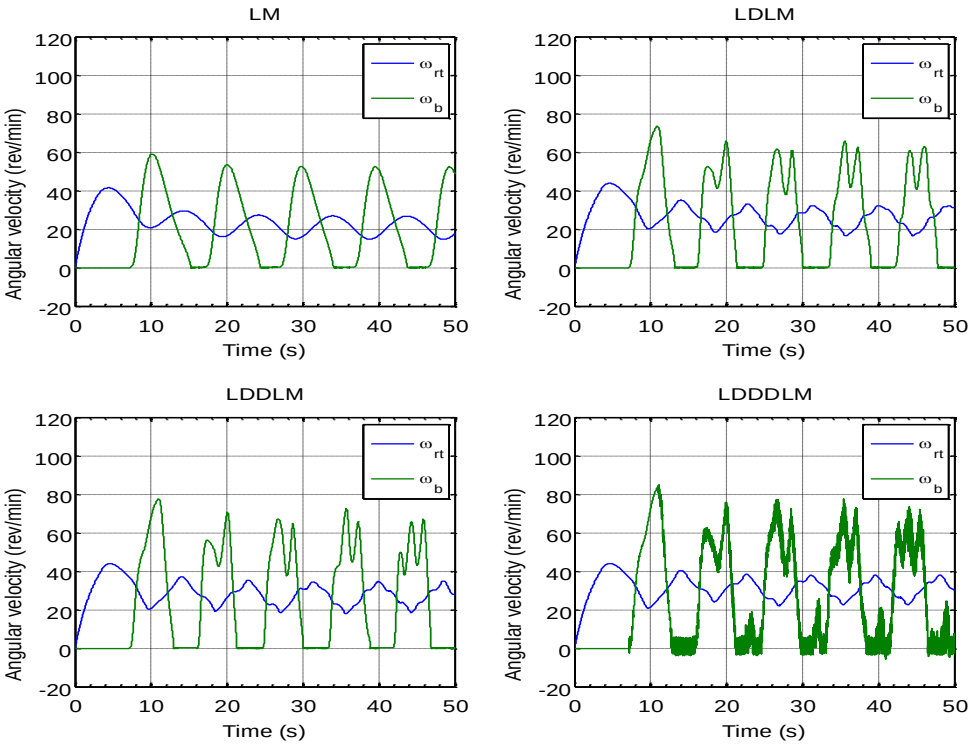

Figure 5-27 Stick-slip at low velocity for the Lumped model (LM) and Distributed-Lumped models (LDLM, LDDLM and LDDDLM) (case 3)

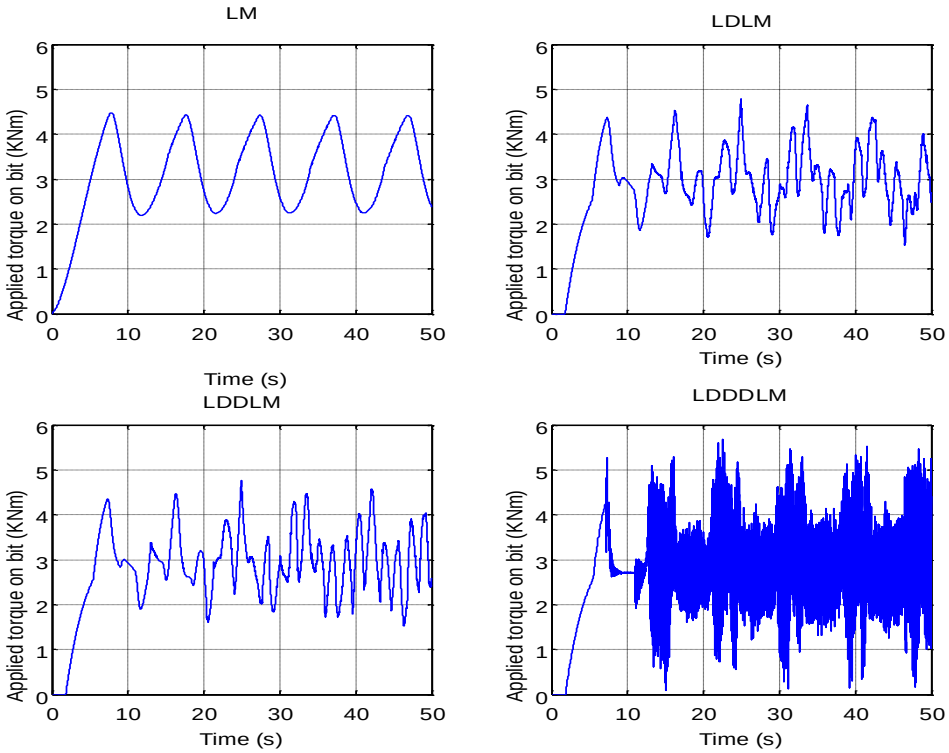

Figure 5-28 Applied torque on the bit in the stick-slip phase for the Lumped model (LM) and Distributed-Lumped models (LDLM, LDDLM and LDDDLM) (case 3)

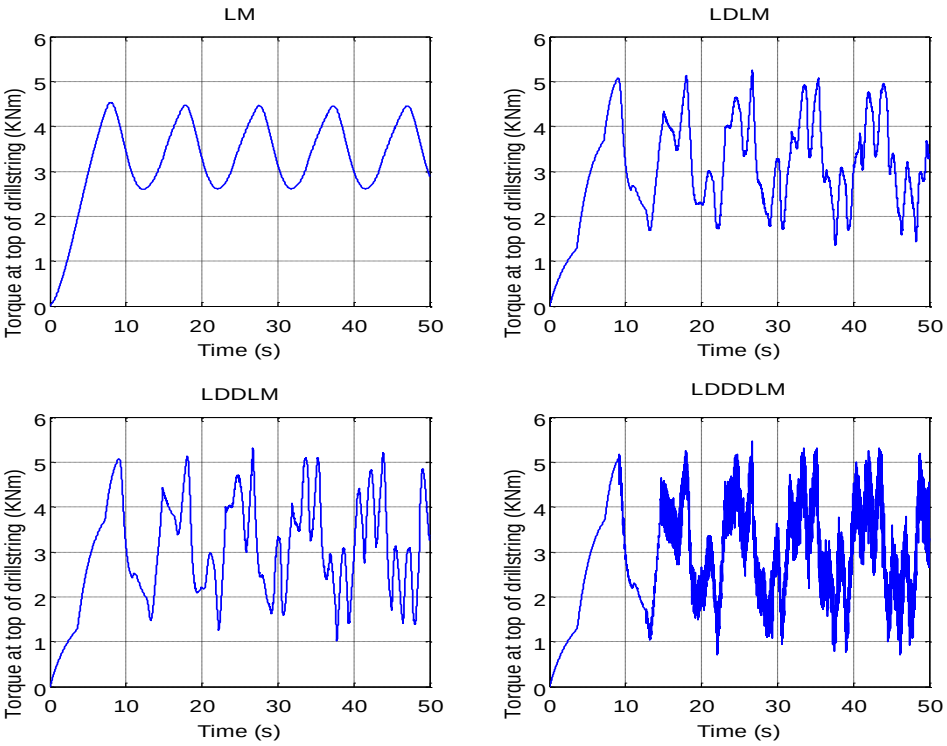

Figure 5-29 Torque at the top of the drillstring in the stick-slip phase for the Lumped model (LM) and Distributed-Lumped models (LDLM, LDDLM and LDDDLM) (case 3)

5.2 Investigating the effect of key drilling parameters on critical speed

During the drilling operation, the stick-slip vibrations occur when the velocity of the rotary table falls below the critical speed (Dufeyte and Henneuse 1991). Therefore, the driller always tries to drill at speeds above this velocity to avoid the stick-slip vibrations. When the critical speed is high, this means that the driller will have to operate at high speed to avoid the stick-slip oscillation, however, drilling with high velocity leads to increase bit wear and lateral vibration, whilst sometimes it is beyond the capacity of the drive system and the bit. Therefore, the target of researchers and engineers is to keep the value of critical speed as low as possible by manipulation of the drilling parameters.

The value of the critical speed depends on many parameters such as the characteristic impedance of the drillpipe (stiffness), the inertia of the drillcollar, weight on the bit, types of rock, types of bit and viscous damping along the drillstring. These parameters can increase or decrease the value of critical speed and, until now, there are no studies that focus on the effects of combinations of these parameters.

In this section, the behaviour of the critical speed under different scenarios is studied to show the effect of the key drilling parameters on the value of critical speed. A single hybrid model (LDLM), which was presented in the previous chapters, has been used to investigate the effect of the parameters. The LDLM was chosen because it would clearly show the transition from slip to stick whereas it would not be as clear in the more detailed LDDL or LDDDL models. This model would be used to study the effects of the characteristic impedance of the drillpipe (ξ_{dp}), the inertia of drillcollar (J_{dc}), the weight on the bit (W_{ob}) and the viscous damping along the BHA (C_{bh}) on the value of critical speed. The characteristic impedance of the drillpipe and inertia of the drillcollar are inherently related to the length and diameter of the drillpipe and the drillcollar respectively, whilst the weight on the bit depends upon the weight of the drillcollar. The type of rock formation determines the minimum weight that can be used to crush the rock and start the drilling, while the type of bit determines the maximum weight can be used. The viscous damping can be changed by adjusting the water content of the mud that is pumped through the cutting interface.

Hence, for the purpose of studying the influence of these parameters on the critical speed, the length of drillpipe, the type of rock and the diameter of the bit will be considered constant using parameters from case study two (Table 4-3).

The diameters of the drillpipe and drillcollar will be changed to get low, medium and high values of the characteristic impedance of drillpipe and inertia of drillcollar. The range of parameter values are listed in Table 5-4.

Table 5-4 Parameter values for the study into critical velocity

No	Parameters	Low	Medium	High
1	Characteristic impedance of the drillpipe(Nms)	72	373	674
2	Inertia of drillcollar(kgm^2)	156	774	1392
3	Weight on bit (KN)	10	80	150
4	Damping along BHA($Nms\ /\ rad$)	15	55	95

5.2.1 Simulation results of the key parameters

Table B-1 in Appendix B shows the numerical results for critical speed under following a full factorial 81 run study (3^4) of the parameters shown in Table 5-4. The numbers -1, 0 and 1 stand for the low, medium and high values of the parameters. First, the interaction plot of drilling parameters is plotted as shown in Figure 5-30 and then the effect of each two parameters on critical speed is plotted as a surface plot as shown in Figure 5-31.

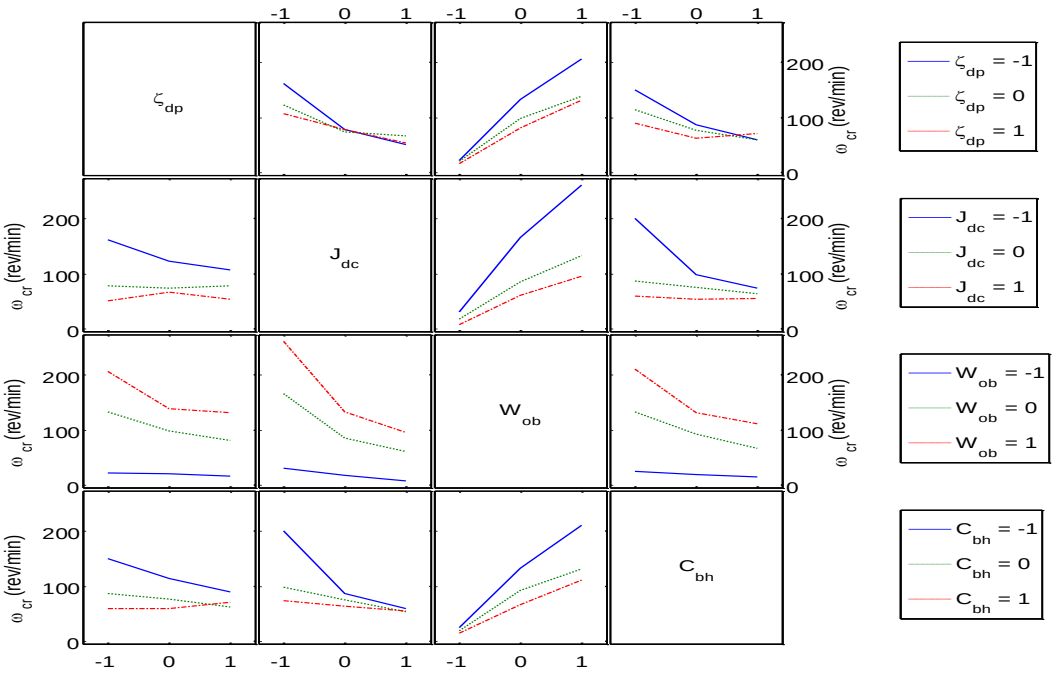

Figure 5-30 Interaction plot of key drilling parameters (characteristic impedance of the drillpipe (ξ_{dp}), inertia of drillcollar (J_{dc}), weight on bit (W_{ob})) and damping along BHA(C_{bh}))

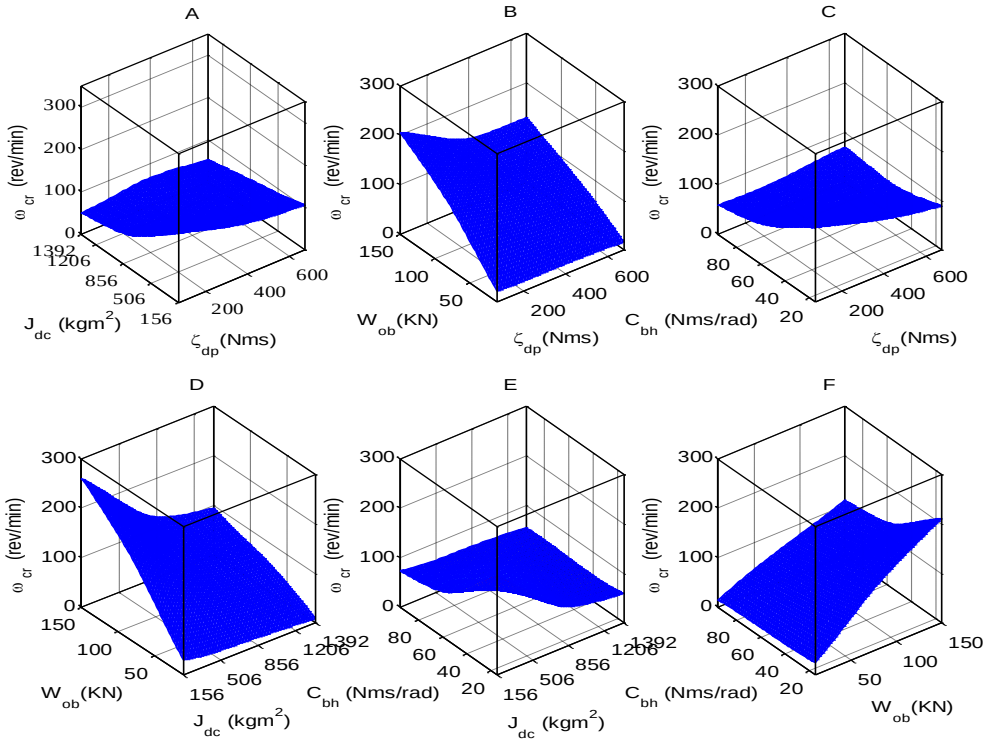

Figure 5-31 Surface plot of the key drilling parameters (characteristic impedance of the drillpipe (ξ_{dp}), inertia of drillcollar (J_{dc}), weight on bit (W_{ob})) vs critical speed (ω_{cr})

The interaction effect between the characteristic impedance of the drillpipe (stiffness) and the inertia of the drillcollar on the critical speed has not previously been studied in any depth by other researchers. When the drilling operation progresses, the stiffness of the drillpipe is reduced due to the increased length. The inertia of the drillcollar is also reduced as a result of its smaller diameter due to the casing process. Hence, for the purpose of simulation, the characteristic impedance of the drillpipe is increased from 72Nms to 674Nms and the inertia of the drillcollar from 156kgm^2 to 1392kgm^2 due to the change in diameter of the drillpipe and drillcollar.

From the interaction plot (Figure 5-30) it can be seen from the shape of the lines that there is not a significant interaction between the characteristic impedance of the drillpipe and the inertia of the drillcollar. Figure 5-31(A) shows that an increase in both the characteristic impedance of the drillpipe and inertia of the drillcollar leads to a decrease in the critical speed of drilling, whilst decreasing the parameters leads to an increase of the critical speed. Also, it can be seen that a drillcollar with high inertia has a significant effect on the critical speed when compared with a drillpipe with high characteristic impedance.

The characteristic impedance has no significant effective on critical speed when compared with the effect of weight on bit as shown in Figure 5-30 and Figure 5-31(B). It can be seen from Figure 5-31(B) that with an increase in the weight on bit the critical speed increases due to the increase in the reactive static torque. When the weight on the bit is low or medium the value of critical speed does not change noticeably with an increase in the stiffness; conversely when the value of weight on the bit is high, an increase in the stiffness of the drillpipe leads initially to a decrease in the value of critical speed and after that, the value does not change with any further increase of the drillpipe stiffness.

During the drilling operation, the mud viscosity is necessary for lubrication and damping as demonstrated in the literature review chapter. The interaction between the stiffness of the drillpipe and the viscosity along the BHA occurs when their values are small as shown in Figure 5-30 and this interaction decreases as the values increase. It can be seen from Figure 5-31(C) that the characteristic impedance of the drillpipe and viscosity along the BHA work together to decrease the value of critical speed. However, the effect of damping has a greater effect than that of stiffness in decreasing the value of critical speed.

The interaction between the inertia of the drillcollar and the weight on the bit is similar to the interaction between the characteristic impedance of the drillpipe and weight on the bit as shown in Figure 5-30. However, the effect of inertia is more pronounced in decreasing the critical speed when compared with that of the stiffness of the drillpipe as shown in Figure 5-31(D). For high loads, the critical speed was found to increase to nearly 250 rev/min when inertia was low and decrease to 100rev/min when the inertia of the drillcollar increased (Figure 5-31-D); while for the same loads an increase in the characteristic impedance of the drillpipe resulted in a change from 200rev/min to near 150rev/min as shown in Figure 5-31(B).

It can be is seen very clearly from the interaction plot of Figure 5-30, and the surface plot of Figure 5-31(E), that the interaction of the inertia of the drillcollar with the damping along the BHA are near-identical with that of the characteristic impedance and damping (Figure 5-31-C). Only slight differences exist in the value of critical speed when the characteristic impedance and inertia of the drillcollar are low.

The interaction of weight on a bit with the viscous damping along the BHA (Figure 5-31(F)) is similar to the interaction with the inertia of the drillcollar and stiffness of the drillpipe as shown in interaction plot Figure 5-30 and surface plot Figure 5-31(B, D & F). From these results, it can be observed that the most dominant factor is weight on the bit as it has the most significant effect on the critical speed.

5.3 Summary

In this chapter, three case studies were presented to address the main differences between the distributed-lumped (hybrid) and purely lumped model in their ability to describe the dynamic behaviour of the key drilling parameters ($T_1, T_{ab}, \omega_{rt}\ and\ \omega_b$) in both the slip phase, when the velocity of the rotary table was 125 rev/min, and in the subsequent stick-slip phase by taking three lengths of drillpipe into consideration (500, 2000 and 5700m).

In case study one, at relatively low drilling depth, it was shown that the general trend of distributed-lumped models (LDLM, LDDLM and LDDDLM) and purely lumped model (LM), in describing the main parameters of drilling in slip phase and stick-slip phase, were similar with only slight differences in the predicted critical speeds.

In case of study two, the increased length of the drillpipe began to highlight the differences between the two types of modelling especially in the value of the critical speed of each model. The differences between LDLM and LDDLM were still slight whilst the LDDDLM showed significant differences from the other three models in describing the stick-slip vibration.

In case of study two, a comparison between the hybrid models and lumped model in the steady-state phase was made with a real measurement from

published literature. The result of this comparison indicated that in general, the hybrid model bore more similarity to the real measurement in its ability to describe the velocity of both the rotary table and the bit in the stick-slip phase when compared to the lumped model.

In case study three, the deepest modelled depth, the differences between the four types of model were very clear with different values of critical speed and responses of applied torque on the bit and torque at the top of drillstring predicted for each model.

The effect of combinations of drilling parameters (ξ_{dp}, J_{dc}, w_{ob}, and C_{bh}) on the value of critical speed were investigated in detail covering the interaction between pairs of parameters. Three levels (low, medium and high) of each parameter were used to calculate the critical speed. The surface plots showed that increases in ξ_{dp}, J_{dc}, and C_{bh} worked to decrease the critical speed, while reducing the w_{ob} increased the critical speed and there was no significant interaction between the parameters ξ_{dp}, J_{dc}, and C_{bh} when compared to the interaction of the same three parameters with the w_{ob}.

CHAPTER 6: OPTIMISATION OF DRILLING PARAMETERS

Chapter 6

Optimisation of Drilling Parameters

In chapter 5, the comparison between two different approaches of drillstring modelling (lumped and hybrid) was carried out by comparing the lumped model (LM) with the three types of hybrid models (LDLM, LDDLM and LDDDLM) to address the main differences between the two types of modelling in describing the dynamic behaviour of the key drilling parameters $(T_{rt}, T_{ab}, \omega_{rt}, \omega_b)$.

In this chapter, based upon the work carried out in chapters 4 and 5, the LDLM will be used to optimise the weight on bit and rotary torque by using a species conserving genetic algorithm (SCGA). The LDL model was selected as it was believed to present the most accurate prediction of the critical speed of the actual drilling system since it incorporates the length of the drillpipe, which is significantly longer than the HWDP and drillcollar. In addition, the viscosity along BHA is taken into consideration. If more detail were required about the actual transient motion the LDDDLM would be more suitable.

First, an introduction to the objective of drilling optimisation during the drilling operation will be presented together with the classification of the drilling parameters (controllable and uncontrollable parameters) and the types of services that the driller receives (Real-time service (RTS) and Next well service (NWS)) to select optimum drilling parameters.

Secondly, a brief explanation of the mechanism of genetic algorithms (GAs) will be explained. The main differences between the conventional approaches of optimisation and GAs, the terminology of GAs and the main operators of GAs

(selection, crossover and mutation) will be introduced. The principle of species conserving genetic algorithms (SCGA) is explained briefly to show the differences between it and other more simpler GAs. In addition, the optimisation problem and the parameters that will be used for the optimisation (weight on bit and rotary torque), objective function and the constraints are presented.

Finally, the three case studies that were used in chapter 5 for comparison are again used in this chapter in order to optimise the weight on bit and torque of the rotary table to prevent stick-slip vibration and obtain all possible values of rate of penetration at the desired speed of drilling (125 rev/min) by using the SCGA technique.

6.1 Drilling optimisation

The objective of drilling optimisation during the drilling operation is to optimise the different drilling parameters in order to save time, minimise the cost of drilling thus increasing the profit and enhance drilling process safety. The drilling parameters can be classified as controllable, or rig and bit related parameters, and environmental, or formation parameters (Kelessidis and Dalamarinis 2009). The controllable parameters which can instantly be changed by the driller comprise of the weight on the bit, rotary torque, velocity of drilling and hydraulic parameters such as mud flow rates, while the environmental parameters which cannot be controlled include categories such as local stresses, mineralogy, formation fluids, rock compaction and abrasion of the formation.

The controlled parameters (weight on bit and velocity of drilling) have a significant influence on the rate of penetration (ROP) and also on the stick-slip oscillation. Irawan, (2012) showed an increase in the velocity of the bit while

keeping the weight on the bit constant lead to an increase in the rate of penetration by 70%, while if the weight on the bit was doubled, but the velocity of the bit remained constant it would result in increasing the rate of penetration by 300%. Increasing the weight on the bit can lead to increased probability of stick-slip vibrations occurring, whilst increasing the velocity of drilling can lead to rapid bit wear; therefore, the optimised value of weight on the bit and velocity of the bit should be carefully chosen by the driller to ensure acceptable rate of penetration and safe drilling without stick-slip vibrations.

The optimum parameters that are used during drilling operations have a significant impact on overall drilling cost reduction. These parameters are selected by the driller before starting the drilling operation and are based upon information about the rock formation, but may also be adjusted in-service dependent upon the feedback provided during the drilling operations. There are two sources of information, or ‘services’, that are given to the driller in order to make a best estimate on the optimum drilling parameters (Bharadwaj and S 2013):

a. Real-time service (RTS), where the surface data allows tracking and monitoring of the drilling behaviour and provides the required information to the driller to select and optimise the optimum drilling parameters in order to increase the rate of penetration, bit life and decrease vibrations

b. Next well service (NWS), collecting past data of similar wells that are drilled at close distances and select the optimum parameters depending on the lesson learned from these drilled wells and construction of a reference knowledge database. The guidelines are then given to the driller in order to improve the performance of the next well.

Stick-slip vibrations are considered to be one of the key causes of increased cost of drilling (Kriesels et al. 1999.), therefore eliminating the stick-slip oscillation will improve the drilling operation and contribute to reduced costs. As shown in the literature review the weight on the bit (Wob) and speed of the bit are the two important factors that can be used by the operator to suppress the stick-slip vibration by either decreasing the weight on the bit or increasing the torque of the rotary table.

The desired speed that is used in oil well drilling is in the region of 120-125 rev/min where there is no stick-slip vibration (Omojuwa et al. 2012). Therefore, the aim of optimisation is to provide the driller with optimised weight on the bit and torque of rotary table to achieve two goals: no stick-slip vibration and maximum rate of penetration.

In this study, the genetic algorithm (GA) optimisation method is used with the LDL model to achieve this goal and also to provide all the possible values of weight on the bit and rotary torque at the desired speed.

6.2 Genetic algorithms (GAs)

Genetic algorithms (GAs) are a powerful optimisation tool for solving search and optimisation problems based on the theory of natural evolution and selection and survival of the fittest (Darwin concept). This method of optimisation was introduced by Holland (1975) in the book "Adaptation in natural and artificial systems" and can be used for solving both constrained and unconstrained optimisation problems.

The GAs have two special elements which are 'individual' and 'population' where the individual represents a single solution in the search space while the population is the group of individuals. The search space, also called state

space, represents the location of all feasible solutions and each point inside the search space represents one possible solution. The principle of GAs depends on mating between the individual (information exchange) to produce new populations and survival of the fittest individual inside the new populations.

Problems including discontinuous functions, non-differentiable, stochastic, or highly nonlinear systems which cannot be solved by conventional optimisation techniques can be solved using genetic algorithms (Falode and Agbarakwe 2016). The difference between the GAs and traditional optimisation techniques can be summarised as follows (Sivanandam et al. 2008):

- The parameters of the problem are coded in the GAs while all the conventional optimisation techniques operate with the problem parameters itself.
- Whole populations of points (strings) are used in GAs to search for the optimum solution while all the traditional optimisation techniques use a single point. This feature increases the probability of GAs reaching a global optimum and decreases the chance of being trapped at a local minimum.
- GAs can be applied to different types of optimisation problems (continuous or discrete) because they use a fitness function to assess the fitness of individuals inside the population for evaluation instead of using derivatives.
- Probabilistic transition operations are used by GAs to make decisions while in traditional optimisation methods the deterministic transition operations are applied to make decisions for the continuous optimisation problem.

Most of the standard terminology relating to GAs is inherited from genetic sciences; therefore it is useful to formally introduce the terminology that will be used throughout this chapter. The terminology can be summarised as follows (Yeten 2003; Onwunalu and Resources Engineering 2006).

- **Individual** is a single feasible solution in the search space.
- **Population** is a set of individuals within the generation.
- **Generation** refers to the iteration stage during the optimisation process.
- **Chromosome** represents the coded notation of the parameters of an individual which is encoded as binary or real numbers.
- **Gene** refers to the single property inside the chromosome.
- **Fitness** represents the value of the objective function for an individual within a population, and this value determines the fittest individual inside the population.
- **Parents** represent for the two fit individuals that are randomly selected to go through reproduction.
- **Offspring** are the Individuals that are produced by the mating of two parents.
- **Selection** is the process of retaining the best performing individual from one generation to the next.
- **Mutation** is the process of causing small random alterations of the bits in a chromosome to prevent the genetic algorithm converging to a local minimum.

The heart of the genetic algorithm is the reproduction process where the search process produces a new generation of the population by selecting the fittest individuals. The reproduction process consists of three steps which are discussed in the following sections.

6.2.1 Selection

Selection is the process of selecting the fitter individual in the current population to go to the next population. The numbers of copies of the individual that will pass to the next generation depend on the fitness value of each where the higher fitness will have more chance to be selected and more copies in the next generation.

6.2.2 Crossover

The crossover operator is considered the most dominant operator in GAs that is responsible for mixing each pair of chromosomes of selecting parents to produce new offspring exhibiting the best properties of each parent. The new child with high fitness value will replace the weaker individuals in the population. The crossover occurs by replacing a part of a chromosome from parent one with a part of a chromosome from parent two in order to produce children. The crossover enables the children to acquire the excellent characteristics of the parents and increase the opportunity for an individual to evolve.

The crossover can be implemented in a single point or multipoint. Figure 6-1 shows the simplest crossover of one point in binary GAs where the parents' chromosomes at a random point are cutting and swapping the two resulting portions. The crossover not performed on all the population but a certain percentage depending on the probability and this value is set arbitrary but is typically greater or equal to 0.6 (Karkoub et al. 2009).

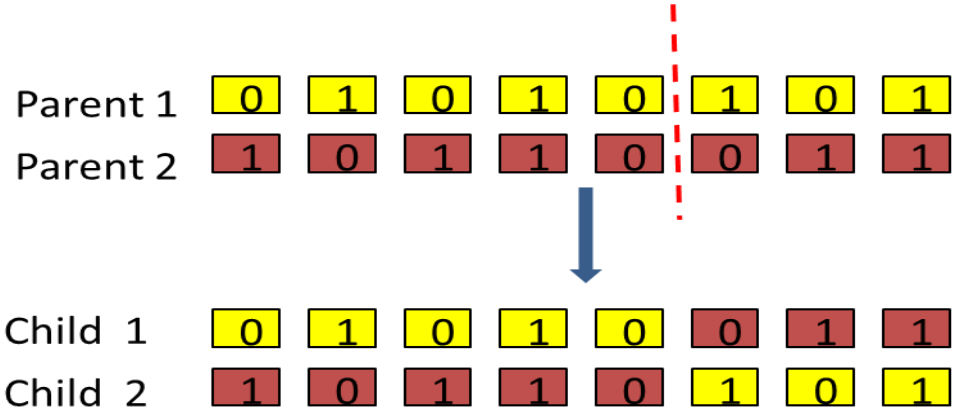

Figure 6-1 A simple one point crossover

6.2.3 Mutation

Mutation is the process of causing small random alterations of the bits in a chromosome and occurs after crossover. This process plays a significant role in recovering the lost genetic materials and prevents the GAs from being trapped at a local minimum. There are many different forms of mutation for the various kinds of representation. A simple mutation applied in binary representation by switching the value of bits at the selected position is shown in Figure 6-2.

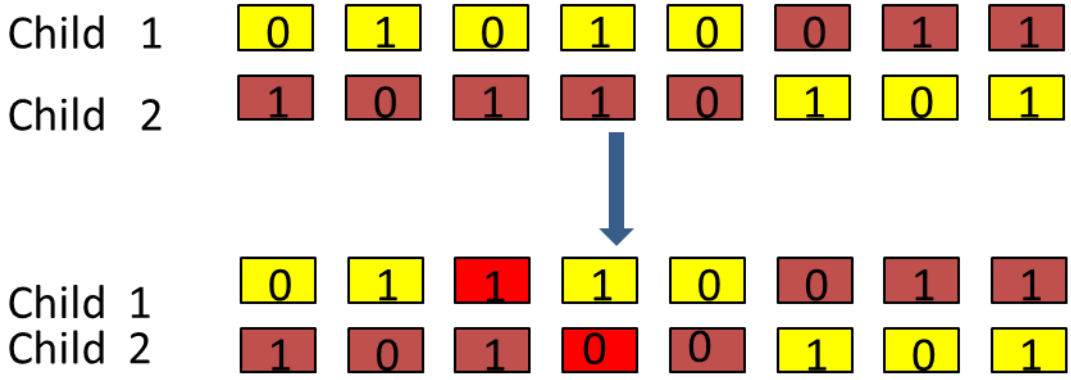

Figure 6-2 Mutation in binary genetic algorithm

6.3 Species Conserving Genetic Algorithms

The simple genetic algorithm converges to a single solution when applied to optimise a multimodal function instead of problems which have many global and local solutions (Goldberg and Richardson 1987). Li et al. (2002) developed a

new technique called species conserving genetic algorithms (SCGA) to search multiple solutions of multimodal optimisation problems on a single run by using a technique for evolving parallel subpopulations.

The SCGA depends on dividing the current population into several species according to their similarity where a species is defined as 'a group of individuals in a population with similar characteristics and is dominated by the best individual, called the 'species seed' (Li 2015). The similarity between any two individuals inside a species is specified by a parameter called species distance (σ_s). Any two individuals are similar if the distance between them is less than the species distance.

The species seed in the current population are conserved by transferring them to the next generation, and this process enables the SCGA to find multiple solutions to multimodal optimisation problems. The ability to find multiple solutions is significant for GAs because it increases the chance of locating the global optimum also the diversity of high-quality solutions provides the optimiser with insight into the nature of the state space which may help to identify innovative alternative solutions (Li et al. 2002).

The species in a population is determined by partitioning the current population (P_n) into a subset of species (S_i) centred upon its dominating individual, called the species seed (x^*). The individual is considered as a dominating individual in its species if for every individual $y \in S_i$

$$f(x^*) \geq f(y)$$

A species S_i is centred upon its species seed $\boldsymbol{x}^*$, if for every individual $\boldsymbol{y} \in \boldsymbol{S_i}$

$$d(x^*, y) < {}^{\sigma_s}/_{2}$$

Where $\sigma_s/2$ stands for the radius of species, and $d(x^*, y)$ is the distance between the species seed ($\boldsymbol{x}^*$) and non-dominating individual $\boldsymbol{y}$.

Figure 6-3 demonstrates a sample distribution of a species in a two-dimensional domain (Li et al. 2002). As can be seen from the figure, each species is formed by the dominant individual (species seed) and non-dominant individual and occupies a region of the feasibility. Some of the individuals are located at the intersection of two or more species, and this is a result of using a fixed radius to determine the species.

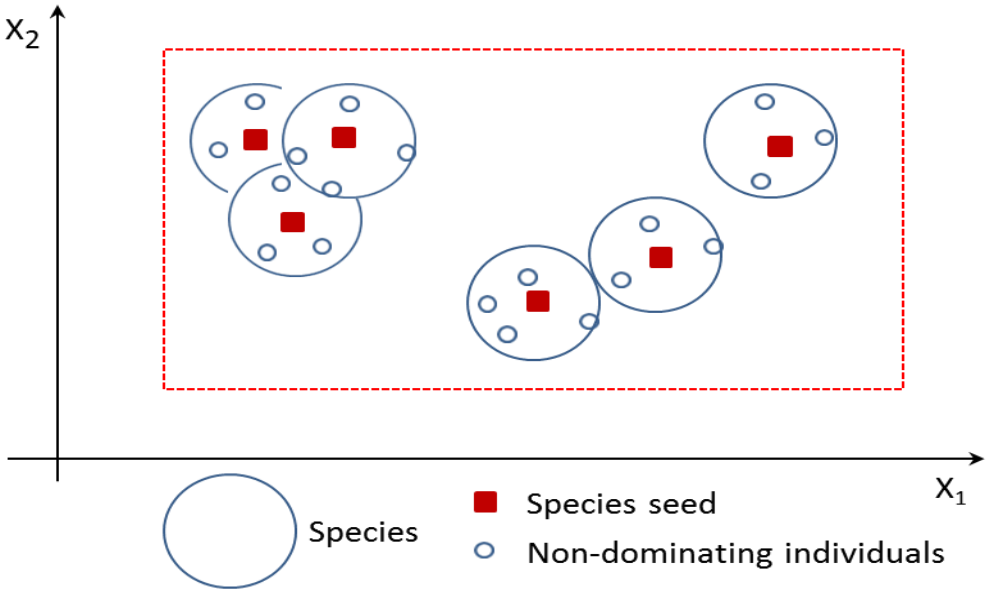

Figure 6-3 A sample distribution of species in a two-dimensional domain (Li et al. 2002)

The structure of the SCGA as introduced by Li et al. (2002) is shown in Figure 6-4

```
Begin
    t = 0;
    Initialize (t) ;
    Evaluate (t) ;
    while (not termination condition) do
        Determine species seeds X_s ;
        Select G(t + 1);
        Crossover G(t + 1);
        Mutate G(t + 1);
        Evaluate G(t + 1);
        Conserve species from X_s in G(t + 1);
        t = t + 1;
    end (while)
    Identify global optima;
end
```

Figure 6-4 The structure of the species conserving genetic algorithm(Li et al. 2002).

The differences between the SCGA and the simple genetic algorithm are that first the species seeds are determined within the current population, and then the species seed will be conserved by moving them into the next generation.

The three steps that are used in applying the SCGA as shown in Figure 6-4 are:

1. Determine the species seeds from a current population.
2. Construct the new population by applying general genetic algorithm operators (selection, crossover and mutation) by copying the identified species seed into the new population.
3. Identifying global solutions from the fittest individual in X_s (the species seed set).

6.4 Optimisation Problems

During a drilling operation, the speed of the rotary table and weight on bit are considered the main variables which can be adjusted to suppress the stick-slip motion, drill string vibration and control the rate of penetration. Therefore,

predicting the best specific operating parameters of these variables can lead to an increase in the efficiency of drilling (Irawan et al. 2012). In a drilling operation, the goal is to drill as fast as possible with low cost by preserving the integrity of the system through prevention of tool failures. In the proposed optimisation strategy, the objective function maximises the rate of penetration, and the constraint of the problem is its integrity limits by drilling with the desired speed and at the same time to ensure there is no stick-slip vibration.

The parameters that will be optimised in this study are the weight on bit and torque of rotary table and these are controllable parameters that can be easily manipulated at the rig. A model for calculating the rate of penetration (ROP) proposed by Spanos et al. (1995) is used in this study. This model relates the rate of penetration with the applied weight on the bit and the speed of the bit as follows:

$$Rop = c_1^* \times Wob\sqrt{\omega_b} - c_2^* \qquad 6.1$$

Where c_1^* and c_2^* represent the characteristics of the rock formation and in this thesis the values of 1.57×10^{-5} and 0.685 respectively have been used. These constants were selected to satisfy a reasonable value of rate of penetration (ROP) for the case of drilling hard rocks (Spanos et al. (1995). The units of rate of penetration, weight on the bit and velocity of the bit are m/hr, N and rev/min respectively.

As previously mentioned, the LDLM will be used to calculate the velocity of the bit, and this model relates the rotary torque, weight on bit and speed of bit as shown in Figure 4-3. The whole drilling system from equation 6.1 and Figure 4-3 is shown again in Figure 6-5 for ease of reference.

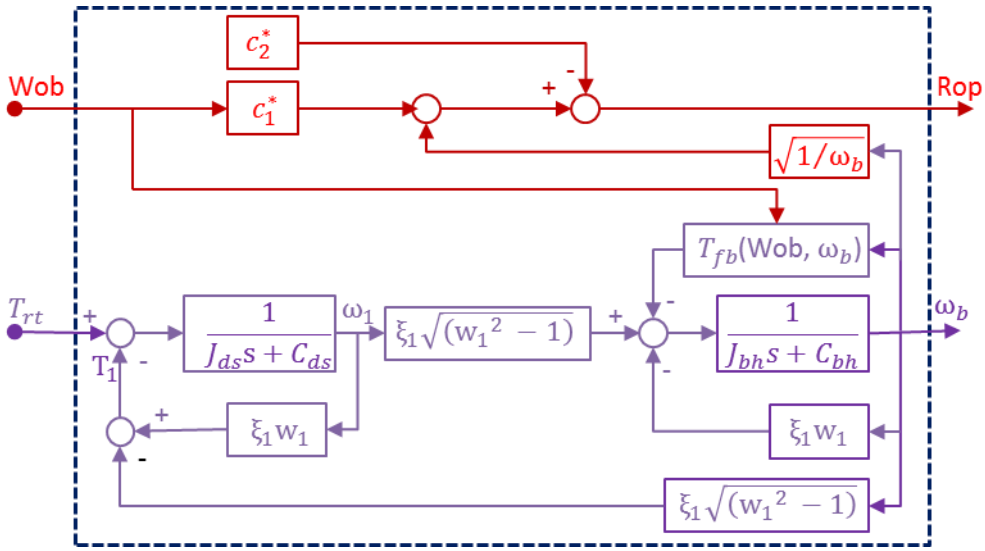

Figure 6-5 Block diagram of the drilling system with two inputs and two outputs

6.4.1 Objective function

In this work, the problem of selecting the optimum drilling parameters (rotary torque and WOB) is converted to an optimisation problem, which is solved by coding the dynamic model of drilling in Matlab software to represent the objective function; a block model of this is shown in Figure 6-6.

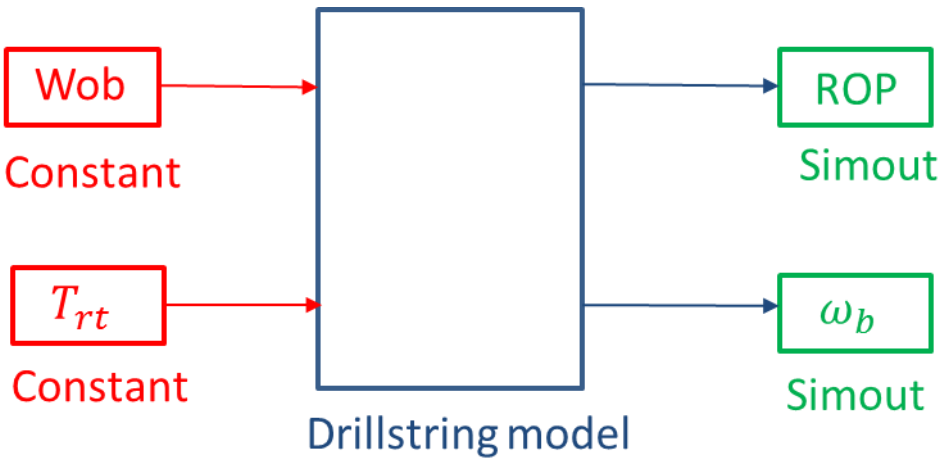

Figure 6-6 Block model representing the objective function

The objective function is coded in Matlab as shown in Figure 6-7 as follows

1. Write a function in Matlab to calculate the maximum rate of penetration from the two input variables, the weight on bit (Wob) and the rotary torque.
2. Use the command *get_param* (get parameter) to specify the input variables to the Simulink model by inputting the name of the model and the location of the input variables (model workspace)
3. Assign the input variables to the model (weight on bit and rotary torque) in the model workspace by using the command *assignin*.
4. Simulate the Simulink model by using the sim command line options and specify the simulation time.
5. Retrieve the output of the model, the bit velocity and rate of penetration, by using the command *get*.
6. To ensure that there was no stick-slip the minimum value of the bit speed must be greater than zero, therefore the minimum speed will be calculated. Also, the velocity of the bit at steady state will be calculated.
7. To use the minimum value of bit velocity in transition and steady state, the two values must be written as global values to be seen by the constraining function.
8. The maximum value of the rate of penetration is calculated during steady state motion.

```
function [max_ROP]=fun(Wob,T_rt)
  hws=get_param('LDLM','modelworkspace');
  assignin(hws,'Weight',Wob);
  assignin(hws,'Torque',T_rt);
  simOut = sim('LDLM', 'StopTime', '100');
  ω_b = get(simOut, 'ω_b');
  ROP = get(simOut, 'ROP');
  min_ω_b=min(ω_b);
  ss_ω_b=mean(ω_b (95000:100001))
  global min_ω_b;
  global ss_ω_b;
  max_ROP=-mean(ROP(95000:100001));
End
```

Figure 6-7 The objective function as coded in Matlab

6.4.2 Constraints

There are two constraints subjected to the objective function which should be achieved to ensure that the optimisation is done appropriately. The first constraint is that the minimum value of bit velocity in the transient phase is greater than zero to make sure that stick-slip will not occur with that WOB and rotary torque. The second constraint is that the velocity of the bit in the steady-state period is equal or less than the desired velocity of drilling.

The optimisation problem is defined as:

maximise $ROP(Wob, T_{rt})$
Subject to:
$\omega_b(t) > 0$; $(any\ t)$
$\omega_b(t) \leq 125$; $(steady\ state; 95 \leq t \leq 100)$

6.5 Results and Discussion

The purpose of optimisation the parameters of drilling are to achieve many targets such as decrease the cost of drilling, reduce the time of drilling, minimise the failure of equipment and increase the efficiency of drilling. Stick-slip is considered to be the main cause of increasing the time of drilling and

increasing the fatigue problem and other issue as demonstrated in the literature chapter. Therefore, suppression of the stick-slip oscillations is significant for the drilling operation. Suppress the stick-slip vibration can be implemented by increasing the velocity of drilling or decreasing the weight on bit, however, increase the velocity can lead to increase the wear of bit also the velocity can not be increased beyond the ability of DC motor. While decreasing the weight on bit can result in decreased the rate of penetration.

Since in real drilling, the drill operator attempts to drill at the desired velocity of approximately 125 rev/min to avoid stick-slip, the target of optimisation is to optimise the weight on the bit and rotary torque to ensure there is no stick-slip vibration at the desired velocity. The other target is to identify the values that will achieve the maximum rate of penetration at this speed. To provide additional insight all the other possible values for the rate of penetration at this velocity will also be obtained. The modelling and optimisation system software (MOS) (Li et al. 2002) is used to apply the SCGA to optimise the Wob and rotary torque for the three different lengths of drillpipe that were modelled in the last chapter with the same parameters of drilling as shown in Table 4-1, Table 4-2, Table 4-3 and Table 4-4.

6.5.1 Case study one (length of drillpipe 500 m)

The MOS, which was used to apply SCGA method, provides multiple solutions of a problem in one run and gives the solution in descending order starting from the maximum objective function value and ending with the minimum value. The optimisation process can be run many times to get a range of solutions. Table 6-1 shows the possible values for weight on the bit (Wob) and torque of the rotary table (T_{rt}) that can be used to ensure that the velocity of the bit is in the range ≤125rev/min without stick-slip vibration. The table also provides the

maximum weight that can be used to get the maximum rate of penetration without stick-slip. Also shown is the threshold value of weight on the bit below which there is no significant value of the rate of penetration.

Table 6-1 Number of solutions at ≤125rev/min (case one)

Number of solution	Weight on bit (kN)	Torque of rotary table (kNm)	Velocity of bit (rev/min)	Rate of penetration (m/hr)
1	61.99929	12.73513	124.9925	10.2167
2	57.23275	12.16514	124.3101	9.3515
3	54.53212	11.86518	124.3402	8.8791
4	51.14188	11.51306	124.8987	8.3047
5	46.00276	10.91813	124.4208	7.3860
6	42.40430	10.51903	124.4590	6.7559
7	40.00977	10.27703	124.9904	6.3508
8	36.51271	9.87842	124.7945	5.7309
9	34.13635	9.58152	124.1029	5.2967
10	29.51254	9.08632	124.5277	4.4955
11	25.42696	8.63711	124.6524	3.7807
12	20.53955	8.1039	124.8893	2.9260
13	16.38712	7.60701	124.1472	2.1876
14	12.48297	7.17977	124.3056	1.5048
15	9.89845	6.88625	124.1794	1.0508
16	7.76104	6.64011	124.0008	0.6752

Figure 6-8 shows that a linear relationship is observed between the ROP, Wob and torque of the rotary table. The rate of penetration increased with an increase in the weight on the bit and rotary torque. The maximum value of the rate of penetration was 10.2167 m/hr when the weight on the bit was 62.0kN and the rotary torque was 12.7 kNm. It can be observed from Figure 6-8 that different rates of penetration can be achieved with the same velocity but with the various values of weight on bit and rotary torque.

Figure 6-9 and Figure 6-10 show the maximum rate of penetration (10.2 m/hr) and the desired speed (125.0 rev/min). The two figures show that at the maximum rate of penetration the velocity of drilling is just above the critical speed and any increase in the weight on the bit or decrease in the rotary torque

will cause the stick-slip vibrations to start. Therefore, the other values, which are located between the maximum and threshold values, can be used to drill at a safe mode without stick-slip vibrations.

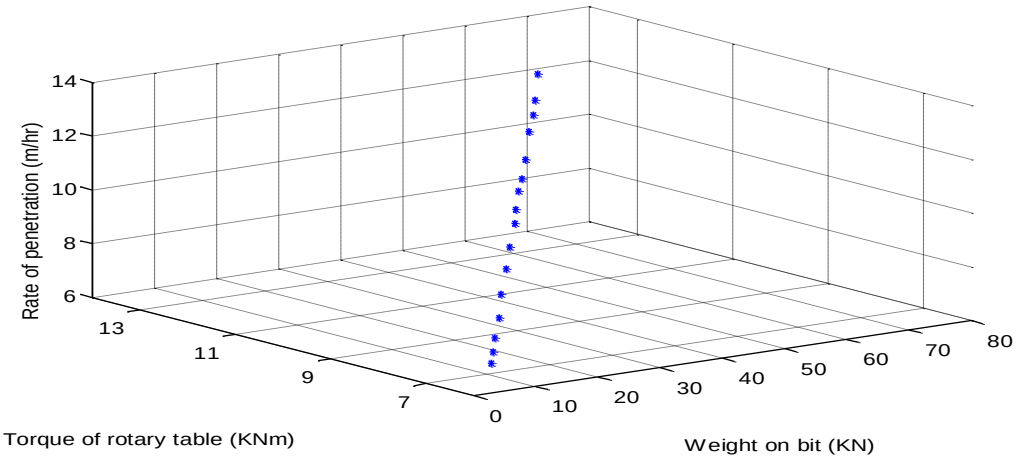

Figure 6-8 Three dimensional plot of rate of penetration (Rop) when velocity of the bit was ≤125rev/min ($l_{dp} = 500m$)

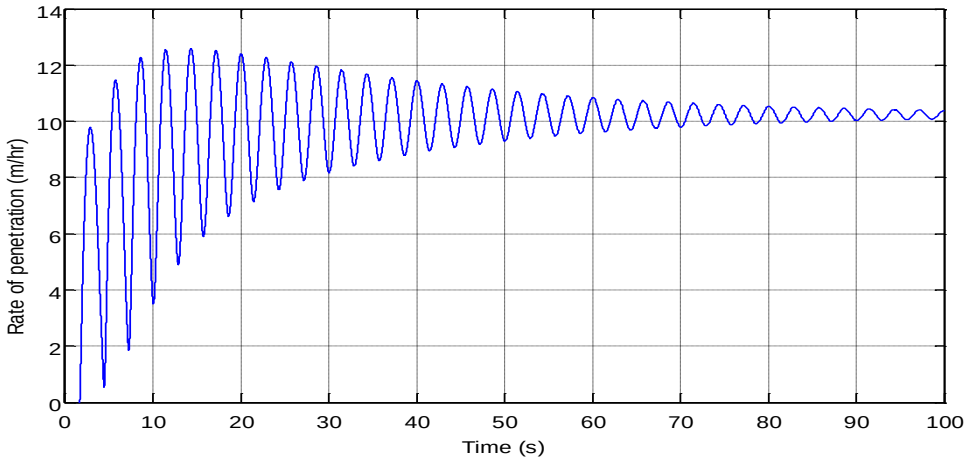

Figure 6-9 Maximum rate of penetration (Rop) at a bit velocity of 124.9925 rev/min ($l_{dp} = 500m$)

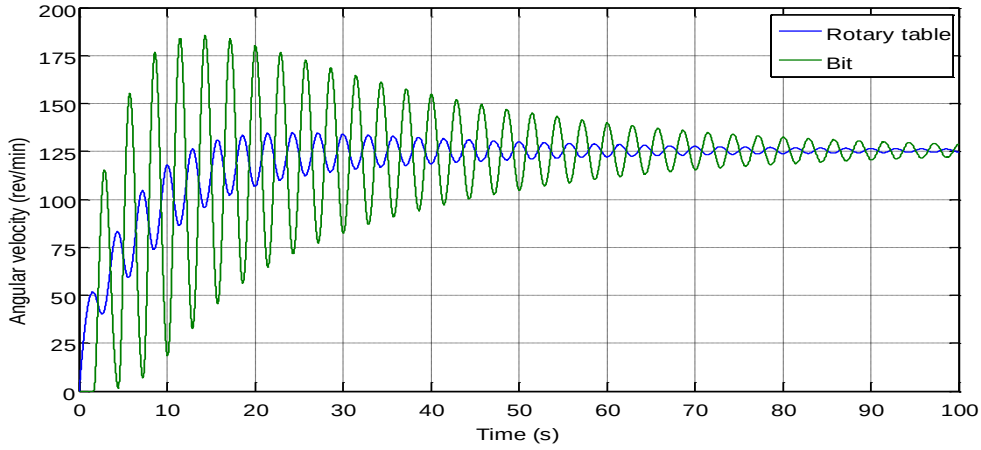

Figure 6-10 Velocity of drilling at maximum rate of penetration (Rop) ($l_{dp} = 500m$)

To have a complete picture of the relationship between the rate of penetration, weight on the bit and the rotary torque, a surface plot can be drawn from the result of Table 6-1. The Rop surface of Figure 6-11 shows that the surface is smooth where there is no stick-slip oscillation and for conditions when the stick-slip starts the surface suddenly begins to fluctuate as the Rop values become unstable due to the effect of stick-slip vibration. This surface plot provides useful information to the driller about the area of stick-slip vibration and the safe values and the corresponding predicted rates of penetration that can be used to ensure there is no stick-slip vibration.

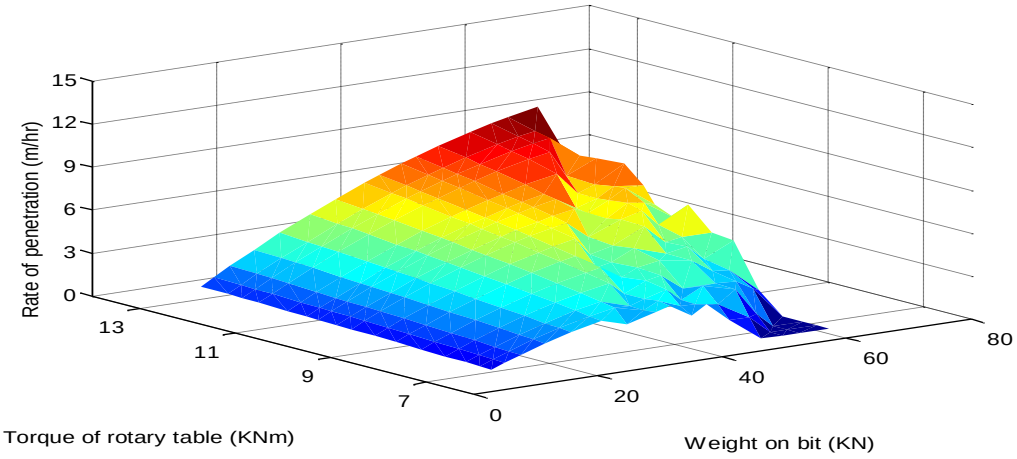

Figure 6-11 Surface plot of rate of penetration (Rop) vs weight on bit (Wob) and torque of rotary table (T_{rt}) ($l_{dp} = 500m$)

During the drilling operation, the driller mostly controls the velocity of drilling instead of the applied rotary torque because the aim is to drill with a velocity above the critical speed where there is no stick-slip vibration. In addition, the velocity of drilling must be appropriate to the type of bit that is used for drilling. Figure 6-12 shows the relationship between the velocity of the bit, torque of the rotary table and the weight on the bit. The surface shows that the relation between the velocity and weight on bit and torque of rotary table is linear and shows that by increasing the weight on the bit the stick-slip will start. This relationship becomes nonlinear, and this is very clear in the surface plot where the fluctuating surface appears due to the change in the value of velocity during the stick-slip vibrations.

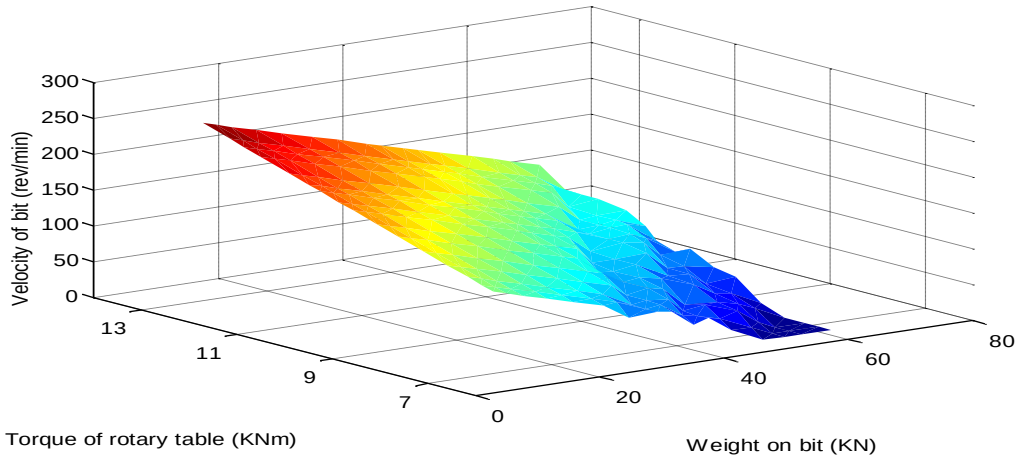

Figure 6-12 Surface plot of velocity of bit (ω_b) vs weight on bit (Wob) and torque of rotary table (T_{rt}) ($l_{dp} = 500m$)

The response surface of Figure 6-13 shows that the rates of penetration, weight on bit and the rotary torque have a linear relationship until the stick-slip begins. It can be seen from the surface plot that the rate of penetration increases with an increase of the weight on the bit and velocity of the bit and then, due to stick-

slip, the fluctuating surface is apparent. From the surface plot of the rate of penetration (Figure 6-13), it can be seen that the weight on the bit has a significant impact on the rate of penetration compared to the effect of velocity.

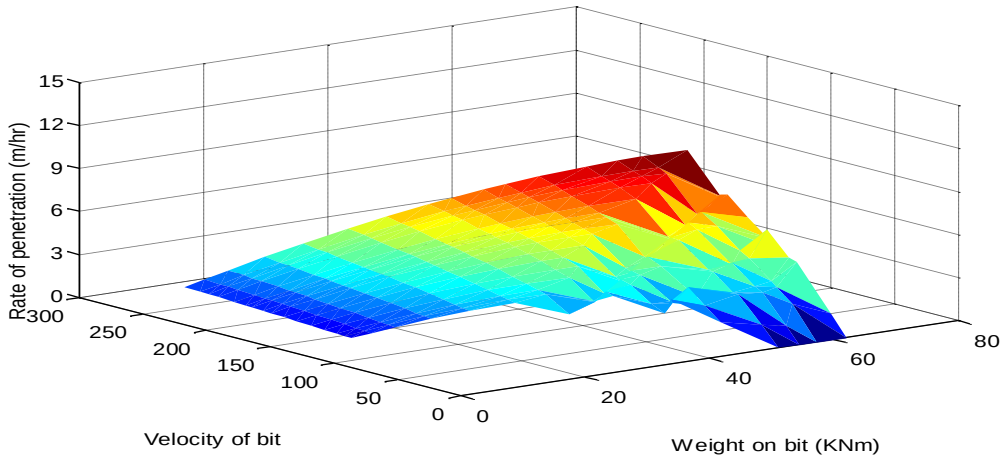

Figure 6-13 Surface plot of rate of penetration (Rop) vs velocity of bit (ω_b) and weight on bit (Wob) ($l_{dp} = 500m$)

6.5.2 Case study two (length of drillpipe 2000 m)

When the drilling operation progresses the length of drillpipe increases and this leads to a decrease in the stiffness of the drillpipe. Typically the hardness of the rock will also increase ad deeper depths. Therefore, the probability of stick-slip occurring will be increased. However, due to the casing operation, the well will be narrower and the diameter of the bit will decrease, this will lead to a reduction in the cutting torque and hence reduces the possibility of stick-slip oscillation.

Table 6-2 shows the all possible values of Wob and T_{rt} that can be used by the driller to drill at the desired velocity (≤125rev/min) without stick-slip vibration.

Table 6-2 Number of solutions at ≤125rev/min (case two)

Number of solution	Weight on bit (kN)	Torque of rotary table (kNm)	Velocity of bit (rev/min)	Rate of penetration (m/hr)
1	96.98548	13.61100	124.4267	16.3300
2	89.07835	12.97489	124.0273	14.9179
3	84.57021	12.66331	124.8418	14.1769
4	78.41521	12.14360	124.0097	13.0493
5	71.87818	11.67385	124.8096	11.9450
6	65.07381	11.1442	124.8031	10.7492
7	61.27486	10.85221	124.8747	10.0848
8	57.34632	10.51749	124.2763	9.3702
9	54.49962	10.31179	124.5990	8.8835
10	51.98037	10.11239	124.5293	8.4387
11	47.563214	9.74539	124.0528	7.6475
12	43.27838	9.42332	124.2911	6.9042
13	39.17841	9.09694	124.1493	6.1814
14	35.34521	8.83245	124.8537	5.5273
15	31.4535	8.5081	124.4222	4.8338
16	28.03672	8.23984	124.3812	4.2336
17	25.58969	8.07529	124.9170	3.8141
18	23.13515	7.84669	124.1451	3.37003
19	21.63465	7.76389	124.8470	3.1178
20	19.82108	7.62354	124.8642	2.7993
21	16.48011	7.3511	124.6098	2.2093
22	12.31354	7.02807	124.6348	1.4780
23	10.7035	6.8816	124.2045	1.1921
24	7.41396	6.61867	124.0689	0.6148
25	3.49884	6.34292	124.6691	0.0696

Figure 6-14 shows the 3D plot of Rop, Wob and $\boldsymbol{T_{rt}}$ at the desired velocity of drilling (≤125rev/min). It can be seen from Table 6-2 and Figure 6-14 that the maximum Rop increased from the 10.2 m/hr of case study one to 16.3 m/hr in case two with associated increase of the weight on the bit and torque of the rotary table. This increase in the rate of penetration without stick-slip is attributed to the decrease in the diameter of the bit due to the casing operation which results in a decrease of the static and dynamic friction torque. Another observation was that the threshold value for weight on the bit was approximately same for the two cases: 7.76kN for case one and 7.41kN for case two because the threshold value depends upon the type of rock.

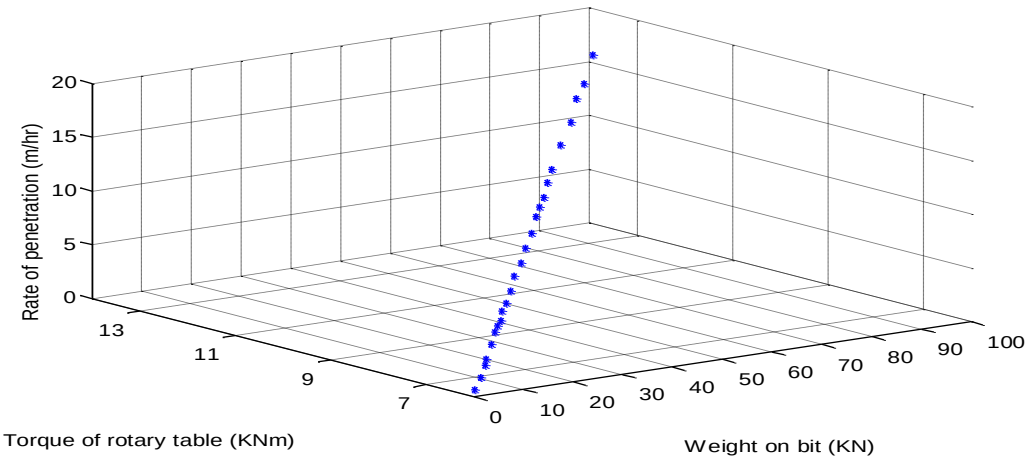

Figure 6-14 Three dimensional plot of rate of penetration (Rop) when velocity of the bit was ≤125rev/min ($l_{dp} = 2000m$)

Figure 6-15 shows the maximum rate of penetration that can be obtained at the desired speed, whilst Figure 6-16 shows the drilling velocity at this rate of penetration without stick-slip oscillation. It can be seen from the two figures that with these parameters, where Wob and T_{rt} are 96.98kN and 13.61kNm, the drilling was just above the critical speed and any change in these parameter by increasing the weight or decreasing the torque of the rotary table will lead to stick-slip vibration. Also, when comparing Figure 6-15 and Figure 6-16 with that of Figure 6-9 and Figure 6-10 in case one, it can be seen that the time of transient response and the vibration are decreased due to the increased damping along the drillstring.

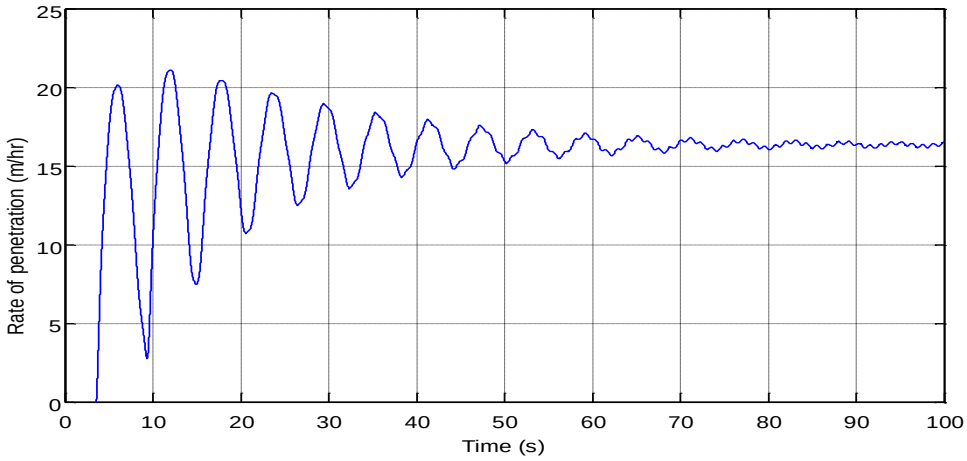

Figure 6-15 Maximum rate of penetration (Rop) at a bit velocity of 124.4267rev/min($l_{dp} = 2000m$)

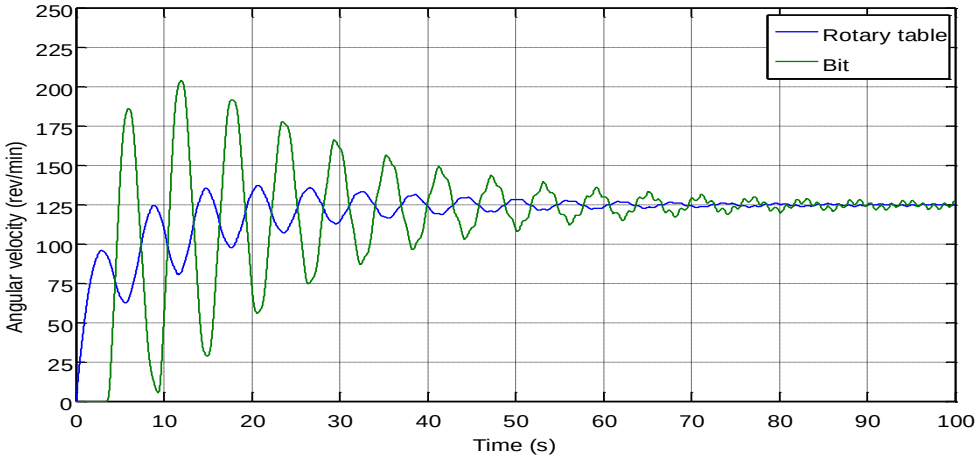

Figure 6-16 Velocity of drilling at maximum rate of penetration (Rop) ($l_{dp} = 2000m$)

As with case study one, the surface plot of Figure 6-17 shows the relationship between the rate of penetration Wob and T_{rt}. It can be seen from the surface plot that the rate of penetration increases with an increase in both weight on the bit and torque of the rotary table and the surface is smooth. However, when the conditions induce stick-slip, a sudden decrease in the Rop causes fluctuations appears in the surface plot before the value goes to zero. The fluctuation of the

Rop is increased when compared with case study one (Figure 6-11) due to the increased length of drillpipe which leads to a reduction in its stiffness.

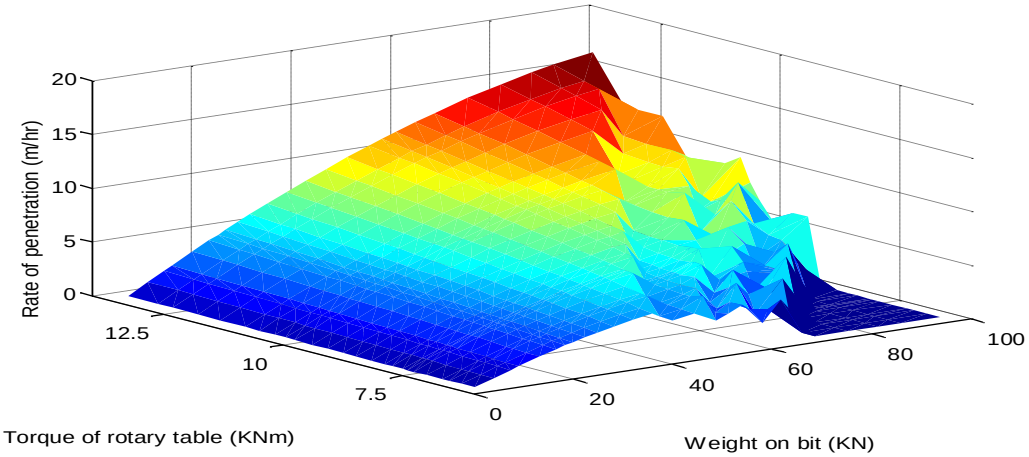

Figure 6-17 Surface plot of rate of penetration (Rop) vs weight on bit (Wob) and torque of rotary table (T_{rt}) ($l_{dp} = 2000m$)

Figure 6-18 shows the response surface created for the velocity of the bit with respect to weight on the bit and torque of rotary table. As with case study one, it can be seen from the surface that in an ordinary mode where there is no stick-slip vibration the surface is smooth and when the stick-slip occurs the fluctuations on the surface appear clearly. The maximum velocity of the drilling in case study two approximately 270 rev/min (Figure 6-18) while in case study one (Figure 6-12) it was approximately 200 rev/min. In addition, the area of stick-slip vibration increased before the velocity fell to zero.

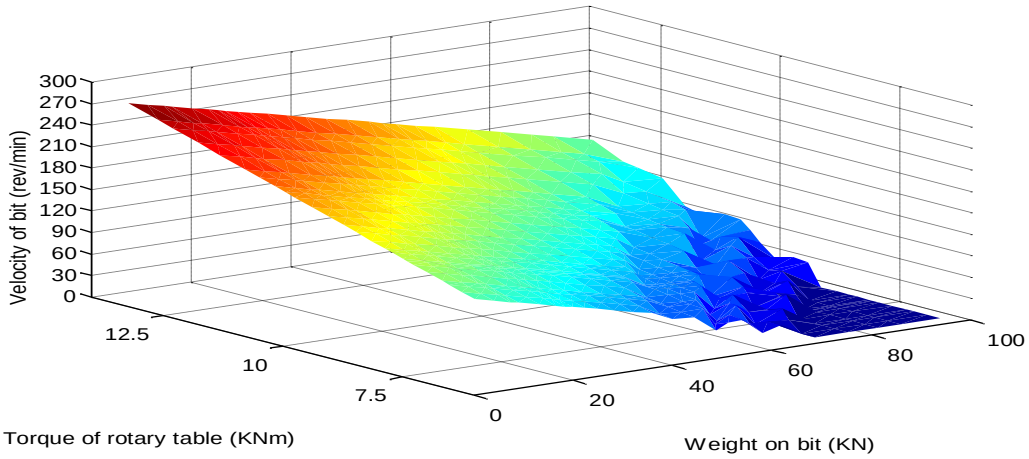

Figure 6-18 Surface plot of velocity of bit (ω_b) vs weight on bit (Wob) and torque of rotary table (T_{rt}) ($l_{dp} = 2000m$)

The relationship between the rate of penetration, the velocity of the bit and the weight on the bit as a surface response is shown in Figure 6-19. It can be seen from the figure that the value of Rop fluctuated when stick-slip occurred and even with an increase in either the weight on the bit or rotary table velocity, the Rop will not increase steadily and the relationship is non-linear.

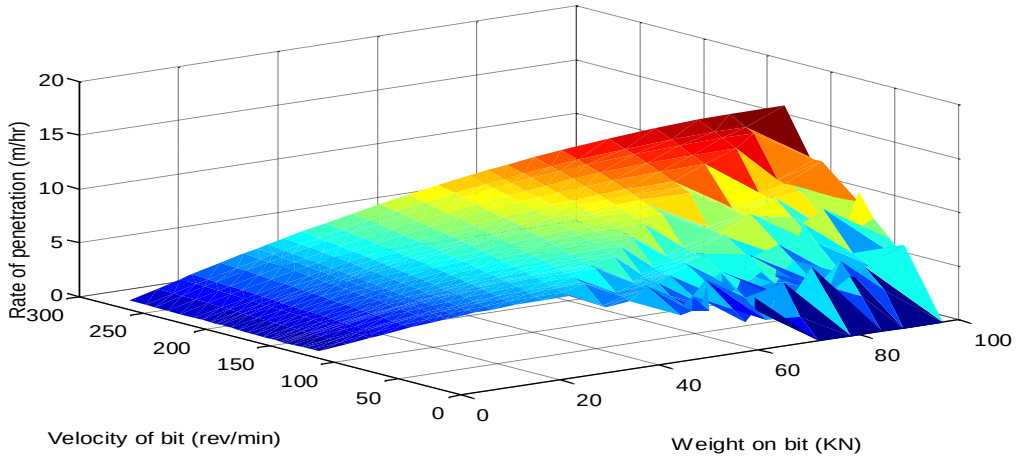

Figure 6-19 Surface plot of rate of penetration (Rop) vs velocity of bit (ω_b) and weight on bit (Wob) ($l_{dp} = 2000m$)

6.5.3 Case study three (length of drillpipe 5700m)

The third case study is when the length of drillpipe is equal to 5700m, where the stiffness of the drillpipe is reduced from 1892Nm/rad in case one to only 166Nm/rad, and it can be seen that now the drillpipe is very soft and the probability of stick-slip is also very high. However, at this length, the diameter of the bit has also reduced from 0.22225m (17.5inch) in case one to 0.1075m (8.5inch). This leads to a decrease in the static and dynamic friction torque from 8890Nm and 5556.3Nm in case one to 4318Nm and 2699Nm in case three, and this helps to decrease the effect of the reduction in stiffness. In addition, the other factor that is crucial to reduce the effect of low stiffness and decrease the possibility of stick-slip is that the diameter of the drillcollar has also changed and which leads to a decrease in the mass moment of inertia of the drillcollar from 445.85 kgm^2 to 137.38 kgm^2.

The results presented in Table 6-3 were calculated by taking more than one run of the SCGA to have a range of results at which there was no stick-slip vibration at the desired speed of drilling. From Table 6-3 it can be seen that the maximum weight on the bit has increased although the drillpipe is very soft; this is attributed to the decrease of static and dynamic friction, decrease in the mass moment inertia of the drillcollar and increase in the damping at the BHA. The threshold value of case three is similar to case one and two because, as mentioned before, this value depends on the type of rock and in this study, it is assumed that the rock is identical in the three case studies.

Table 6-3 Number of solutions at ≤125rev/min (case study three)

Number of solution	Weight on bit (kN)	Torque of rotary table (kNm)	Velocity of bit (rev/min)	Rate of penetration (m/hr)
1	178.26837	16.48141	124.6707	30.6202
2	170.88398	16.04705	124.0764	29.2520
3	166.11137	15.78923	124.1004	28.4188
4	160.56247	15.48913	124.1107	27.4478
5	155.46645	15.22915	124.3952	26.5861
6	151.11643	14.98114	124.1652	25.7986
7	145.7525	14.72913	124.8567	24.9296
8	138.07329	14.3216	124.9845	23.5925
9	134.19892	14.11325	124.9927	22.9121
10	128.96581	13.81923	124.7573	21.9707
11	122.12162	13.44871	124.7244	20.7656
12	120.04973	13.29933	124.0370	20.3434
13	116.62344	13.16764	124.9969	19.82219
14	109.57558	12.75524	124.4139	18.5380
15	100.18099	12.27175	124.8527	16.9209
16	94.07835	11.94089	124.8298	15.8470
17	89.61743	11.68123	124.4870	15.0415
18	84.96749	11.45117	124.8664	14.2483
19	77.11873	10.98327	124.0583	12.8250
20	73.50195	10.83971	124.9975	12.2401
21	70.01242	10.6502	124.9782	11.6256
22	67.54456	10.51353	124.9219	11.1890
23	64.32181	10.33357	124.8215	10.6180
24	60.28729	10.12342	124.9518	9.9146
25	57.66354	9.98147	124.9376	9.4527
26	52.45846	9.65606	124.1190	8.5075
27	48.2804	9.46826	124.8122	7.7990
28	42.86373	9.18311	124.9589	6.8517
29	35.29702	8.76889	124.8399	5.51848
30	33.84355	8.6872	124.7788	5.2616
31	29.91968	8.47388	124.7517	4.5717
32	23.56342	8.09360	124.0843	3.4441
33	18.36392	7.81364	124.0978	2.5333
34	11.66394	7.46963	124.4130	1.3621
35	7.66346	7.28537	124.9893	0.6634
36	6.32659	7.19755	124.7045	0.4271

Figure 6-20 shows the 3D plot of the Rop with respect to torque of the rotary table and weight on the bit. It can be seen from the figure that the maximum Rop is high (30.6m/hr) when compared with case one and case two and this is due to low static and dynamic friction torque because the radius of the bit is smaller at this length. Also, the number of the solutions has increased and this

gives the driller more flexibility in choosing the desired parameters of drilling (weight on the bit and torque of the rotary table) without stick-slip vibrations.

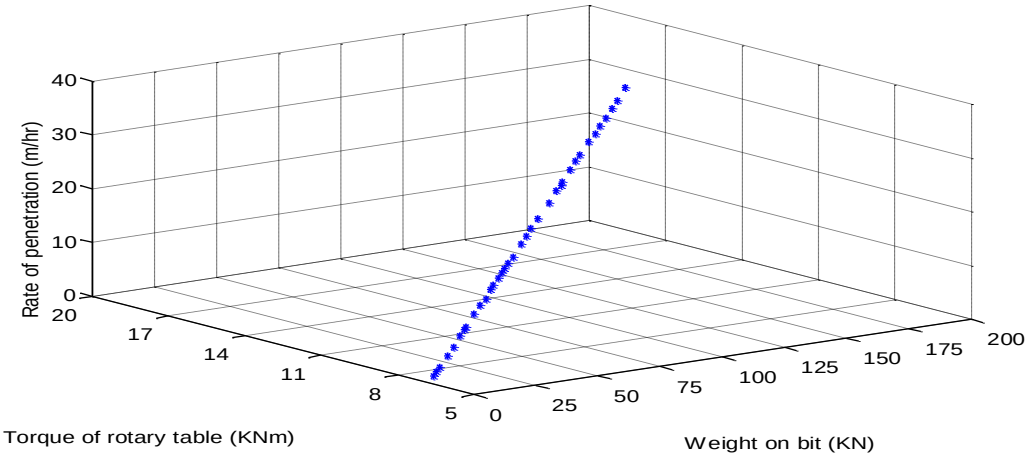

Figure 6-20 Three dimensional plot of rate of penetration (Rop) at a velocity of ≤125rev/min ($l_{dp} = 5700m$)

Figure 6-21 shows the response of maximum rate of penetration at the desired speed (Figure 6-22). It can be seen that the transient response time is very low when compared to case one and case two and this is due to two reasons: the first is the increase in the damping and the second is due to the decrease of the mass moment inertia of the bottom hole assembly (BHA).

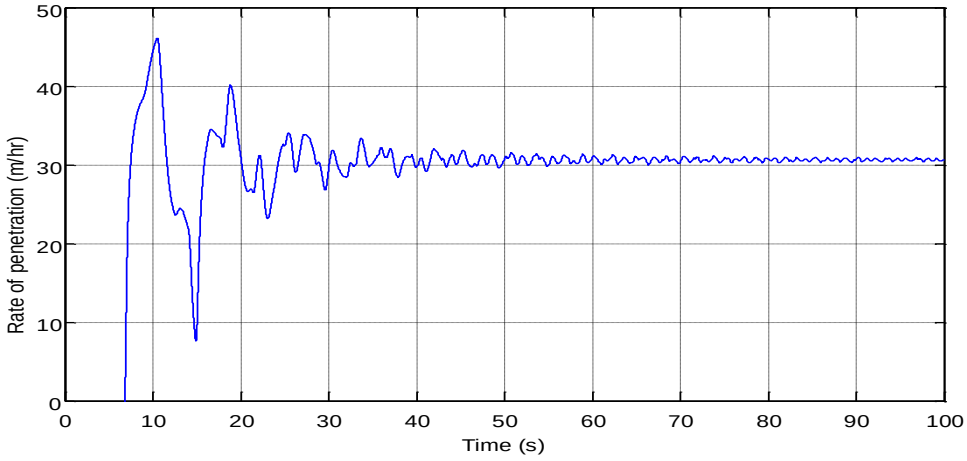

Figure 6-21 Maximum rate of penetration (Rop) at a bit velocity of 124.4267rev/min ($l_{dp} = 5700m$)

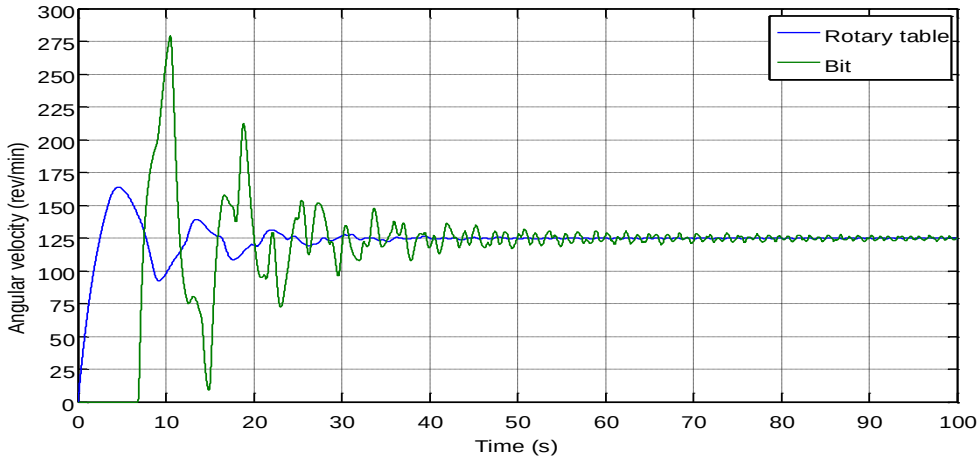

Figure 6-22 Velocity of drilling at maximum rate of penetration (Rop) ($l_{dp} = 5700m$)

The response surface for the Rop is shown in Figure 6-23. It can be seen from the figure is that the transfer from slip phase to stick-slip phase is more sharp when compared to case one (Figure 6-11) and case two (Figure 6-17). In addition, the fluctuation of the Rop in the stick-slip area is very high when compared with case one and case two; this is due to the effect of the low stiffness of the drillpipe.

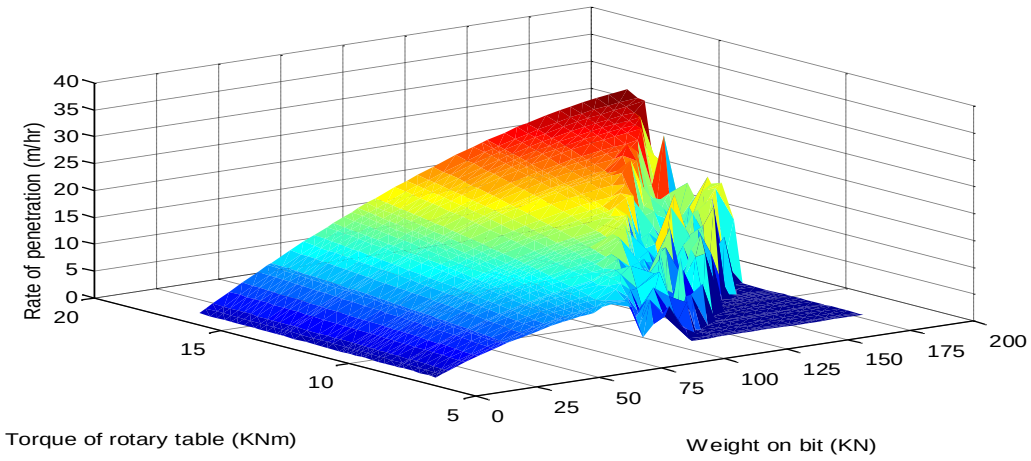

Figure 6-23 Surface plot of rate of penetration (Rop) vs weight on bit (Wob) and torque of rotary table (T_{rt}) ($l_{dp} = 5700m$)

Figure 6-24 shows the response surface of the velocity of the bit and rotary table. It is clear from the figure why the fluctuation of the Rop is high in the stick-slip area, and this is due to the high fluctuation in the velocity of the bit because of the low stiffness of the drillpipe. The fluctuation is high when compared to case one (Figure 6-12) and case two (Figure 6-18) because the stiffness of the drillpipe very low when compared to case one and two.

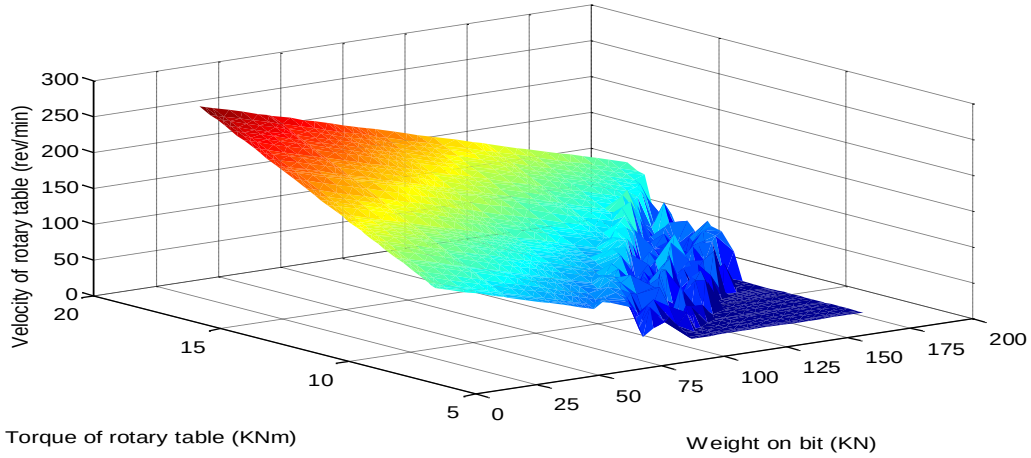

Figure 6-24 Surface plot of velocity of bit (ω_b) vs weight on bit (Wob) and torque of rotary table (T_{rt}) ($l_{dp} = 5700m$)

The 3D surface response of Rop (Figure 6-25) shows a linear relationship between the Rop and the weight on the bit and velocity of the bit in the ordinary mode as in case one (Figure 6-13) and case two (Figure 6-19). However, the non-linearity is very high in the stick-slip phase when compared to case one and two. From Figure 6-25 it can be seen that the inclination in the value of Rop is very high in the stick-slip phase when compared with case one and case two and this is due to an increase in the time of sticking compared to the time of slipping. Increase in the time of sticking can be attributed to the decrease in the stiffness of the drillpipe; this means more twist is generated in the drillpipe to get torque higher than the static torque in order to release the bit and start to rotate the bit again.

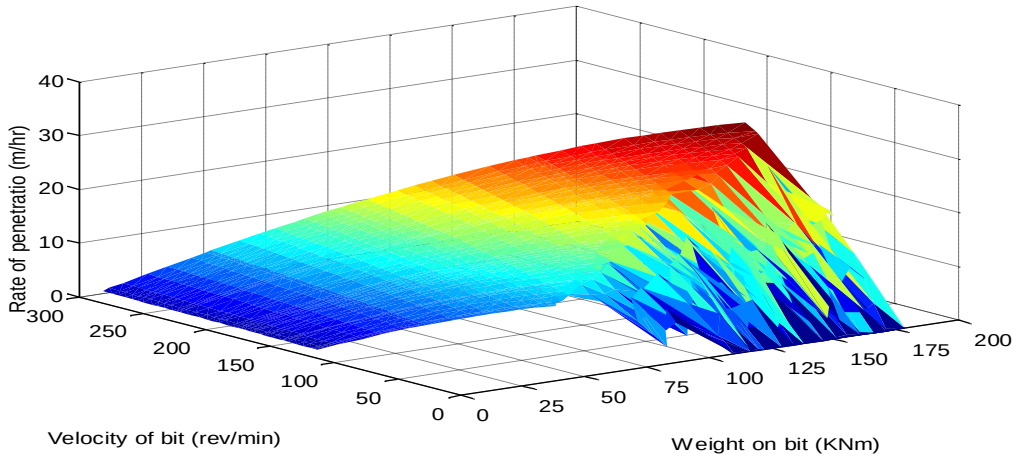

Figure 6-25 Surface plot of rate of penetration (Rop) vs velocity of bit (ω_b) and weight on bit (Wob) ($l_{dp} = 5700m$)

6.6 Summary

This chapter presented an overview of the objective of drilling optimisation and the classification of the drilling parameters as controllable and uncontrollable parameters, and the classification of the services (real-time service (RTS) and Next well service (NWS)) that are provided to the driller to select optimum drilling parameters.

The concept of genetic algorithms (GAs) and the main differences between the GAs and conventional optimisation approaches were presented. The main steps that were used to apply the reproduction process (selection, crossover and mutation) inside the GAs were explained. The details relating to species conserving genetic algorithms (SCGA) were presented, and the principle of working were introduced briefly

The optimisation problem was explained, and the relation between the drilling parameters (weight on bit and rotary torque) were shown in Figure 6-5. The objective function and the constraints were also introduced.

Three case studies were used to optimise the weight on bit and rotary torque. The results show that a decrease in the radius of the bit led to an increase in the rate of penetration and increase in the number of the solutions despite a reduction in the stiffness of drillpipe due to increasing the length. Also, the surface response showed that the area of the slip phase was smooth while the area of the stick-slip phase produced fluctuations. The desired speed at the maximum rate of penetration can be considered as the critical speed because any change in the weight on the bit or torque of the rotary table was shown to initiate stick-slip vibration. The results showed that the hybrid modelling technique combined with the SCGA method can be used effectively to optimise the drilling parameters and to get surface plot represent the slip phase and stick-slip phase which occur during the drilling process. This information would be valuable to the drilling operator and company in their quest to reduce the cost of drilling and increase the speed.

CHAPTER 7: CONCLUSION AND RECOMMENDATIONS FOR FURTHER WORK

Chapter 7

Conclusion and Recommendations for Further Work

This chapter deals with the major findings of the comparison between the distributed-lumped models (hybrid) and lumped model in modelling and simulation of stick-slip phenomena as shown in chapters 4 and 5 and the optimisation of drilling parameters as shown in chapter 6. Recommendations for further work are also included in this chapter.

7.1 Summary

The overall aim of this thesis was divided into two subjects. First, to develop a new model for the modelling and simulation of stick-slip vibration in an oil well drilling system in which the drillstring was modelled as a distributed-lumped model system (hybrid). Secondly, using species conserving genetic algorithms (SCGA) to optimise the weight on bit and torque of the rotary table to prevent stick-slip vibrations and to obtain all possible solutions at the desired speed of drilling.

A literature review on the modelling and simulation of drillstring of oil drilling system to study the stick-slip vibration showed that all previous published work had treated the drillstring solely as either a lumped model or distributed model and that there was no work in which the drillstring had been modelled as a composition of lumped and distributed components (hybrid). However, in reality the drillstring consists of distributed elements such as, drillpipe, HWDP and drillcollar which have inertia, stiffness and mass distributed over many meters of length; and pointwise concentrated elements such as, drill bit, gearing and

rotary table which are considered as a part of the drilling system when modelling the drillstring.

In this work, the distributed-lumped model (hybrid) was used to model the drillstring to study the stick-slip motion. The rotary system components and the drill bit were treated as lumped elements and their dynamics were represented by ordinary differential equations. The three pipes of the drillstring (drillpipe, HWDP and drillcollar) were treated as distributed elements, represented by the partial differential equations, to represent the distributed nature of these pipes. This resulted in developing three drillstring models (LDLM, LDDLM and LDDDLM) based upon the distributed-lumped modelling technique. Another lumped model with two degrees of freedom was developed based upon the lumped modelling approach. Also the drilling parameters (torque of rotary table and weight on bit) were optimised to prevent stick-slip vibration at the desired speed by using the species conserving genetic algorithm (SCGA) method.

From the comparison between the two models in three case studies as shown in chapters 5 and 6 and also the comparison with real measurements from past research, the following conclusions can be drawn:

1. The comparison between the new model (DLM) and the conventional model (LM) showed that there was a significant difference between the two models in reflecting the response of drilling parameters especially in the transient response due to the effect of distributed mass, inertia and stiffness of the drillstring and showed the importance of taking into consideration the length of drillstring when modelling the drilling system.

2. The new method of modelling permits more detailed modelling of the drillstring and its vibrations and has shown the ability to predict the response of different parameters along the drillstring. It was shown that taking the length of the HWDP in consideration when modelling the drillstring had little impact on the output response while the drillcollar had a big impact on the output response.

3. The method has been shown to mimic the response of the real system with more accuracy and detail and this confirmed the ability of the hybrid model to predict the actual response of the distributed nature of the drillstring when compared to the lumped model. Therefore, the DLM method is far more suited to use with real time measurements in order to improve the efficiency of the drilling process.

The contribution to knowledge based on the work in this thesis is a new model (DLM) for oilwell drillstring modelling which has the ability to consider the drillstring as a distributed mass, inertia and stiffness by taking the length of drillstring on consideration. This new model was efficient with the incorporation of the distributed nature of the drillstring when compared to other methods of modelling such as FEM, and can be used effectively to study the response of drilling parameters and for real time measurements.

7.2 Recommendations for Further Work

The recommendations for further work are summarised as follows.

- The validation of the distributed-lumped model and lumped model of an oil well drillstring was performed by comparing the velocity responses obtained from the LDLM and LM with the actual measurements in

published studies (Veeningen 2011). The validation of the two types of modelling by measuring the velocity response or torque response on a drilling system was not possible because of the non-availability of such testing facilities to the author. However, the velocity responses obtained from real measurements (Kriesels et al. 1999.; Veeningen 2011; Ledgerwood et al. 2013) gave good agreement with the hybrid model response. The obvious differences between the two actual measurements were the accuracy of measuring the response due to the development of sensors and measuring devices. Therefore, the focus should be placed on the measurement of the velocity response and torque response on a real oil drilling system with high accuracy measuring instruments to further validate such models.

- In this study, the focus was on the modelling and the effect of drillpipe length on the parameters of drilling. Therefore, the optimisation technique assumed that the same layer of rock was experienced with different length of drillpipe; it is understood that this is not necessarily the case in reality. The optimisation method can be modified to handle different layers of rock with different length of drillpipe by updating the parameters of drilling with the progress of the drilling operation from a real measurement of an oil well if possible.
- Friction in the real system is greater than that modelled in this and past studies. Friction between the drillstring and the wall and stabiliser and the wall (static and dynamic) was not modelled. Therefore, to improve the accuracy more emphasis should be placed on measuring and modelling these effects.

References

Abbassian, F. and Dunayevsky, V. A. (1998) Application of stability approach to torsional and lateral bit dynamics. *SPE Drilling and Completion* 13 (2), 99-107.

Abdulgalil, F. and Siguerdidjane, H. (2005) PID based on sliding mode control for rotary drilling system. In *EUROCON 2005 - The International Conference on Computer as a Tool, November 21, 2005 - November 24, 2005.* Belgrade, Yugoslavia: Vol. I. Inst. of Elec. and Elec. Eng. Computer Society. 262-265.

Al-Hiddabi, S. A., Samanta, B. and Seibi, A. (2003) Non-linear control of torsional and bending vibrations of oilwell drillstrings. *Journal of Sound and Vibration* 265 (2), 401-415.

Apostal, M. C., Haduch, G. A. and Williams, J. B. (1990) A study to determine the effect of damping on finite element based, forced frequency response models for bottomhole assembly vibration analysis. In *In: SPE-20458, Presented at SPE Annual Technical Conference and Exhibition.* New Orleans, LA, USA. 537– 550.

Armstrong-Helouvry, B., Dupont, P. and Canudas De Wit, C. (1994) Survey of models, analysis tools and compensation methods for the control of machines with friction. *Automatica* 30 (7), 1083-1138.

Bailey, J. J. and Finnie, I. (1960) An analytical study of drillstring vibration. *Journal of Engineering for Industry, Transactions of the ASME* 82 (2), 122-128.

Bailey, J. R., Biedigner, E., Sundararaman, S., Carson, A. D., Elks, W. C. and Dupriest, F. E. (2008) Development and application of BHA vibrations model. In *In: Proceedings of the International Petroleum Technology Conference.* Kuala Lumpur, Malaysia.

Bailey, J. R. and Remmert, S. M. (2009) Managing drilling vibrations through BHA design optimization. In *in Proceeding of the International PetroleumTechnology Conference (IPTC '09).* Doha, Qatar. 921–930.

Baker Houghes INTEQ (1996) *Oil field familiarization: Train Gudie*. Houston, Tx 7703, United States of America, Baker Houghes INTEQ.

Beck, B. E., Desbrandes, R., Johnson, P. W., Lyons, W. C. and Miska, S., et al. (1996) *Drilling and well completions.* In W. C. Lyons (Ed.), Standard handbook of petroleum and natural gas engineering. Vol. 1. Houston, Texas: Gulf Publishing Company.

Besselink, B., Van De Wouw, N. and Nijmeijer, H. (2011) A semi-analytical study of stick-slip oscillations in drilling systems. *Journal of Computational and Nonlinear Dynamics* 6 (2).

Bharadwaj, A. M. and S, V. (2013) Drilling Optimization: A Review. *International Journal on Theoretical and Applied Research in Mechanical Engineering* 2 (1), 31-35.

Bourgoyne Jr, A. T., Millheim, K. K., Chenevert, M. E. and Young Jr, F. S. (1986) *Applied drilling engineering* SPE Textbook Series. Vol. 2. Richardson, Texas: Society of Petroleum Engineering.

Boussaada, I., Cela, A., Mounier, H. and Niculescu, S.-I. (2013) Control of drilling vibrations: A time-delay system-based approach. *11th Workshop on Time-Delay Systems, TDS 2013, February 4, 2013 - February 6, 2013.* Grenoble, France. IFAC Secretariat.

Boussaada, I., Mounier, H., Niculescu, S.-I. and Cela, A. (2012) Analysis of drilling vibrations: A time-delay system approach. *2012 20th Mediterranean Conference on Control and Automation, MED 2012, July 3, 2012 - July 6, 2012.* Barcelona, Spain. IEEE Computer Society.

Brett, J. F. (1992) The Genesis of Torsional Drillstring Vibrations. *SPE Drilling Engineering.* 7, 169-174.

Brown, F. T. (2001) *Engineering system dynamics.* United States of America: Marcel Dekker, Inc.

Canudas-de-Wit, C., Corchero, M. A., Rubio, F. R. and Navarro-Lopez, E. (2005) D-OSKIL: A new mechanism for suppressing stick-slip in oil well drillstrings. In *44th IEEE Conference on Decision and Control, and the European Control Conference, CDC-ECC '05, December 12, 2005 - December 15, 2005.* Seville, Spain: Vol. 2005. Inst. of Elec. and Elec. Eng. Computer Society. 8260-8265.

Challamel, N. (2000) Rock destruction effect on the stability of a drilling structure. *Journal of Sound and Vibration* 233 (2), 235-254.

Chen, S. L., Blackwood, K. and Lamine, E. (2002) Field investigation of the effects of stick-slip, lateral, and whirl vibrations on roller-cone bit performance. *SPE Drilling and Completion* 17 (1), 15-20.

Cherutich, S. K. (2009) *Rig selection and comparison of top drive and rotary table systems for cost effective drilling projects in keniya.* Iceland: *http://www.os.is/gogn/unu-gtp-report/UNU-GTP-2009-08.pdf.* Accessed 26 March 2015.

Christoforou, A. P. and Yigit, A. S. (2001) Active Control of Stick-Slip Vibrations: The Role of Fully Coupled Dynamics. In *SPE Middle East Oil Show, March 17, 2001 - March 20, 2001.* Bahrain, Bahrain. Society of Petroleum Engineers (SPE). 215-221.

Christoforou, A. P. and Yigit, A. S. (2003) Fully coupled vibrations of actively controlled drillstrings. *Journal of Sound and Vibration* 267 (5), 1029-1045.

Crowther, A. R. and Singh, R. (2007) Analytical investigation of stick-slip motions in coupled brake-driveline systems. *Nonlinear Dynamics* 50 (3), 463-481.

Dareing, D., Tlusty, J. and Zamudio, C. (1990) Self-excited vibrations induced by drag bits. *Journal of Energy Resources Technology, Transactions of the ASME* 112 (1), 54-61.

Dawson, R., Lin, Y. Q. and Spanos, P. D. (1987) Drill-string stick-slip oscillations. In *In the Proceedings of the Spring Conference on Experimental Mechanics (SEM'87).* Houston, Tex, USA. 590-595.

Dubinsky, V. S. and Baecker, D. R. (1998) Interactive drilling dynamics simulator for drilling optimization and training. In *Proceedings of the 1998 SPE Technical Conference and Exhibition. Part Omega, September 27, 1998 - September 30, 1998.* New Orleans, LA, USA: Vol. Delta. Soc Pet Eng (SPE). 639-648.

Dufeyte, M. and Henneuse, H. (1991) Detection and monitoring of the slip-stick motion: field experiments. In *Proceedings of the SPE/IADC Drilling Conference.* Amsterdam, The Netherlands: March, 1991. Vol. SPE. 429–438.

Duff, R. (2013) *An experimental and computational investigation of rotating flexible shaft system dynamics in rotary drilling assemblies for down hole drilling vibration mitigation.* PhD thesis. Graduate Faculty of the Louisiana State University and Agricultural and Mechanical College.

Dunayevsky, V. A., Abbassian, F. and Judzis, A. (1993) Dynamic stability of drillstrings under fluctuating weight on bit. *SPE Drilling and Completion* 8 (2), 84-92.

Dykstra, M. W., Neubert, M., Hughes, B., Hanson, J. M. and Meiners, M. J. (2001) Improving drilling performance by applying advanced dynamics models. In *SPE/IADC Drilling Conference, February 27, 2001 - March 1, 2001.* Amsterdam, Netherlands: Vol. 1. Society of Petroleum Engineers (SPE). 101-118.

Falode, O. A. and Agbarakwe, C. J. (2016) Optimisation of Drilling Parameters for Directionaland Horizontal Wells Using Genetic Algorithm. *Journal of Scientific Research & Reports* 11 (2), 1-10.

Fear, M. J., Abbassian, F., Parfitt, S. H. L. and McClean, A. (1997) The destruction of PDC bits by severe slip-stick vibration. In *Proceedings of the SPE/IADCDrilling Conference, SPEno. 37639.* Amsterdam, The Netherlands.

Finnie, I. and Bailey, J. J. (1960) An experimental study of drill-string vibration. *Journal of Engineering for Industry, Transactions of the ASME* 82 (2), 129–135.

Fubin, S., Linxiu, S., Lin, L. and Qizhi, Z. (2010) Adaptive PID control of rotary drilling system with stick slip oscillation. In *2010 2nd International Conference on Signal Processing Systems, ICSPS 2010, July 5, 2010 - July 7, 2010.* Dalian, China: Vol. 2. IEEE Computer Society. V2289-V2292.

Ghasemloonia, A., Geoff Rideout, D. and Butt, S. D. (2015) A review of drillstring vibration modeling and suppression methods. *Journal of Petroleum Science and Engineering* 131, 150-164.

Goldberg, D. E. and Richardson, J. (1987) Genetic algorithms with sharing for multimodal function optimization. In *Proceedings of the Second International Conference on Genetic Algorithms.* Lawrence Earlbaum, Hillsdale, New Jersey. 41–49.

Gradl, C., Eustes, A. W. and Thonhauser, G. (2012) An analysis of noise characteristics of drill bits. *Journal of Energy Resources Technology, Transactions of the ASME* 134 (1).

Guerrero, C. A. and Kuli, B. J. (2007) Deployment of an SeROP predictor tool for real-time bit optimization. In *SPE/IADC Drilling Conference and Exhibition 2007, February 20, 2007 - February 22, 2007.* Amsterdam, Netherlands: Vol. 1. Society of Petroleum Engineers (SPE). 284-297.

Gulyaev, V. I., Khudolii, S. N. and Glushakova, O. V. (2009) Self-excitation of deep-well drill string torsional vibrations. *Strength of Materials* 41 (6), 613-622.

Halsey, G. W., Kyllingstad, A. and Kylling, A. (1988) Torque feedback used to cure slip-stick motion. In *Proceedings: 1988 SPE Annual Technical Conference and Exhibition, October 2, 1988 - October 5, 1988.* Houston, TX, USA: Vol. DELTA. Publ by Soc of Petroleum Engineers of AIME. 277-282 18049.

Henneuse, H. (1992) Surface detection of vibrations and drilling optimization: field experience. In *Drilling Conference - Proceedings, February 18, 1992 - February 21, 1992.* New Orleans, LA, USA. Soc of Petroleum Engineers of AIME. 409-423.

Irawan, S., Abd Rahman, A. M. and Tunio, S. Q. (2012) Optimization of weight on bit during drilling operation based on rate of penetration model. *Research Journal of Applied Sciences, Engineering and Technology* 4 (12), 1690-1695.

Jain, J. R., Ledgerwood, L. W., Hoffmann, O. J., Schwefe, T. and Fuselier, D. M. (2011) Mitigating torsional stick/slip vibrations in oilwell drilling through PDC-bit design: Putting theories to the test. *JPT, Journal of Petroleum Technology* 63 (12), 79-80.

Jansen, J. D. (1993) *Nonlinear dynamics of oilwell drillstrings*. Ph.D. Thesis. Delft, Netherlands: University of technology.

Jansen, J. D., Steen, L. v. d. and Zachariassen, E. (1994) Active damping of torsional drillstring vibrations with a hydraulic topdrive. In *Proceedings of the European Petroleum Conference. Part 1 (of 2), October 25, 1994 - October 27, 1994.* London, UK. Society of Petroleum Engineers (SPE). 457-464.

Jansen, J. D. and van den Steen, L. (1995) Active damping of self-excited torsional vibrations in oil well drillstrings. *Journal of Sound and Vibration* 179 (4), 647-668.

Jansen, J. D., van den Steen, L. and Zachariasen, E. (1995) Active damping of torsional drillstring vibrations with a hydraulic top drive. *SPE Drilling and Completion* 10 (4), 250-254.

Janwadkar, S. S., Fortenberry, D. G. and Roberts, G. K. (2006) BHA and drilling modeling maximizes drilling performance in lateral wells of Barnett shale gas field of N.Texas,. In *in Proceedings of the SPE Gas Technology Symposium, vol. 100589 of SPE.* Calgary,Canada.

Jardine, S., Malone, D. and Sheppard, M. (1994) Putting dampers on drilling's bad vibrations. *Oilfield Rev.* 6 (1), 15-20.

Javanmardi, K. and Gaspard, D. (1992a) Soft torque rotary system reduces drillstring failures. *Oil and Gas Journal* 90 (41), 68-71.

Javanmardi, K. and Gaspard, D. T. (1992b) Application of soft-torque rotary table in mobile bay. In *Drilling Conference - Proceedings, February 18, 1992 - February 21, 1992.* New Orleans, LA, USA. Publ by Soc of Petroleum Engineers of AIME. 645-650.

Jijon, R. B., Canudas-De-Wit, C., Niculescu, S.-I. and Dumon, J. (2010) Adaptive observer design under low data rate transmission with applications to oil well drill-string. In *2010 American Control Conference, ACC 2010, June 30, 2010 - July 2, 2010.* Baltimore, MD, United states. IEEE Computer Society. 1973-1978.

Johnson, P. A., Savage, H., Knuth, M., Gomberg, J. and Marone, C. (2008) Effects of acoustic waves on stick-slip in granular media and implications for earthquakes. *Nature* 451 (7174), 57-60.

Johnson, S. (2008) A new method of producing laterally stable PDC drill bits. *SPE Drilling and Completion* 23 (3), 314-324.

Kamel, J. M. and Yigit, A. S. (2014) Modeling and analysis of stick-slip and bit bounce in oil well drillstrings equipped with drag bits. *Journal of Sound and Vibration* 333 (25), 6885-6899.

Kapitaniak, M., Vaziri Hamaneh, V., Páez Chávez, J., Nandakumar, K. and Wiercigroch, M. (2015) Unveiling complexity of drill–string vibrations: Experiments and modelling. *International Journal of Mechanical Sciences* 101-102, 324-337.

Karkoub, M., Abdel-Magid, Y. L. and Balachandran, B. (2009) Drill-string Torsional Vibration Suppression Using GA Optimized Controllers. *Journal of Canadian Petroleum Technology, 48(12), 32–38* 48 (12), 32-38.

Karnopp, D. (1985) Computer simulation of stick-slip friction in mechanical dynamic systems. *Journal of Dynamic Systems, Measurement and Control, Transactions of the ASME* 107 (1), 100-103.

Kelessidis, V. C. and Dalamarinis, P. (2009) Monitoring drilling bit parameters allows optimization of drilling rates. *9th International Multidicsciplinary Scientific Geoconference and EXPO, SGEM 2009, June 14, 2009 - June 19, 2009.* Albena, Bulgaria, Vol. 1. International Multidisciplinary Scientific Geoconference.

Khulief, Y. A. and Al-Naser, H. (2005) Finite element dynamic analysis of drillstrings. *Finite Elements in Analysis and Design* 41 (13), 1270-1288.

Khulief, Y. A., Al-Sulaiman, F. A. and Bashmal, S. (2005) Modeling of stick-slip in multibody drilling systems. *DETC2005: ASME International Design Engineering Technical Conferences and Computers and Information in Engineering Conference, September 24, 2005 - September 28, 2005.* Long Beach, CA, United states, Vol. 6 B. American Society of Mechanical Engineers.

Khulief, Y. A., Al-Sulaiman, F. A. and Bashmal, S. (2007) Vibration analysis of drillstrings with self-excited stick–slip oscillations. *Journal of Sound and Vibration* 299 (3), 540-558.

Kovalyshen, Y. (2013) A simple model of bit whirl for deep drilling applications. *Journal of Sound and Vibration* 332 (24), 6321-6334.

Kriesels, P. C., Keultjes, W. J. G., Dumont, P., Huneidi, I., Furat, A., Owoeye, O. O. and Hartmann, R. A. (1999.) Cost Savings through an Integrated Approach to Drillstring Vibration Control. In *in the SPE/IADC Middle East Drilling Technology Conference.* Abu Dhabi. SPE/IADC 57555.

Kyllingstad, A. and Halsey, G. W. (1988) Study of slip/stick motion of the bit. *SPE drilling engineering* 3 (4), 369-373.

Kyllingstad, A. and Nessjen, P. J. (2009) A new stick-slip prevention system. In *SPE/IADC Drilling Conference and Exhibition 2009, March 17, 2009 - March 19, 2009.* Amsterdam, Netherlands: Vol. 2. Society of Petroleum Engineers (SPE). 912-925.

Kyllingstad, A. and Nessjen, P. J. (2010) Hardware-in-the-loop simulations used as a cost efficient tool for developing an advanced stick-slip prevention system. In *IADC/SPE Drilling Conference and Exhibition 2010, February 2, 2010 - February 4, 2010.* New Orleans, LA, United states: Vol. 1. Society of Petroleum Engineers (SPE). 429-441.

Ledgerwood, L. W., Jain, J. R., Hoffmann , O. J. and Jr. et al. (2013) Downhole measurement and monitoring lead to an enhanced understanding of drilling vibrations and polycrystalline diamond compact bit damage. *SPE Drill Completion* 28 (3), 254-262.

Leine, R. I. (2000) *Bifurcations in discontinuous mechanical systems of filippov-type*. Ph.D. Thesis. Netherlands: Technical University of Eindhoven.

Leine, R. I. and Van Campen, D. H. (2005) Stick-slip whirl interaction in drillstring dynamics. *IUTAM Symposium on Chaotic Dynamics and Control of Systems and Processes in Mchanics: Proceedings of the IUTAM Symposium held in Rome, Italy, 8-13 June 2003.* Vol. 122. Springer Verlag. http://dx.doi.org/10.1007/1-4020-3268-4-27.

Leine, R. I., Van Campen, D. H., De Kraker, A. and Van Den Steen, L. (1998) Stick-slip vibrations induced by alternate friction models. *Nonlinear Dynamics* 16 (1), 41-54.

Leonov, G. A., Kuznetsov, N. V., Kiseleva, M. A., Solovyeva, E.P. and Zaretskiy, A. M. (2014) Hidden oscillations in mathematical model of drilling system actuated by induction motor with a wound rotor. *Nonlinear Dynamics* 77, 277-288.

Li, J.-P. (2015) Truss topology optimization using an improved species-conserving genetic algorithm. *Engineering Optimization* 47 (1), 107-128.

Li, J.-P., Balazs, M. E., Parks, G. T. and Clarkson, P. J. (2002) A species conserving genetic algorithm for multimodal function optimization.

Lin, Y.-Q. and Wang, Y.-H. (1991) Stick-slip vibration of drill strings. *Journal of engineering for industry* 113 (1), 38-43.

Liu, S., Liu, Z. and Sun, Y. (2013a) Research on drill string stick-slip vibration and its soft-torque control. *32nd Chinese Control Conference, CCC 2013, July 26, 2013 - July 28, 2013.* Xi'an, China. IEEE Computer Society.

Liu, X., Vlajic, N., Long, X., Meng, G. and Balachandran, B. (2013b) Nonlinear motions of a flexible rotor with a drill bit: Stick-slip and delay effects. *Nonlinear Dynamics* 72 (1-2), 61-77.

Liu, Y. (2015) Suppressing stick-slip oscillations in underactuated multibody drill-strings with parametric uncertainties using sliding-mode control. *IET Control Theory & Applications* 9 (1), 91-102.

Macdonald, K. A. and Bjune, J. V. (2007) Failure analysis of drillstrings. *Engineering Failure Analysis* 14 (8), 1641-1666.

Macpherson, J. D., Jogi, P. N. and Kingman, J. E. E. (2001) Application and analysis of simultaneous near bit and surface dynamics measurements. *SPE Drilling and Completion* 16 (4), 230-238.

Macpherson, J. D., Mason, J. S. and Kingman, J. E. E. (1993) Surface measurement and analysis of drillstring vibrations while drilling. *Proceedings of the 1993 SPE/IADC Drilling Conference, February 23, 1993 - February 25, 1993.* Amsterdam, Neth. Publ by Soc of Petroleum Engineers of AIME.

Mason, J. S. and Sprawls, B. M. (1998) Addressing BHA whirl: The culprit in Mobile Bay. *SPE Drilling and Completion* 13 (4), 231-236.

Mensa-Wilmot, G., Booth, M. and Mottram, A. (2000) New PDC bit technology and improved Operational practices. In *SPE/IADC Drilling Conference.* New Orleans.

Millheim, K., Jordan, S. and Ritter, C. J. (1978) Bottom-hole assembly analysis using the finite element method. *SPE* (6057), 265–74.

Mitchell, R. F., Miska, S., Aadnɣ, B. S. and Society of Petroleum, E. (2011) *Fundamentals of drilling engineering.* eBook: Society of Petroleum Engineers. Accessed Book, Whole.

Mongkolcheep, K. (2009) *A Lyapunov Exponent Approach for Identifying Chaotic Behavior in a Finite Element Based Drillstring Vibration Model*. Master of Scince. Texas A&M University.

Navarro-Lopez, E. M. (2009) An alternative characterization of bit-sticking phenomena in a multi-degree-of-freedom controlled drillstring. *Nonlinear Analysis: Real World Applications* 10 (5), 3162-3174.

Navarro-Lopez, E. M. and Cortes, D. (2007a) Avoiding harmful oscillations in a drillstring through dynamical analysis. *Journal of Sound and Vibration* 307 (1-2), 152-171.

Navarro-Lopez, E. M. and Cortes, D. (2007b) Sliding-mode control of a multi-DOF oilwell drillstring with stick-slip oscillations. *2007 American Control Conference, ACC, July 9, 2007 - July 13, 2007.* New York, NY, United states. Institute of Electrical and Electronics Engineers Inc.

Navarro-Lopez, E. M. and Suarez, R. (2004) Practical approach to modelling and controlling stick-slip oscillations in oilwell drillstrings. In *2004 IEEE International Conference on Control Applications, September 2, 2004 - September 4, 2004.* Taipei, Taiwan: Vol. 2. Institute of Electrical and Electronics Engineers Inc. 1454-1460.

Navarro-López, E. M. and Licéaga-Castro, E. (2009) Non-desired transitions and sliding-mode control of a multi-DOF mechanical system with stick-slip oscillations. *Chaos, Solitons and Fractals* 41 (4), 2035-2044.

Oil and Gas Portal (2014) *Drilling.* http://www.oil-gasportal.com/drilling/technologies Accessed 26 March 2015.

Omojuwa, E., Osisanya, S. and Ahmed, R. (2011) Dynamic analysis of stick-slip motion of drillstring while drilling. In *Society of Petroleum Engineers Nigeria Annual International Conference and Exhibition 2011, August 1, 2011 - August 3, 2011.* Abuja, Nigeria. Society of Petroleum Engineers. 220-229.

Omojuwa, E., Osisanya, S. and Ahmed, R. (2012) Measuring and controlling torsional vibrations and stick-slip in a viscous-damped drillstring model. In *International Petroleum Technology Conference 2012, IPTC 2012, February 7, 2012 - February 9, 2012.* Bangkok, Thailand: Vol. 1. Univeristy of Zagreb. 217-229.

Onwunalu, J. M. s. R., Department of Energy and Resources Engineering, S. U., California. (2006) *Optimization of Nonconventional Well Placement Using Genetic Algorithms and Statistical Proxy*. Master's Report. Stanford University, California.

Paic, B., Gaurina-Medimurec, N. and Matanovic, D. (2007) Wellbore instability: Causes and consequences. *Rudarsko Geolosko Naftni Zbornik* 19, 87-98.

Pastusek, P., Brackin, V. and Lutes, P. (2005) A fundamental model for prediction of hole curvature and build rates with steerable bottomhole assemblies. *SPE Annual Technical Conference and Exhibition, ATCE 2005, October 9, 2005 - October 12, 2005.* Dallas, TX, United states. Society of Petroleum Engineers (SPE).

Patil, P. A. and Teodoriu, C. (2013a) A comparative review of modelling and controlling torsional vibrations and experimentation using laboratory setups. *Journal of Petroleum Science and Engineering* 112 (0), 227-238.

Patil, P. A. and Teodoriu, C. (2013b) Analysis of bit-rock interaction during stick-slip vibration using PDC cutting force model. *Oil Gas European Magazine* 39 (3), 124-129.

Patil, P. A. and Teodoriu, C. (2013c) Model development of torsional drillstring and investigating parametrically the stick slips influencing factors. *ASME J. Energy Resour. Technol.* 135 (1), 0131031-0131037.

Pavković, D., Deur, J. and Lisac, A. (2011) A torque estimator-based control strategy for oil-well drill-string torsional vibrations active damping including an auto-tuning algorithm. *Control Engineering Practice* 19 (8), 836-850.

Pavone, D. R. and Desplans, J. P. (1994) Application of high sampling rate downhole measurements for analysis and cure of stick-slip in drilling. In *Proceedings of the SPE Annual Technical Conference & Exhibition, September 25, 1994 - September 28, 1994.* New Orleans, LA, USA: Vol. Delta. Society of Petroleum Engineers (SPE). 335-345.

Placido, J. C. R., Santos, H. M. R. and Galeano, Y. D. (2002) Drillstring vibration and wellbore instability. *Journal of Energy Resources Technology, Transactions of the ASME* 124 (4), 217-222.

Rao, S. S. (1995) *Mechanical vibrations.* Wokingham; Reading, Mass: Addison-Wesley.

Rich Mineral Corporation (2007) *How oil drilling works. http://www.richminerals.ca/m6.html.* Accessed 26 March 2015.

Richard, T. (2001) *Self-excited stick-slip oscillations of Drag bit.* Ph.D. Thesis. USA: University of Minnesota, USA.

Richard, T., Germay, C. and Detournay, E. (2004) Self-excited stick–slip oscillations of drill bits. *Comptes Rendus Mécanique* 332 (8), 619-626.

Richard, T., Germay, C. and Detournay, E. (2007) A simplified model to explore the root cause of stick-slip vibrations in drilling systems with drag bits. *Journal of Sound and Vibration* 305 (3), 432-456.

Rudat, J. and Dashevskiy, D. (2011) Development of an innovative model-based stick/slip control system. In *SPE/IADC Drilling Conference and Exhibition 2011, March 1, 2011 - March 3, 2011.* Amsterdam, Netherlands: Vol. 1. Society of Petroleum Engineers (SPE). 585-596.

Saldivar, B., Boussaada, I., Mounier, H., Mondié, S. and Niculescu, S. I. (2014a) An Overview on the Modeling of Oilwell Drilling Vibrations. *IFAC Proceedings Volumes* 47 (3), 5169-5174.

Saldivar, B., Knüppel, T., Woittennek, F., Boussaada, I., Mounier, H. and Niculescu, S. I. (2014b) Flatness-based Control of Torsional-Axial Coupled Drilling Vibrations. *IFAC Proceedings Volumes* 47 (3), 7324-7329.

Saldivar, B., Mondie˙, S., Loiseau, J.-J. and Rasvan, V. (2011) Stick-slip oscillations in oillwell drillstrings: dsitributed parameter and neutral type retarded model approaches. In *Preprints of the 18th IFAC World Congress.* Milano (Italy) August 28-September 2. International Federation of Automatic Control (IFAC). 284-289.

Saldivar, B., Mondi´e, S., Loiseau, J. J. and R˘asvan, V. (2013) Suppressing Axial-Torsional Coupled Vibrations in Drillstrings. *Control Engineering and Applied Informatics* 15 (1), 3-10.

Saldivar, B. and Mondié, S. (2013) Drilling vibration reduction via attractive ellipsoid method. *Journal of the Franklin Institute* 350 (3), 485-502.

Sananikone, P., Kamoshima, O. and White, D. B. (1992) Field method for controlling drillstring torsional vibrations. In *Drilling Conference - Proceedings, February 18, 1992 - February 21, 1992.* New Orleans, LA, USA. Publ by Soc of Petroleum Engineers of AIME. 443-452.

Sassan, A. and Halimberdi, B. (2013) Design of a controller for suppressing the stick-slip oscillations in oil well drillstring. *Research Journal of Recent Science* 2 (6), 78-82.

Schwarz, R. J. and Friedland, B. (1965) *Linear systems.* London; New York; etc: McGraw-Hill.

Serrarens, A., van de Molengraft, R., Kok, J. J. and van den Steen, L. (1998) H control for suppressing stick-slip in oil well drillstrings. *IEEE Control Systems Magazine* 18 (2), 19-30.

Sivanandam, S. N., Deepa, S. N. and Books24x, I. (2008) *Introduction to genetic algorithms.* New York;Berlin; eBook: Springer.

Spanos, P. D., Sengupta, A. K., Cunningham, R. A. and Paslay, P. R. (1995) Modeling of roller cone bit lift-off dynamics in rotary drilling. *Journal of Energy Resources Technology, Transactions of the ASME* 117 (3), 197-207.

Stroud, K. A. (1995) *Engineering mathematics: programmes and problems.* Basingstoke: Macmillan.

Sun, Y. Q. and Simson, S. (2008) Wagon–track modelling and parametric study on rail corrugation initiation due to wheel stick-slip process on curved track. *Wear* 265 (9–10), 1193-1201.

Tang, L., Zhu, X., Shi, C., Tang, J. and Xu, D. (2015) Study of the influences of rotary table speed on stick-slip vibration of the drilling system. *Petroleum* 1 (4), 382-387.

Tarng, Y. S. and Cheng, H. E. (1995) An investigation of stick-slip friction on the contouring accuracy of cnc machine tools. *International Journal of Machine Tools and Manufacture* 35 (4), 565-576.

Tikhonov, V. S. and Safronov, A. I. (2011) Analysis of postbuckling drillstring vibrations in rotary drilling of extended-reach wells. *Journal of Energy Resources Technology, Transactions of the ASME* 133 (4).

Veeningen, D. (2011) Nonel high speed telemetry system with measurments along the string mitigate drilling risk and improve drilling efficiency. In *In Proceedings of the Brazil Offshore Conference and Exhibition.* Macae', Brazil 533-544.

Warren, T. M. and Oster, J. H. (1998) Torsional resonance of drill collars with PDC bits in hard rock. In *Proceedings of the 1998 SPE Technical Conference and Exhibition. Part Omega, September 27, 1998 - September 30, 1998.* New Orleans, LA, USA: Vol. Delta. Soc Pet Eng (SPE). 625-637.

Whalley, R. (1988) The response of distributed-lumped parameter system. *Proceedings of the Institution of Mechanical Engineering, Part C: Journal of Mechanical Engineering Science.* 202 (C6), 9.

Whalley, R. (1990) Interconnected spatially distributed systems. *Transactions of the Institute of Measurement and Control* 12 (5), 262-270.

Worrall, R. N., Stulemeijer, I. P. J. M., Jansen, J. D. and Van Walstijn, B. G. G. (1992) *Method and system for controlling vibrations in borehole equipment.* 5117926. www.google.com/patents/EP044689A2?cl=en Accessed 26 March 2015.

Yeten, B. (2003) *Optimum Deployment of Nonconventional Wells*. Ph.D. Stanford University, California.

Yigit, A. S., Al-Ansary, M. D. and Khalid, M. (1996) Active and passive control of drillstring vibrations by mode localization. In *Proceedings of the 1996 1st European Conference on Structural Control, May 29 - 31 1996.* Barcelona, Spain. 603-603.

Yigit, A. S. and Christoforou, A. P. (1998) Coupled torsional and bending vibrations of drillstrings subjected to impact with friction. *Journal of Sound and Vibration* 215 (1), 167-181.

Yigit, A. S. and Christoforou, A. P. (2000) Coupled torsional and bending vibrations of actively controlled drillstrings. *Journal of Sound and Vibration* 234 (1), 67-83.

Zamanian, M., Khadem, S. E. and Ghazavi, M. R. (2007) Stick-slip oscillations of drag bits by considering damping of drilling mud and active damping system. *Journal of Petroleum Science and Engineering* 59 (3–4), 289-299.

Zhu, X., Tang, L. and Yang, Q. (2015) A Literature Review of Approaches for Stick-Slip Vibration Suppression in Oilwell Drillstring. *Advances in Mechanical Engineering* 6, 967952-967952.

Zill, D. G. and Cullen, M. R. (2000) *Advanced engineering mathematics.* Vol. 2nd. Sudbury, Mass: Jones and Bartlett.

Appendix A

A.1 Electrical transmission line

The electrical transmission line is a well-known example of a distributed element where the current and voltage depend on both time and space. Due to the analogy between the electrical transmission line and other physical systems (i.e., their differential equations are identical), understanding of the behaviour of the transmission line can be used to understand other systems (Schwarz and Friedland 1965). Therefore, in this section, the general equation of a distributed element will be derived by using the electrical network theory and the procedure of deriving this equation can be used to derive the equation of any distributed physical system, for example, mechanical systems.

Figure A 1 represents a circuit model of a section of transmission line of length Δx consisting of resistance per unit length (R), inductance per unit length (L), capacitance per unit length (C), and conductance per unit length (G). The voltage and current at time t, and point (x) are v(x,t) and i(x,t), respectively. The resistance and inductance represent the losses in the transmission line and if R and G are included in the analysis, the transmission line is called a lossy transmission line. On the other hand, If there are no losses the model could be reduced to an ideal transmission line ("lossless transmission line") consisting of only inductance (L) and capacitance(C). Hence the differential equation for a lossy transmission line and a lossless transmission line can be derived.

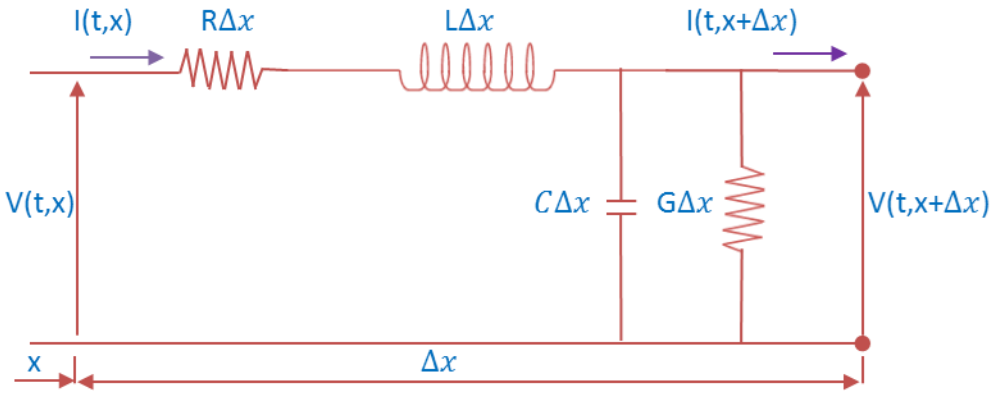

Figure A-1 Generic transmission-line section

A.1.1 Lossy transmission line

The circuit of a lossy transmission line consists of L, C, R and G as shown in Figure A-1 and the model can be derived as follows.

According to Kirchhoff's voltage law the change in voltage between the ends of the section can be obtained as follows:

$$v(x+\Delta x,t) - v(x,t) = -\left[L\frac{\partial i(x,t)}{\partial t} + Ri(t,x)\right]\Delta x \qquad \text{A.1}$$

Dividing by Δx and take $(\text{limit}\ \Delta x \to 0)$

$$\frac{\partial v(x,t)}{\partial x} = -L\frac{\partial i(x,t)}{\partial t} - Ri(x,t) \qquad \text{A.2}$$

Similarly, the change of current can be calculated using Kirchhoff's current law.

$$i(x+\Delta x,t) - i(x,t) = -\left[C\frac{\partial v(t,x+\Delta x)}{\partial t} + Gv(x+\Delta x,t)\right]\Delta x \qquad \text{A.3}$$

Dividing by Δx and taking the limit $(\Delta x \to 0)$, we obtain the partial differential equation

$$\frac{\partial i(x,t)}{\partial x} = -C\frac{\partial V(x,t)}{\partial t} - Gv(x,t) \qquad \text{A.4}$$

Taking the Laplace transformation of equation A.2 and A.4 with initial conditions equal to zero (assume linear system):

$$\frac{dV}{dx}(x,s) = -(Ls+R)I(x,s) \quad \text{A.5}$$

$$\frac{dI}{dx}(x,s) = -(Cs+G)V(x,s) \quad \text{A.6}$$

x and s are independent variables.

Differentiating equation A.6 with respect to x:

$$\frac{d^2I}{dx^2}(x,s) = -(Cs+G)\frac{dV(x,s)}{dx} \quad \text{A.7}$$

Substituting A.5 in A.7:

$$\frac{d^2I}{dx^2}(x,s) - (Ls+R)(Cs+G)I(x,s) = 0 \quad \text{A.8}$$

Similarly, differentiating equation A.5 with respect to x and substituting equation A.6 in it gives:

$$\frac{d^2V}{dx^2}(x,s) - (Ls+R)(Cs+G)V(x,s) = 0 \quad \text{A.9}$$

Let $\Gamma = \sqrt{(\mathrm{Ls}+\mathrm{R})(\mathrm{Cs}+\mathrm{G})}$ A.10

Where Γ is known as the propagation constant.

Then equation A.8 and A.9 can be written as:

$$\frac{d^2I}{dx^2}(x,s) - \Gamma^2 I(x,s) = 0 \quad \text{A.11}$$

$$\frac{d^2V}{dx^2}(x,s) - \Gamma^2 V(x,s) = 0 \quad \text{A.12}$$

The general solution of equations A.11 and A.12 can be found in any mathematics book, e.g. (Stroud 1995; Zill and Cullen 2000) and is shown in Appendix B:

$$V(x,s) = A\cosh\Gamma x + B\sinh\Gamma x \quad \text{A.13}$$

$$I(x,s) = C'\sinh\Gamma x + D\cosh\Gamma x \quad \text{A.14}$$

The constants of equations A.13 and A.14, (A, B, C', D) can be calculated from the boundary conditions (B.C) as follows:

First from B.C at x=0 substitute in A.13 and A.14:

$V(0, s) = A$

$I(0, s) = D$

Differentiating equations A.13 and A.14 with respect to x:

$\frac{dV(x,s)}{dx} = A\,\Gamma sinh\,\Gamma x + B\ \Gamma cosh\,\Gamma x$ A.15

$\frac{dI(x,s)}{dx} = C'\,\Gamma cosh\,\Gamma x + D\,\Gamma sinh\,\Gamma x$ A.16

Substituting equation A.5 and A.6 into equations A.15 and A.16:

$-(Ls + R)\,I(x, s) = A\,\Gamma sinh\,\Gamma x + B\ \Gamma cosh\,\Gamma x$ A.17

$-(Cs + G)V(X, s) = C'\,\Gamma cosh\,\Gamma x + D\,\Gamma sinh\,\Gamma x$ A.18

Then substitute x=0 (B.C) into equations A.17 and A.18:

$-(sL + R)\,I(0, s) = B\Gamma$ A.19

$-(Cs + G)V(X, s) = C'\Gamma$ A.20

Substitute equation A.10 into equations A.19

$-(sL + R)\,I(0, s) = B\sqrt{(sL + R)(Cs + G)}$

Rewrite $(sL + R)$and $(Cs + G)$ in the root form as $(\sqrt{sL + R})(\sqrt{sL + R})$ and$(\sqrt{sC + G})(\sqrt{sC + G})$, then substitute into equations A.19 and A.20

$$B = \frac{-(\sqrt{sL + R})(\sqrt{sL + R})I(0, s)}{\sqrt{(sL + R)(Cs + G)}}$$

$B = -\sqrt{\frac{(sL+R)}{(Cs+G)}}\ \ I(0, s)$ A.21

$$C' = \frac{-(Cs+G)V(0,s)}{\Gamma} = \frac{-(\sqrt{sC+G})(\sqrt{sC+G})\,V(0,s)}{\sqrt{(sL+R)(Cs+G)}}$$

$$C' = -\,1\Big/\sqrt{\frac{(sL+R)}{(Cs+G)}}\;\; V(x,s) \qquad \text{A.22}$$

Let $\xi = \sqrt{\frac{(sL+R)}{(Cs+G)}}$ A.23

Where ξ, is known as the characteristic impedance of the line, which has the units of ohms.

By substituting equation A.23 into equations A.21 and A.22:

$B = -\xi\, I(0,s)$

$C' = -\xi^{-1}\, V(x,s)$

Substitute the value of, B, C' and D in A.13 and A.14:

$$V(x,s) = V(0,s)cosh\,\Gamma x - \xi\, I(0,s)\, sinh\,\Gamma x \qquad \text{A.24}$$

$$I(x,s) = -\xi^{-1}V(0,s)\, sinh\,\Gamma x + \xi I(0,s)\, cosh\,\Gamma x \qquad \text{A.25}$$

Therefore, the equations A.24 and A.25 can be used to calculate the voltage and the current at any distance from the beginning of the segment and can be expressed in matrix form as:

$$\begin{bmatrix} V(x,s) \\ I(x,s) \end{bmatrix} = \begin{bmatrix} cosh\,\Gamma x & -\xi_j\, sinh\,\Gamma x \\ -\xi_j{}^{-1}\, sinh\,\Gamma x & cosh\,\Gamma x \end{bmatrix} \begin{bmatrix} V(0,s) \\ I(0,s) \end{bmatrix} \qquad \text{A.26}$$

Now if there are (i) numbers of segments and i=1, 2, 3,…, n, and the input to the segment j and output j+1 and j=ith element -1, then

At the input $x = 0$:

$V(0,s) = V_j(s)$, $I(0,s) = I_j(s)$

The output at $(x = l)$ can be written as:

$$V(l,s) \;=\; V_{j+1}(s)$$

$$I_j\big(l_j,s\big) \;=\; I_{j+1}(s)$$

Substituted into equation A.26:

$$\begin{bmatrix} V_{j+1}(s) \\ I_{j+1}(s) \end{bmatrix} = \begin{bmatrix} cosh\,\Gamma_j\, l_j & -\xi_j\, sinh\,\Gamma_j l_j \\ -{\xi_j}^{-1}\, sinh\,\Gamma_j l_j & cosh\,\Gamma_j l_j \end{bmatrix} \begin{bmatrix} V_j(s) \\ I_j(s) \end{bmatrix} \qquad \text{A.27}$$

From equation A.27.

$$V_{j+1}(s) \;=\; cosh\,\Gamma_j l_j \;\; V_j(s) \;- \xi_j\, sinh\,\Gamma_j l_j \;\; I_j(s) \qquad \text{A.28}$$

$$I_{j+1}(s) \;= -{\xi_j}^{-1}\, sinh\,\Gamma_j l_j V_j(s) \;\; + \;\; cosh\,\Gamma_j l_j \;\; I_j(s) \qquad \text{A.29}$$

From equation A.29:

$${\xi_j}^{-1}\, sinh\,\Gamma_j l_j\, V_j(s) \;= -I_{j+1}(s) \;\; + cosh\,\Gamma_j l_j \;\; I_j(s)$$

Divided into both sides of the equation on $({\xi_j}^{-1}\, sinh\,\Gamma_j l_j\,)$

$$V_j(s) \;= -\,\xi_j \frac{1}{sinh\,\Gamma_j l_j} I_{j+1}(s) \;\; + \xi_j \frac{cosh\,\Gamma_j l_j}{sinh\,\Gamma_j l_j} I(s) \qquad \text{A.30}$$

Sub equation A.30 in A.28.

$$V_{j+1}(s) \;= cosh\,\Gamma_j l_j \left(-\,\xi_j \frac{1}{sinh\,\Gamma_j l_j} I_{j+1}(s) \;\; + \xi_j \frac{cosh\,\Gamma_j l_j}{sinh\,\Gamma_j l_j} I_j(s) \right) - \xi_j\, sinh\,\Gamma_j l_j \;\, I_j(s)$$

$$V_{j+1}(s) \;= \left(-\,\xi_j \frac{cosh\,\Gamma_j l_j}{sinh\,\Gamma_j l_j} I_{j+1}(s) \;\; + \xi_j \frac{cosh^2\,\Gamma_j l_j}{sinh\,\Gamma_j l_j} I_j(s) \right) - \xi_j\, sinh\,\Gamma_j l_j \;\, I_j(s)$$

Since $cosh^2\,\Gamma_j l_j \;= sinh^2\,\Gamma_j l_j \;+ 1$

$$V_{j+1}(s) \;= \left(-\,\xi_j \frac{cosh\,\Gamma_j l_j}{sinh\,\Gamma_j l_j} I_{j+1}(s) \;\; + \xi_j \frac{\left(sinh^2\,\Gamma_j l_j \;+ 1\right)}{sinh\,\Gamma_j l_j} I_j(s) \right) - \xi_j\, sinh\,\Gamma_j l_j \;\, I_j(s)$$

$$V_{j+1}(s) = \left(-\xi_j \frac{\cosh \Gamma_j l_j}{\sinh \Gamma_j l_j} I_{j+1}(s) + \xi_j \frac{\left(\sinh^2 \Gamma_j l_j\right)}{\sinh \Gamma_j l_j} I_j(s) + \xi_j \frac{1}{\sinh \Gamma_j l_j} I_j(s) \right)$$

$$- \xi_j \sinh \Gamma_j l_j \; I_j(s)$$

$$V_{j+1}(s) = \left(-\xi_j \frac{\cosh \Gamma_j l_j}{\sinh \Gamma_j l_j} I_{j+1}(s) + \xi_j \sinh \Gamma_j l_j \; I_j(s) + \xi_j \frac{1}{\sinh \Gamma_j l_j} I_j(s) \right)$$

$$- \xi_j \sinh \Gamma_j l_j \; I_j(s)$$

$$V_{j+1}(s) = -\xi_j \frac{\cosh \Gamma_j l_j}{\sinh \Gamma_j l_j} I_{j+1}(s) + \xi_j \frac{1}{\sinh \Gamma_j l_j} I_j(s)$$

$$V_{j+1}(s) = \xi_j I_j(s) \operatorname{csch} \Gamma_j l_j - \xi_j I_{j+1}(s) \operatorname{ctnh} \Gamma_j l_j \qquad \text{A.31}$$

Where

$$\operatorname{ctnh} \Gamma_j l_j = \frac{\cosh \Gamma_j l_j}{\sinh \Gamma_j l_j}$$

$$\operatorname{csch} \Gamma_j l_j = \frac{1}{\sinh \Gamma_j l_j}$$

Similarly from equation A.28:

$$V_j(s) = \xi_j I_j(s) \operatorname{ctnh} \Gamma_j l_j - \xi_j I_{j+1}(s) \operatorname{csch} \Gamma_j l_j \qquad \text{A.32}$$

Equation A.31 and A.32 can be written in matrix form:

$$\begin{bmatrix} V_j(s) \\ V_{j+1}(s) \end{bmatrix} = \begin{bmatrix} \xi_j \operatorname{ctnh} \Gamma_j l_j & -\xi_j \operatorname{csch} \Gamma_j l_j \\ \xi_j \operatorname{csch} \Gamma_j l_j & -\xi_j \operatorname{ctnh} \Gamma_j l_j \end{bmatrix} \begin{bmatrix} I_j(s) \\ I_{j+1}(s) \end{bmatrix} \qquad \text{A.33}$$

Since from trigonometric relations

$$\operatorname{ctnh} x = \frac{e^{2x} + 1}{e^{2x} - 1}$$

Then

$$\operatorname{ctnh} \Gamma_j l_j = \frac{e^{2\Gamma_j l_j} + 1}{e^{2\Gamma_j l_j} - 1}$$

If the following relationship is given

$$w_j(s) = cnth\, \Gamma_j l_j$$

Then

$$w_j(s) = \frac{e^{2\Gamma_j l_j} + 1}{e^{2\Gamma_j l_j} - 1}$$

Since

$$csch\, \Gamma_j l_j = \sqrt{ctnh^2\, \Gamma_j l_j - 1}$$

Then

$$csch\, \Gamma_j l_j = \sqrt{\left(w_j{}^2(s) - 1\right)}$$

Substituting the above relationships into Equation A.33:

$$\begin{bmatrix} V_j(s) \\ V_{j+1}(s) \end{bmatrix} = \begin{bmatrix} \xi_j w_{j\,(s)} & -\xi_j \sqrt{\left(w_j{}^2(s) - 1\right)} \\ \xi_j \sqrt{\left(w_j{}^2(s) - 1\right)} & -\xi_j w_j\,(s) \end{bmatrix} \begin{bmatrix} I_j(s) \\ I_{j+1}(s) \end{bmatrix} \qquad \text{A.34}$$

Equation A.34 represents the general equation for calculating the voltage and current at any point along the transmission line. Now if we consider that U(t, x) and Y(t, x) represent the input and output to any distributed element, their partial differential equations are identical to transmission line equation. Thus, equation A.34 can be written for a distributed element as follows.

$$\begin{bmatrix} U_j(s) \\ U_{j+1}(s) \end{bmatrix} = \begin{bmatrix} \xi_j w_{j\,(s)} & -\xi_j \sqrt{\left(w_j{}^2(s) - 1\right)} \\ \xi_j \sqrt{\left(w_j{}^2(s) - 1\right)} & -\xi_j w_j\,(s) \end{bmatrix} \begin{bmatrix} Y_j(s) \\ Y_{j+1}(s) \end{bmatrix} \qquad \text{A.35}$$

Therefore equation A.35 is the general equation of a distributed element.

A.1.2 Lossless transmission line

In this model, we assume there are no losses in the transmission line and the resistance and conductance equal to zero. This assumption means that the signal is transmitted from the input to the outlet without losses or distortion but only delay.

The same procedure used for the derivation of the lossy transmission line will apply except that R=G=0.

The equations A.2 and A.4 of the lossy transmission line will reduce to

$$\frac{\partial v(x,t)}{\partial x} = -L\frac{\partial i(x,t)}{\partial t} \quad \text{A.36}$$

$$\frac{\partial i(x,t)}{\partial x} = -C\frac{\partial V(x,t)}{\partial t} \quad \text{A.37}$$

Also characteristic impedance and propagation constant will reduce to

$$\Gamma = s\sqrt{LC} \quad \text{A.38}$$

$$\xi = \sqrt{\frac{L}{C}} \quad \text{A.39}$$

By using the same procedure of deriving the equation for a lossy transmission line, the final equation of the lossless transmission line is the same except the difference in the value of impedance and propagation constant as follows.

$$\begin{bmatrix} V_j(s) \\ V_{j+1}(s) \end{bmatrix} = \begin{bmatrix} \xi_j w_{j\,(s)} & -\xi_j\sqrt{\left(w_j{}^2(s) - 1\right)} \\ \xi_j\sqrt{\left(w_j{}^2(s) - 1\right)} & -\xi_j w_j\,(s) \end{bmatrix} \begin{bmatrix} I_j(s) \\ I_{j+1}(s) \end{bmatrix} \quad \text{A.40}$$

For any distributed element without losses along the element.

$$\begin{bmatrix} U_j(s) \\ U_{j+1}(s) \end{bmatrix} = \begin{bmatrix} \xi_j w_{j\,(s)} & -\xi_j\sqrt{\left(w_j{}^2(s) - 1\right)} \\ \xi_j\sqrt{\left(w_j{}^2(s) - 1\right)} & -\xi_j w_j\,(s) \end{bmatrix} \begin{bmatrix} Y_j(s) \\ Y_{j+1}(s) \end{bmatrix} \quad \text{A.41}$$

Therefore equation A.41 can be used to represent a mechanical system where the input and output represent the torque and velocity of a distributed long slender shaft such as the drillpipe in an oil drilling system.

Appendix B

B.1 General solution of second order linear differential equation

$$\frac{d^2y}{dx^2} - k^2y = 0 \qquad \text{B.1}$$

Auxiliary equation of Eq. B.1

$$m^2 - k^2 = 0$$

From auxiliary equation

$m_1 = k$ and $m_2 = -k$

Since the auxiliary equation has two unequal real roots, then it has two solutions

$y_1 = e^{m_1 x} = e^{kx}$ and $y_2 = e^{m_2 x} = e^{-kx}$

Since these equations are linearly independent on $(-\infty, \infty)$ then the general solution of Eq. B.1 is

$$y = a_1 e^{kx} + a_2 e^{-kx} \qquad \text{B.2}$$

If $a_1 = a_2 = 1/2$ and $a_1 = \frac{1}{2}$, $a_2 = -1/2$ in Eq.B.2, then the particular solution is

$y = \frac{1}{2}(e^{kx} + e^{-kx}) = \cosh kx$ and $y = \frac{1}{2}(e^{kx} - e^{-kx}) = \sinh kx$

Since $\cosh kx$ and $\sinh kx$ are linearly independent on any interval of the x-axis, an alternative form for the general solution of Eq. B.1 is

$$y = a_1 \cosh kx + a_2 \sinh kx$$

Appendix C

Table C-8-1 Simulation results of the key parameters

No.	Case	ξ_{dp}	J_{dc}	W_{ob}	C_{bh}	T_{rt}	ω_{cr}
1	LLLL	72	156	10	15	3470	59
2	LLLM	72	156	10	55	2410	32
3	LLLH	72	156	10	95	1980	21
4	LLML	72	156	80	15	19350	285
5	LLMM	72	156	80	55	13160	138
6	LLMH	72	156	80	95	10880	85
7	LLHL	72	156	150	15	33500	474
8	LLHM	72	156	150	55	23160	228
9	LLHH	72	156	150	95	19310	140
10	LMLL	72	774	10	15	2100	28
11	LMLM	72	774	10	55	1830	18
12	LMLH	72	774	10	95	1710	15
13	LMML	72	774	80	15	11820	120
14	LMMM	72	774	80	55	10970	94
15	LMMH	72	774	80	95	10400	77
16	LMHL	72	774	150	15	20740	192
17	LMHM	72	774	150	55	19140	150
18	LMHH	72	774	150	95	18340	122
19	LHLL	72	1392	10	15	1510	12
20	LHLM	72	1392	10	55	1480	10
21	LHLH	72	1392	10	95	1460	8.5
22	LHML	72	1392	80	15	9550	72
23	LHMM	72	1392	80	55	9400	64
24	LHMH	72	1392	80	95	9300	57
25	LHHL	72	1392	150	15	16860	113
26	LHHM	72	1392	150	55	16360	97
27	LHHH	72	1392	150	95	16530	89
28	MLLL	373	156	10	15	2710	41
29	MLLM	373	156	10	55	2220	28
30	MLLH	373	156	10	95	1960	20
31	MLML	373	156	80	15	14970	190

32	MLMM	373	156	80	55	13350	142
33	MLMH	373	156	80	95	11520	97
34	MLHL	373	156	150	15	26190	315
35	MLHM	373	156	150	55	22190	209
36	MLHH	373	156	150	95	20190	156
37	MMLL	373	774	10	15	1780	20
38	MMLM	373	774	10	55	1670	15
39	MMLH	373	774	10	95	1590	13
40	MMML	373	774	80	15	10450	90
41	MMMM	373	774	80	55	10260	80
42	MMMH	373	774	80	95	10110	71
43	MMHL	373	774	150	15	18310	144
44	MMHM	373	774	150	55	17990	125
45	MMHH	373	774	150	95	17750	111
46	MHLL	373	1392	10	15	1390	8
47	MHLM	373	1392	10	55	1365	6
48	MHLH	373	1392	10	95	1355	5
49	MHML	373	1392	80	15	9200	64
50	MHMM	373	1392	80	55	9240	60
51	MHMH	373	1392	80	95	9250	55
52	MHHL	373	1392	150	15	16330	101
53	MHHM	373	1392	150	55	16360	93
54	MHHH	373	1392	150	95	16370	86
55	HLLL	674	156	10	15	2470	36
56	HLLM	674	156	10	55	2080	25
57	HLLH	674	156	10	95	1860	18
58	HLML	674	156	80	15	13350	155
59	HLMM	674	156	80	55	12450	124
60	HLMH	674	156	80	95	11590	98
61	HLHL	674	156	150	15	23100	249
62	HLHM	674	156	150	55	21100	187
63	HLHH	674	156	150	95	20260	158
64	HMLL	674	774	10	15	1690	17
65	HMLM	674	774	10	55	1590	13
66	HMLH	674	774	10	95	1550	11

67	HMML	674	774	80	15	10130	85
68	HMMM	674	774	80	55	10070	76
69	HMMH	674	774	80	95	9970	68
71	HMHL	674	774	150	15	17900	134
71	HMHM	674	774	150	55	17700	119
72	HMHH	674	774	150	95	17550	107
73	HHLL	674	1392	10	15	1370	8
74	HHLM	674	1392	10	55	1350	6
75	HHLH	674	1392	10	95	1340	5
76	HHML	674	1392	80	15	9240	66
77	HHMM	674	1392	80	55	9210	59
78	HHMH	674	1392	80	95	9230	55
79	HHHL	674	1392	150	15	16320	102
80	HHHM	674	1392	150	55	16360	94
81	HHHH	674	1392	150	95	16380	87